2019

NETWORKED MICROGRID OPTIMIZATION AND ENERGY MANAGEMENT

Robert S. Jane
Michigan Technological University, rsjane@mtu.edu

NETWORKED MICROGRID OPTIMIZATION AND ENERGY MANAGEMENT

By

Robert S. Jane

A DISSERTATION

Submitted in partial fulfillment of the requirements for the degree of

DOCTOR OF PHILOSOPHY

In Mechanical Engineering - Engineering Mechanics

MICHIGAN TECHNOLOGICAL UNIVERSITY

2019

This dissertation has been approved in partial fulfillment of the requirements for the Degree of DOCTOR OF PHILOSOPHY in Mechanical Engineering - Engineering Mechanics.

Department of Mechanical Engineering - Engineering Mechanics

Dissertation Co-advisor: *Dr. Gordon G. Parker*

Dissertation Co-advisor: *Dr. Steven Y. Goldsmith*

Committee Member: *Dr. Wayne W. Weaver*

Committee Member: *Dr. Denise M. Rizzo*

Department Chair: *Dr. William W. Predebon*

Dedication

This dissertation is dedicated to the various members of my extended and immediate family, especially my mother **Lisa A. Jane** and my father **Robert T. Jane** for always supporting me, and providing me with the ability to pursue an education in the field of Mechanical Engineering - Engineering Mechanics. I would also like to recognize my **favorite** sister-in-law **Tania Castro** and brother **Micheal T. Jane** for providing additional moral support and drive to obtain my doctorate before the birth of my nephew. Further, I am grateful to my grandparents, aunts, uncles, and cousins for supporting me.

Contents

List of Figures

List of Tables

Preface

Copyright Permission

Components of Chapter 2 are reprinted with permission from "Of Fuel-Optimal Strategies for Vehicle Supported Military Microgrids," *SAE International* Technical Paper 2016-01-0312, 2016, doi:10.4271/2016-01-0312. SAE International. Further use or distribution is not permitted without permission from SAE. I performed the literature review, constructed various simulation components, tabulated the data, and wrote the paper. The remaining coauthors proofread and peer reviewed the paper for technical correctness.

Chapter 3 are reprinted with permission from "Optimal Power Management of Vehicle Sourced Military Outposts," *SAE International Journal of Commercial Vehicles* 10(1):pp.132-143 SAE International. Further use or distribution is not permitted without permission from SAE. Both myself and Ronald Matthews performed the literature review, constructed various simulation components, tabulated the data, and wrote the paper. The remaining coauthors proofread and peer reviewed the paper for technical correctness. The letter of permission can be found in Appendix D.

Disclaimer

This work was partially supported by the U.S. Army Combat Capabilities Development Command (CCDC) Ground Vehicle Systems Center (formerly the U.S. Army Tank Automotive Research Development and Engineering Center (TARDEC)). The views and conclusions contained in this document are those of the authors and should not be interpreted as representing the official policies, either expressed or implied, of the CCDC Ground Vehicle Systems Center or the U.S. Government.

This work was also partially supported by the U.S. Army Research Laboratory (ARL). Reference herein to any specific commercial company, product, process, or service by trade name, trademark, manufacturer, or otherwise, does not necessarily constitute or imply its endorsement, recommendation, or favoring by the United States Government or the Department of the Army (DoA). The opinions of the authors expressed herein do not necessarily state or reflect those of the United States Government or the DoA, and shall not be used for advertising or product endorsement purposes.

Acknowledgments

There are many individuals, and organizations, which I have interacted with over the course of my graduate work, their contributions have made it possible for me to obtain both a Masters and Doctorate degrees.

First, I would like to acknowledge both my advisors, Dr. Gordon G. Parker, and Dr. Steven Y. Goldsmith. My advisers have provided me with exceptional technical and professional expertise in the field of Engineering, and provided me with the ability to participate in multiple research endeavors while perusing my higher education.

Additionally, I would like to acknowledge my other dissertation committee members Dr. Wayne W. Weaver, and Dr. Denise M. Rizzo. All of my committee members have provided extensive technical knowledge and their individual contributions to my research cannot be overstated, and is much appreciated.

I would also like to acknowledge Michigan Technological University's (MTU) faculty, staff, and fellow students who contributed their time and effort during various stages of my academic career.

I have deep gratitude to the men and women who serve our military. I am thankful to the support and funding from the U.S. Army Research Laboratory (ARL) of the U.S.

Army Research Development and Engineering Command (RDECOM).Additional support and funding were provided by the U.S. Army Combat Capability Development Center (CCDC) and Ground Vehicle Systems Center (USACCDCGVSC) for military microgrid optimization and control. Notably, I would like to acknowledge Bruce R. Geil, Morris S. Berman, Donald H. Porschet, and Gail T. Vaucher for providing exceptional technical, professional, and educational expertise.

This work was partially supported by the U.S. Army Combat Capabilities Development Command (CCDC) Ground Vehicle Systems Center (formerly the U.S. Army Tank Automotive Research Development and Engineering Center (TARDEC)). The views and conclusions contained in this document are those of the authors and should not be interpreted as representing the official policies, either expressed or implied, of the CCDC Ground Vehicle Systems Center or the U.S. Government.

This work was partially supported by the U.S. Army Research Laboratory (ARL). Reference herein to any specific commercial company, product, process, or service by trade name, trademark, manufacturer, or otherwise, does not necessarily constitute or imply its endorsement, recommendation, or favoring by the United State Government or the Department of the Army (DoA). The opinions of the authors expressed herein do not necessarily state or reflect those of the United State Government of the DoA, and shall not be used for advertising or product endorsement purposes.

List of Abbreviations

AAM	Autonomous Agile Microgrid
AC	Alternating Current
AKC	Acknowledgment
AMMPS	Advanced Medium Mobile Power Source
ARIMA	Autoregressive Integrated Moving Average
ARL	U.S. Army Research Laboratory
BC	Battery Commander
BCIL	Base Camp Integration Laboratory
BN	Battalion
CAN	Controller Area Network
CAT	Caterpillar Inc.
CCDC	Combat Capabilities Development Command
CESS	Composite Energy Storage System
COC	Combat Operations Center
COM	Communication
COMM	Communication
COP	Combat Outpost or Coefficient of Performance
COTS	Commercial off the Shelf

DC	Direct Current
DCLC	Decentralized Closed Loop Controller
DG	Distributed Generation
DGM	Distributed Grid Management
DMBC	Decentralized Model Based Control
DoA	Department of the Army
DOD	Department of Defense
DS	Distributed Storage
ECU	Electronic Control Unit or Environmental Control Unit
EMS	Energy Management Strategy
ESS	Energy Storage Systems
FOB	Forward Operating Base
GEP	General Engine Products
GFA	Generator Forecasting Agent
GFE	Government Furnished Equipment
GVSETS	Ground Vehicle Systems Engineering and Technology Symposium
HEMMTT	Heavy Expanded Mobility Tactical Truck
HIL	Hardware in the Loop
HMMWV	High Mobility Multipurpose Wheeled Vehicle
HQ	Headquarters
HVAC	Heating, Ventilation, and Air Conditioning

ID	Identification Number
IP	Internet Protocol
ISG	Integrated Starter Generator
JLTV	Joint Light Tactical Vehicle
LC	Local Controller
LEP	Leader Election Protocol
LFA	Load Forecast Agent
LFC	Load Frequency Control
LIN	Local Interconnected Network
LOG	Logistics
LTO	Long Term Optimal
MANET	Mobile Ad Hoc Network
MATLAB	Matrix Laboratory
MGCC	Microgrid Central Controller
MOST	Media Oriented System Transport
MPC	Model Predictive Control
MPPT	Maximum Power Point Tracking
MRAP	Mine Resistance Ambush Protected
MTVR	Medium Tactical Vehicle Replacements
NARX	Nonlinear AutoRegressive Network with Exogenous Inputs
NOCT	Normal Operating Cell Temperature

ODB	On-Board Diagnostic
OP	Outpost
OPF	Optimal Power Flow
OPSEC	Operations Security
OPSo	Operations
PCC	Points of Common Coupling
PEV	Plug-in Electric Vehicles
PFCA	Power Flow and Control Agent
PHEV	Plug-in Hybrid Electric Vehicles
PSCA	Power Scheduling and Coordination Agent
PV	Photovoltaic Array
QRF	Quick Response Force
RDECOM	United States Army Research, Development, and Engineering Command
RESCU	Rugged Energy Storage Containment Unit
RFA	Renewable Forecast Agent
RH	Relative Humidity
RL	Resistance and Inductance
RMS	Root Mean Square
RPM	Revolutions per Minute
RTDS	Real-Time Digital Power Systems Simulator

SAE	Society of Automotive Engineers
SEES	Small Electric Energy Systems
SFA	Storage Forecast Agent
SGT	Sergeant
SIL	Software in the Loop
SOC	State of Charge
SPIDERS	Smart Power Infrastructure Demonstration for Energy Reliability and Security
STC	Standard Test Conditions
SVM	Support Vector Machines
SWE	Sea Wave Energy
SYN	Synchronize
TCP	Transmission Control Protocol
TIG	Transmission Integrated Generator
TQG	Tactical Quiet Generator
TTCAN	Time Triggered Controller Area Network
TVGM	Tactical to Vehicle Module
UDP	User Datagram Protocol
UML	Unified Modeling Language
V2G	Vehicle to Grid
V2V	Vehicle to Vehicle

VANET	Vehicular Ad-Hoc Network
VI	Voltage Current
VP	Voltage Power
WOT	Wide Open Throttle
WT	Wind Turbines
ZoH	Zero Order Hold

Abstract

Military vehicles possess attributes consistent with a microgrid, containing electrical energy generation, storage, government furnished equipment (GFE), and the ability to share these capabilities via interconnection. Many military vehicles have significant energy storage capacity to satisfy silent watch requirements, making them particularly well-suited to share their energy storage capabilities with stationary microgrids for more efficient energy management. Further, the energy generation capacity and the fuel consumption rate of the vehicles are comparable to standard diesel generators, for certain scenarios, the use of the vehicles could result in more efficient operation. Energy management of a microgrid is an open area of research especially in generation constrained scenarios where shedding of low-priority loads may be required. Typical metrics used to assess the effectiveness of an energy management strategy or policy include fuel consumption, electrical storage energy requirements, or the net exergy destruction. When considering a military outpost consisting of a stationary microgrid and a set of vehicles, the metrics used for managing the network become more complex. For example, the metrics used to manage a vehicle's onboard equipment while on patrol may include fuel consumption, the acoustic signature, and the heat signature. Now consider that the vehicles are parked at an outpost and participating in vehicle-to-grid power-sharing and control. The metrics used to manage the grid

assets may now include fuel consumption, the electrical storage's state of charge, frequency regulation, load prioritization, and load dispatching. The focus of this work is to develop energy management and control strategies that allow a set of diverse assets to be controlled, yielding optimal operation. The provided policies result in both short-term and long-term optimal control of the electrical generation assets. The contributions of this work were: (1) development of a methodology to generate a time-varying electrical load based on (1) a U.S. Army-relevant event schedule and (2) a set of meteorological conditions, resulting in a **scenario rich environment** suitable for **modeling and control of hybrid AC/DC tactical military microgrids**, (2) the development of a **multi-tiered hierarchical control architecture**, suitable for development of both **short and long term optimal energy management strategies** for hybrid electric microgrids, and (3) the development of blending strategies capable of blending a diverse set of **heterogeneous assets** with multiple **competing objective functions**. This work could be extended to include a more diverse set of energy generation assets, found within future **energy networks**.

Chapter 1

Motivation

An electrical network which contains power generation, energy storage, and electrical loads which are capable of connecting with other electrical networks are a microgrid. An example of a typical microgrid includes electrical networks constructed on a temporary basis for disaster relief or military operations. Such operations require careful moderation of the available resources, in order to maintain the electrical grid for extended periods of time. The availability of the resources may be restricted due to meteorological, hydrological, monetary, or dynamic operating conditions. Common practices usually require the microgrid to include portable diesel generators and electrical storage.

Consider a ten bus electrical grid, shown in Figure 1.1, with two 30 kW diesel generators, a 30 kW electrical storage device, a 30 kW photovoltaic (PV) array, and four constant electrical loads totaling 40 kW, contained within an AC electrical network operating with a unity power factor, and negligible losses operating for a twenty-four hour period. In the next few paragraphs, we'll compare several power flow solutions and examine their effect on fuel consumption.

First, consider the case where the PV and storage are not used, and each of the generator's fuel consumption characteristics are identical, such that the fuel consumption was modeled as shown in Figure 1.2. For this example, there is an infinite number of feasible power flow solutions. Further assume that secondary control strategies are applied to each of the generation assets, such as speed and frequency control, and maximum power point tracking. For example, in order to obtain sufficient power flow within the electrical grid, the AC voltage magnitude and angle at each electrical bus must be controlled. One feasible power flow solution is to share the electrical load equally, where each generator is operating at 20 kW consuming 109.76 gallons. Due to the generator efficiency curve of Figure 1.2, an optimal power apportionment solution is to operate one generator at 30 kW and the other at 10 kW, consuming 104.64 gallons.

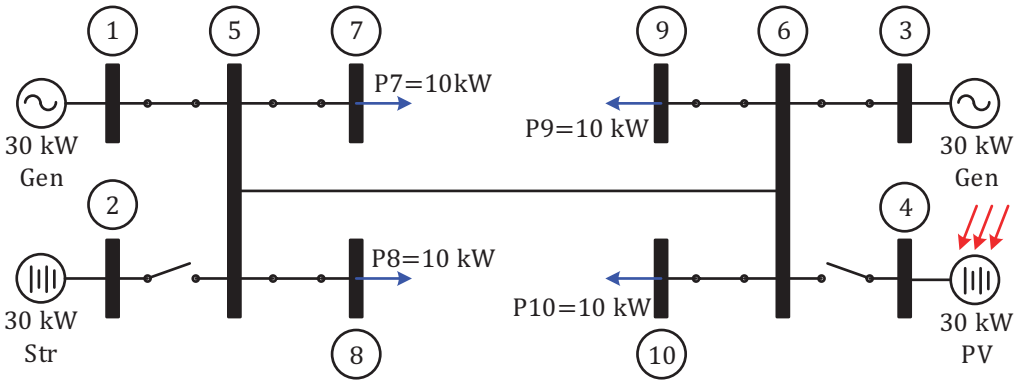

Figure 1.1: The AC electrical network with two 30 kW generators, a 30 kW electrical storage device, a 30 kW photovoltaic (PV) array, and 40 kW electrical load, where the storage device and PV asset are disconnected.

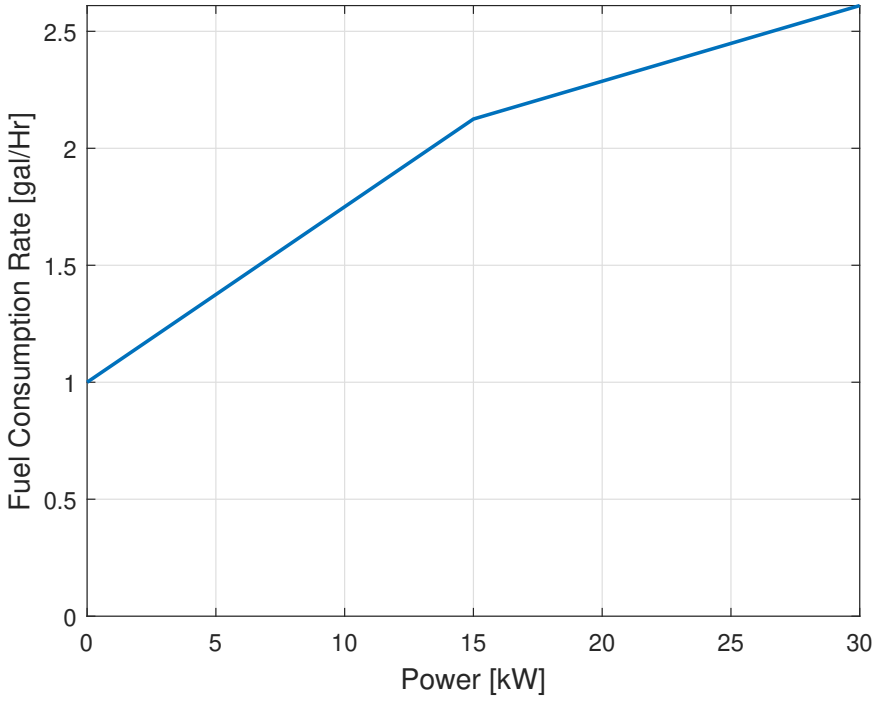

Figure 1.2: The fuel consumption characteristics as a function of electrical power produced by each of the two generators.

Next, consider the same electrical network where the electrical storage is now operable, as shown in Figure 1.3. The minimum fuel solution is to run both 30 kW generators for the first twelve hours at 30 kW, servicing the electrical load while simultaneously charging the storage device at 20 kW. For the remaining twelve-hour period, a single 30 kW generator operates at 20 kW, while the electrical storage discharges at 20 kW consuming a total of 90.08 gallons. It's important to note that this fuel savings comes a cost of energy storage capacity. For this solution the electrical storage capacity is 864 MJ, or roughly 445, 12 volt batteries, rated for 45 AHr.

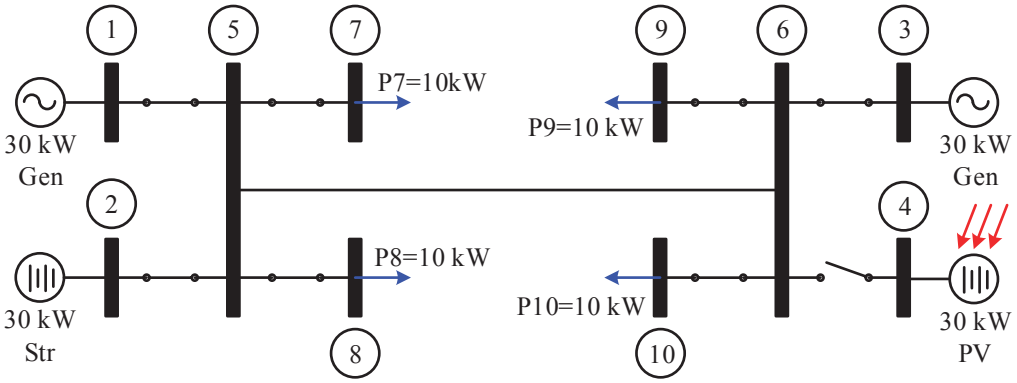

Figure 1.3: The same network of Figure 1.1 where the electrical storage device is now connected.

Finally, consider the case where both electrical storage and the PV asset are connected as shown in Figure 1.4. Also consider that the PV array could provide 10 kW of power for an eight hour period centered around noon, at all other times the PV array is incapable of generating power. A minimum fuel solution is to run both 30

kW generators for the first eight hours at 30 kW, servicing both the electrical load and charging the electrical storage at 20 kW. For the next eight hours, a single 30 kW generator is run at 30 kW, and the battery state of charge remains unchanged. For the final eight hours, a single 30 kW generator is operated at 20 kW, while the electrical storage is discharged at 20 kW. Here the fuel consumption is 80.93 gallons and the storage capacity is 576 MJ. This final configuration used 26% less fuel than the first scenario and 32% less storage than the second scenario.

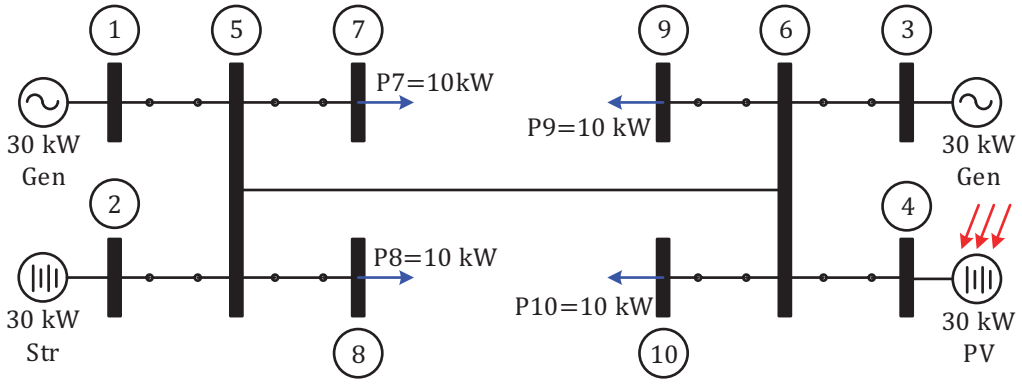

Figure 1.4: The same network of Figure 1.1 where the electrical storage device and PV are connected.

This example illustrates the potential benefit, in terms of fuel savings, when energy storage and PV are used in conjunction with complete knowledge of both the future load and PV output. It's important to note that if the PV had been treated simply as a negative load, the fuel savings would have been much less.

In order to manage an electrical network with multiple power generation and load

assets, a numerical optimization scheme based on mathematical models and weather forecasts is required. This dissertation focuses on developing energy management strategies which are capable of harmonizing a microgrids heterogeneous assets using both load and meteorological forecasts.

The remainder of the document is separated into six chapters. Chapter 2 introduces some challenges and opportunities of using vehicles as either an electrical generator or energy storage in addition to other standard power generation assets. Some relevant literature is introduced while concluding by identifying some of the research gaps addressed in subsequent chapters of this dissertation.

Chapters 3 and 4 address two aspects of microgrids whose electrical power is sourced from a combination of diesel generators and vehicles. Chapter 3 considers energy management during the first 72 hour deployment of a military outpost. Chapter 4 addresses the problem of maintaining a grid when vehicles, who are fully or in part supplying the electrical energy, leave on short notice. Chapter 5 moves away from vehicle sourced grids to consider the effect of meteorological forecast quality on fuel optimal grid control whose assets include diesel generators, PV and energy storage.

Chapter 6 then combines the fuel optimal grid control of Chapter 5 with a method to blend dissimilar diesel fuel based assets including diesel generators and military vehicles. Chapter 7 summarizes the findings and conclusions and provides suggestions for further study.

Chapter 2

Problem Description

[1] In Chapter 1, the motivation behind developing energy management strategies for an electrical grid was presented. Modeling complexities lead to non-obvious optimal fuel solutions, requiring more sophisticated energy management and control algorithms to improve energy efficiency.

Expeditionary military outposts are constructed in response to rapid deployment of armed forces which require a self-sustaining base of operations. The military outposts are sometimes referred to as tactical military microgrids. The microgrids require

[1] "Components of Chapter 2 are reprinted with permission from "Of Fuel-Optimal Strategies for Vehicle Supported Military Microgrids," *SAE International* Technical Paper 2016-01-0312, 2016, doi:10.4271/2016-01-0312. SAE International, reproduced with permission of SAE International in the format Thesis/Dissertation via Copyright Clearance Center. "

multiple electrical generation resources which typically range from commercial-off-the-shelf (COTS) diesel generators, portable electrical storage, and portable gasoline or diesel generators. The generators and electrical storage are traditionally used to allow the microgrid to operate external to a macrogrid, and during the outpost buildup. If possible, preexisting electrical grid infrastructure may be used to allow the microgrid to operate from the macrogrid, typically referred to as "shore" power.

When an expeditionary military outpost is constructed physical barriers are established to provide security. After the physical barriers are established, the outpost's equipment and personnel are transported to the physical location using a variety of vehicles including Medium Tactical Vehicle Replacements (MTVRs) or Heavy Expanded Mobility Transport Trucks (HEMTTs) for equipment, and Mine Resistance Ambush Protected (MRAPs), Joint Light Tactical Vehicle (JLTVs), or High Mobility Multipurpose Wheeled Vehicle (HMMWVs) to transport personnel. Once at the location, the microgrid components are unpacked and setup by combat engineers, who utilize electrical storage and gasoline generators (secondary generation assets) to build up the military outpost. When the generation capacity becomes limited, Advanced Medium Mobile Power Sources (AMMPS) or Tactically Quiet Generators (TQGs) are brought on-line to boost the generation capacity and provide stable electrical power for the outpost.

Advancements in technology have led to a rise in advanced capabilities and improved

reliability for military vehicles. Military vehicles traditionally were designed to safely and reliably transport military personnel. Due to the ever-changing dynamic working environment, military vehicles are being built to serve dual purposes which extend and support military personnel in complex dynamic situations. One such functionality includes the use of military vehicles for silent watch operations[2, 3]. Military vehicles which are capable of conducting silent watch operations require excess electrical storage capacity, which enables them to operate on-board sensors and weapons suites while the vehicle's engine remains inoperable. The goal of silent watch operations is to minimize thermal and acoustic signatures. The design requirement that military vehicles can be used to serve dual purposes, this led to vehicle variants that export electrical power.

While deployed, it has been estimated that military vehicles spend only 5% of the time performing mobility functions and remain stationary and relatively unused for the remaining 95% of the time [4]. Additionally, when the vehicle is in use, a large percentage of the time, the vehicle is idling. When Vehicle-to-Grid (V2G) and Vehicle-to-Vehicle (V2V) electrical resources are brought together a power apportionment schema is required to effectively use the assets within the electrical grid. Optimal power apportionment strategies with advanced controls could be implemented to reduce the total consumed fuel for the military assets. Consuming less fuel within an Outpost (OP) or Forward Operating Base (FOB) would mean less fuel needs to be

transported to the location via air or ground convoys. A reduction in military resupply convoys, results in additional fuel savings. The average cost incurred to transport fuel between a base is estimated to be $400 - 800$ $\$/gal$.

There is also the potential to increase the overall effectiveness of vehicle variants to provide force protection and amplification effects during various military operations. The effectiveness of the vehicle's operations could be extended through the use of a network of military vehicles engaged in vehicle-centric electrical resource sharing and control. In order for multiple vehicles to form vehicle-centric electrical microgrids and participate in resource sharing and control, the V2G or V2V networks would require a secure communication link. The communication between the individual vehicles as well as the grid operators could increase the ability to diagnose and respond to vehicle maintenance related issues. A greater return on investment for military vehicles is envisioned when vehicle-centric military microgrids are constructed.

Both V2G and V2V electrical resource sharing requires greater communication throughput, without which the use of vehicle assets for electrical resource sharing and control cannot be achieved. The added communication throughput would include information regarding the current fuel, energy storage capacity, or anticipated use. Without this added information, more optimal energy management of an electrical grid containing vehicles is unlikely, as the vehicles must be able to serve their primary roles while deployed, and providing electrical grid support is likely only a

secondary objective. Secure, reliable communication between the vehicles and the electrical grid is required, due to the sensitive nature of military operations, the added communication would likely be achieved using a physical connection using TCP/IP or UDP. Malicious users could potentially implement malicious code designed to disrupt military networks, causing various components within the military network to fail (Stuxnet[5]) for individual assets or networked assets. Additionally, failure to implement realistic power apportionment strategies could lead to logistical issues, or affect the grid stability.

Military vehicles which possess electrical storage, onboard sensors and/or weapons suites (loads), and the ability to export electrical power (source) effectively make military vehicles such as the MRAP, JLTV, or HMMWV a mobile microgrid. If interfaced with preexisting electrical networks, vehicle-based ad-hoc networked microgrids could be constructed and controlled. The added dimensionality of vehicle electrification could effectively alter the electrical and communication network, leading to potential cybersecurity threats not previously considered.

Consider a microgrid with both vehicle and stationary diesel generator assets. The decision of when to use the vehicle assets is based on the relative efficiency between the vehicle's electrical subsystems and the diesel generators consumption rate for the operational scenario. Under certain conditions, the vehicle's electrical efficiency may be higher than the generators' efficiency, in this case it may be more useful to rely on

the vehicles for grid support, conversely when the generator is operating at inefficient loads it may be favorable to increase the generator load by (1) charging the vehicles battery or (2) operating any of its government furnished equipment (GFE). The additional draw would then force the diesel generator to operate at higher efficiencies, potentially saving fuel. Several studies have been conducted for civilian vehicle-to-grid (V2G) applications, including [6] and [7], which showed that large scale power generation and storage opportunities seem to be viable for (1) aggregate frequency regulation and (2) aggregate peak power shaving using civilian type vehicles.

Additional research efforts regarding power management stability and control for V2G architectures were completed. In [8], the authors proposed a distributed V2G power management control strategy based on droop control to maintain frequency, accomplished through the use of power electronic circuits. In [9], an optimal energy management control strategy is proposed as it pertains to aggregate small electric energy systems (SEESs) including microgrids. In [10], coordinated V2G control is considered as it pertains to microgrids which contain wind power generation. The authors propose a robust conventional load frequency control (LFC) in addition to a battery state-of-charge (SOC) deviation control, enhanced performance and robust stability is achieved by optimizing both control strategies using particle swarm modeling techniques coupled with H_2/H_∞. In [11] plugin-hybrid-electric-vehicles (PHEVs) bidirectional charger systems are identified as critical components which facilitate voltage regulation, aggregate peak power shaving, and reactive power compensation

for various charging modes of the PHEVs. The study found that reactive power compensation is possible under level one charging (three to four different charging levels are supported for electric vehicles). In [12], intelligent solutions used to monitor and control electrical grids are considered which contain plug-in electric vehicles (PEV). The proposed intelligent controllers include fuzzy load and fuzzy voltage controllers optimized for grid stability, resulting in increased reliability and efficiency of an electrical grid.

On the other side of the spectrum, military type vehicles also possess the ability to provide grid support through the use of their integrated starter generators and batteries. Multiple studies were conducted to further investigate the use of military-type vehicles for electrical grid support. Military microgrids usually have prioritized electrical loads, and the electrical loads range in terms of kW of electrical power as compared to MW or GW for a macrogrid. In[13, 14] military hybrid vehicles were conceptualized as a self-contained microgrid. By optimizing the state of charge usage over a drive cycle, fuel economy improvements can be achieved. Furthermore, the optimization strategies provided for a single vehicle could be extended for multiple vehicles engaged in cooperative control, yielding more efficient operation of multiple vehicles. Then in [15], a simulation was developed intended to provide optimal sizing of hybrid electric vehicle components based on specific combat missions. Based on the specific missions, it was identified that the use of the battery could supplement the use for mechanical power delivered by the engine for load compensation. Engine

mechanical power requirements decrease with the addition of hybrid vehicle components, including electric drive motors and a flywheel. Due to the stringent design and operational requirements, no military hybrid electric vehicle architectures are currently deployed, however many civilian-based vehicle manufacturers offer hybrid vehicles. Research has shown that the use of hybrid electric vehicle architectures, yield more optimal performance resulting from efficiency gains, reducing the dependency on expensive fossil fuels. Additional studies which consider military vehicle variants which utilize hybrid electric vehicle powertrains for improved performance include [16, 17, 18].

Military vehicle variants have the potential to export electrical power commensurate with traditional military grade diesel generators, despite the lack of hybrid electrical vehicle powertrains. In [19], a simulation was developed with multiple types of electrical generation assets applied to a 72 Hr build-up of a military outpost. The results presented suggest that due to exportable power capabilities of the vehicle's, electrical power from the vehicle could be used to supplement electrical power from the diesel generators, potentially reducing the logistical supply chain required to establish a military outpost. Methods to provide more optimal energy use was applied to minimize the unnecessary electrical losses within both the power distribution network and the vehicle platform. Finally, in [4] V2G/V2V electrical resource sharing was proposed and demonstrated using four military vehicle variants including two MRAPs and two HMMWVs at the base camp integration laboratory (BCIL). This

demonstration was completed in response to "multiple operational energy gaps identified by the Department of Defense (DoD)" [4], resulting in reduced fuel usage when compared to conventional methods. In addition to the vehicle's exportable power capabilities, these vehicles also possess components which enable the vehicle to operate in silent watch, presumably making the vehicle more useful during deployments.

From the provided material, it is clear that military vehicles have the potential to provide additional functionalities, used to further extend the operational capacity of military operations. Any of the previously defined applications could be extended for disaster relief operations.

In [20] an optimal control of a microgrid was considered for an electrical network containing renewable generators, electrical storage devices, and points of common coupling (PCC) assumed to be an infinite utility grid. The network of assets was optimized to minimize the overall cost of energy imported from a utility grid while maintaining adequate power flow. The optimization solution was recursive, which combined dynamic allocation with traditional power flow solvers. Electrical storage assets were used as the primary control assets, differential voltages were computed based on storage energy measurements, power output was then derived, followed by a network power flow completed using Gauss-Seidel or Newton-Raphson, assuming the power flow solution was feasible, this solution would be identified as viable, this

process is recursively solved for all times and energies. This optimization solution provides a method to circumvent the numerical complexities for normal optimal power flow problems. Then in [21] another optimal energy/power control methodology is presented which utilizes mixed-integer-linear-programing and a rolling horizon window to optimize a network containing electrical storage devices and renewable power generation in the form of solar arrays and wind generators. The optimization problem was formulated to minimize the cost associated with buying/selling electrical power. The optimization policy considered the electrical power generation limits for each asset and enforced that at the end of the horizon, the battery energy levels must end approximately where it began. The optimization routine yielded a computationally efficient optimization routine that could be applied to electrical only networks but could be extended to enable more diverse assets.

Electrical microgrids can be either stationary or transient in the form of military vehicles or perhaps that of a military warship. In [22] a shipboard microgrid was considered, and a novel approach to control the grid was developed based on load frequency control. The electrical network of a naval vessel is the perfect example of an islanded microgrid with multiple electrical generation, loads, and electrical storage. Stringent marine pollution protocols have led to the potential to integrate wind turbines (WTs), solar generation, sea wave energy (SWE), and energy storage systems. Control of the grid's assets was archived using a load frequency controller (LFC) using fuzzy logic coupled with a proportional derivative (PD) controller. The

algorithm was deployed using an OPAL-RT HIL simulation. The algorithm developed was computationally efficient and can be tailored for various electrical networks, and was suitable for real-time operation.

2.1 Research Gaps

As identified within the literature review, multiple research efforts have been completed to identify acceptable power apportionment schemas relating to individual AC, DC, and AC/DC electrical grids. Most lack specifics pertaining to vehicles, the studies that have been conducted thus far typically contain a limited number of assets which may include vehicles, however, the particular specifics regarding the vehicle assets are usually limited to civilian-based vehicles which have fundamentally different capabilities than military vehicles. Civilian-based vehicles have smaller exportable power capabilities when compared to military vehicles, this requires large groups of vehicles in order to achieve cooperative control aimed at achieving aggregate peak shaving or frequency control for electrical grids. Additionally, the rated electrical generation capacity for civilian vehicles are not commensurate to a macrogrids electrical load. However, military vehicles which remain stationary at FOBs, Combat Outpost (COP), or OPs possess exportable power capabilities which are comparable to the traditional diesel generators and known to operate at higher efficiencies for larger loads when multiple diesel generators are required to meet the same load

demands.

Many of the power apportionment strategies concerning V2G and V2V include some kind of flexible optimal charging/discharging strategy for electrical storage. Most attempt to quantify the strategies for a limited number of assets, those that attempt to quantify multiple assets reformulate the optimization within a distributed network. The problems are recast as an advanced scheduling and coordination problem, which provides greater insight for more extensible dynamic modeling environments, which are far from field implementation. The existing techniques which are applied to V2G and V2V applications seem to be quite limited in regards to the specific application area which includes military ground vehicle optimization for generator-centric, vehicle-centric, generator vehicle-centric applications and the union of the two regimes.

2.2 Research Goals and Approach

This work focuses on developing and implementing energy management strategies for networked microgrids containing diverse electrical assets. Networked microgrids contain multiple electrical generation, distribution, and load assets interconnected to form an electrical grid. The motivation for this work is networked microgrids that are not intended for permanent operation and can operate

with minimal communication while ensuring **safe, reliable operation**, avoiding additional complexities which could inadvertently affect current operations.

These microgrids rely heavily on small portable generation assets, including both gasoline and diesel generators, in addition to electrical storage assets, and possibly renewable generation assets or military grade vehicles. Renewable power generation is a function of the current operating conditions and is traditionally considered to be a secondary power generation asset. Similarly, the primary responsibility of military vehicles is to transport military personnel, but can also be used as secondary power generation for an electric grid. Gasoline or diesel generators and electrical storage are generally considered to be the primary power generation assets. To maintain continuous operation, the generators require regular maintenance and consistent resupply missions. If the resupply missions or maintenance are delayed, normal grid operation may be greatly affected. **To efficiently use these assets, control algorithms are required**.

In order to develop advanced control algorithms, the electrical components found within a microgrid need to be modeled. **Mathematical models were developed for diesel generators, electrical storage assets, renewable based assets including PV arrays, and military grade vehicles**. The combination of these components yielded a diverse scenario rich environment well suited for the development of energy management strategies.

To illustrate the energy management control strategies, case studies were created. Value stream impacts such as fuel consumption or electrical energy used by the assets are tabulated, to assess the operation of the energy management policy.

The remainder of the dissertation is broken up into five additional chapters. In Chapter 3, a simulation was constructed which utilized a dynamic electrical load governed by a deterministic event schedule which focused on a 72 Hr buildup of a military OP. The event schedule was used to (1) induce additional loads, and (2) used to control an asset's ability to provide electrical power. The individual assets were controlled using a centralized optimal control strategy, computing an asset's operating points (voltage magnitude and angle) to yield minimal fuel consumption. A secondary control strategy was introduced to enable load shedding, should the generation capacity be insufficient to meet the desired electrical load, resulting from the absence of available generation assets governed by the event schedule. This control strategy was capable of handling both stationary assets (gasoline and diesel generators and electrical storage) and transient assets (military vehicles) with minimal or no knowledge regarding future use of the assets.

Using similar mathematical models and a control architecture provided in Chapter 3, a simulation was constructed using object-oriented modeling techniques in Chapter 4 with a cooperative optimal control policy. This was achieved by (1) modularizing the centralized control algorithms and distributing them among the generation assets to

form an agent control architecture, (2) developing a leader election protocol (LEP) which use time-varying leader election criteria to adaptively elect a primary and secondary leader, and (3) used current and future information limited to a fifteen minute look-ahead This yielded a realistic implementation of a centralized control architecture, distributed to each of the generation assets.

Two different communication protocols were introduced; (1) the nearest neighbor algorithm for conducting leader election, and (2) bidirectional communication, for feedback control. The culmination of these components helped to provide insight regarding the integration of stationary and transient assets with future system knowledge regarding deterministic events. This yielded more efficient energy management of the generation assets.

In Chapter 5, additional dynamic models were developed. The models included an energy based model for introducing a dynamic electrical load subject to the meteorological conditions in addition to a deterministic event schedule. The resulting system model was used to develop and assess a long-term optimal (LTO) energy management strategy using estimates of meteorological forecasts and the resulting future grid thermal and electrical loads. The effectiveness of the LTO's energy management policy was evaluated using measured solar radiation and temperature for four meteorological conditions including clear, partly cloudy, full overcast, and monsoon sky conditions.

Building on the conclusions and results collected from the previous research endeavors, a methodology or strategy which could blend a set of heterogeneous assets with competing objective functions was provided in Chapter 6. The different competing objective functions considered include fuel consumption and electrical energy. Both diesel generators and military vehicles require diesel fuel, consumed to generate electrical power for electrical resource sharing. Most if not all microgrid architectures also use electrical storage, whether it be dedicated electrical storage or collocated electrical storage associated with renewable or vehicle assets. The fuel consumption rates for diesel generators can often be modeled as cubic or quadratic polynomials with a single degree of freedom including the electrical load, assumed to be operating at either 50 Hz or 60 Hz. Conversely, the fuel consumption rates for vehicles are often modeled as a multidimensional surface, with a minimum of two degrees of freedom including engine speed and torque. Using concatenation and permutation techniques, a computationally efficient strategy for identifying the optimal fuel trajectories for generation assets that have different efficiency and power characteristics was derived. This methodology was extended for the vehicle assets and using the vehicle platform characteristics, a two degree of freedom fuel consumption model can be reduced to a single degree of freedom fuel consumption model, similar to a diesel generator fuel consumption models. These two methods were combined, to harmonize the competing optimal fuel trajectories and coupled with additional energy management strategies to yield more optimal fuel usage.

Finally, in Chapter 7, the main conclusions from the individual research efforts are summarized, proceeded by future research endeavors.

Chapter 3

Optimal Power Management of Vehicle Sourced Military Outposts

[1] In this chapter, dynamic models of an AC electrical grid are developed, coupled with a prioritized electrical load subject to an event schedule and shelter equipment list. The event schedule effects both the time history of the electrical load as well as the power generation asset's availability, which may affect the ability to satisfy the electrical load. Operating points for each asset are generated using a centralized optimization algorithm, which utilized a prioritization level and shelter equipment list to shed loads when insufficient power generation assets arise. An energy management

[1] "Chapter 3 are reprinted with permission from "Optimal Power Management of Vehicle Sourced Military Outposts," *SAE International Journal of Commercial Vehicles* 10(1):pp.132-143 SAE International, reproduced with permission of SAE International in the format Thesis/Dissertation via Copyright Clearance Center."

strategy was applied to minimize energy losses for an electrical grid containing stationary assets (diesel generators and electrical storage) and transient assets (military vehicles).

3.1 Introduction

Ad-hoc military outposts contain multiple generation, storage, vehicle, and load assets. Initially, a mix of batteries, vehicles, and portable generators are used to power the communication equipment for a combat operations center (COC). As the outpost grows, additional gasoline generators are incorporated. Sometime thereafter, stationary diesel generators are brought online to charge the energy storage units and provide the outpost with reliable electrical power. At this point, the outpost has a base electrical load, and very limited functionality. As time progresses, additional assets are incorporated incrementally to increase the outpost's functionality, ultimately resulting in a fully functional installation capable of providing force amplification and support.

Military vehicles may possess the ability to export electrical power or contain vast reserves of energy storage, making the military vehicle a microgrid which has the potential to provide electrical resource sharing using either vehicle-to-grid (V2G)

or vehicle-to-vehicle (V2V) architectures [14]. Using standard grid tied electrical resources in addition to military vehicles, it may be possible to (1) reduce the number of military assets required to establish an outpost, and (2) allow V2V or V2G networked microgrid architectures to be constructed, resulting in more efficient operation.

Several studies were completed, which identify potential V2G applications including power management, stability, and control. In [8], the authors proposed a distributed V2G power management control strategy based on droop control. In [9], an optimal energy management control strategy was proposed for small electric energy systems (SEESs) including microgrids. In [10], coordinated V2G control is considered for microgrids with significant wind power assets. The authors propose a robust conventional load frequency control (LFC) in addition to battery state-of-charge (SOC) deviation control, enhanced performance and robust stability was achieved by optimizing both control strategies using particle swarm optimization coupled with H_2/H_{infty} control. In [11] plugin-hybrid-electric-vehicles (PHEVs) bidirectional charger systems are used for voltage regulation, aggregate power peak shaving, and reactive power compensation for various charging modes. The study found that reactive power compensation is possible under level one charging. In [12], methods for using PEVs as source assets for electrical grids were described. Optimized, fuzzy control schemes were developed that showed the grid's reliability and efficiency were enhanced.

Several studies have been conducted which identify military vehicles as viable electrical generation and storage resources, which could be used for V2G and V2V applications including [14, 23, 24, 25], and [26]. In [14], an optimal power management method was considered for hybrid military vehicles. The single vehicle provided a base framework for fuel optimization, and provided insight into extending the optimal power management to multiple military vehicles. In [23], an optimal energy management strategy was postulated for a microgrid which utilized both distributed generation and energy storage. In [24], the use of renewable sources and military vehicles was considered for frequency and voltage regulation for a military microgrid. In [25], coordinated multi-microgrid optimal control algorithms were postulated to form a smart decentralized distribution management system. While the study was conducted on a civilian microgrid, the control methodology provided framework which could be extended for military applications. In [26], a V2G microgrid simulation was created to evaluate the reliability of a microgrid. It also introduced a control strategy, which identified acceptable times to charge/discharge the vehicles to provide peak power shaving and smooth the grid load during islanded operation.

Experiments have also been conducted to supplement the simulation studies described above. In [27], results from the Smart Power Infrastructure Demonstration for Energy Reliability and Security (SPIDERS) project were presented. A goal of the SPIDERS program was to identify the potential to use tactical microgrids to provide greater control and stability for military electrical networks. Military vehicles were identified

as viable assets which could be used to provide added reliability and functionality. In [28], a web-centric frequency control system was introduced. The main research effort was to test the system response in terms of latency, precision and stability of the microgrid.

In this chapter, an optimal power management and control strategy applied to the 72-hour evolution of a military outpost. After describing the scenario, individual components which make up the microgrid are presented. An optimal power apportionment strategy is considered and evaluated using a *MATLAB/Simulink* implementation.

3.2 Problem Definition

The military outpost considered is sized for a battalion of 800-1000 soldiers separated into six equal sized companies. Each military vehicle used in the outpost required four soldiers while on patrol or responding to a contact. Under normal operations, companies A and B are responsible for providing base security for the military installation, companies C and D are responsible for conducting patrols until the outpost is operational, and companies E and F are responsible for constructing the outpost's infrastructure. Under abnormal operations (patrol comes under fire, or contact is reported), a quick reaction force (QRF) from companies A and B depart using the military vehicles to assist the patrol that has called for assistance,

simultaneously companies E and F stop construction of the outpost, shut down systems which have not been configured to work with the primary grid assets, and assist in defense of the outpost. After the QRF returns to the outpost, abnormal operation is suspended and normal operations resume. The evolution of the electrical load is shown in Figure 3.1. The "Tier" designation indicates load priority with Tier 1 being the highest priority load. The electrical loads for squads E and F, responsible for grid deployment, are given in Figure 3.2.

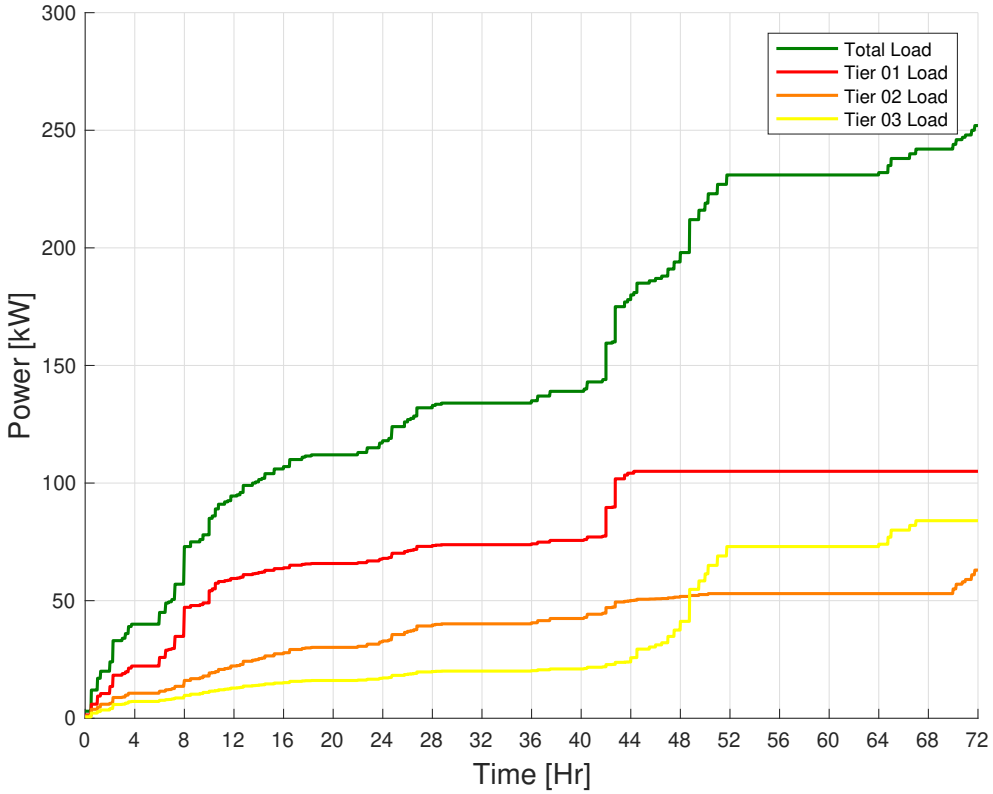

Figure 3.1: The outpost's total electrical load for the first 72-hour buildup, after which point the military outpost is fully manned and operated. As time progresses the outpost's load increases due to its increased functionality.

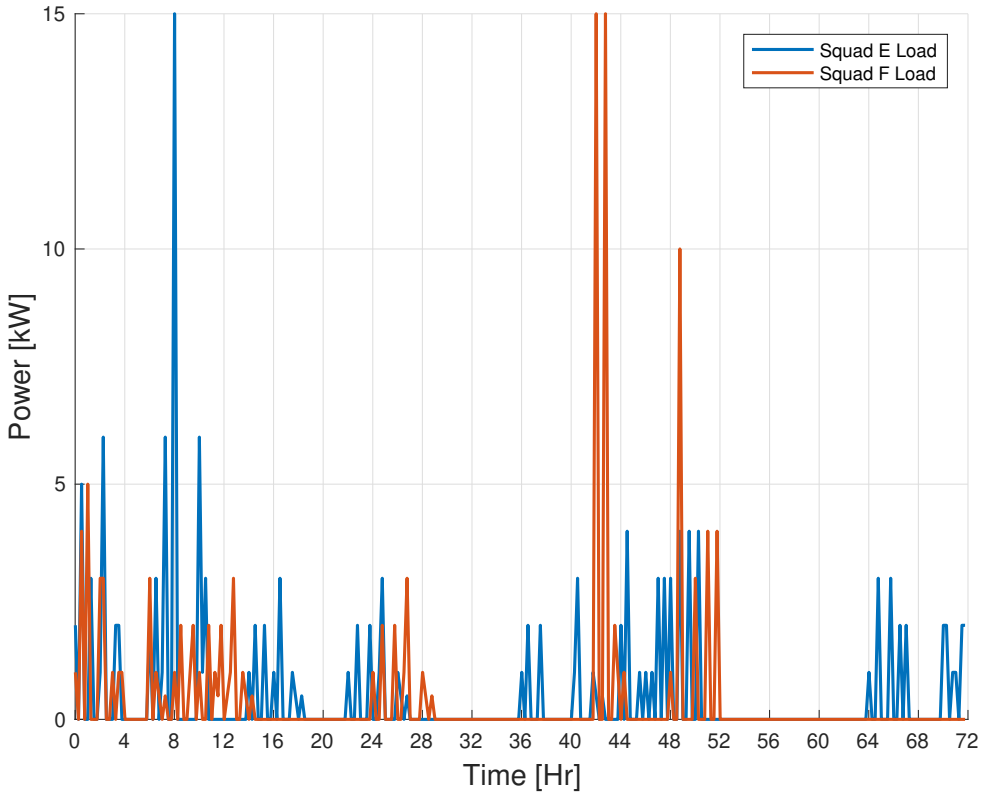

Figure 3.2: The individual loads attributed to the two squads responsible for bringing the outpost's functionally online.

The grid asset inventory included: four military vehicles, two gasoline generators, and two electrical storage units. The gasoline generators are considered secondary assets and are the sole source of power until the primary assets, the vehicles, are connected.

The two operational scenarios considered are: (1) uninterrupted outpost construction, and (2) interrupted outpost construction due to a security threat. The presence of a security threat leads to an interruption of the outpost construction, and potentially

a loss of primary grid assets, resulting in load deficits, which require low priority load shedding. The event schedules for both scenarios, which dictate the operational load profile and dynamic events for the simulation studies, are shown in Figure 3.3 and Figure 3.4.

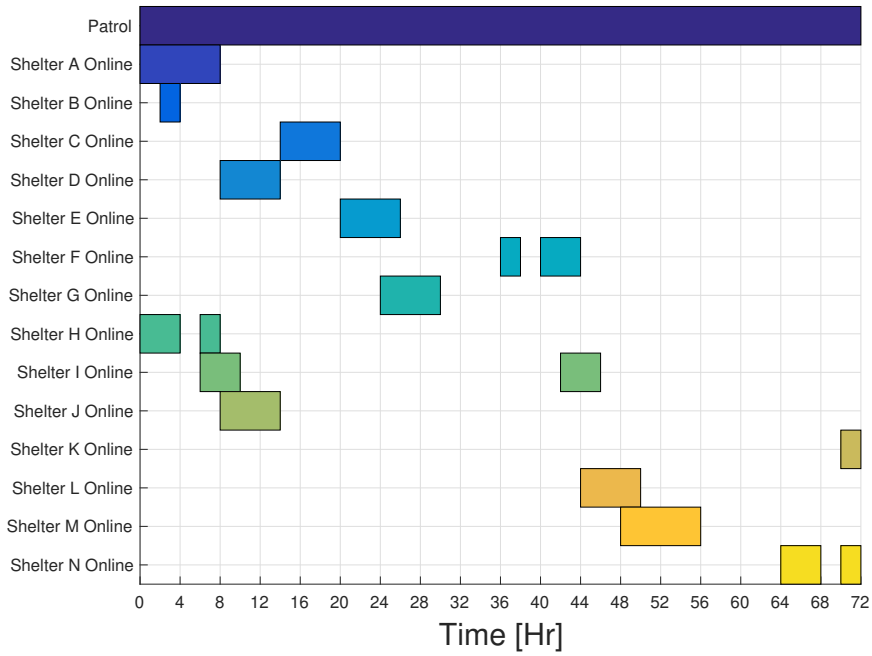

Figure 3.3: The uninterrupted outpost construction event schedule. This event schedule lacks events, which would cause the base's security level to increasing.

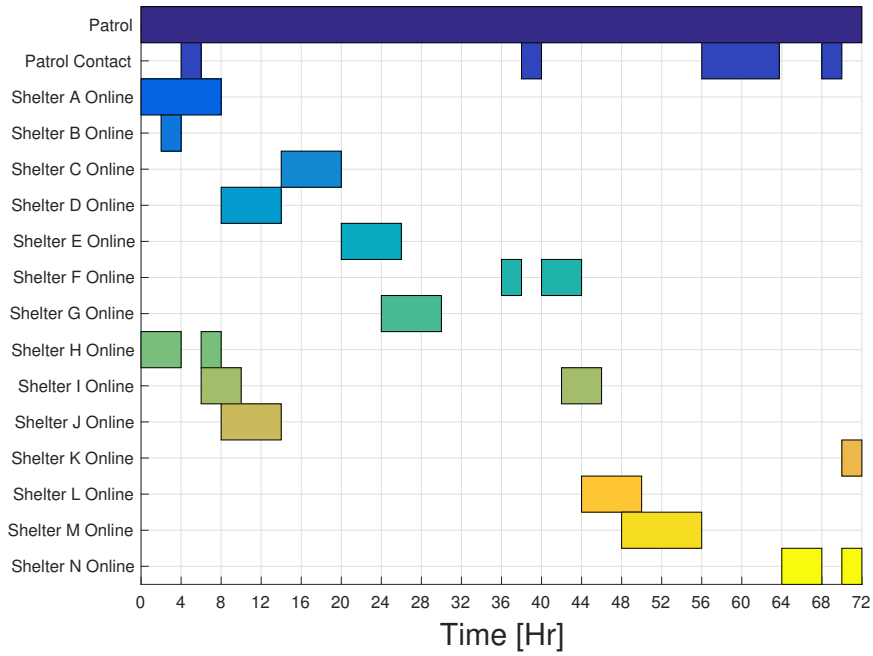

Figure 3.4: The interrupted outpost construction event schedule. This event schedule includes events where the continuous patrols report a contact, which causes the base to enter a heightened state of security, which leads to an interruption of construction.

Lettered shelter names are used instead of functional names for brevity with a mapping given in Table 3.1.

The final piece of information to complete the interrupted scenario definition is the vehicle use for squads A and B and is shown in Figure 3.5. For the uninterrupted outpost scenario all four vehicles are available to power the outpost.

Generic Shelter Designation	Technical Shelter Designation
Shelter A	BN COC
Shelter B	Fires
Shelter C	CO HQ COC
Shelter D	CO A COC
Shelter E	CO B COC
Shelter F	CO C COC
Shelter G	CO Weapons COC
Shelter H	COM Shake
Shelter I	Motor Pool
Shelter J	LOGs
Shelter K	BC SGT M OPSo Offices
Shelter L	Chow Hall
Shelter M	Enlisted Quarters
Shelter N	Officer Quarters

Table 3.1
Mapping of lettered shelter designation to their functional names.

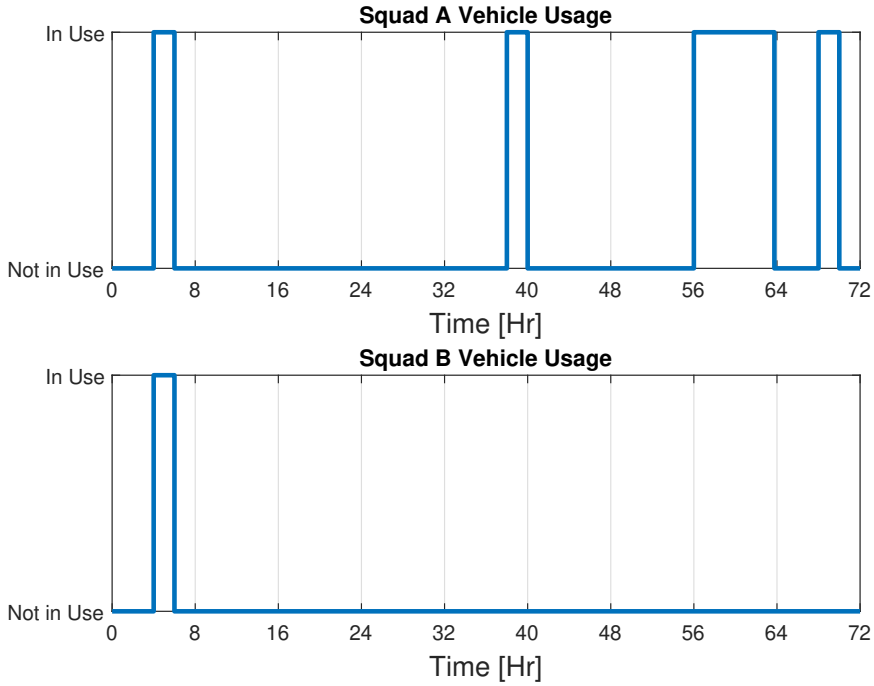

Figure 3.5: Planned vehicle usage for squad A and squad B during the interrupted outpost construction scenario. When a vehicle is in use it is unavailable to provide electrical power to the microgrid.

The grid architecture used is shown in Figure 3.6 and has five buses. Each primary microgrid, contains a military vehicle and multiple, prioritized electrical loads. The secondary microgrid, contains two gasoline generators and two Lithium-Ion battery packs.

Both scenarios have several operational elements in common: (1) the military vehicles are the primary grid assets, and (2) the gasoline generators and energy storage units are the secondary grid assets, (3) the gasoline generators are operated continuously during the 72 hour build up, and (4) the batteries remain operational for a short period of time when the load power P_{load}; is less than 35 kW.

When higher loads are encountered, additional generation assets are brought online increasing the power generation capacity. If the generation capacity is sufficiently larger than the load demand, batteries may be charged. The loads are separated into three tiers. The first tier contains all critical loads. These are loads that must be operational at all times such as the Combat Operations Centers (COCs), medical equipment, and critical communications equipment. The second tier contains non-critical loads. These are loads that are required for extended operations such as motor pools (vehicle repair shops) and mess halls. The third tier contains comfort loads such as lighting, non-critical communications, and moral boosting devices. Additionally, if the generation capacity is significantly reduced (vehicles become inoperable or are unavailable) the batteries are brought

online and allowed to discharge to achieve the maximum power generation capacity. Once the maximum power generation capacity is achieved, and the total tiered load for the networked microgrid exceeds the total power generation capacity, the lowest priority loads are shed until the power generation exceeds the total microgrid load. This deficit could be either planned (long term) or transient. In the transient case, rapid charge/discharge of the battery occurs which aids in stability.

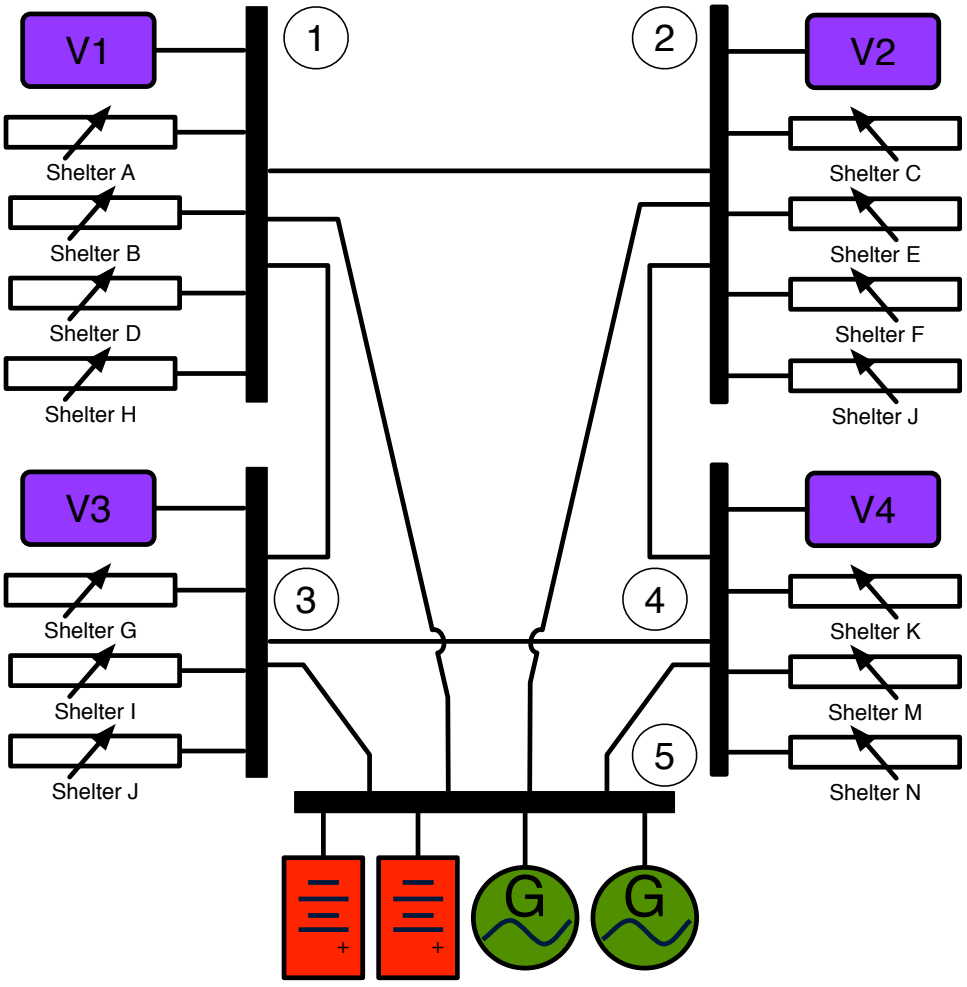

Figure 3.6: The networked microgrid architecture.

The system is modeled using *MATLAB/Simulink* using both AC and DC power sources. Since power transfer is done via DC transmission lines, the AC sources are rectified. The simulation is made up of six components including - (1) electrical storage (battery) model, (2) vehicle models, (3) gasoline generator models, (4) a grid model, (5) an optimal power flow controller, and (6) a power-coordination controller.

3.2.1 Electrical Storage Model

The battery module is modeled as a controlled voltage behind a series resistance as described in [29]. Three points on the battery's discharge curve are used for the model: $(V_{full}, 0)$, (V_{exp}, Q_{exp}), and (V_{nom}, Q_{nom}). The discharge curve is for a Nickel-Metal Hydride battery is provided in Figure 3.7.

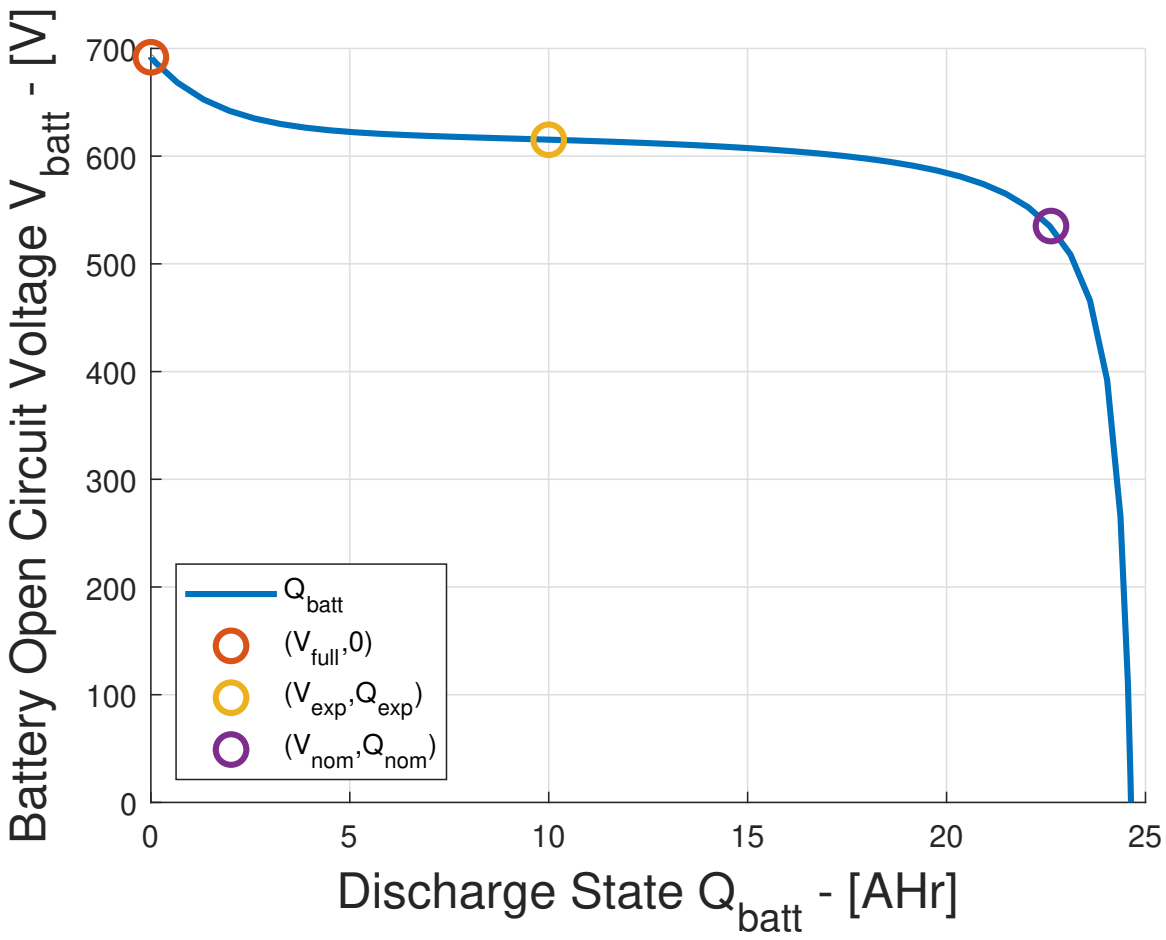

Figure 3.7: The electrical storage's discharge state varies as a function of its chemical composition, the discharge state for a Nickel-Metal Hydride battery is provided.

In the provided figure, Q_{batt} is the discharge state in AHr, and V_{batt} is the voltage between at the terminals of the battery. Three points are used to characterize the discharge state of the battery, as shown in Figure 3.7, they include: (1) $(V_{full}, 0)$ this is the point at which the battery is fully charged (red circle), (2) (V_{exp}, Q_{exp}), this is the point at which the exponential zone ends (yellow circle), (3) and (V_{nom}, Q_{nom}) is the point at which the nominal zone of operation ends (purple circle). The battery

voltage is governed by the discharge state of Equation 3.1,

$$V_{batt} = V_o - K\left(\frac{Q}{Q - Q_{batt}}\right) + Ae^{-B(it)} \tag{3.1}$$

where

$$A = V_{full} - V_{exp} \tag{3.2}$$

is the voltage drop in the exponential zone,

$$B = \frac{3}{Q_{exp}} \tag{3.3}$$

is the charge at the end of the exponential zone,

$$K = \frac{V_{full} - E_{nom} + A(e^{-BQ_{nom}} - 1)(Q - Q_{nom})}{Q_{nom}} \tag{3.4}$$

is the polarization voltage,

$$Q_{batt} = \int i_{batt}(t) \quad dt \tag{3.5}$$

is the discharge state of the battery, and

$$V_o = V_{full} + K + R_{batt}i_{rated} - A \tag{3.6}$$

is the voltage constant of the battery, where i_{rated} is the rated discharge current. It should be noted here that time is in hours and all charges are in AHr. The series

resistance of the battery is then,

$$R_{batt} = V_{nom}\frac{1-\eta}{0.2Q_{nom}} \tag{3.7}$$

where η is the battery efficiency ranging between 0 and 1[29]. The battery characteristics vary depending upon the materials utilized in construction. Four types of batteries are considered which are the most common. These are Lead-Acid, Lithium-Ion, Nickel-Cadmium, and Nickel-Metal-Hydride. The parameters for each battery type are listed in Table 3.2. The required inputs are the nominal voltage V_{nom}, and the rated capacity Q. The values in Table 3.2 are taken from [30].

	Lead Acid	Li-Ion	Ni-Cd	Ni-MH
V_{full}	$1.08V_{nom}$	$1.16V_{nom}$	$1.15V_{nom}$	$1.17V_{nom}$
i_{rated}	$0.05Q$	$0.2Q$	$0.2Q$	$0.2Q$
Q_{nom}	$0.5Q$	$0.935Q$	$0.905Q$	$0.762Q$
V_{exp}	$1.025V_{nom}$	$1.03V_{nom}$	$1.03V_{nom}$	$1.05V_{nom}$
Q_{exp}	$0.009Q$	$0.85Q$	$0.4Q$	$0.2Q$

Table 3.2
Battery characteristics of materials, commonly used to construct batteries.

3.2.2 Military Vehicle Model

The military vehicle model can be subdivided into three components, including (1) a mechanical system, which is used to generate mechanical power (prime mover), (2) the mechanical to electrical generator often referred to as an integrated starter/generator

(ISG), and (3) a rectifier.

Two different military vehicles are modeled, they include a M1152 high mobility multipurpose-wheeled vehicle (HMMWV) and a Max Pro mine resistance ambush protected (MRAP) vehicle. The HMMWV utilizes a General Engine Product (GEP) 6.5L 205 HP engine, with a $30kW$ ISG. The Max Pro MRAP utilizes a CAT C7 350 HP Engine which is tied to a transmission integrated generator (3TIG) 125 kW ISG. The engines are approximated using the frequency-power curves of Figure 3.8 and Figure 3.9. The fuel consumption rates for vehicle i is assumed quadratic in output power P_i, which is provided in Equation 3.8, where the fuel consumption coefficients for each vehicle are provided in Table 3.3.

$$\dot{m}_i = a_{0,i}P_i^2 + a_{1,i}P_i + a_{2,i} \quad (gal/hr) \tag{3.8}$$

Vehicle	$a_{0,i}$ $\left(\frac{gal}{kW^2Hr}\right)$	$a_{1,i}$ $\left(\frac{gal}{kWHr}\right)$	$a_{1,i}$ $\left(\frac{gal}{Hr}\right)$
1	2.54E-04	6.08E-02	1.28E+00
2	3.27E-05	6.04E-02	5.63E-01
3	2.54E-04	6.08E-02	1.28E+00
4	3.27E-05	6.04E-02	5.63E-01

Table 3.3
Fuel consumption coefficients for the military vehicle engines.

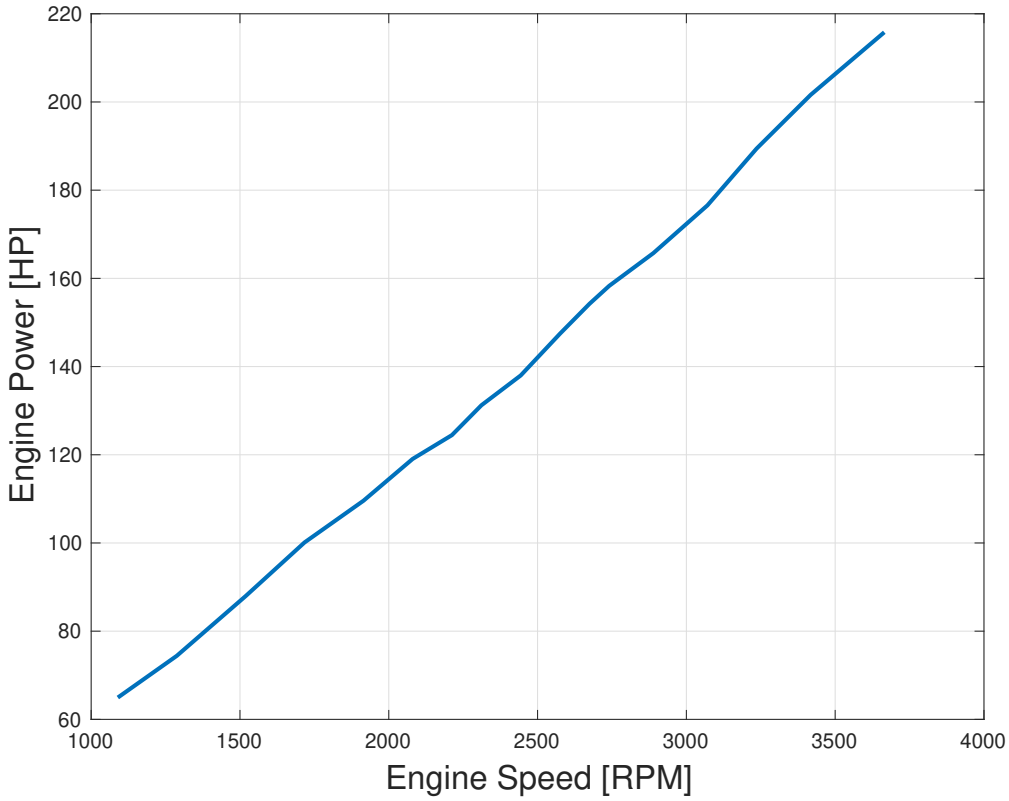

Figure 3.8: Engine power curve for the M1152 HMMWV, which utilizes a GEP Optimizer 6500 215 HP. The curves were derived using public data, a linear fit could be used for the provided engine speeds.

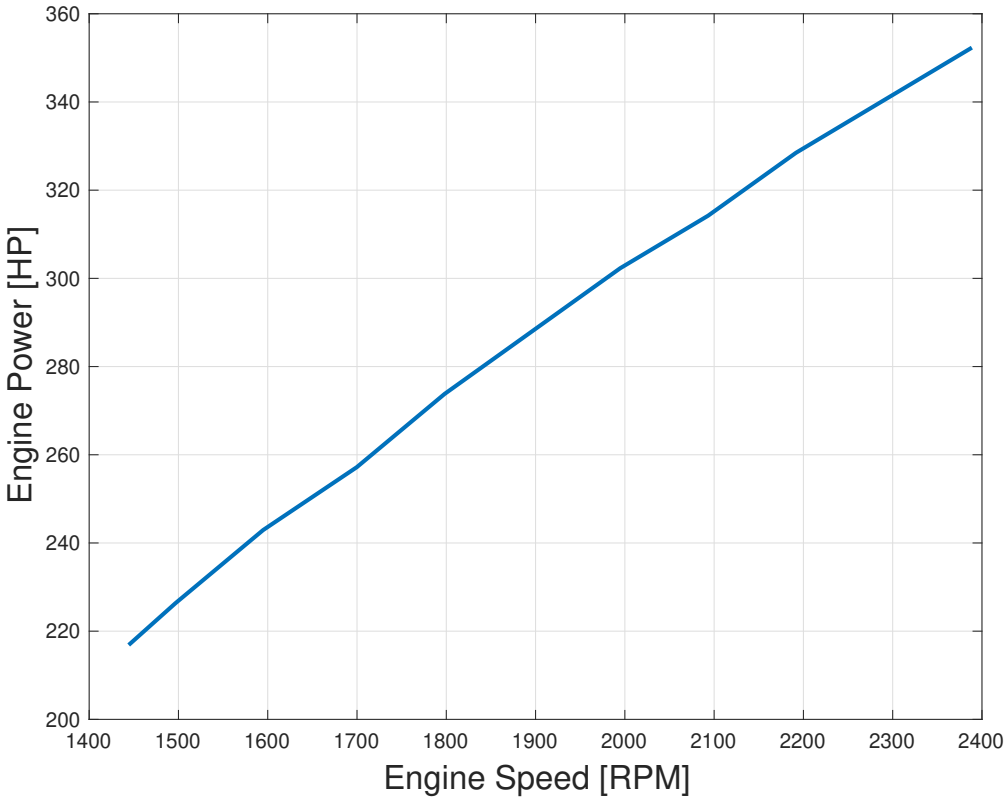

Figure 3.9: Engine power curve for the Max Pro MRAP which utilizes a CAT C7 engine. The curves were derived using public data, a linear fit could be used for the provided engine speeds.

3.2.3 Three Phase Synchronous Generator Model

In order to reduce the number of simulation states, a 2-pole generator model was used. The generator is modeled assumes steady state sinusoidal operation at a fixed voltage and variable frequency. The fuel consumption rates for generator i is assumed quadratic in output power P_i, which is provided in Equation 3.9, where the fuel

consumption coefficient for each vehicle have been provided in Table 3.4 [31].

$$\dot{m}_i = a_{0,i}P_i^2 + a_{1,i}P_i + a_{2,i} \quad (gal/hr) \tag{3.9}$$

Let $V_{RMS,LL,k}$ be the RMS line-to-line voltage at the terminals of the generator. The

Generator	$a_{0,i}$ $\left(\frac{gal}{kW^2Hr}\right)$	$a_{1,i}$ $\left(\frac{gal}{kWHr}\right)$	$a_{1,i}$ $\left(\frac{gal}{Hr}\right)$
1	2.00E-03	2.23E-01	3.63E-01
2	2.00E-03	2.23E-01	3.63E-01

Table 3.4
Fuel consumption coefficients for the gasoline generator.

peak line to neutral voltage V_p is then

$$V_p = \sqrt{2/3}V_t \tag{3.10}$$

In the simulations, a value of $V_t = 208$ V is assumed for all generators. A 3-phase diode bridge rectifier is used in combination with a boost converter as shown in Figure 3.10. The steady state average voltage at the dc-dc link between the diode bridge and the boost converter is

$$V_{low} = \frac{3\sqrt{3}}{\pi}V_p \tag{3.11}$$

as discussed in [28] is assumed.

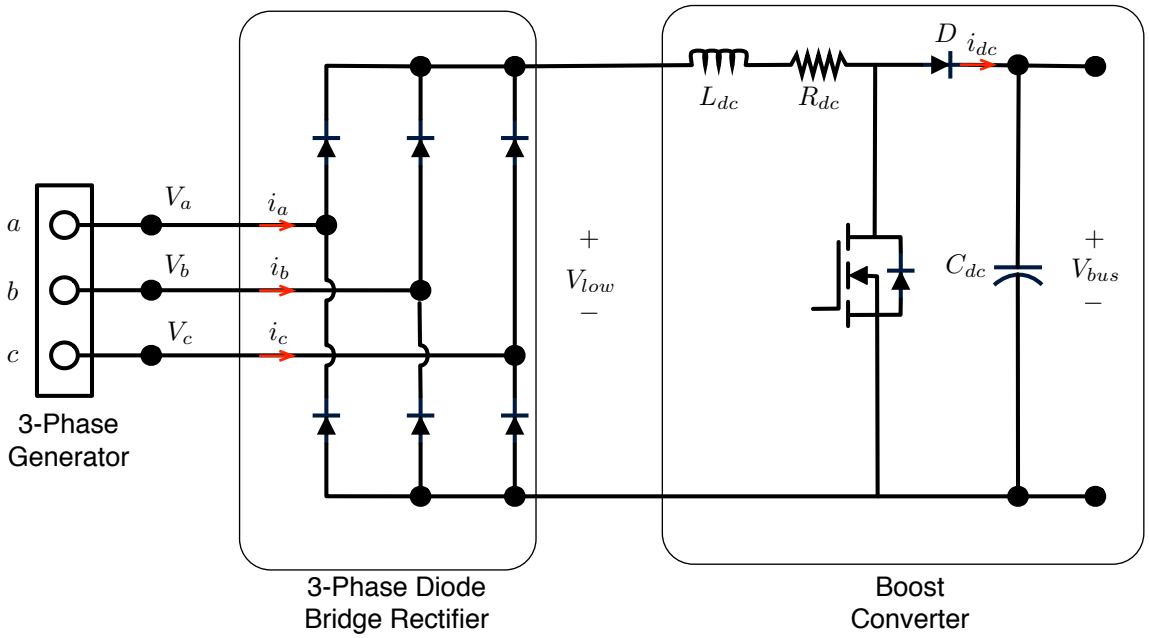

Figure 3.10: Three-diode bridge rectifier and boost converter connected to 3 phase source.

The current i_{dc} is then

$$L_{dc}\frac{di_{dc}}{dt} = V_{low} - i_{dc}R_{dc} - DV_{bus} \tag{3.12}$$

where D is the duty cycle, L_{dc} is the line inductance, R_{dc} is the inductor resistance, V_{bus} is the bus voltage, and C_{dc} is the output capacitance. Feedforward control is used to drive the voltage to the reference voltage V_{ref} such that

$$D = \frac{V_{low} - i_{dc}R_{dc}}{V_{ref}} \tag{3.13}$$

For the system modeled, $L_{dc} = 0.001$ H, $R_{dc} = 0.1\ \Omega$, and $C_{dc} = 0.0001$ F.

3.2.4 Grid Model

The dc grid is modeled as shown in Figure 3.11. There is a 100 μF capacitor at each bus (not shown). The line resistance and inductance values are provided in Table 3.5. There is a total of 9 buses. Buses 1, 2, 3, 4, 8, and 9 are generator buses. These are the buses that have either a diesel or gasoline generator present. Buses 6 and 7 are the storage buses. These are the buses that have a battery present. Bus 5 has no generation available. The loads of the system are connected directly to buses 1, 2, 3, and 4.

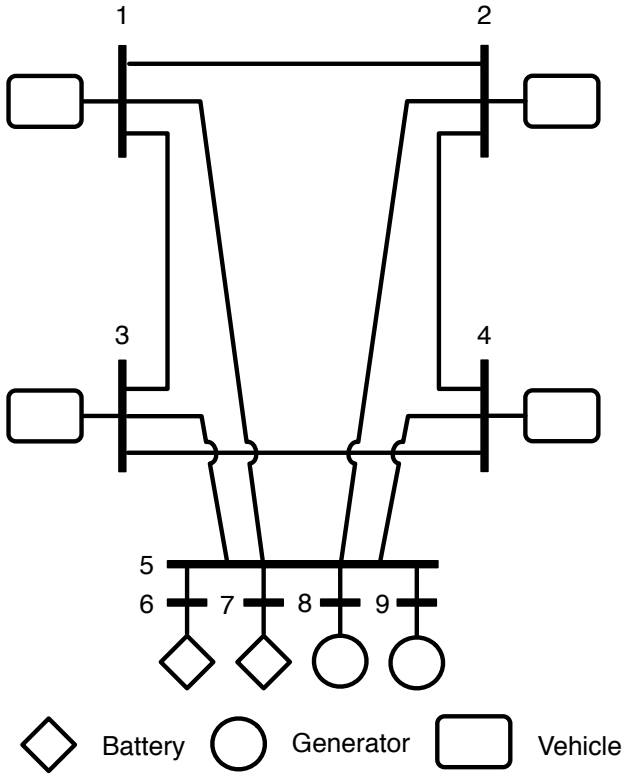

Figure 3.11: The electrical grid topology for all source assets. For simplicity, the load has been removed from the depiction of the grid architecture.

The dc transmission lines modeled have a per unit resistance of 4.8 Ω/mi (3 $m\Omega/km$) and a per unit length inductance of 1.7 mH/mi (1.05 mH/km). The system is spread out over an area of about one square mile. The geometric spacing of the buses (line lengths) are used to derive the resistance and inductance values provided in Table 3.5.

From	To	Res. (Ω)	Ind. (H)
1	2	4.32E-02	1.53E-03
2	4	4.65E-02	1.65E-03
4	3	4.32E-02	1.53E-03
3	1	4.56E-02	1.61E-03
5	1	4.80E-03	3.04E-04
5	2	3.84E-02	1.36E-03
5	3	4.61E-02	1.63E-03
5	4	6.05E-02	2.14E-03
5	6	4.80E-03	3.40E-04
5	7	4.80E-03	3.40E-04
5	8	4.80E-03	3.40E-04
5	9	4.80E-03	3.40E-04

Table 3.5
DC Grid transmission line resistance and inductance values.

3.2.5 Optimal Power Flow Controller Model

It is desired to minimize fuel consumption. Each generator has an associated fuel efficiency curve relating the rate of fuel consumption to its output power.

The batteries in the system are charged at opportune times and drained only as a last

resort. Therefore, a larger weighting of their contribution to the objective function was assigned to the batteries. The optimal power flow wad updated every 30 seconds. The fuel consumption was computed by integrating the fuel rates for the vehicles and the gasoline generators, defined in Equation 3.8 and Equation 3.9 respectively. For the two batteries, the objective functions are,

$$J_6 = 10P_6^2 \quad (gal/hr \quad equiv.) \tag{3.14}$$

$$J_7 = 10P_7^2 \quad (gal/hr \quad equiv.) \tag{3.15}$$

The optimal power flow problem was to find the generator, vehicle, and electrical storage asset's output electrical power commands P_i which minimizes,

$$J = \sum_{i \epsilon G} \dot{m}_i + \sum_{i \epsilon B} f_i \tag{3.16}$$

using Newton-based optimal power flow, subject to,

$$\left[g_k = \sum_{i=1}^{n} V_k \left(V_k - V_i \right) Y_{k,i} = 0 \right]_{k=1}^{n} \tag{3.17}$$

$$[V_{min,k} \leq V_k \leq V_{max,k}]_{k=1}^{n} \tag{3.18}$$

$$[P_{min,k} \leq P_k \leq P_{max,k}]_{k=1}^{n} \tag{3.19}$$

where $n = 9$ is the number of buses, $G = 1, 2, 3, 4, 8, 9$ is the set of buses with a

generator or vehicle, and $B = 6, 7$ is the set of buses with a battery. The constraints g_k enforce a power balance. The quantity V_k is the voltage at bus k and P_k is the power injected into bus k from the power source at that bus, and $P_{min,k}$ and $P_{max,k}$ are the lower and upper bounds on the source power k respectively. These constraints are provided by an overarching controller that provides estimates for the available power for each source. These values change throughout the simulation based upon fuel availability, generator availability, and battery state of charge. $V_{min,k}$ and $V_{max,k}$ are the lower and upper bounds on voltage at bus k respectively. For the system modeled, all upper limits are set to 990 volts and all lower limits are set to 1010 volts.

The optimal power flow calculation are performed every 30 seconds using finite differences to approximate derivatives. The output of the optimization block provides both voltage and current reference (target) values to be utilized by controllers as needed. For bus k, $V_{k,ref}$ is the reference voltage and $I_{k,ref}$ is the reference current.

3.2.6 Power Coordination Controller Model

The purpose of this controller is to compute the total electrical power generated via the generation assets in relation to the event profile and the vehicle usage policies. The event profile dictates which events are active, and the approximate time for its

completion, and the associated electrical load. The coordination controller will perform load shedding to maintain grid stability should outpost build-up be interrupted. Load shedding is determined using the shelter designations in addition to the tired allocation.

3.3 Uninterrupted Outpost Construction

The uninterrupted outpost construction case study means that the build-up progresses without any security threat interruptions. Events that would cause the threat level to increase include reported contact with military patrols, or a call for fire actions against targets. During the construction of the outpost, there are no events, which cause the security threat level to increase, meaning the construction of the outpost is uninterrupted throughout the simulation epoch.

The control strategy used for this scenario assumes the load power and the power reserve margin can be abbreviated as P_{load} and P_{res} respectively. Under low load conditions ($P_{load} < 30$) kW, only the secondary grid generation assets, the gasoline generators and electrical storage units, are used to supply power where each gasoline generator and electrical storage unit is capable of producing 10 kW. Under medium-low load conditions ($30 \leq P_{load} < 70$) kW, the two electrical storage units are taken offline, simultaneously two of primary grid generation assets are brought

online. The additional generation assets, which are brought online, include the two vehicles with the lowest generation capacity (30 kW). Under medium load conditions ($70 \leq P_{load} < 195$) kW, an additional primary generation asset (one of the vehicles capable of exporting 125 kW of power) is brought online. Finally, under high load conditions ($P_{load} > 195$) kW, an additional primary generation asset (the final vehicle capable of exporting 125 kW of power) is brought online. Throughout the simulation epoch, the electrical storage units are only used to supply power under low load conditions, under all other load conditions, the electrical storage units may be permitted to charge depending on the electrical storage state of charge level as well as the power reserve margin. If the power reserve margin is low ($20 \leq P_{res} < 30$) kW then the electrical storage units may be allowed to charge under low charge conditions (2 kW). If the power reserve margin is medium ($30 \leq P_{res} < 50$) kW, then the electrical storage units may be allowed to charge under medium charge conditions (4 kW). Finally, if the power reserve margin is high ($P_{res} \geq 50$) kW, the electrical storage units may be allowed to charge under high charge conditions (6 kW). If the state of charge of an electrical storage unit is less than ninety percent ($SOC < 90$) % and the reserve margin lies within the three predefined charge conditions the electrical storage units are permitted to charge, if the state of charge exceeds the ninety percent SOC limit, the electrical storage unit remains inactive at its current state of charge.

3.4 Interrupted Outpost Construction

The interrupted outpost construction case study includes the presence of multiple events which cause an increase in the security threat level. It was assumed that the total generation capacity P_{gen}, was the sum of the available primary/secondary grid assets. The control strategy used for this scenario is similar to the one provided within the previous section; the major differences arise due to the planned vehicle usage and their unavailability for providing power. If a vehicle was "in use" then all secondary grid assets are used to satisfy the load. If ($P_{load} > P_{gen}$), then some or all of the tier three loads are shed, if the load still exceeds the generation capacity, some or all tier two loads are shed in addition to the tier three loads. If all tier three and two loads have been shed and the load power still exceeds the generation capacity, some of the tier one loads are shed such that load power is less than the power generation capacity ($P_{load} < P_{gen}$). Tiered load shedding was completed as need, if partial load shedding is required (some tier one/two/three loads are active while some are not) the methodology used to determine which tiered load is shed is based off the shelter designations. For example, during a patrol contact, if the load power exceeded the generation capacity, and all tier three and two loads were shed, but the load power still exceeded the generation capacity, lower priority shelters loads (chow hall, enlisted quarters, etc.) were shed before higher priority shelter loads (communication shake, fires shake, etc.).

3.5 Simulation Studies

Two cases are simulated. In the first case study, the outpost was built successfully from start to finish without any interruptions. In the second case study, security threats arise, temporarily halting outpost construction. It was expected that no load shedding was required for the first case. Conversely, for the second case, load shedding was required to maintain grid stability.

3.5.1 Uninterrupted Outpost Construction

The results obtained from simulating the 72-hour uninterrupted outpost construction are provided in Figure 3.12 - 3.14.

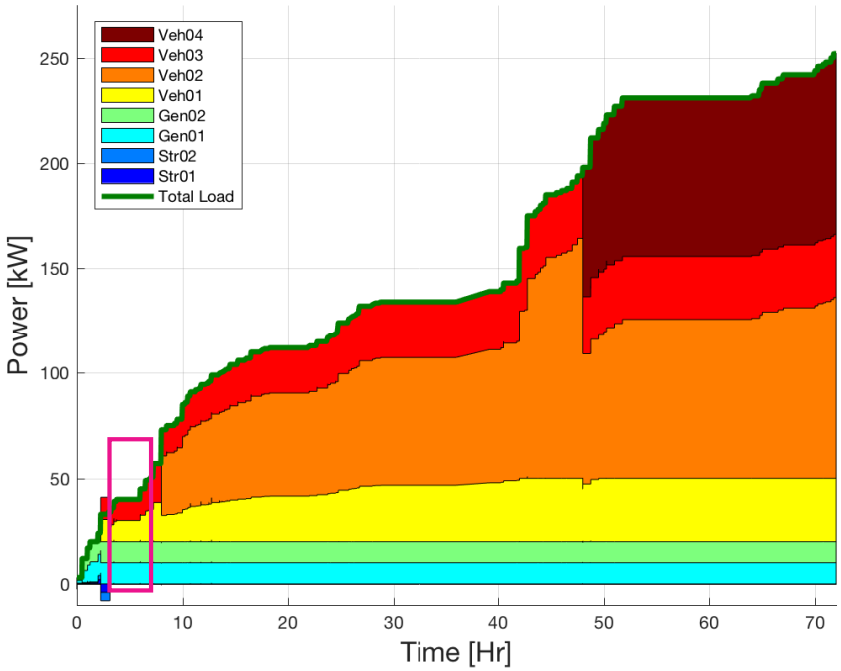

Figure 3.12: Contributions of all assets (four vehicles, 2 generators and 2 storage devices) during the 72 hour buildup.

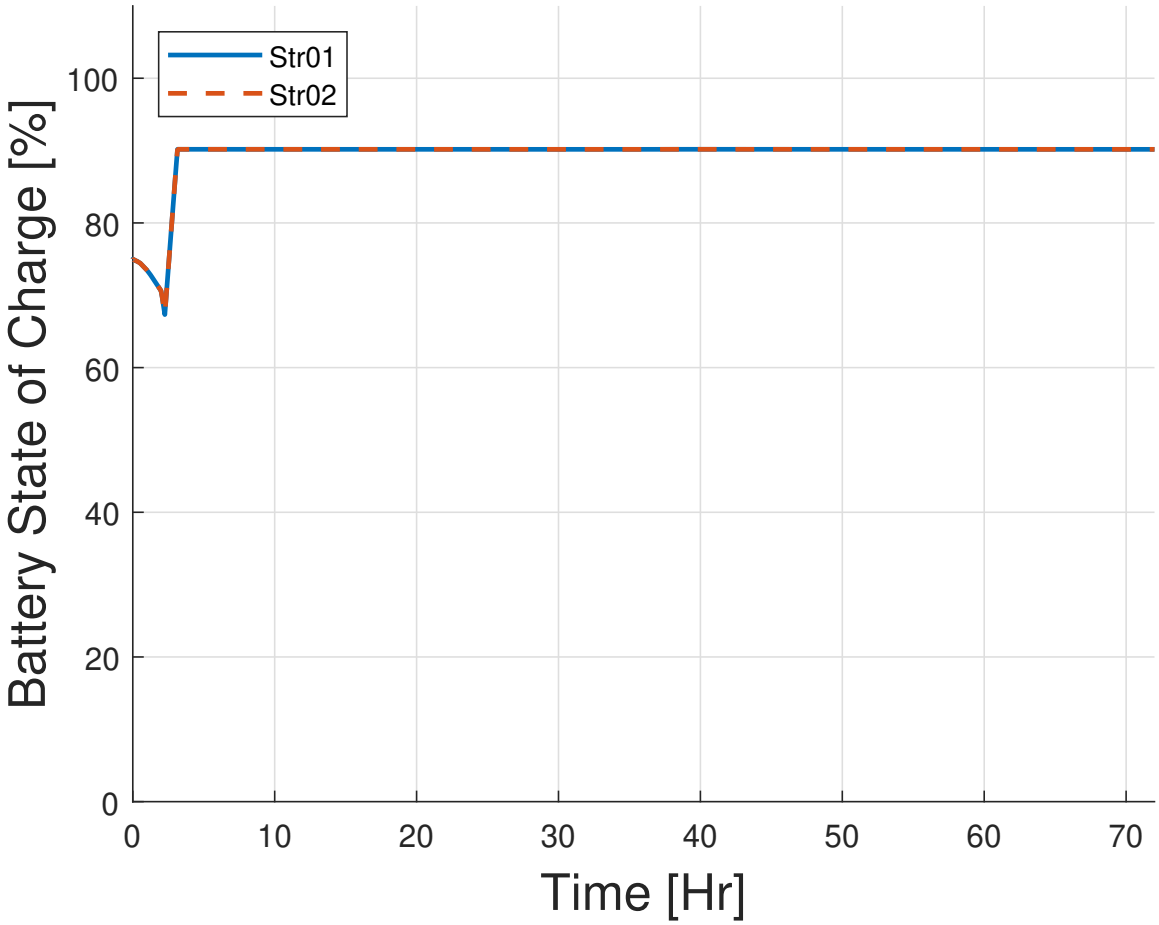

Figure 3.13: The electrical storage (battery) state of charge levels. Notice that the storage was initially exporting power. After sometime, the power-coordination control allows the electrical storage to charge for the uninterrupted outpost construction.

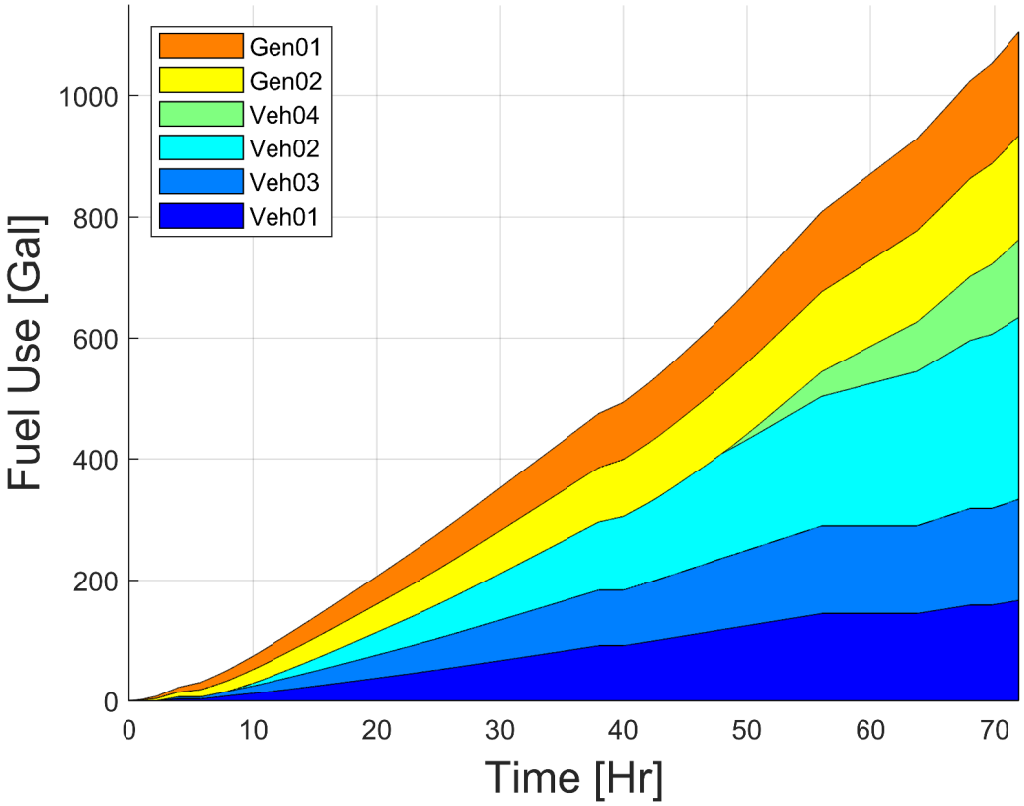

Figure 3.14: The estimated fuel use for the contingent of vehicles and generators was computed to be 1105 gallons of gasoline and diesel fuel for the uninterrupted outpost construction.

In Figure 3.12, we see that as the outpost matures, new primary grid assets are brought online to ensure that the power generation capacity was always greater than the actual load. It can also be seen that when the power generation far exceeds the load (purple region), the electrical storage units are allowed to charge until they reach 90% (as shown in Figure 3.13). Additional controls were introduced within the power-coordination controller to limit the electrical storage units exportable/importable

power capabilities. To prevent overcharging/discharging, the power-coordination controller limits the electrical storage units' from achieving more than 90% SOC (maximum SOC limit reached as shown in Figure 3.13) or less than 20% SOC (limit not reached within the simulation). Finally, Figure 3.14 shows the total fuel consumption for both the primary and secondary grid assets. The contingent of vehicles and gasoline generators consumed 1105 gallons of fuel to meet all tier one, two, and three loads throughout the simulation epoch. One should notice the fuel consumption for the various assets increase as the load increase. Additionally, different generation assets come online at different times, this can be seen when Figure 3.12 and Figure 3.14 are compared. When a vehicle begins to supply power (Figure 3.1 time in which a new color i.e. a new asset comes online), the fuel consumption immediately responds, simultaneously other loads seem to momentarily be reduced as the new grid asset begins to take a fraction of the total load.

3.5.2 Interrupted Outpost Construction

The results obtained from simulating the 72-hour interrupted outpost construction are shown in Figure 3.15 - 3.18.

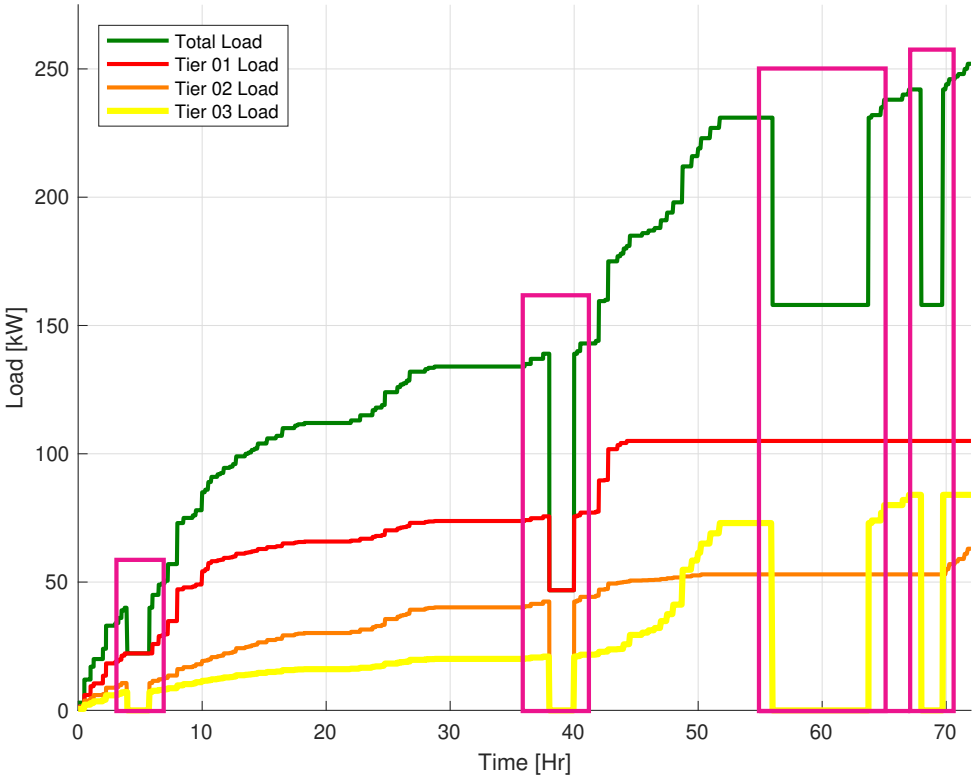

Figure 3.15: The total networked microgrid operational load profile, which consists of tier one, two, and three loads. During the interrupted outpost construction, the power-coordination controller registers power deficit, to alleviate deficit partial load shedding of tier one, two, and three are required to maintain the stability of the microgrid. Power deficits occur in the purple boxed regions are caused by vehicles leaving the grid.

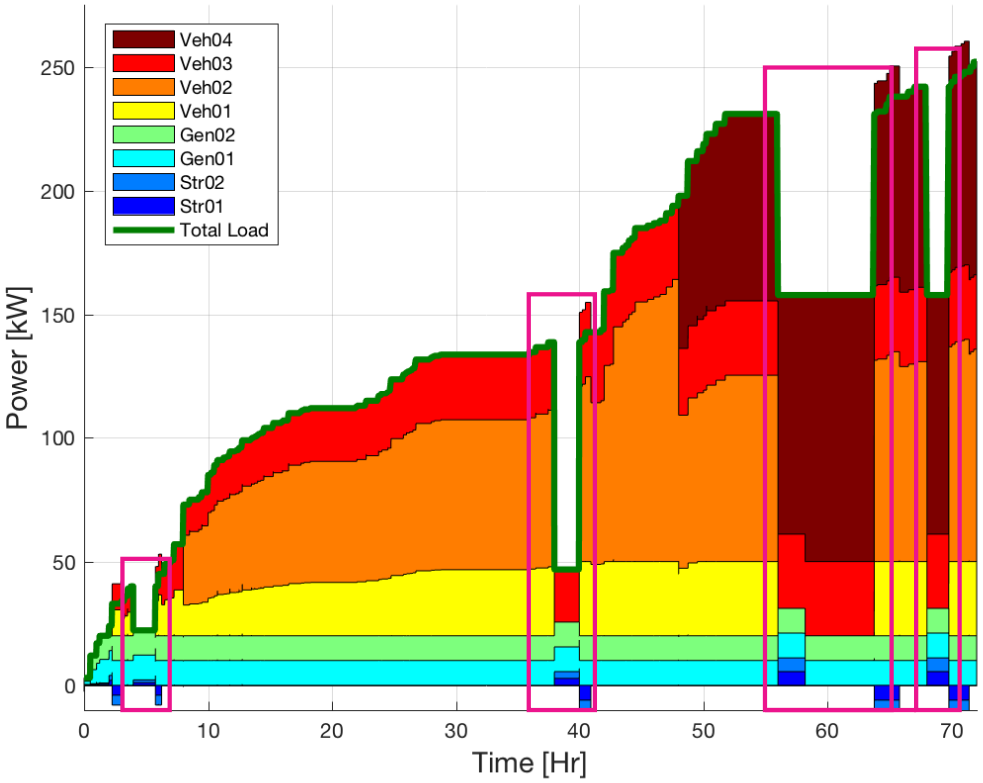

Figure 3.16: Contributions of all assets (four vehicles, 2 generators and 2 storage devices) during the 72 hour build up for the Interrupted scenario. During times when the power-coordination controller identifies power deficits, the electrical storage units are used to lessen the deficit, until the load deficit clears the system.

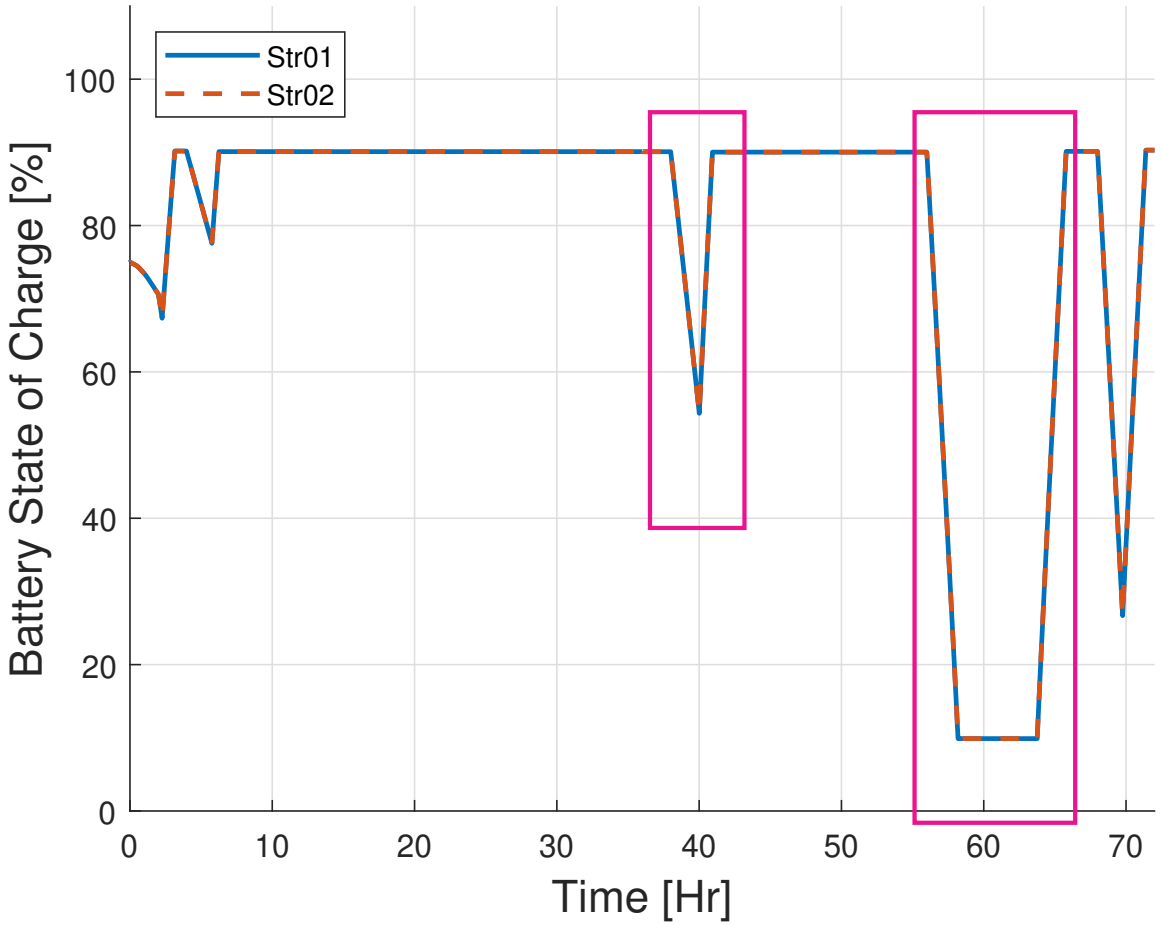

Figure 3.17: The electrical storage (battery) state of charge levels. Notice throughout the simulation epoch the storage was both discharged and charged. The storage charges when the generation capacity exceeds total load, and discharges when the power-coordination controller identifies power deficits.

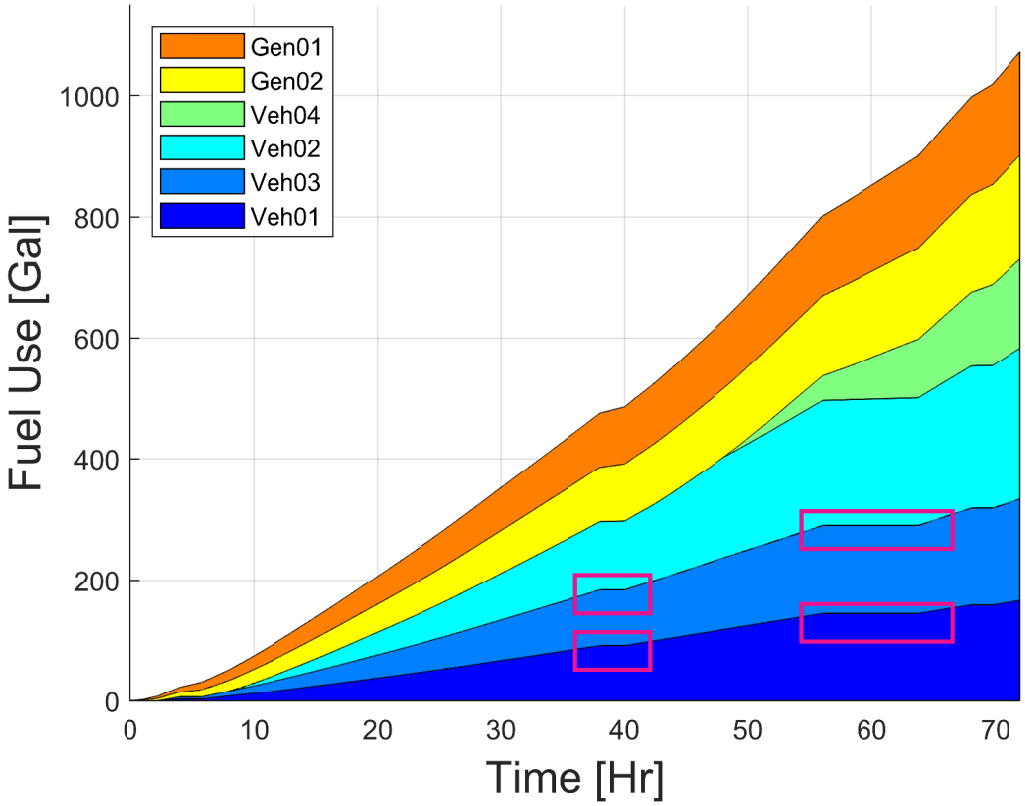

Figure 3.18: The estimated fuel use for the contingent of vehicles and generators was computed to be 1207 gallons of gasoline and diesel fuel for the interrupted outpost construction.

Recall in the interrupted outpost construction scenario, there are events, which cause a heightened level of security. The heightened level of security leads to some or all of the primary grid assets being unavailable for multiple periods throughout the simulation. Due to the unavailability, load shedding was required in order to ensure the generation capacity exceeds the actual load profile as shown in Figure 3.15 (purple/-magenta region). When the power-coordination controller identifies a power deficit has occurred, the lowest level priority loads are shed, if the power deficit remains, the

mid-level priority loads are shed, this process was continued until the power deficit was eliminated. If, however, partial load shedding (not all tier one loads can be achieved so some tier one loads were on while others were off) was required knowledge regarding the shelter designation was used to ensure loads, which are superfluous, are removed. Throughout the interrupted simulation epoch there were four registered power deficits, which required partial load shedding. After the deficit cleared the system, (primary grid assets returned to the outpost) normal operations resumed. In Figure 3.12, the individual load contributions for each primary and secondary grid assets are shown. Notice throughout the simulation epoch, the gasoline generators are continually used, and vehicles one and two are absent for multiple periods of time, during which time the load deficits were registered and the electrical storage units were brought online to minimize the deficit. After the events which caused the load deficits end, the storage was charged, this is notable as the total power generation exceeds the total load. In Figure 3.17, the effect of the electrical storage controls are observed. Throughout the simulation epoch when the generation capacity far exceeds the load, the storage was charged. Conversely, when the load far exceeds the generation capacity, the electrical storage units are discharged to minimize deficits, additional load shedding was used to further minimize the deficit until it became nonexistent and the events causing the load deficit had cleared. Additionally, the battery controls can also be identified upon inspection of Figure 3.17, after the electrical storage units were discharged, they were charged to 90% SOC, and powered

down. Conversely, when the battery discharges to 10 % SOC, the electrical storage was powered down to limit the battery degradation. Finally, the contingent of vehicles and gasoline generators consumed 1207 gallons of fuel to meet all active (load shedding required as power deficit was identified by power-coordination controller) tier one, two, and three loads as shown in Figure 3.18. Figure 3.18 can also be used to identify the periods where the individual vehicles are available for use, during this time no fuel consumption can be monitored (purple region), so the fuel consumption for a specific vehicle was held constant indicating no additional fuel was consumed.

3.6 Conclusions and Future Work

An optimal power management and power-coordination control strategy was developed and applied to the build-up phase of a military microgrid. During the 72-hour outpost buildup, it was shown that depending on the available electrical storage capacity as well as the generation capacity, a vehicle centric microgrid architecture could be constructed and controlled. The results showed that the four military vehicles (two M1152 HMMWVs with a 30 kW ISG, and two Max Pro MRAPs with a 3TIG integrated 125 kW ISG) were capable of producing sufficient power throughout the outpost construction to satisfy the outpost's load for the ideal case (uninterrupted construction). Conversely having limited primary grid assets adversely affected the outpost's load for the non-ideal case (interrupted construction) as tier

one, two, and three loads were shed to reduce the load deficit. Failure to reduce load deficits throughout the outpost construction could potentially lead to a voltage collapse. Adverse effects could be mitigated by allocating more vehicles with exportable power capabilities during the construction of a military outpost. Further allocation between primary and secondary vehicles could eliminate any agnostic power deficits caused by agnostic loads.

For the uninterrupted outpost construction, the storage capacity was sufficient to meet load demand. In the second scenario, it was concluded that the selected electrical storage was insufficient to mitigate a large portion of the load deficit that arose when the vehicles were absent. It was computed that the electrical storage was undersized by approximately 930 kWh. As a conservative estimate, we assume that our electrical storage units are discharging at the lowest controlled voltage of 550 V. The maximum time duration which the batteries would need to operate was assumed to be 8 Hr operating at 75 kW, it was estimated that the two electrical storage units would have to be rated at 550 AHr to ensure the generation capacity exceeds the load demand.

Additionally, higher fidelity models could be used for simulation purposes for the both the vehicle models, generator models, as well as the power-coordination controller. In regards to the vehicle models, fuel consumption models of the vehicles engines were based on commercial off the shelf data, which may be inaccurate measures of fuel consumption for military grade vehicles. Both the vehicle and generators AC

components have been significantly reduced to mitigate the effects of states such that a 72-hour simulation could be executed. Using higher fidelity models could show lower level of consumed fuel, and could show more deviation between which assets are used throughout the simulation epoch.

Chapter 4

Adaptive Leader Election for Control of Tactical Microgrids

[1] In Chapter 3, a centralized optimal control strategy was applied to an AC microgrid containing diesel generators, electrical storage, and military based vehicles, whose ability to generate electrical power was dictated by an event schedule. If an asset's availability resulted in insufficient power generation capabilities to meet the electrical load, load shedding was conducted based on the electrical load's prioritization level in addition to the shelter equipment list. Applying a centralized control strategy to AC electrical grid requires large communication throughput, and is ultimately vulnerable to destabilization should the communication between assets be severed. In

[1] "The material contained in this chapter was submitted to *The Journal of Defense Modeling and Simulation*"

this chapter, a distributed centralized control is applied to a similar AC electrical grid containing stationary and transient assets (diesel generators and military ground vehicles). Similarly an event schedule was used to dictate an asset's availability to provide electrical power, which also included a fifteen minute look ahead event schedule, which enables assets to be transitioned to or from an "on" or "off" state. Unlike Chapter 3, each of the assets were constructed using object oriented programming techniques to construct agents, which employ an adaptive leader election protocol to conduct cooperative control of a microgrid subject to sudden architecture changes, mitigated by the election of both a primary and secondary leader. This research effort builds upon the previously completed work in terms of implementing a deployable version of a centralized control strategy which would help reduce communication redundancies and provide improved scalability and robustness for energy management of an electrical grid. In Chapter 3 and 4, the control strategies required perfect knowledge of the electrical load, in practice this is a very generous assumption as the electrical load and operating conditions of a microgrid vary as a function of meteorological or hydrological conditions. In Chapter 5, the ability to control a set of heterogeneous assets was achieved by implementing a model predictive control technique, applied to an AC microgrid containing traditional generation assets (diesel generators and electrical storage), and photovoltaic (PV) arrays. The goal of the research effort was to understand the ability to perform long-term energy management of the electrical grid using a model predictive controls, subject to variable meteorological weather

scenarios with variable forecast prediction intervals.

4.1 Introduction

Ad-hoc microgrids typically include portable stationary diesel generators, battery storage, and renewable energy generation devices. Microgrids are commonly constructed during military operations, or for disaster relief [32, 33] operations. Electrical microgrids which include heterogeneous assets require constant communication, without which grid stability may be compromised. For larger systems, computationally efficient communication protocols are required to minimize communication throughput. One such communication protocol which achieves this includes leader election protocols. Commonly, leader election protocols elect leaders solely based on a unique identification number[34]. This type of leader election criteria is particularly vulnerable to node failures as a result of deterministic events including maintenance, remaining fuel capacity, or sudden topology changes. As a result grid instability may occur, further complicating relief efforts or military operations. For this reason, an adaptive leader election protocol was developed using time varying condition-based leader desirability criteria.

When microgrids are constructed, the individual microgrid components are transported, unpacked, and interconnected to form a generator-centric microgrid which

potentially contains i generators, j battery storage, and k renewable energy generation devices, requiring extensible control schemes to flow power. The previously defined microgrid does not include the use of vehicles as grid assets, this was primarily because earlier variants of vehicles lacked physical hardware capable of interfacing with grid-tied components.

Modern military equipment must provide safe, reliable operation during complex missions, which support flexibility and adaptability in an ever-changing kinetic environment. In particular, military vehicles are being built to serve dual purposes, including (1) transportation of units or supplies, (2) provide additional support through use of any government furnished equipment (GFE), and (3) provide electrical grid support using any exportable power capabilities. Vehicles such as the mine resistance ambush protected (MRAP) or the joint light tactical vehicle (JLTV) possess energy storage, GFE (loads), and the ability to export electrical power. Military vehicles which possess these three components are self-contained microgrids, optimization methods were applied and implemented for real-time control and system level design of a military microgrid for a single vehicle[14]. This research effort established a baseline architecture which could be extended for multiple vehicles. During silent watch operation, vehicles use their on-board GFE for long-range surveillance and must maintain maximum readiness for multiple hours without running the engine. If a contingent of military vehicles participates in silent watch operations, vehicle-centric microgrids could be exploited to extend silent watch operations using networked power flow

control strategies.

The integration of the vehicular platform within an electrical network could offer added functionally and capabilities not yet previously considered within military microgrids, including voltage and frequency regulation. Complete integration of the vehicle platform would lead to a more diverse asset pool, providing greater energy security and reliability for an ever changing working environment[18]. Additionally, the research effort identified acceptable times when the vehicle could be used for grid regulation. When military outposts are constructed, the result is an ad-hoc military microgrid, because vehicle variants like the MRAP are microgrids, a networked microgrid modeling approach should be used to control the flow of power for either vehicle to grid (V2G) or vehicle to vehicle (V2V) architectures. The microgrid architecture could potentially contain i stationary grid assets, and j transient assets (military vehicles), which require extensible distributed control schemes to facilitate the flow of power between grid assets.

The flow of power can only be achieved if the vehicles and grid-tied electrical resources communicate, which means communication protocols are required. Military vehicles represent transient grid assets, for this reason extensible plug-and-play communication protocols are required. Due to the nature of the control schema (distributed controls), some sort of multicast communication protocol may be required. A major prerequisite for mobile ad hoc networks (MANETs) is the ability to broadcast and

discover services of connected devices, without which misuse of an asset is likely to occur. Further, inefficiencies of the communication protocol due to redundant packet transmission potentially limit the extensibility of the communication network. To mitigate these effects, a more efficient alternative group-based service discovery protocol for MANETs was developed[35]. Similarly, vehicular ad hoc networks (VANETs) a subset of MANETs, likely require similar protocols for effective use of the network's assets. Vehicular based application areas are normally separated into two application areas, including safety and comfort[36]. While the study was conducted for the civilian based vehicles, it provided insight into unique challenges which plague VANET communication networks, which may coincidentally effect military VANETs.

Military vehicles and stationary grid-tied electrical hardware are designed to achieve two fundamentally different objectives, which require vastly different control schemas for each individual asset. In order to maintain control over the networked microgrid it is postulated that some sort of supervisory control is required to meter the flow of power. Further, to exploit the individual assets, it is also postulated that each individual group of assets (stationary diesel generators and military vehicles) use a leader election protocol to mitigate unnecessary data propagation. Two separate leader election protocols intended to be used for MANETs were developed[37]. The rationale behind the two separate versions of the leader election protocol was to construct distributed and highly adaptive leader election protocols which could account for single topology changes as well as node failures within the network. The work

completed provide insight regarding the use and potential construction of a leader election protocol.

A *MATLAB/Simulink* simulation was developed capable of modeling both generator and vehicle assets. The generation assets are contained within an AC electrical distribution network, and were constructed using modular components. The modularity of the components, was done out of necessity regarding the implementation of an adaptive leader election protocol which is responsible for managing the grid assets. The adaptive leader election allows either stationary or transient assets to be elected as either a primary or secondary leader. The primary leader was charged with maintaining control over the grid assets, and the secondary leader was introduced to mitigate the effect of a node failure. To ensure the best leaders are in charge, rolling elections are conducted. Condition based, time varying measurement data was used within the leader election protocol to assess an asset's ability to lead. Node failures within a communication network intended to control an electrical grid could lead to large voltage or frequency fluctuations. If the leader node fails, grid stability may be compromised, added protection is required to mitigate node failures. The desirability criteria was primarily based on an asset's longevity to provide electrical power. Such criteria included total fuel capacity, remaining fuel, energy storage capacity, and remaining availability which considers a 15 Min look ahead event schedule. The extended use of an asset leads to a reduction in available fuel, without resupply, the asset's longevity decreases. The time varying leader desirability criteria reflects the

asset's diminishing desirability to lead, increasing the probability that it is not elected to lead. This means the leader election protocol is less susceptible to the leader experiencing a node failure resulting from insufficient fuel or energy storage capacity (deterministic events). The contribution of this chapter is a new centralized control architecture using distributed agents engaged in cooperative control. An adaptive leader election protocol suitable for control of both stationary and transient assets was developed and implemented to mediate communication and control of an AC network. The work provides a foundation which could be extended for optimal energy management and control polices to include heterogeneous assets. The remainder of this chapter describes the model components, focusing more on the leader election protocol including the roles of both the leader and the subordinates.

4.2 Model Dynamics

The *MATLAB/Simulink* simulation developed was capable of modeling an AC network containing both grid-tied components (diesel generator) and transient assets (vehicles) participating in cooperative control. The simulation's core electrical grid was broken up into three major components including, (1) generators, (2) vehicles, and (3) the grid architecture/topology. The generator assets are based on commercial off the shelf (COTS) diesel generators. The vehicle assets were constructed assuming the vehicle model contained four distinct components; (1) a battery, (2) an engine,

(3) GFE, and (4) an alternator. Each generation asset was separated into modular components which are responsible for modeling the dynamic behavior of the asset and implementing the power flow commands, subject to the control policy. The overall system dynamics and electrical grid architecture were defined using the complex nodal admittance matrix. This assumed that the grid was operating within a sinusoidal steady state where transient response was negligible, the complex nodal admittance matrix simplifies the electrical dynamics to a set of algebraic equations.

4.2.1 Generator Assets

The electrical grid architecture used for modeling a generator is provided in Figure 4.1. The generator model was a COTS AC diesel generators operating at 60 Hz with a variable voltage behind a reactance[19]. Two different generator types were used for the simulation studies, including an advanced medium mobile power sources (AMMPS) and the tactically quiet generators (TQGs).

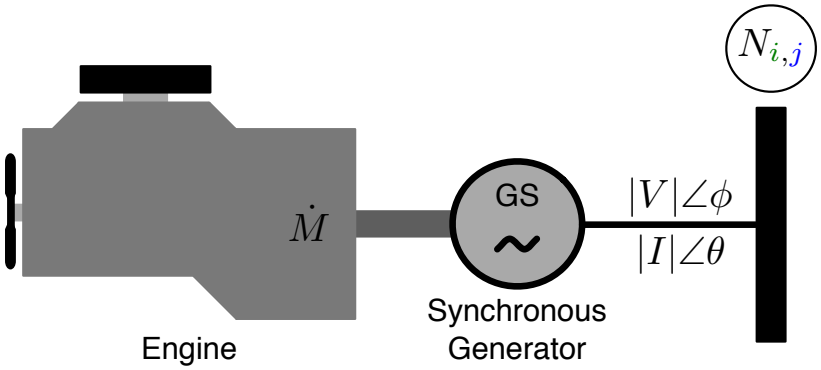

Figure 4.1: The electrical circuit diagram used to model the generator assets assumes the generator consumes diesel fuel $\dot{m}$ to produce electrical power, with a single degree of freedom $\dot{m} = f(P_{elc})$.

4.2.2 Vehicle Assets

The electrical schematic used for modeling a vehicle is provided in Figure 4.2, and assumes a vehicle contains (1) a battery, (2) a six phase self-rectifying alternator, (3) an engine, and (4) a variable load. The battery model was based on a genetic battery algorithm[38]. The alternator model was based on a Niehoff alternator, operating at 28 volts DC (V_{alt}), capable of exporting either 30 kW or 125 kW of power for a high mobility multipurpose wheeled vehicle (HMMWV) or MRAP respectively[39]. The alternator model is similar to current alternators used by the JLTV, and scaled appropriately to achieve similar exportable power capabilities of each vehicle. Two vehicle variants were considered, the HMMWV utilizes a GEP Optimizer 6500 215 HP and the Max Pro MRAP possess a Caterpillar C7 engine[40]. The vehicle model

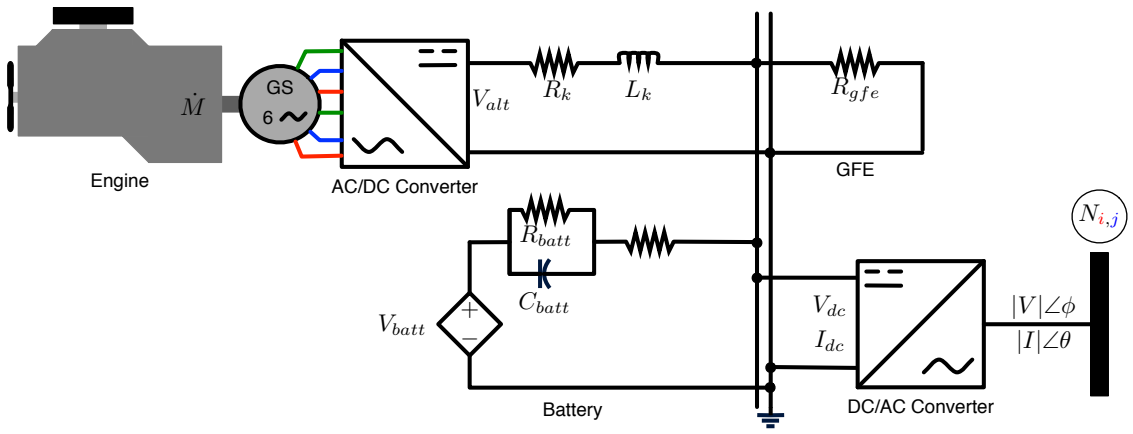

Figure 4.2: The electrical circuit diagram used to model the vehicle assets assumes the vehicle consumes diesel fuel $\dot{m}$ to produce electrical power, with two degrees of freedom $\dot{m} = f(\tau_{eng}, \omega_{eng})$. Mechanical power was converted to electrical power, which could be exported to an AC electrical network.

dynamics are based on [19].

4.2.3 Grid Architecture

We assume that electrical transients are negligible (when compared to the mechanical transients), and the grid has reached sinusoidal steady state, which omits the frequency deviation of the stationary diesel generators. Further to achieve power flow between the vehicle platform, TARDEC has constructed the tactical to vehicle module (TVGM) which was intended to allow the vehicle platform to operate at a variable frequency and flow power between other vehicles and an AC distribution network[4]. Applying these assumptions, the differential equations used to model the electrical architecture are reduced to a set of algebraic equations formulated within

the complex nodal admittance matrix. The nodal connections defined by the complex nodal admittance matrix defines the grid topology based on Ohm's Law rewritten to include the complex nodal admittance matrix provided in Equation 4.1,

$$\vec{I} = [Y_{bus}]\vec{V} \tag{4.1}$$

where $\vec{V}$ is a vector of complex voltages, $\vec{I}$ is a vector of complex currents, and Y_{bus} is a square matrix, containing the known admittances for the transmission network. The complex nodal admittance matrix was used in conjunction with the nodal voltages, to compute the nodal currents. The optimal power apportionment strategy computed the optimal voltage set-points that minimized value stream impacts such as consumed fuel or transmission losses which are based on the AC power flow Equations of [41].

4.3 Leader Election Protocol

Leader election was selected to manage and control a set of heterogeneous assets including diesel generators and military vehicles. For the case of a distributed system with minimal communication capabilities, one way to manage each individual asset would be to implement droop or isochronous control, which effectively enables each asset to compute $1/N^{th}$ of the power flow solution, which should result in sufficient power flow from the contingent of assets. This type of control methodology is robust,

however it does not necessarily ensure any of the assets will operate efficiently which could lead to more fuel or energy storage requirements. In order to manage the diverse assets and compute a complete power flow, the assets must communicate with each other and come to some type of consensus with the acceptable level of power sharing each asset should provide to accommodate an electrical load. In order to implement leader election to manage the generation and load assets, a single asset must be elected from the contingent of assets. Multiple leaders cannot be elected and active at the same time. If this were the case, differences resulting from communication latency and measurement based data would lead to continuous updates, grid instability is likely to occur.

The simplest leader election protocol uses an asset's unique identification (ID) number to select a leader from the contingent of assets. Usually the asset with the lowest unique identification number is selected as the leader. According to [42] the five most prominent leader election algorithms are (1) Bully Algorithm presented by Gracia-Molina in 1982, (2) Improved Bully Election Algorithm in Distributed System presented by A. Arghavani in 2011, (3) Modified Bully Election Algorithm in Distributed Systems presented by M. S. Kordafshari and group, (4) Ring Algorithm, and (5) Modified Ring Algorithm. The original bully algorithm requires that every process knows the identity of every other process, with N^2 communication complexity. The improved bully election algorithm first elects a coordinator, and then selects a backup coordinator should the original leader experience a node failure. This algorithm has

a complex structure, and requires a large database to implement. To mitigate the potential disadvantages of the bully election algorithms the modified election algorithm was developed. When a process notices the leader is not responding, the election process is initiated, election messages to all processes with higher priority numbers are sent, if no responses the process wins the election. The algorithm is time bounded, and still requires that all process know the priority of the others, and usually has less computational complexity than N^2. The ring algorithm assumes that the processes are physical or logically ordered. When the leader process is not functioning, an election message is constructed by the asset which has identified the leader is not functioning. The election message contains its own process number, this message is sent to its successor. The successor will amended the election message to include its own process number and passes this along until a new leader is elected, resulting in at most $2N$ messages with $2N$ latency. Finally, the modified ring algorithm was constructed to mitigate the large messaging structure of the ring algorithm. In this algorithm, an asset obtains messages from the previous asset, compares it's unique ID or priority to the previous message, the highest priority number is forwarded to the next asset, the resulting algorithm results in at most $2N$ communications to elect an new leader, and does not require a large database to select a leader.

Our leader election protocol had multiple features including (1) the ability to elect an adaptive leader using condition based data, and (2) the ability to elect both a primary and secondary leader. The leader election protocol was triggered at the start of the

simulation, at topology changes, and periodically using rolling leader elections (every minute). There are two different roles an asset may fill including (1) the primary leader or (2) a subordinate which also includes the secondary leader.

The primary leader was charged with four responsibilities; (1) to complete the negotiation process between the leader and a subordinate, thereby establishing and confirming a communication link between the subordinate and the leader, (2) invoke an optimization routine intended to identify the acceptable level of power sharing among networked assets, (3) smoothly transitioning an asset to and from an on/off state to mitigate bus voltage deviation, and (4) perform bidirectional communication among the subordinates to obtain sensor data, and implement the commands generated within the optimization process.

The subordinates on the other hand have a single responsibility including performing bidirectional communication between the asset and the leader by updating sensor data and implementing the commands issued by the leader. The secondary leader's responsibilities are nearly the same as a subordinate. If the primary leader experiences a node failure, the secondary leader assumes the role of the primary leader. The various components or features are described in greater detail in subsequent sections.

4.3.1 Leader Election Criteria

An adaptive leader election protocol was introduced to manage and control a finite number of generation and load assets. Military microgrids such as an outpost (OP), forward operating base (FOB), or disaster relief operations are physically contained in small geographic regions, assumed to be less than two square miles in area. Additionally it was assumed that of the vehicle assets present, half of the assets are capable of providing grid support. Finally the total number of assets defined within the network was less than or equal to 100. Due to the finite number of generation assets it was postulated that an adaptive leader election algorithm could be used to manage the electrical grid. The leader election protocol was selected to manage both stationary and transient based assets due to the distributed nature of the algorithm and relative size of the asset pool. Without use of such a protocol, transient assets (vehicles) may be underutilized, limiting the potential to implement more efficient control strategies. Additionally, various leader election protocols have been developed, which could be used to reduce redundant communications, which limit the scalability and efficiency of the communication network[34].

Due to the kinetic working environment of military operations or disaster relief efforts, unexpected node failures brought on by mechanical or communication failure may be more likely to occur for ad-hoc networks. In an attempt to mitigate more deterministic

node failures, time varying condition based leader election criteria was used to elect a leader. This type of functionality was introduced in order to mitigate the potential that an asset with diminishing properties or forecasted operational deficiencies could be elected leader and force the grid to experience power disruption brought on by a node failure.

Additionally, some capabilities or features of an asset may be better suited to handle high speed transient or perhaps lead to a reduction in energy usage. Features such as assumed fuel efficiency at half/full load or current fuel level could greatly affect the ability of an asset to operate efficiently or for an extended period of time within the network. It was for this reason that the leader election criteria provided within Table 4.1 was established to assess an asset's desirability to lead. Information regarding the availability and type of the assets are used to help skew the selected leader away from deterministic node failures (topology change, insufficient fuel) to mitigate the potential that a node failure could affect the grid stability.

#	Signal Information	Units	Variable
1	Unique Asset ID	-	NaN
2	Ratio Between Rated Power and Current Load	-	β_1
3	Rated Load	kW	β_2
4	Total Fuel Capacity	gal	β_3
5	Remaining Fuel Capacity	%	β_4
6	Half Load Fuel Efficiency	-	β_5
7	Full Load Fuel Efficiency	-	β_6
8	Total Energy Capacity	AHr	β_7
9	Remaining Energy Capacity	AHr	β_8
10	Half Load Storage Efficiency	-	β_9
11	Full Load Storage Efficiency	-	β_{10}
12	Inertia	kgm^2	β_{11}
13	Asset Type	-	β_{12}
14	Availability	sec	β_{13}

Table 4.1
The criteria used to assess an asset's desirability to become a leader was based on machine parameters which effect the assets ability to provide prolonged assistance to the grid as well as efficient operation.

Using the values provided within the table an asset's desirability to lead can be

computed using Equation 4.2.

$$\mathscr{LD} = \sum_{i=1}^{13} k_i \beta_i \tag{4.2}$$

Within Equation 4.2, the gains k_i (assumed to be a one) are introduced to form non-dimensional values which allow an asset's net desirability to lead to be computed. In the event of a tie, the asset with the lowest unique identification number was elected as the primary leader. If there are no ties than the asset with the next highest desirability to lead may be elected as the secondary leader. An exception to this rule exists, if the primary leader has been identified as a vehicle, the asset with the next highest desirability to lead may not be selected as the secondary leader. Vehicles are transient assets, this means without notice a vehicle may leave resulting in a sudden node failure. If a vehicle asset has been identified as the primary leader, the asset with next highest desirability may be ignored, in place of this asset, a generator asset with the highest desirability to lead was elected as the secondary leader. If no generator assets are available, than the asset with the next highest desirability to lead was elected as the secondary leader, regardless of type. The choice to elect a generator as a secondary leader when a vehicle is the primary leader, reduces the possibility that two unexpected node failures may occur within a short period of time, which could occur if both primary and secondary leaders are vehicles.

From analysis of Table 4.1, let it be understood, if a vehicle and generator have next to identical characteristics, the vehicle would have a higher desirability to lead over

a generator due to the absence of components which allow the generator to store electrical energy. This type of behavior was justified as vehicle variants such as the MRAP have excess electrical storage capabilities for silent watch operations, as such the addition of their electrical components make the asset more suitable to handle high-speed transients, which in a real system would be limited by the generators inertia.

As mentioned previously some of the leader desirability criteria was introduced to help skew the election of a leader. One such criteria includes the asset's forecasted availability. The availability is a measure of how long the asset will be available for, limited to a fifteen minute period measured in seconds. If an asset such as a vehicle was slated to depart or undergo maintenance fifteen minutes from now the desirability criteria remains unchanged. During the next rolling leader election, the leader desirability criteria for the availability was reduced based on the remaining time the asset was expected to be available. Using this type of behavior, assets which are schedule to depart or be taken off-line drastically lose their desirability to lead around forecasted topology changes. As a result, if the leader was forecasted to depart within the next fifteen minutes, the leader desirability decreases to the point in which the asset was not favored to lead the asset pool, meaning the asset transfers the leadership responsibly prior to embarking from the asset pool.

4.3.2 Rolling Leader Election

Rolling leader elections were induced periodically (every minute) in an attempt to minimize the potential that an asset with deteriorating capabilities could be elected to lead. All leader elections are conducted using the nearest neighbor algorithm, assumed to be arranged within a ring configuration as shown in Figure 4.3. Using this type of communication strategy, the communication complexity yields at most $2N$ which saves $N(N-2)$ communications when compared to a fully connected network. The ring configuration was updated to exclude assets which were identified as disconnected, if this was the case, the corresponding signals used to invoke the leader election protocol are routed to the next available asset within the chain.

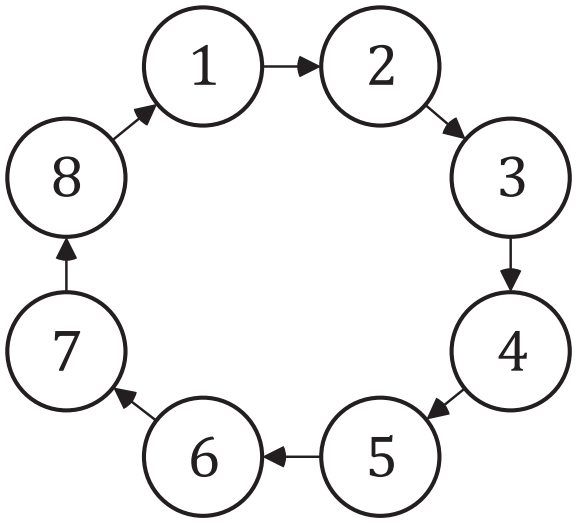

Figure 4.3: The nearest neighbor algorithm coupled with a ring configuration.

4.3.3 Negotiation Protocol

The negotiation protocol was completed following a topology change in which an asset connects/disconnects with the electrical grid. When a newly connected asset was identified by the leader, the leader attempted to establish and confirm connection by transmitting a flag to the asset. If the asset received the flag, a separate flag was set, and transmitted in response back to the leader. After a series of successful transmit/receive flags had been set by the newly connected asset and the leader, the asset set a flag confirming the communication link had been established and active, the leader than identified the newly connected asset as a viable asset from which it may begin to flow power to/from the grid based on updated measurement data. The unified modeling language (UML) sequence diagram for the negotiation process has been provided in Figure 4.4. In the event that an asset became disconnected, the flag used to confirm that the communication link was established and active yielded multiple unsuccessful transmit/receive transmissions, this indicated that the asset has disconnected from the network. The leader then identified the asset as inactive and omits it from the power flow solution. All stored data regarding the asset was reset in preparation for a new asset to connect to the network.

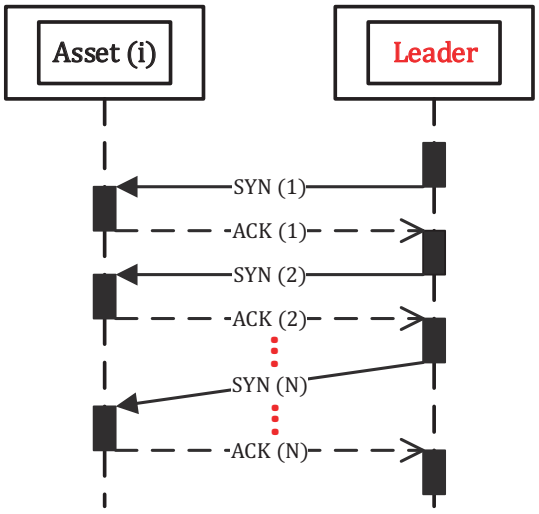

Figure 4.4: The negotiation protocol sequence diagram. The sequence is initiated via the leader which waits for multiple acknowledgments from the subordinate to establish and confirm the communication with the leader. Failure to achieve this results in disconnection.

4.3.4 Optimal Power Flow

Each generation asset included within the simulation was created to be modular, and possess a single power flow and control agent (PFCA). The PFCA agent was charged with implementing subordinate or superior communication between networked assets. In the event that an asset had been identified as the leader, the asset in question was then responsible for negotiating between its subordinates to establish a communication link, after the link was established and the subordinates provide information regarding their current states, the leader generated a set of active and reactive power flow commands based on the measured load. The power flow commands must then

be converted into optimal actuation commands that satisfy the power flow equations for the electrical network in the form of voltage magnitude and angle commands.

To achieve this an approximate, feasible solution to the power flow equations were computed by applying the DC power flow for an AC microgrid approximately satisfying the AC power flow equations. The DC power flow was computed using the grid's complex nodal admittance matrix where a single-phase power network and per-unit values were used. A balanced three phase system was assumed, which allows the use of a single phase model and the DC power flow solution. At every node of the electrical network the complex power flows are represented using Equation 4.3, where S_k represents the net complex power flow into the k^{th} node, S_{gk} is the complex power generated at the k^{th} node, and S_{dk} is the complex power flow away from the k^{th} node.

$$S_k = S_{gk} - S_{dk} \tag{4.3}$$

The complex power at any node can be computed assuming the complex voltage and current are known, resulting in Equation 4.4, where V_k is the complex voltage at the k^{th} node, and I_k^* is the complex conjugate of the complex current at the k^{th} node.

$$S_k = V_k I_k^* \tag{4.4}$$

The complex power of Equation 4.4 can be separated into real and imaginary components leading to Equation 4.5, where P_k and Q_k are the real and reactive power injected at the k^{th} node.

$$S_k = P_k + iQ_k \tag{4.5}$$

The current and voltage are related by the nodal admittances, Y_{kj}, which lie between the k^{th} and j^{th} node, as shown in Equation 4.6.

$$I_k = \sum_{j=1}^{N} Y_{kj} V_k \tag{4.6}$$

The nodal admittance can be rearranged into real and the complex components resulting in Equation 4.7, where G_{kj} and B_{kj} represents the resistive and reactive component of the admittance, between the k^{th} and j^{th} nodes.

$$Y_{kj} = G_{kj} + iB_{kj} \tag{4.7}$$

Equation 4.7 can be rearranged to form the complex nodal impedance of Equation 4.8, where R_{kj} and X_{kj} are the resistive and reactive components of the impedance between the k^{th} and j^{th} nodes.

$$Z_{kj} = \frac{1}{Y_{kj}} = R_{kj} + iX_{kj} \tag{4.8}$$

The power flow of Equation 4.4 can be rearranged to form Equation 4.9, where θ_k

and θ_j are the phasor angles for the k^{th} and the j^{th} nodes.

$$\begin{aligned} P_k &= \sum_{j=1}^{N} |V_k||V_j| \left[G_{kj}\cos(\theta_k - \theta_j) + B_{kj}\sin(\theta_k - \theta_j)\right] \\ Q_k &= \sum_{j=1}^{N} |V_k||V_j| \left[G_{kj}\sin(\theta_k - \theta_j) - B_{kj}\cos(\theta_k - \theta_j)\right] \end{aligned} \tag{4.9}$$

The full derivation of the DC power flow[41] yields Equation 4.9, applying multiple assumptions can yield an approximate, feasible solution which provides an efficiency boost for subsequent optimization routines of an AC network. The solution can be obtained by imposing four assumptions: (1) the resistive component of the impedance is very small when compared to the reactive component ($2 \leq X/R \leq 10$), (2) the phase angle separation between nodes is less than $10 - 15$ degrees, (3) all reactive power generated at a node is contained in the control volume (complex nodal admittance matrix), and (4) all magnitudes are known and equal to one another. If these assumptions are made, the power flow equations provided in Equation 4.9 can be simplified resulting in Equation 4.10.

$$\begin{aligned} P_k &= \sum_{j=1}^{N} |V_k||V_j| \left[G_{kj}(\theta_k - \theta_j)\right] \\ Q_k &= \sum_{j=1}^{N} |V_k||V_j| \left[-B_{kj}\right] \end{aligned} \tag{4.10}$$

Analysis of Equation 4.10 reveals that using both the real and reactive equations at every node of the network results in an overdetermined system. To solve for the nodal voltages, the real component of Equation 4.10 can be used to solve for the unknown

phasor angles. Prior to solving the system of equations governed by the real power injected at each node, the equations can be arranged into matrix form. Careful inspection of the matrix equations reveals (1) the sign of the reactive component is opposite of the reactive component within the complex nodal admittance matrix, and (2) the matrix equations are not linearly independent. An invertible system can be constructed by making one of the assets "slack" with a zero phase angle and eliminating its corresponding rows and columns from the matrix equations. This solution method assumes all phase angles are referenced to the slack asset and provides a very fast approximate, feasible solution which can then be used to seed optimal solution algorithms, increasing the efficiency of the subsequent power flow.

The optimal power flow (OPF) algorithm uses *MATLAB's* fmincon optimization algorithm, seeded with a feasible initial guess as described above. The design variables of the OPF include the individual nodal voltage and phase angles that satisfy the power flow equations subject to the set of matrix equations defined using the complex nodal admittance matrix. Using a variably sized set of matrix equations can be computationally inefficient, for this reason, the OPF includes additional logic which reduces the set of design variables at each iteration based on the actuation estimates generated, further improving its convergence time over an initial guess of zero.

The OPF objective function can be any quantity of interest. For the studies conducted here, dissipated power, given in Equation 4.11, where R_{kj} is the resistive component

of the branch connecting the k^{th} and the j^{th} node, and $|I_{kj}^2|$ is the square of the absolute value of the complex current between the k^{th} and the j^{th} node, was used.

$$J = \sum_{i=1}^{n} R_{kj}|I_{kj}|^2 \tag{4.11}$$

Equation 4.11 represents the dissipated losses incurred due to the flow of power between nodes in the network. The cost function can be modified to allow the OPF to minimize custom objective functions. The OPF solution is also subject to the equality and inequality constraints of Equation 4.12 and Equation 4.13.

$$\begin{aligned} P_k &= Re(V_k I_k^*) \\ Q_k &= Im(V_k I_k^*) \end{aligned} \tag{4.12}$$

$$\begin{aligned} |V|_{k,min} \leq |V|_k \leq |V|_{k,max} \\ \angle V_{k,min} \leq \angle V_k \leq \angle V_{k,max} \end{aligned} \tag{4.13}$$

At every simulation iteration, the real power constraints for each source asset were constructed. Similarly, both real and reactive power constraints were imposed for each node. Using similar logic used to reduce the number of design variable previously mentioned, only the applicable power constraints were applied. With the reduction made to both the design variables and the constraint equations, computational efficiency was increased to accommodate a dynamically sized network. If the optimization routine fails to find a solution in a specified amount of time, then the

previous feasible solution generated from the DC power flow was passed as opposed to defaulting all assets to a nominal value. Since the swing asset has been assigned to the electrical storage, power balance was maintained. The resulting power flow provides efficient and scalable optimization methodology to optimize an AC distribution network.

4.3.5 Smooth Transition of Asset

Proceeding the departure of an asset or immediately following the arrival of an asset, the asset's ability to export power to the grid was ramped down/up. This was completed to mitigate voltage excursions which may arise due to the reduction of current injected. To achieve this the reported rated power of an asset was scaled using a cubic polynomial as shown in Figure 4.5. By doing this, an asset which was scheduled to depart or has recently connected is smoothly transitioned to an on/off state. In doing so especially if an asset is to depart, the asset was commanded to output zero power, to achieve this within the AC distribution network, the asset's voltage should track the corresponding bus voltage. In doing so the voltage magnitude and angle error should be minimal, when a switch was thrown voltage excursions should be negligible, mitigating potential voltage instability.

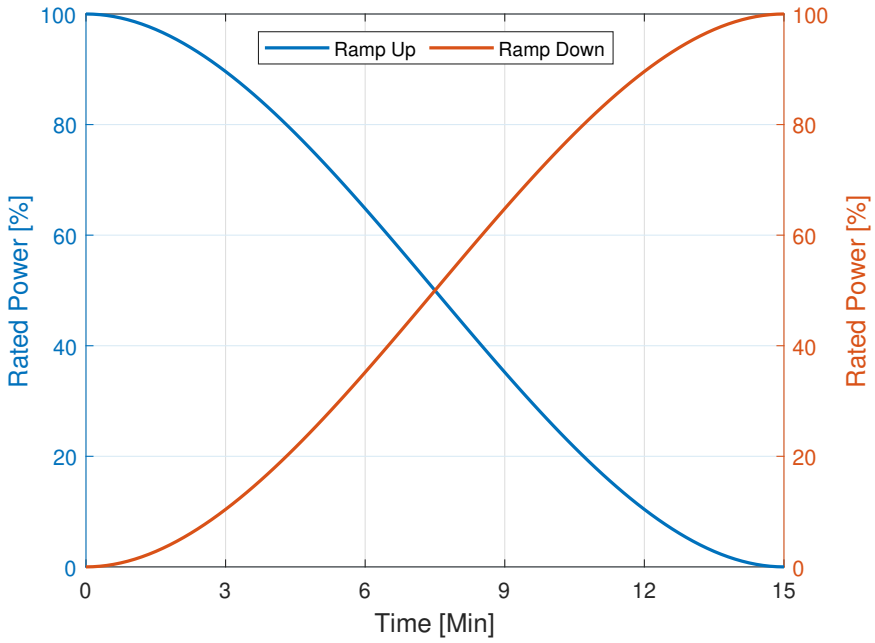

Figure 4.5: Smooth transitioning polynomial used to ramp down/up an asset. The polynomial was used prior to a forecasted topology change in which an asset was forecasted to embark, or immediately following the addition of an asset to a running state. The asset achieves a running state after the subordinate has completed the negotiation process.

4.3.6 Bidirectional Communication

Immediately after the leader election has ended and the individual assets have identified the leader, all communication which uses the nearest neighbor algorithm was halted. At which point the only communication which is now complete includes the communication between the leader and the subordinates as shown in Figure 4.6, with a communication complexity of at most $2N$. Communication which originates in the

asset and transmitted to the leader contains current sensor measurement data. Conversely communication which originate in the leader and transmitted to a subordinate were considered commands, generated via the power flow agent.

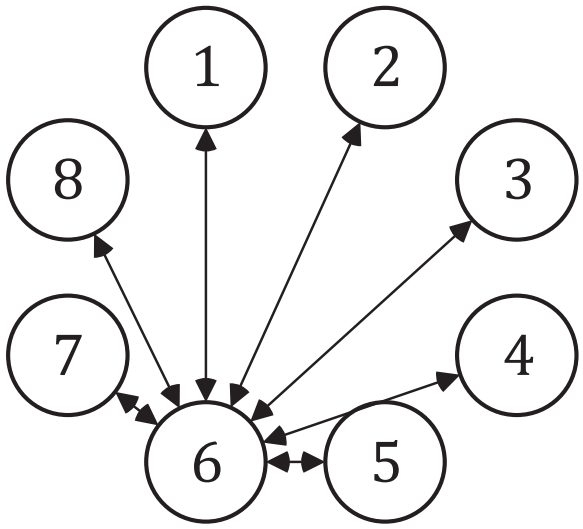

Figure 4.6: Communication between individual assets and leader, where asset 6 has been elected to lead the asset pool.

4.4 Scenario Definition

To highlight the ability to use leader election to manage grid assets, a scenario was defined consisting of three diesel generators, one 30 kW TQG, one 30 kW AMMPS, and one 60 kW TQG. In addition to the stationary assets, there are two HMMWVs capable of exporting 30 kW using integrated starter generators, and a single MRAP capable of exporting a maximum of $125kW$ using its 3000 transmission integrated

generator (3TIG). All generation assets are directly connected to a centralized AC electrical distribution node. The corresponding electrical architecture is provided in Figure 4.7. Each asset's node is connected to the distribution node through a 50 ft three phase wire with wound copper conductors. We assume the electrical grid operates at a nominal 60 Hz and that the startup dynamics and high speed transients were neglected.

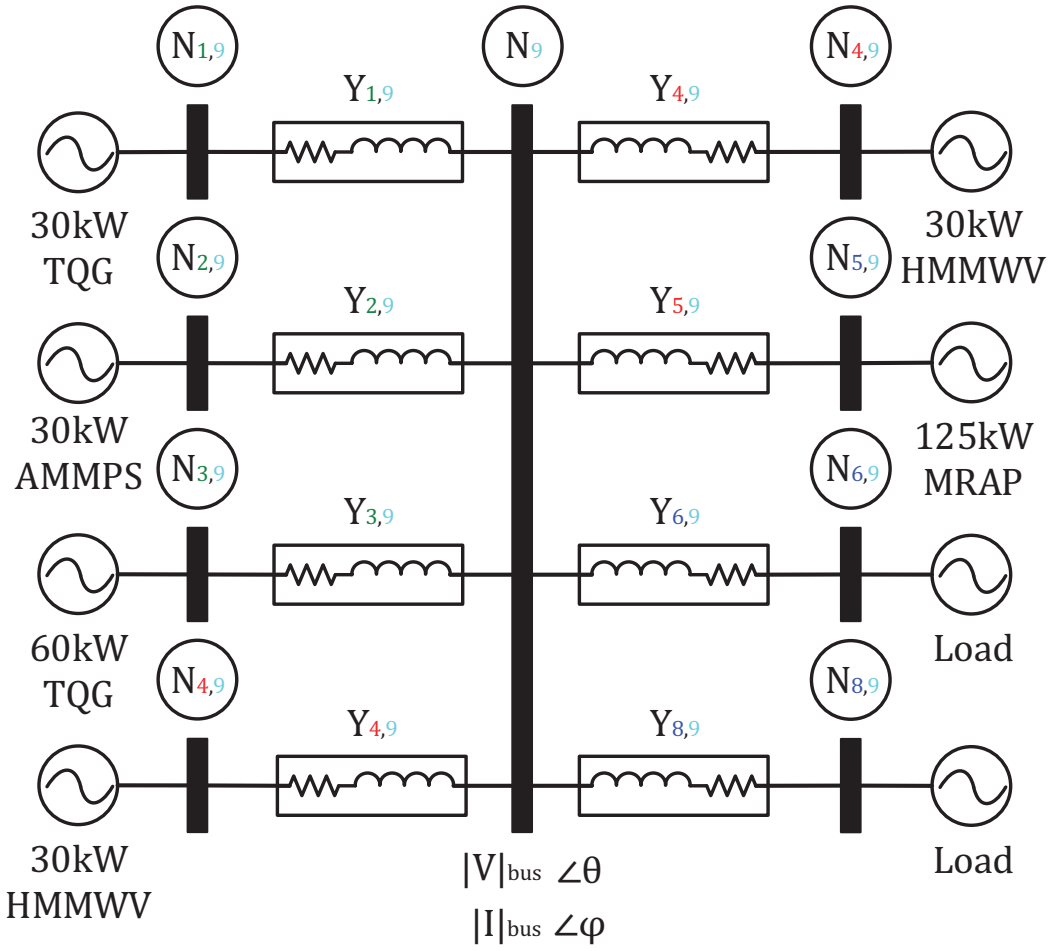

Figure 4.7: The electrical architecture consisting of three stationary diesel generators, three transient vehicle assets, and two load assets, within an AC distribution network.

In addition to six source assets, there are two load assets which equally share a predefined load profile provided in Figure 4.8. The load profile is assumed to be complex with a constant power factor of $\phi = 0.95$, for this reason only the active power profile has been provided.

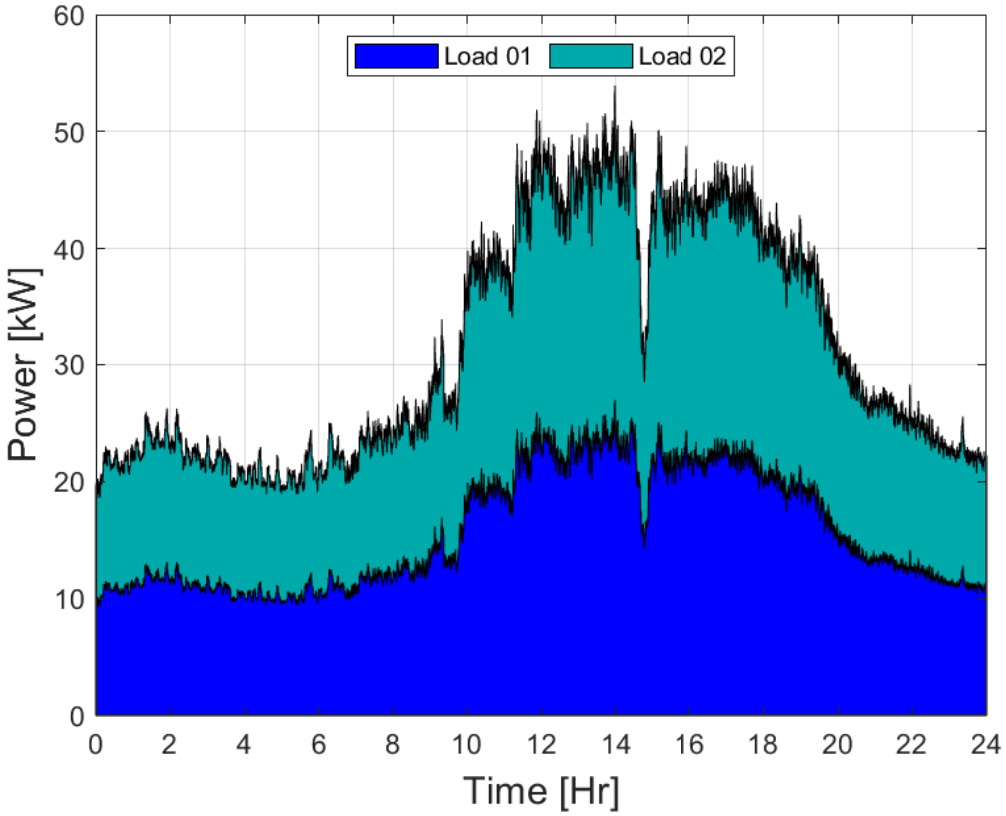

Figure 4.8: The total load is shown decomposed into two equal components.

The scenario is ultimately governed by an event schedule provided in Figure 4.9. The event schedule defines the asset's availability, i.e. active or inactive. Initially all three generators are operational, at time $t = 6$ Hr the 60 kW TQG which has been elected as the leader had experienced a node failure, the asset remains off-line for the duration of the simulation epoch. Because the node failure is not a planned event, it was omitted within the event schedule. The remaining contingent of generators continue to operate for an extended period of time, at which point the three transient assets

became available and are brought on-line. After the transient assets are operating, the stationary generation assets were taken off-line and become inactive for a limited amount of time indicative of scheduled maintenance. After the scheduled maintenance the two 30 kW generators were brought back on-line, the vehicle assets disconnect and become inactive, this is indicative of a patrol being dispatched. The power apportionment and leader election protocols utilize two separate event schedules, the first event schedule included information regarding current active/inactive assets, while the second event schedule included future information regarding the asset's state active or inactive. The future event schedule identifies an asset's forecasted active/inactive state with a fifteen minute look ahead. The use of both event schedules is crucial, enabling assets to be ramped up/down prior to a topology change, and also mitigates the potential for a node failure to affect grid stability.

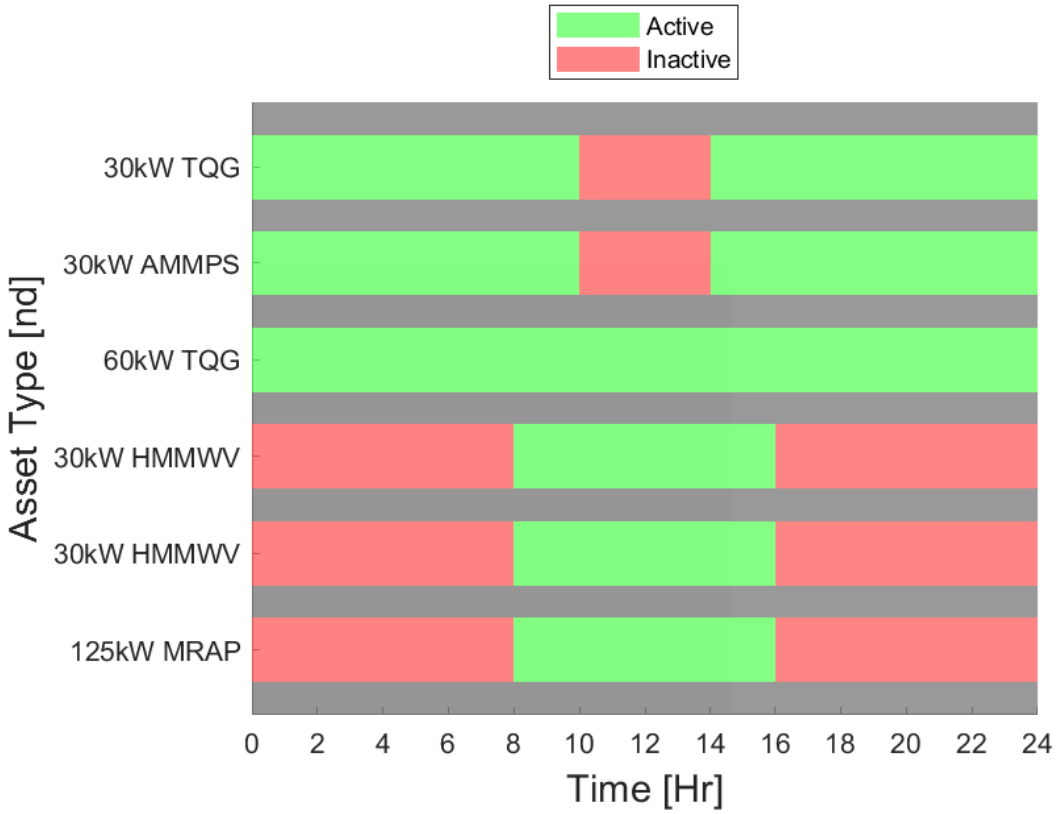

Figure 4.9: The default event schedule provided as a reference to compare the resulting event schedule which occurs within the case study, including non-deterministic events.

Using a combination of built-in *Simulink* block sets, and user defined *MATLAB* and C s-function, the *Simulink* model components were created, and can be separated into eight distinct components arranged as shown in Figure 4.10. Two of the components shown within the figure are repeated multiple times, this is to form the individual dynamic models for a generator (subsystems labeled with a 1) and a vehicle (subsystems labeled with a 2). Subsystem 3 is the subsystem which loads in predefined signals

such as the event schedule or load profile, and also computes the complex nodal admittance matrix throughout the simulation epoch. Subsystem 4 is perhaps one of the most important components of the model, this subsystem/function collects signals output from each asset, and identifies the primary and secondary leader's unique identification number and distributes it to subsystem 5, 6, and 7, enabling the leader command and communication signals to be routed correctly from the leader to the subordinates. Subsystem 5 implements the nearest neighbor algorithm, assuming a ring configuration. Subsystem 6 concatenated a vector from each source asset to construct a matrix, the matrix was passed to the elected leader. The matrix constructed in this subsystem contains communication signals used to conduct the handshakes between the leader and the subordinates, and provides additional information regarding the current state of each asset used for the power apportionment. Subsystem 7 routes the leader commands generated by the power flow agent (PFCA) to the corresponding asset. Finally, subsystem 8 extracts the updated matrix constructed by subsystem 6 after it was passed and updated by the leader, and decomposes the matrix back to a set of vectors, routed back to the originating asset allowing the handshaking process to be completed.

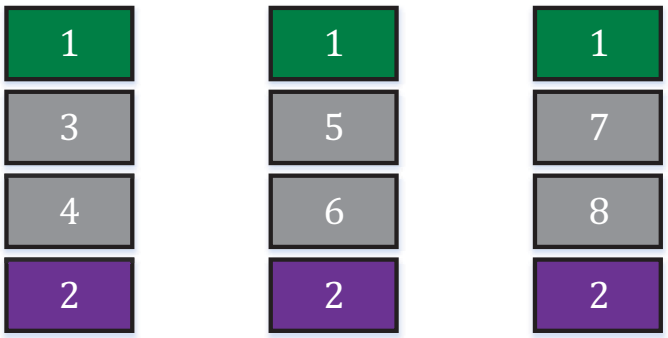

Figure 4.10: The generic architecture used within the *Simulink* model to construct the mathematical model and the communication network. The green and purple blocks represent the generator and vehicle asset blocks, while the gray blocks represent the components responsible for loading in scenario data and facilitating the appropriate signal routing.

Within each subsystem labeled with a 1 or a 2, there exists multiple C s-function which implement the various dynamics and functionality described for each asset, and a single MATLAB codded s-function which invokes the PFCA and any required communication. Each PFCA has three modes of operation, including (1) leader operation, (2) secondary leader operation, and (3) subordinate operation. The leader operation as it suggests is only invoked after an asset has been identified as a leader, and allows the asset to conduct a series of handshakes to confirm connection between the leader and a subordinate. After the handshaking process has completed, the leader was permitted to invoke the power flow. As a reminder the power flow was invoked after the handshaking process was completed. The power flow solution only considers assets which have completed the negotiation process. The secondary leader

may also conduct the handshaking process and had the ability to execute the power flow, these functionalities are only available if a node failure was identified, specifically it had to register that current leader experienced a node failure. Node failure of any other asset was managed by the primary leader. Finally there is the subordinate operation. The subordinate operation invokes a component of the handshaking protocol which was initiated by the leader. The subordinate also passes updated sensor measurement signals required by the power flow optimization.

4.5 Results

Using the *Simulink* model in conjunction with the predefined scenario, event schedules, and the individual components described previously, the model was simulated. The results collected from the simulation are provided within Figure 4.11 - Figure 4.18. The resulting event schedule which was obtained as a result of the node failure has been provided in Figure 4.11. The event schedule has been overlaid with markers indicating the selected primary and secondary leaders throughout the simulation epoch. The leader election process was initiated at known topology changes, and periodically throughout the simulation, termed rolling leader elections. Because the leader desirability criteria was based on time varying measurements such as current fuel or current state of charge, the leader desirability changes as a function of use. This ability to change the leader desirability as a function of time

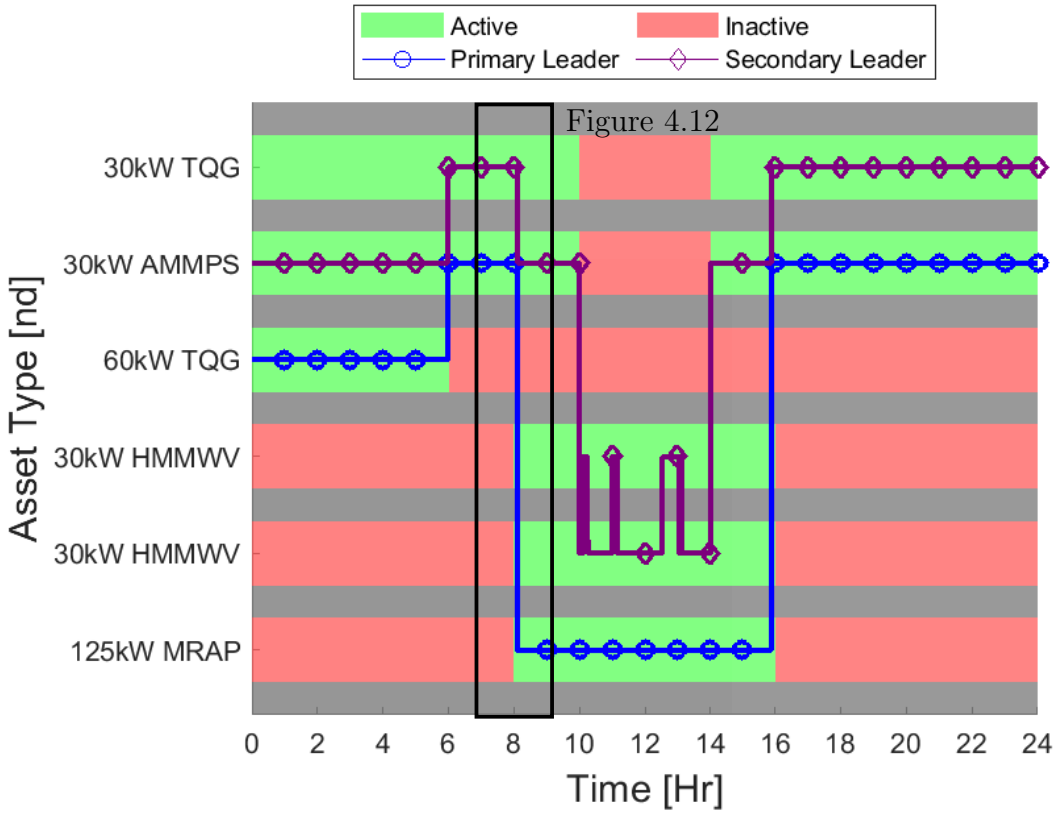

Figure 4.11: The resulting event schedule amended to include the unexpected node failure overlaid with the elected primary and secondary leader.

leads to the potential for the primary and secondary leader to change. This type of behavior can be seen upon observation of Figure 4.11, specifically focus on the time interval of $10 - 14$ Hr. Notice that throughout this epoch, one of the two HMMWVs are continuously being identified as the secondary leader. This behavior only occurs during the epoch, where the vehicles are the only active assets. If both vehicles and generators are active, and a vehicle was elected as a leader, the stationary asset with the highest desirability to lead was identified as the secondary leader. If no stationary assets were active, the vehicle with the next highest desirability to lead

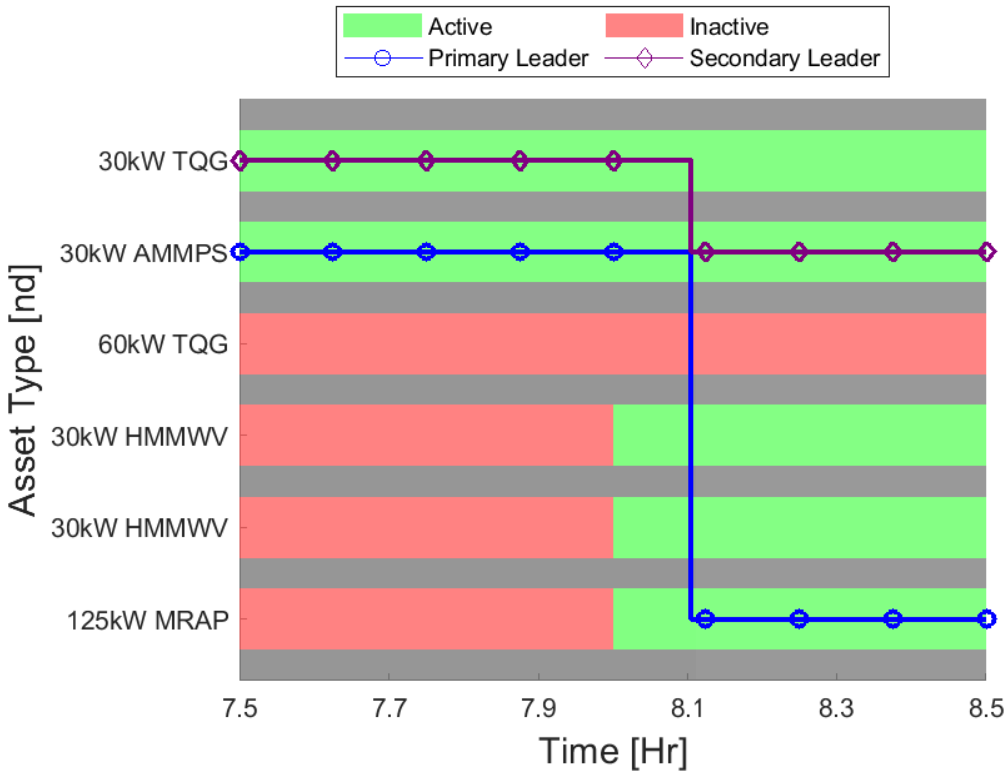

Figure 4.12: The event schedule centered around a topology change. Not long after the topology change, a vehicle was elected to be the primary leader, the secondary leader was then identified to be a stationary asset, i.e. the former primary leader.

was identified as the secondary leader. This type of behavior was implemented to mitigate the potential for power flow interruptions should a node failure occur. If a node failure occurred simultaneously for both the primary and secondary leaders (more likely to occur for transient assets), the grid would be forced into a state in which insufficient generation assets could be allocated. Throughout the simulation epoch multiple topology changes occur. Immediately following a topology change, any newly connected assets must first complete a series of handshakes. The hand shaking protocol was implemented to ensure that the newly connected asset and

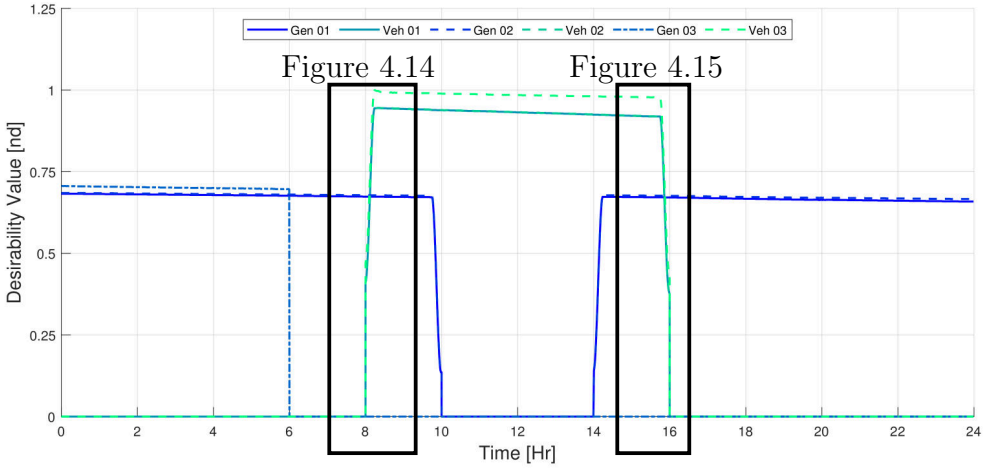

Figure 4.13: The individual assets desirability to become a leader throughout the simulation. Notice that when assets are ramped up/down, the assets desirability to lead was affected. The process forces assets which are soon to be disconnected/connected to look less/more desirable, skewing the leader election to elect assets which are active for longer periods of time. Let it also be known that because of the leader selection criteria, vehicle based assets tend to have a higher desirability to lead due to the presence of both mechanical and electrical components which can be used to provide electrical power to the AC distribution network.

the leader of the assets were synced. Conversely, if an asset becomes disconnected, the leader must also identify the asset has failed to communicate and cease communication between the assets. Once the hand shaking protocol concludes, the asset were permitted for use within the optimal power flow apportionment strategy. If the asset recently completed the connection process, the primary leader ramps the asset up as a function of the assets rated power. For subsequent rolling leader elections, the assets desirability was also ramped up based on the future event schedule. This type of behavior can be seen in both Figure 4.13 and Figure 4.14. As the leader desirability increases for a newly connected asset, the asset becomes more desirable to lead, if the desirability surpasses the current leaders desirability to lead which occurs

at $T \approx 8.1$ Hr a new leader was elected. Alternatively proceeding a topology change in which assets were forecast to be disabled or depart, the ramp down functionality was applied, this type of behavior is visible as shown in Figure 4.13 and Figure 4.15. When a vehicle was identified as the primary leader, a generator was elected as the secondary leader and not another vehicle, this behavior is shown in Figure 4.12.

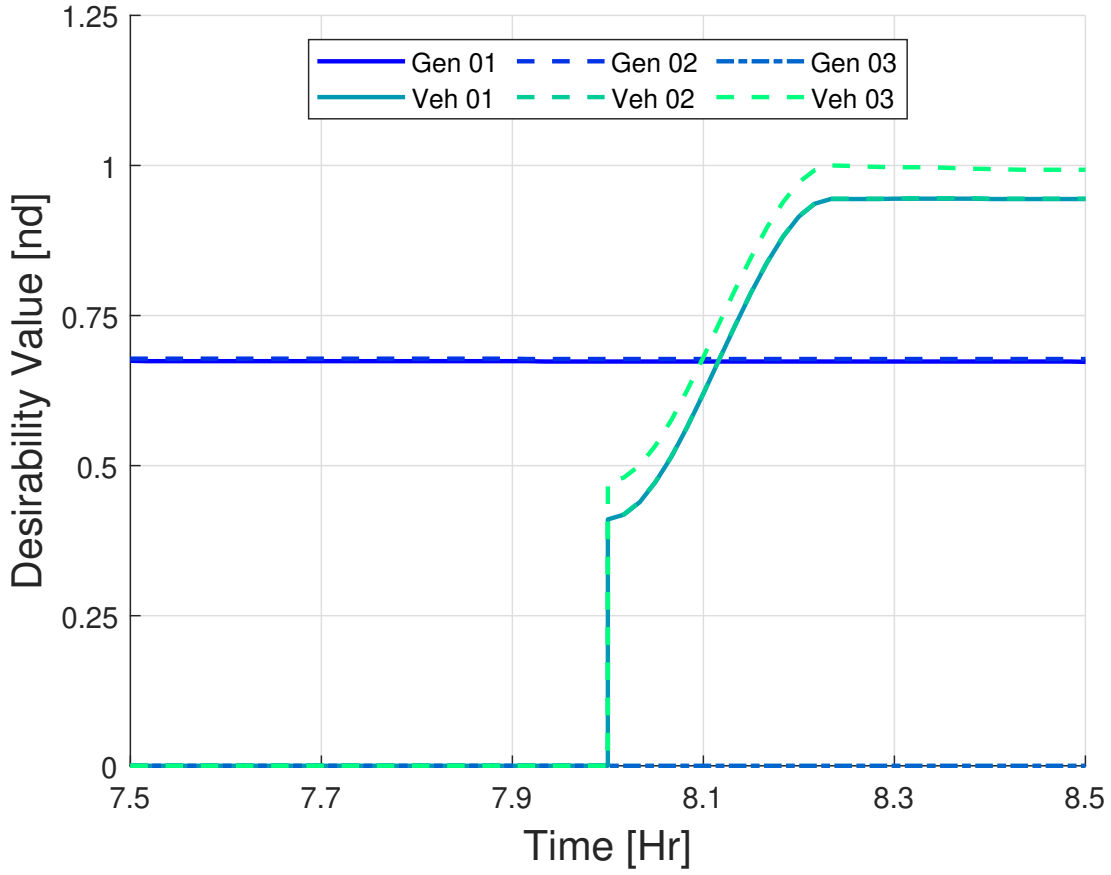

Figure 4.14: The leader desirability metric, centered around a topology change in which new assets are connected to the grid. Notice, as the simulation progresses the desirability of a vehicle to lead gradually increases, primarily due to the transition smoothing algorithm being applied to gradually allow the vehicle to provide greater electrical power to mitigate voltage fluctuations. Eventually a vehicle's desirability to lead exceeds current primary and secondary leader's desirability, resulting in a leader change where one of the vehicles was elected as the primary leader.

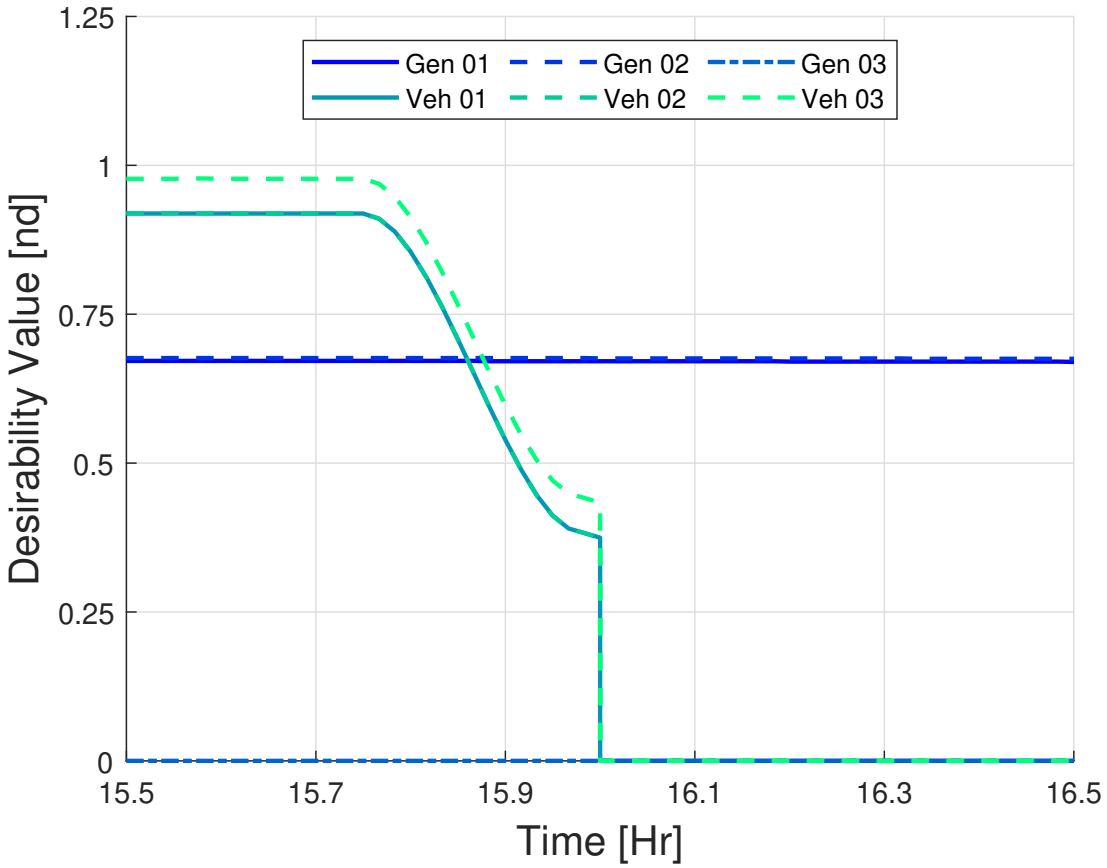

Figure 4.15: The leader desirability metric, centered around a topology change in which new assets are preparing to disconnect from the grid. Notice, as the simulation progresses the desirability of a vehicle to lead gradually decrease, primarily due to the transition smoothing algorithm being applied to gradually limit the vehicle to provide minimal electrical power to mitigate voltage fluctuations. Eventually the vehicle's desirability to lead drops below a subordinate's leader desirability value, resulting in a leader change, where a generator becomes the primary and secondary leader.

The remaining figures to be analyzed include Figure 4.16 - Figure 4.18, the figures contain information pertinent to the power apportionment strategy implemented by leader of the assets. From analysis of Figure 4.16 and Figure 4.17, it was determined that the contingent of generation assets was able to meet both the active and reactive power commands throughout the vast majority of the simulation. Immediately

following load changes, the optimal power apportionment routine was invoked to re-optimize subject to the new load conditions. New load conditions require new voltage set-points, without which insufficient power may be generated by the generation assets, resulting in load deficits. Following a topology change in which multiple asset become connected and have finished the hand shaking protocol, the leader ramps up the asset to allow the asset to provide electrical power. Conversely, prior a topology change, the leader ramps down the asset to the point in which it no longer exports electrical power to the grid, enabling the asset to disconnect without causing a power deficit or significant voltage fluctuation. The leader uses information about the assets rated power in addition to the anticipated time in which an asset was predicted to be available which was limited for a fifteen minute period.

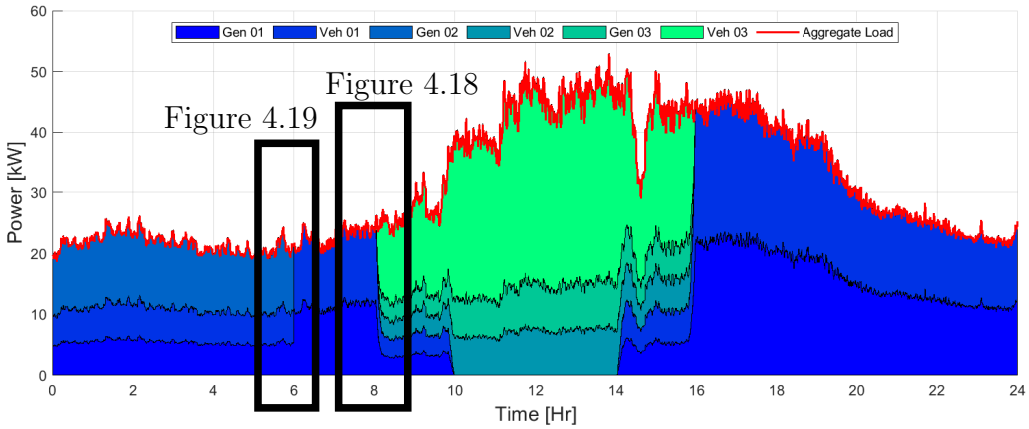

Figure 4.16: The resulting operational load profile illustrating the individual power apportionment for the individual sources. Prior too or proceeding an event, various source assets are ramped up/down via the elected leader.

When a newly connected asset completes the negotiation process, its rated power

was assumed to be zero. For subsequent leader election processes, the rated power was scaled using a cubic polynomial which ranges from zero to one, over an assumed epoch of fifteen minutes. This enables the asset to ramped up and provide electrical power. Conversely if an asset becomes disconnected, the inverse is also true, the only exception, is the asset was ramped down prior to the topology change. Figure 4.18 contains a magnified view of the active power contribution during a topology change, which illustrates the ability to ramp an asset up.

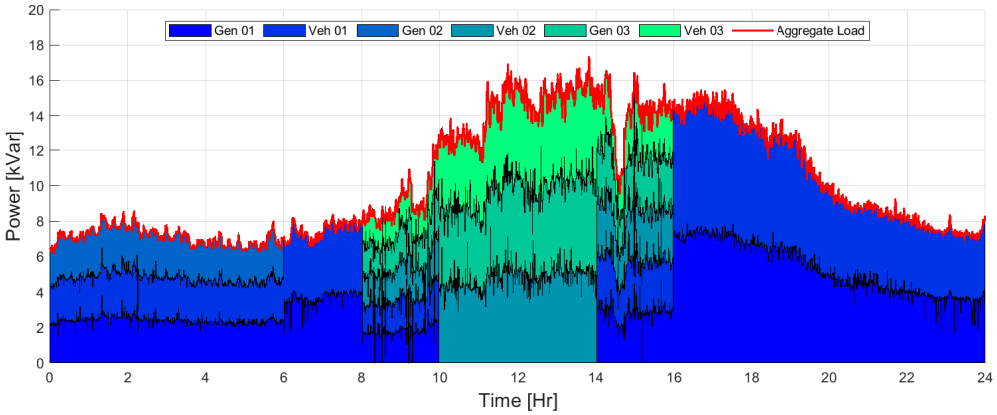

Figure 4.17: The resulting operational load profile illustrating the individual power apportionment for the individual sources. Prior too or proceeding an forecasted event, various source assets are ramped up/down via the elected leader.

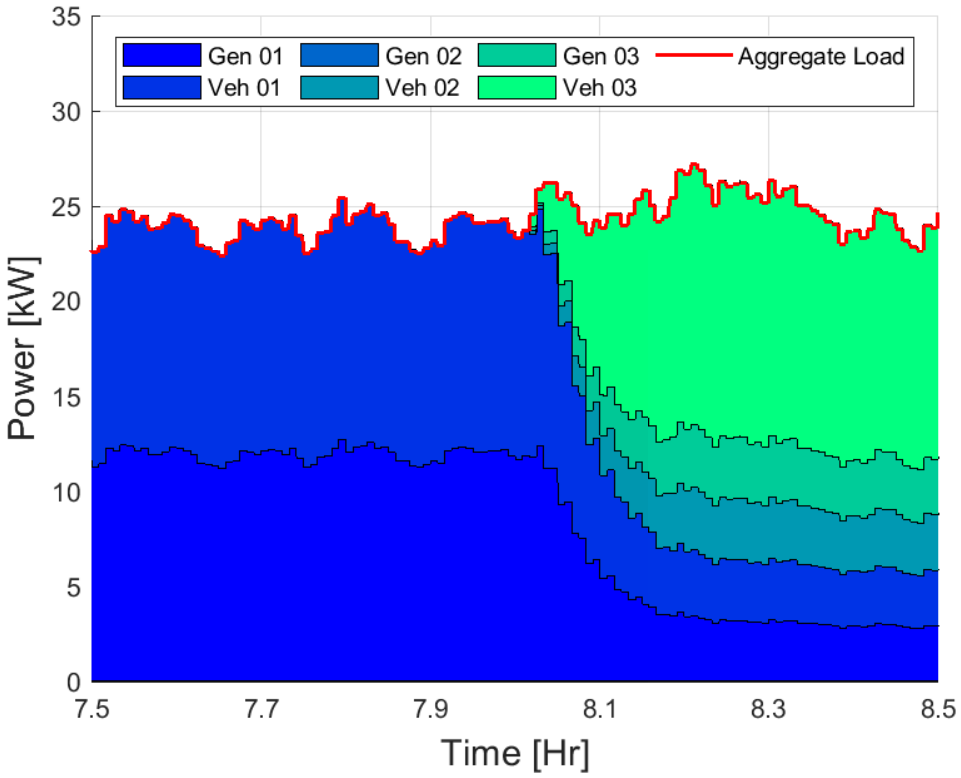

Figure 4.18: Magnification of the power apportionment centered around a connection event. The assets are ramped up within accordance with the assets rated power, scaled using the smoothing algorithm provided in Figure 4.5.

In the event an unexpected node failure, the primary leader has sufficient functionality to appropriately correct for a power mismatch however a voltage excursion may be observed. If however the primary leader experiences a node failure (Figure 4.19), the subordinates would need to first identify a node failure has occurred and then elect a new leader, however detecting a node failure may not be a trivial exercise. One option could be to simply pass the past solution to continue the operation of the grid, however this can be extremely dangerous, resulting in a load deficit. To mitigate this

type of issue our adaptive leader election protocol simply transitions from the primary leader to the secondary leader. The secondary leader then invokes the leader election process and computes a new power apportionment strategy. In order to minimize the load deficit encountered due to an unplanned topology change, the remaining assets must be ramped up to again provide the desired electrical power.

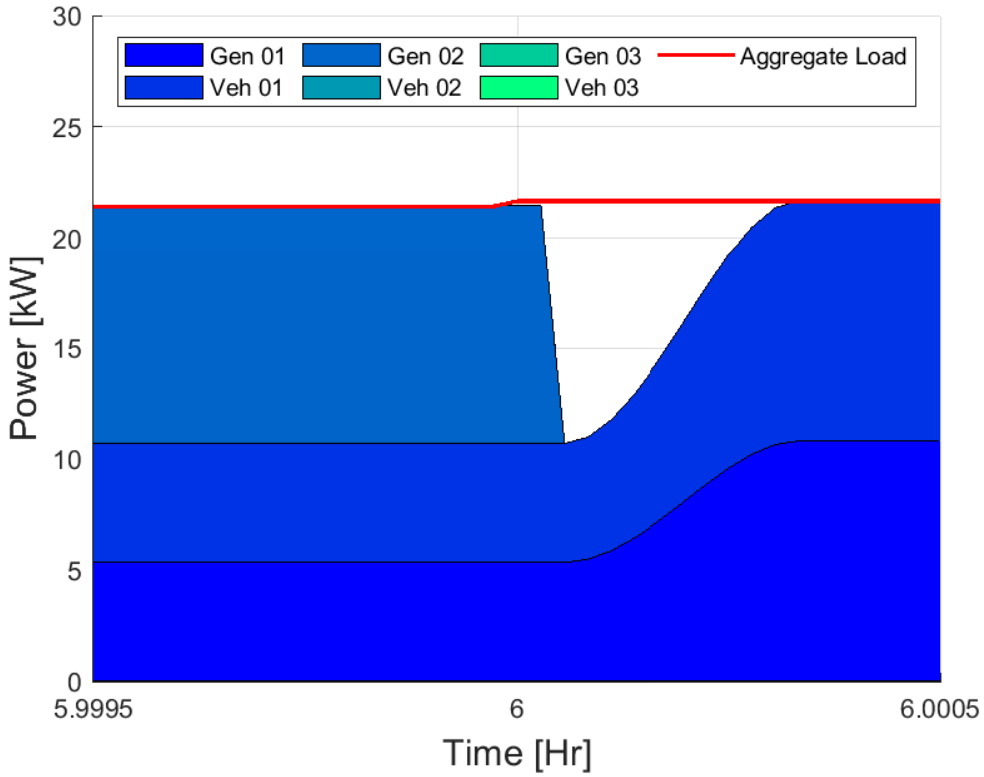

Figure 4.19: Magnification of the power apportionment for centered around the node failure. The node failure causes an abrupt power flow mismatch requiring the secondary leader to generate a new power flow solution.

4.6 Conclusions

In this chapter we established the ability to manage and control a contingent of assets for cooperative control of a microgrid using leader election. The main reason for implementing a leader election protocol was to implement a distributed control methodology, enabling heterogeneous assets to be controlled. The distributed adaptive leader election control strategy results in a resilient leader election process capable of rejecting node failures which are deterministic (insufficient fuel, or state of charge). While in theater, damage to critical components used for the distribution and flow of power are crucial to ensure uninterrupted operation. Distributing the components capable of implementing the strategies to flow power within the electrical distribution network results in a resilient control hierarchy. Further by identifying both a primary and secondary leader, should the primary leader experience a node failure the secondary leader could assume the responsibilities of the primary leader to maintain the grid's resiliency.

Using a leader election protocol, enables both stationary and transient assets to be used to service a prescribed electrical load. More efficient leader election protocols exist, which solely rely on an assets unique identification number to identify a leader among the asset pool. For this reason careful consideration of an asset's unique identification number is required. Having a constant unique ID also precludes the ability

to elect a new leader periodically assuming no topology changes occur, despite being subject to conditions which may induce a node failure. A node failure may occur for multiple reasons, including communication failure, insufficient resources available to provide grid support (fuel or charge), scheduled maintenance, or mechanical malfunction. As illustrated in Figure 4.19, node failures within an electrical grid ultimately result in some sort of power deficit, which could be detrimental for critical infrastructure. Many of the root causes of deterministic events have been identified, however deterministic events such as scheduled maintenance can be inferred from diagnostic signals, such signals would indicate that an asset may be low on fuel or operating incorrectly. If this were the case, information such as these should be factored into the leader desirability criteria used to identify a leader. It is for this reason that our leader election protocol uses information relating to planned events and diagnostic information to assess an asset's desirability to lead. This results in a time varying desirability to lead the contingent of assets. Should one of the assets identify as having minimal fuel remaining, this greatly affects the assets ability to be elected as a leader, which means a more suitable leader was likely be elected.

Further, certain assets such vehicle or electrical storage may be more adequately equipped to be a leader. For instance military based vehicles possess the ability to export/import electrical power or operate additional on-board loads making the asset a microgrid. It is for this reason that assets like storage device or vehicle may be more well equipped to handle high speed transients. These capabilities effectively

make the assets more desirable to lead, further strengthening the rational that the leader should be identified using leader desirability criteria, rather than constant unique identification number.

4.7 Future Work

The work completed thus far provides insight regarding the operation and control of a network of assets using a leader election protocol with a primary and secondary leader. Future working using the algorithm in questioned would include adding desirability criteria which includes information pertaining to computational abilities of an assets. Additionally modifying the power apportionment strategy to consider value stream impacts such as fuel consumed or energy charged/discharged. The power apportionment strategy implemented only considers the rated power of an asset and fails to consider the efficiency of the asset. It would be more beneficial to incorporate efficiency based aspects for the optimal power. This could be added into the power flow agent, or implemented in some form of a hierarchical energy management based control agent.

Both types of generation assets provided within the study require diesel fuel to operate, as such while they are fundamentally different types of assets, their own respective competing objectives are similar, which make optimization of the combined energy

usage possible. However what if additional assets were included which did not rely on fuel, perhaps photovoltaic arrays or wind turbines? Such assets have fundamentally different competing objective based functions which are hard to compare. Future work would include the ability to harmonize a set of heterogeneous assets with multiple competing objective functions. We also intend to generalize the energy network to enable a more agnostic interpretation of the individual assets to include a more diverse contingent of assets.

Chapter 5

Using Meteorological Forecasts to Improve Microgrid Performance

[1] In Chapter 4, a distributed centralized control architecture was presented which used an adaptive leader election protocol to elect a primary and secondary leader. The primary leader is charged with generating an optimal power flow solution using data provided from the subordinates to archive minimal fuel consumption. Object oriented programming techniques were used to generate the centralized control algorithm distributed amongst each asset. Further adaptive leader election criteria was coupled with rolling leader elections to continually identify more desirable primary

[1] "The material contained in this chapter is in preparation for submission to *IEEE Transactions on Smart Grid*"

and secondary leaders, resulting in a more robust and resilient control strategy in regards to communication failures or topology changes. This chapter shifts away from vehicle aspects of tactical grid management and towards meteorological effects. A long-term energy management strategy for an AC microgrid controlled using model predictive control techniques and optimization routines is presented, with the goal of understanding the effect of weather conditions on energy management where there is significant coupling between the grid's thermal and electrical loads.

5.1 Introduction

Microgrids are electrical energy networks that have four attributes: generation, storage, loads, and the ability to operate independently or share power with other networks. Generation can be from multiple sources, such as diesel generators, vehicles, solar or wind. Remote and provisional microgrids are envisioned that use a mix of fossil and renewable generation assets. These applications could have electrical loads that vary significantly from day to day based on local meteorological conditions. A tactical military microgrid, whose loads are dominated by its shelter's heating, ventilation and air conditioning (HVAC) systems, is one example. Meteorological variability makes electrical load estimation and renewable asset integration a challenge requiring energy storage if the renewable assets are to be used efficiently [43] and [44]. The **energy management system** (EMS) described in this paper combines the ability

to **forecast the electrical load and power generated** by a PV array derived from **meteorological forecasts**.

A breif review of literature is provided below concerning forecasting: (1) meteorological conditions (Section 5.1.1), (2) estimated PV array output power (Section 5.1.2) , (3) and the electrical load (Section 5.1.3). Finally, energy management of a microgrid is considered in Section 5.1.4.

5.1.1 Meteorological Forecasting

Since the power generated by a PV array depends on solar radiation and its cell temperature, forecasts of these quantities enables PV output estimation which in turn can aid microgrid energy management. Reikard [45] addressed solar irradiance forecasting at temporal resolutions of 5, 15, 30, and 60 minutes. The best results were found using an Autoregressive Integrated Moving Average (ARIMA) model along with a data prefiltering scheme and the inclusion of the extraterrestrial horizon component of solar irradiance, humidity, the turbulence coefficient, the Richardson number, and cloud cover data. The accuracy of the predictions decreased with increasing cloud cover variability. Chow [46] developed a method using cloud imager data sampled at 0.2 Hz to predict solar irradiance. Validation was performed over a 2 km area using an array of pyronemters. The sky imaging technique matched the pyronmeter

measurements 70% of the time up to a 5 minute forecast horizon. The hardware performed well for identifying sudden high frequency changes; an attribute useful for an EMS requiring short term deterministic predictions.

The two previous studies considered solar irradiance prediction, similarly, the ambient temperature affects electrical load and power generated by PV sources. Aal [47] compared abductive network (AN) and neural network models to estimate hour-ahead and day-ahead temperature. The models were created using past temperature measurements. For the cases considered, the AN was more accurate than the NN. Dombaycı [48], developed a method to predict the daily mean ambient temperature using a NN. The paper's case study showed good agreement between predicted and measured temperatures.

5.1.2 PV Power Forecasting

The tie between irradiance and temperature forecasting to PV power estimation is considered next. Shi et al. [49] developed algorithms to forecast the output power of a PV array, based on weather classification using a support vector machine (SVM). Weather conditions were divided into four categories: clear, cloudy, foggy, and rainy. The results indicated that the SVM models for sunny and foggy conditions were the most accurate, while the rainy and cloudy models were more prone to error. It was

concluded that model error increased commensurate with the daily variability in the meteorological conditions. Tao et al. [50] used a Nonlinear Autoregressive network with Exogenous inputs (NARX) NN, as well as a Hottels radiation model [51] to predict PV power. The NN model was developed using a public dataset with half the data used for training and the other half for testing. The trained model predicted daily temperature trends, regardless of sky condition classifications, and showed good agreement with the measured and PV output power estimates.

Yang et al. [52] developed a multi-stage process to estimate PV output with a 24 hour horizon using historical PV output and meteorological data along with current meteorological measurements. The steps were (1) classification of weather conditions and corresponding PV output (2) within each classification, a NN was trained to predict irradiance and (3) a forecast agent was used to select the best trained model based on current meteorological data. The results showed that the proposed approach achieved better prediction accuracy over ANNs and simple support vector regression. Bouzerdoum et al. [53] developed a short term power forecasting method combining seasonal ARIMA models, and support vector machines (SVM) using electrical data from the PV arrays. This direct approach did not require intermediate forecasts of temperature and solar irradiance.

5.1.3 Load Forecasting

Load forecasting is often used in large power grids to secure the lowest cost energy. Microgrid load forecasting, as used in this paper, aids its efficient operation in terms of fuel consumption and energy storage requirements. Large grid load forecasting is discussed below that was found to be relevant to this work. Hong et al. [54] addressed the problem of generating probabilistic, long-range electrical load estimates used by regional electric companies. They showed that using hourly samples of historical electrical load and weather data improved load estimation as compared to the common practice of using monthly samples for electrical load predictions. Hernandez et al. [55] published a survey article on electrical demand predictions, focusing on model type and application. The paper considered prediction method attributes including (1) the amount of data required, (2) computational speed, and (3) prediction performance.

5.1.4 Energy Management Systems

The articles above addressed forecasting of (1) meteorological conditions, (2) PV output power, and (3) electrical load demand. If available, an EMS can exploit this information to operate a power grid to satisfy an objective such as resiliency or reduced cost of operation. Several EMS studies are presented below as an introduction

to the optimal EMS discussed later in this paper. DC Microgrid energy management was the focus of Zhou et al. [56], addressing the best use of their composite energy storage system (CESS), consisting of both batteries and ultra-capacitors. Their solution was to match the load and storage device frequency responses where loads with low-frequency content were serviced by the batteries while high-frequency loads were shifted to the ultra-capacitors.

Lu and Francois [57], developed a hierarchical microgrid energy management strategy. Energy supervision was implemented using a central energy management strategy for the microgrid, and decentralized power management for the individual generation assets. Information was passed between the two management policies, forming power and load predictions. Short-term primary power generation was achieved using droop control; while long-term planning was obtained daily using a 24-hour schedule. The long-term planning was amended every hour to account for the new storage, renewable, and generator states. The distribution of the control authority was based on time, load forecasting was conducted daily which incorporated the electricity market and Renewable Energy Resource (RES). Load management was then completed on an hourly basis, using the load forecasts, RES, and energy storage. Droop control was carried out every second, and extremely short-term (milliseconds) power balancing required use of energy storage coupled with the PV array and a micro-gas turbine.

Shi et al. [58], developed a distributed optimal energy management system for microgrids using an ideal schedule. The energy management system used a graph theory approach to identify the grid architecture. If there were multiple buses, the first one encountered was designated as a feeder with fixed voltage and flexible power injection. The system then classified the remaining buses as a load or source where sources included: (1) distributed generation (DG), (2) distributed storage (DS), (3) wind turbines (WT), and (4) PV arrays. In order to solve the nonlinear optimization problem to minimize resistive losses, the asset's local controllers (LCs) performed local power flow optimization based on local voltage and current measurements. The individual power flow solutions were passed to the microgrid's central controller (MGCC) which coordinated the individual power flows and computed a complete power flow solution. The combination of local and global optimization enabled joint energy management, and optimal asset scheduling, minimizing electrical losses, and the cost to generate and store power.

In this paper a model predictive control (MPC) based EMS is developed to minimize fuel consumption and energy storage requirements. The EMS attempted to operate the diesel generators at peak efficiency and storing any excess energy. This allowed the microgrid to operate from battery power to further save fuel. Meteorological weather predictions, using a persistent forecast were used to estimate (1) PV output power, and (2) the electrical load of the heating, ventilation, air conditioning (HVAC) or ECUs. The estimates were incorporated into a long-term optimal (LTO) optimization

routine. The energy management strategy was evaluated used four sky conditions; (1) clear, (2) partly cloudy, (3) overcast, and (4) monsoon, with a particular interest in understanding the effect of the update frequency of the persistent forecast had on fuel consumption and energy storage requirements.

The remainder of this document is organized as follows: Section 5.2 describes the model components needed by the EMS, Section 5.3 develops the LTO and its relationship to the energy management strategy. Section 5.4 introduces a case study whose electrical loads are dominated by meteorological conditions. Section 5.5 presents the case study results showing that both fuel consumption and energy storage requirements increase with increasing persistent forecast period and that this has some variation with sky conditions. Finally, Section 5.6 provides some conclusions and areas for further study.

5.2 Model Description

The optimal energy management strategy, described in Section 5.3, can be applied to a wide range of microgrid configurations including single or multiple bus or a network of connected microgrids. Models of the microgrid's components are needed for both implementation of the energy management strategy and for evaluating its performance in simulation. The energy management strategy apportions power flow among assets,

such as diesel generators, PV sources, energy storage units at the bus or collocated with PV, to meet the electrical loads. Electrical load estimates are also required by the energy management system. It is assumed that the net electrical load can be divided into two parts: (1) an event-based load with an available estimation strategy and (2) a weather dependent load, for example, due to HVAC climate control. This second part of the load is of primary interest in this chapter where lumped parameter models of shelters are used in the example in Section 5.4. It should be noted that other weather dependent loads could be accommodated assuming there exist models that predict their electricity consumption due to weather conditions. Furthermore, it is important that all models used by the energy management system execute sufficiently fast to be used for real-time control. The remainder of this section describes generator, storage, PV, and shelter component models used in the example of Section 5.4.

5.2.1 Generator Model

As will be seen later, the optimal energy management strategy exploits load dependent, diesel generator efficiency to reduce fuel consumption and energy storage requirements. Thus, this behavior must be captured in the generator's model where the total fuel mass burned, m, is

$$m(t) = \int_0^t \dot{m}(P_g, \vec{\alpha}_g) d\tau \tag{5.1}$$

where P_g is the generator's time-varying power output, $\vec{\alpha}_g$ is a vector of generator-specific, parameters and $\dot{m}(P_g, \vec{\alpha}_g)$ is the generator's load-dependent, steady-state mass flow rate, often characterized by a generator's flow rate versus power curve. In general the $\vec{\alpha}_g$ can be time-varying if aging effects are of interest. In the subsequent example, the microgrid contains four Tactical Quiet Generators (TQGs) [59], two rated at 30 kW and two rated at 60 kW. Their flow rate versus power characteristics [60] are modeled as shown in Eq. 5.2

$$\dot{m}(P_g, \vec{\alpha}_g) = \alpha_{g,1} e^{\alpha_{g,2} P_g} + \alpha_{g,3} e^{\alpha_{g,4} P_g} \tag{5.2}$$

where the elements of $\vec{\alpha}_g$ are determined to minimize the error between Eq. 5.2 and the generator's flow rate versus power data and are shown in Table 5.1 for the generators considered later with their corresponding plots in Figure 5.1.

Rated Power (kW)	$\alpha_{g,1}$ (kg/hr)	$\alpha_{g,2}$ (kW^{-1})	$\alpha_{g,3}$ (kg/hr)	$\alpha_{g,4}$ (kW^{-1})
30	2.896	0.031	−2.896	−0.273
60	5.793	0.016	−5.791	−0.136

Table 5.1
Parameters used for the generator flow rate versus power characteristics.

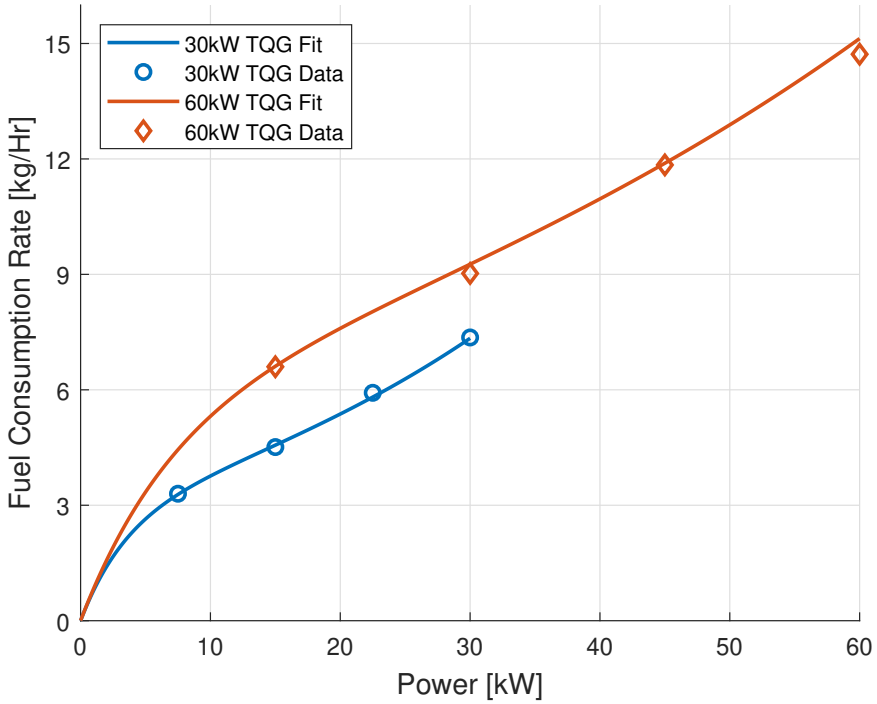

Figure 5.1: Fuel flow rate versus power curves for the 30 kW and 60 kW TQGs using Eq. 5.2 with the parameters of Table 5.1.

5.2.2 Battery Model

Energy storage is usually needed in a microgrid to make full use of renewable sources when there is more generation than load or vice versa. Distributed storage can be used, for example collocated with PV sources, to make renewable sources appear to the ESM as a consistent generator. This can also reduce resistive losses and the complexity of transmitting power to a centralized storage unit.

The energy storage model used in the ESM, shown in Eq. 5.3, is similar in form to

the generator and tracks the current energy state of the device

$$\dot{E}_s = -P_s(E_s, \vec{\alpha}_s, t) \tag{5.3}$$

where E_s is its current energy state, $\vec{\alpha}_s$ is a set of device-specific parameters, and P_s is the power entering or exiting the device. The negative sign is used to specify that power leaving is considered adding to the microgrid's power. Its dependence on E_s is required for some devices whose ability to source or sink energy depends on its energy state.

In the example of Section 5.4 two storage devices are used: (1) at the microgrid's main bus and (2) collocated with the PV array. Both devices have the same device-agnostic model shown in Eq. 5.4.

$$E_s(t) = E_s(0) - \begin{cases} \alpha_{s,1} \int_0^t P_s(\tau) d\tau, & P_s(t) \geq 0, \quad \text{(discharging)} \\ \alpha_{s,2} \int_0^t P_s(\tau) d\tau, & P_s(t) < 0, \quad \text{(charging)} \end{cases} \tag{5.4}$$

where the parameters $\alpha_{s,1}$ and $\alpha_{s,2}$ are the efficiencies for discharging and charging respectively. The values used in the example of Section 5.4 were $\alpha_{s,1} = 1.2$ and $\alpha_{s,2} = 0.8$. Since this study focuses on storage energy requirements, $E_s(0) = 0$, though not physical, its energy state was allowed to go negative. The lowest negative storage value specifies the amount of initial storage required to meet all loads during the time period considered. Similarly, the largest positive storage value specifies the

storage capacity required.

The battery model assumed an electrical current was applied, producing a voltage, thereby discharging energy stored within the battery, providing electrical power. The battery dynamics (electrical storage) were modeled after Equation 5.5-Equation 5.8,

$$V_{batt} = 300 \tag{5.5}$$

$$E_{max} = 3600\,(V_{batt})\,(Q_{batt}) \tag{5.6}$$

$$E_{lod} = E_{max}\,(SOC_0) - \int P_{lod} \quad dt \tag{5.7}$$

$$SOC = \frac{E_{max} - E_{lod}}{E_{max}} \tag{5.8}$$

where V_{batt} is the battery voltage in volts, Q_{batt} is the maximum battery capacity in AHr, SOC_o is the initial state of charge in %, P_{lod} is the induced battery load in kW, SOC is state of charge as a function of the battery is discharged/charged, and E_{max} is the maximum electrical energy capacity in Joules. The battery was assumed to be excessively large, to avoid the possibility that the individual batteries would fully charge/discharge. This attribute enabled the battery to operate within a linear voltage region of the non-linear discharge curve. Losses were lumped by assuming that 20% of the energy going into and out of the energy storage device was lost.

5.2.3 Photovoltaic Array Model

A PV array model is needed by the EMS to convert meteorological forecasts of temperature, $T(t)$ (°C), and irradiance, $G(t)$ (W/m^2), into output power, $P_{pv}(t)$ (kW). To be consistent with the fidelity of the generator and energy storage models described above, a steady-state approach is used here with the general form of Eq. 5.9

$$P_{pv} = P_{pv}(G, T, \vec{\alpha}_{pv}) \tag{5.9}$$

where $\vec{\alpha}_{pv}$ is a set of panel-specific parameters. The model used in the example of Section 5.4 was adapted from the approach of Vergura et al. [1] that used parameters typically found on manufacturer data sheets. The parameter values used here are shown in Table 5.2 and can be arranged in any convenient order to create the $\vec{\alpha}_{pv}$ of Eq. 5.9.

Symbol	Description	Unit	Value
P_s	Cell series resistance	W	180
V_{oc}^0	Open Circuit Voltage at STC	V	45
I_{sc}^0	Short Circuit Current at STC	A	5.25
V_{mpp}^0	Voltage at Maximum Power at STC	A	36.8
I_{mpp}^0	Current at Maximum Power at STC	A	4.87
$NOCT$	Nominal Operating Cell Temperature	^oC	48
$\alpha_{I_{sc}}$	Short Circuit Current Temperature Coefficient	$\%/^oC$	0.1
$\alpha_{V_{oc}}$	Open Circuit Voltage Temperature Coefficient	$\%/^oC$	0.1
N_s	Number of Series Cells	#	9
N_p	Number of Parallel Cells	#	7

Table 5.2
PV parameters used for the example of Section 5.5 with the model form of [1].

5.2.4 Dynamic Electrical Load

The total dynamic electrical load consisted of two components, (1) an Equipment Load that was time varying, but independent of meteorological conditions and (2) an HVAC Load that was also time varying and heavily dependent on meteorological conditions.

Equipment Load

The equipment electrical load varies as a function of an event schedule. The event schedule is directly linked to the individual shelter designations and shelter electrical equipment list. There were eight distinctly different shelter designations, they included (1) billeting, (2) shower, (3) latrine, (4) kitchen, (5) laundry, (6) combat operation center (COC), (7) communications (COMM), and (8) office shelters. A shelter was defined as a physical structure that contained various electrical devices, such as computers, lights, ovens, warmers, hot-water heaters, and perhaps a Heating, Ventilation, and Air Conditioning unit (HVAC). For the subsequent simulation studies, there were eighteen shelters, 8 billeting, 2 shower, 2 latrine, a single kitchen, COC, COMM, laundry, and 2 offices, resulting in eighteen different shelters. As a result of the variable shelter designations and shelter electrical equipment list, the individual equipment electrical loads for each shelter were generalized resulting in Eq. 5.10,

$$P_{equip,k} = \sum_{i=0}^{n} \alpha_{equip,k} \beta_{evt,n} P_{rated,k} \tag{5.10}$$

where $P_{equip,k}$ is the aggregate equipment electrical load for the k^{th} shelter, $\vec{\alpha}_{equip,k}$ was a vector of constants which dictate the number of distinctly different electrical equipment contained within the shelter i.e. the number of computes, phone chargers, fans, etc., $\vec{\beta}_{evt,n}$ was a binary vector, zero for inactive, and one for active, defined as the event schedule which resulted in load increases or decreases, and $\vec{P}_{rated,k}$ was a vector of constants which described the rated power for the electrical equipment.

The equipment electrical load was linked to the event schedule, the event schedule consisted of ten events; (1) shower, (2) pre-meal, (3) meal, (4) post-meal, (5) briefing, (6) training, (7) wash cycle, (8) dry cycle, (9) maintenance, and (10) supply refit event. The billeting shelters were affected by the meal and shower events, the kitchen shelters were only affect by meal events, shower shelters were affected by shower events, the laundry shelter was affected by the wash and dry cycles, the COC, COMM, and offices were affected by the briefing and training events, and the latrine shelter was invariant of all events. As a result of the event schedule which is provided within the Section 5.4.2, the internal equipment electrical load will increase, the eight distinctly different electrical equipment load profiles have been provided in Appendix B. The event schedule was assumed constant, with no uncertainty, this ultimately lead to a constant equipment electrical load for all subsequent simulation studies.

HVAC Load

As stated previously, the HVAC load was heavily dependent on the current and future meteorological conditions, resulting from the operation of an HVAC to supply thermally controlled air and maintain a desired temperature. The HVACs can operate in four separate modes; (1) off, (2) fan only, (3) heating, and (4) cooling coupled with an on-off scheme with $\pm 5\ ^{o}F$ hysteresis band around the shelter's temperature set-point. In the case studies considered below, both the mode and temperature set-points for the HVAC were held constant, and assumed to be operating in a cooling mode with a temperature set-point of $T_{set} = 63^{\circ}$ F.

The HVAC consumed power subject to,

$$P_{hvac} = \frac{Q_{rated}}{COP} \tag{5.11}$$

where P_{hvac} is the power consumed to cool/heat or run the fan in kW, Q_{rated} is the rated electrical load in kW for a respective process (fan only, cooling/heating), and COP is the coefficient of performance for the heat or cooling pump which was non-dimensional. The HVAC power was zero if turned "off"; and consumed a constant amount of power in "fan only" mode, where Equation 5.11 did not apply. As the HVAC operated, the HVAC's airflow to the corresponding shelter was governed by,

$$\dot{m}_{hvac} = \frac{\dot{Q}_{pwr}\rho}{3600} \tag{5.12}$$

where ρ is the density of air in kg/m^3, $\dot{Q}_{pwr}$ is a volumetric flow rate m^3/Hr, and $\dot{m}_{hvac}$ is mass flow rate of air in kg/s for a specific process (fan only, cooling/heating). If the HVAC was "off", the mass flow rate was zero. The corresponding temperature of the delivered air to the shelter was then,

$$T_{hvac} = T_{room} \pm \frac{Q_{rated}}{\dot{m}_{hvac}C_{p,air}} \tag{5.13}$$

where T_{room} is the room temperature in Kelvin (K), $C_{p,air}$ is the specific heat of air in kJ/kg/K, $+/-$ for heating/cooling, and T_{hvac} temperature of the air delivered to the

shelter in K. If the HVAC was operating in "fan only" mode, Equation 5.13 did not apply. The air temperature delivered to the shelter was simply the ambient temperature. The air returned to the shelter gave rise to the dynamic models representing the shelter cooling/heating effects of the HVAC, represented by the 1D heat transfer equations,

$$C_{wall}\dot{T}_{wall} = \frac{1}{R_{wall}}T_{amb} - \left(\frac{1}{R_{wall}} + \frac{1}{R_{room}}\right)T_{wall} + \frac{1}{R_{room}}T_{room} \tag{5.14}$$

$$C_{room}\dot{T}_{room} = \eta P_{equip} + P_{ocu} + \dot{m}_{hvac}c_{p,air}\left(T_{hvac} - T_{room}\right) + \frac{1}{R_{room}}\left(T_{wall} - T_{room}\right) \tag{5.15}$$

where T_{room} and T_{wall} are the room and wall temperatures in K, R_{wall} and R_{room} are the reciprocal of the thermal resistance in kW/K, C_{room} and C_{wall} are the thermal capacitance of the room and wall in kJ/K, P_{equip} is the electrical equipment power, η is the heat to electrical power efficiency which is non-dimensional, P_{ocu} is the amount of power transferred from a constant number of occupants in kW, and finally T_{amb} is the ambient temperature in K. The effects of radiation were neglected as a result of the studies completed in [61] and [62], which indicated that they would have a minimal effect on the systems operation.

As stated previously, there were eighteen shelters, of the eighteen shelters, variability was introduced by varying the thermal parameters used to model the 1D heat transfer equations, the individual thermal constants and parameters are provided in Table B.1

and Table B.2 provided in Appendix B. Of the eighteen shelters, fifteen shelters had HVACs, the remaining three did not (refer to Section 5.4.5), all HVACs were modeled as shown previously and used the parameters provided in Table 5.3.

Symbol	Description	Unit	Value
$Q_{rated,cool}$	Rated Electrical Load	kW	18
$\dot{Q}_{pwr,cool}$	Volumetric Flow Rate	m^3/Hr	3250
$COP_{pwr,cool}$	Coefficient of Performance	nd	1.5
$Q_{rated,heat}$	Rated Electrical Load	kW	10
$\dot{Q}_{pwr,heat}$	Volumetric Flow Rate	m^3/Hr	5175
$COP_{pwr,heat}$	Coefficient of Performance	nd	1.8
$Q_{rated,fan}$	Rated Electrical Load	kW	6
$\dot{Q}_{pwr,fan}$	Volumetric Flow Rate	m^3/Hr	5250
$COP_{pwr,fan}$	Coefficient of Performance	nd	1

Table 5.3
The HVAC's parameters.

5.3 Energy Management System

The EMS developed, assumed that both power generated by a PV array and the aggregate electrical load of a microgrid could be estimated or predicted provided an

event schedule and or meteorological forecasts. The predictions were then passed to an optimization routine to minimize the use of the expensive diesel fuel, while managing the electrical storage. The complete control architecture is provided in Figure 5.2.

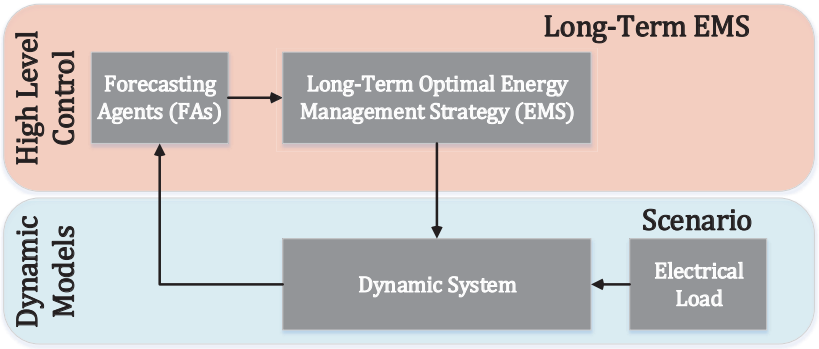

Figure 5.2: The control architecture was developed to minimize the energy use of the assets for a 24 Hr period.

5.3.1 Forecasting Agents

The energy management strategy requires meteorological weather forecasts, the forecasts were passed through two forecasting agents; (1) the load forecast agent (LFA), and (2) the renewable forecast agent (RFA). The LFA and RFA were used to predict the anticipated electrical load and the power generated by the PV arrays respectively. The models provided in Section 5.2.3 and Section 5.2.4 were used to construct the forecasting agents. The only major difference regarding the implementation of the

forecasting agents was the use of forecasts as inputs, as opposed to the measured weather profiles.

5.3.2 Energy Management Strategy

The long term optimal (LTO's) energy management policy used a model predictive control (MPC) strategy to compute long-term optimal generator and PV power set-points for the next 24 hours at 15-minute intervals, resulting in 96 evenly spaced epochs. Scalability was an important consideration in developing the MPC strategy. A typical approach was to find the 96 optimal operating points for each generator. Since the time-to-solution increased with the cube of the number of operating points, this approach was not practical due to the lack of scalability. For example, if a 2 generator grid requiring 192 solution points was scaled up to a 4 generator grid, 384 operating points are required, the time to a solution would increase by a factor of 8. Eventually, a solution would not be practical in the 15-minute window. To limit the solution space and improve the scalability of the optimization routine, each generator's fuel consumption trajectories were concatenated to form a complete fuel trajectory, which doubles as a power apportionment strategy. For the subsequent simulation studies, there were two 30 kW TQGs, and two 60 kW TQGS, the individual fuel trajectories shown in Figure 5.1 were concatenated to form Figure 5.3.

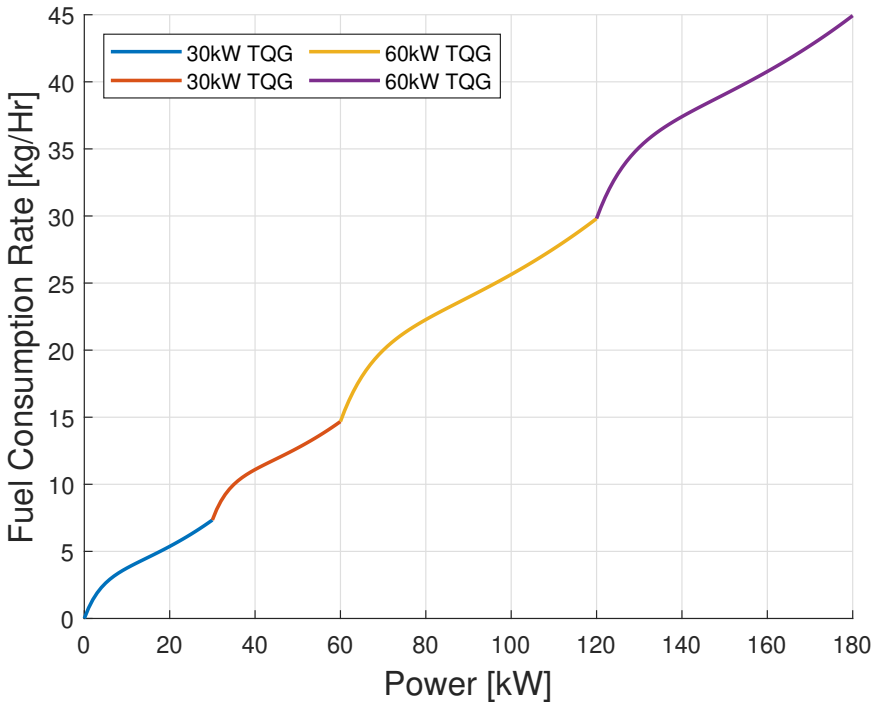

Figure 5.3: The concatenation fuel trajectories double as a power apportionment strategy. For example assume the diesel generators must provide 100 kW, using the fuel trajectory, both of the 30 kW TQGs should be operating at their maximum rated electrical power, and one of the 60 kW TQGs should be providing 40 kWs, consuming an estimated 26 kg/Hr.

Every 15 minutes, the LTO's energy management policy was executed. The meteorological forecasts for the solar radiation G_{amb} and the ambient temperature T_{amb} were collected, and passed through the forecasting agents to generate the anticipated power generated via the PV array P_{pv} and the aggregate electrical load $P_{lod} = P_{equip} + P_{hvac}$. Both the power delivered by the diesel generators P_{gen} and the power generated via the renewable asset $P_{pv,sys}$ were assumed to negatively impact the total electrical load. The quantity $P_{pv,sys}$ is the combined output power of a renewable asset which

assumed power was harnessed by both the PV array P_{pv}, and the PV's collocated electrical storage $P_{str,pv}$. If insufficient power was generated via the PV array to meet the required output electrical demand of the renewable asset, the PV storage discharged. If power was overproduced by PV array, the excess power was used to charge the PV storage. By subtracting these values from the aggregate electrical load, the resulting power delivered to or from the bus storage is computed using Equation 5.16.

$$P_{str,bus} = (P_{hvac} + P_{equip}) - P_{pv,sys} - P_{gen} \tag{5.16}$$

Similarly the power delivered to or from the collocated electrical storage of the PV array is given by Equation 5.17.

$$P_{str,pv} = P_{pv,sys} - P_{pv} \tag{5.17}$$

The optimization routine will find both the aggregate diesel generator operating points P^*_{gen}, and the aggregate output electrical power of the renewable assets $P^*_{pv,sys}$, and minimize the fuel consumed by the diesel generators using Equation 5.18,

$$J_i = \int_{t_i}^{t_f} \dot{m} \quad dt \tag{5.18}$$

where $\dot{m}$ is the fuel consumption rate in kg/Hr, which was computed using the concatenated fuel trajectory of Figure 5.3. Equation 5.18 was minimized subject to the

energy storage constraint provided in Equation 5.19,

$$E_{str,bus}(t_f) + E_{str,pv}(t_f) = E_{str,bus}(t_o) + E_{str,pv}(t_o) \tag{5.19}$$

where $E_{str,bus}$ is the bus storage energy, $E_{str,pv}$ is the PV storage energy, t_f is the final simulation time, and t_o is the initial simulation time. The storage constraint was introduced in an attempt to leave the system no worse than where it started, in-terms of stored electrical energy. The bus and PV storage energy is then computed using Equation 5.20 and Equation 5.21,

$$E_{str,bus} = \int_{t_i}^{t_f} P_{str,bus} \quad dt + E_{str,bus}(t_i) \tag{5.20}$$

$$E_{str,pv} = \int_{t_i}^{t_f} P_{str,pv} \quad dt + E_{str,pv}(t_i) \tag{5.21}$$

where $E_{str,bus}(t_i)$ is the current measurement of the bus storage's stored energy, and $E_{str,pv}(t_i)$ is the current measurement of the PV storage's stored energy. The measurements terms were introduced to allow feedback control, these terms enabled the LTO's energy management solution to correct for additional losses within the electrical network.

For the first execution of the optimization routine, a set of initial conditions was generated for the generator and PV power set-points. The initial conditions were

generated assuming any and all energy contained within the bus storage was iteratively discharged to satisfy the electrical load, until no energy remained. With no electrical energy available to service the remaining electrical load, the diesel generators were used, limited according to the generator's maximum rated electrical power. For all simulation studies, the initial conditions were generated assuming the electrical storage was empty. For every subsequent optimization, the previous optimal solutions were used as the initial conditions. As stated previously there are two design variables, each design variable was a vector of length 96 for the first execution of the optimization routine, for subsequent executions of the optimization routine, the length of each design variables decreased by one.

At the end of the simulation epoch, any deviation from the individual and the net asset's initial energy state was tabulated and used to compute the additional fuel reduction/consumption value, based on either more or less electrical storage. This assumed a single generator was operated at it's maximum rated electrical power P_{max} in kW, consuming $\dot{m}$ in kg/Hr, the time required to charge/discharge the storage was computed. Using this time, in addition to the fuel consumption rate, a fuel cost was computed. This process brought the final storage state back to the initial storage state. The computed value was used to compute the equivalent fuel consumption, which was used as an added metric to assess the LTO's complete energy management solution for a particular scenario.

5.4 Study Description

The study consisted of five components, including (1) meteorological conditions, (2) the event schedule which dictates part of the electrical load which is invariant to the meteorological conditions, (3) the resulting electrical load, (4) a meteorological forecasting methodology, and (5) the microgrid architecture. Detailed information regarding each of the five components are provided within the subsequent sections.

5.4.1 Meteorological Scenario

The meteorological scenarios consisted of four atmospheric conditions: (1) clear sky (CLR), (2) partly cloudy (PC) sky, (3) overcast (OVC), and (4) monsoon (MON) sky conditions (the monsoon scenario began with a clear sky, transitioned to partly cloudy skies, and ended with an overcast sky); see Figure 5.4 - Figure 5.7.

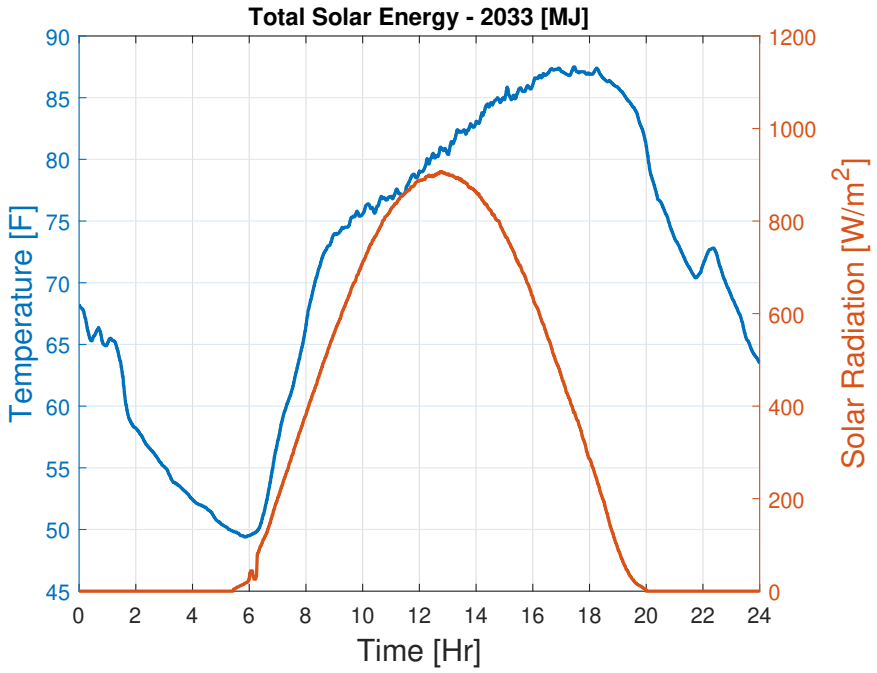

Figure 5.4: The clear sky solar radiation and temperature time series. The clear sky surface solar radiation is characterized by its consistently smooth curve.

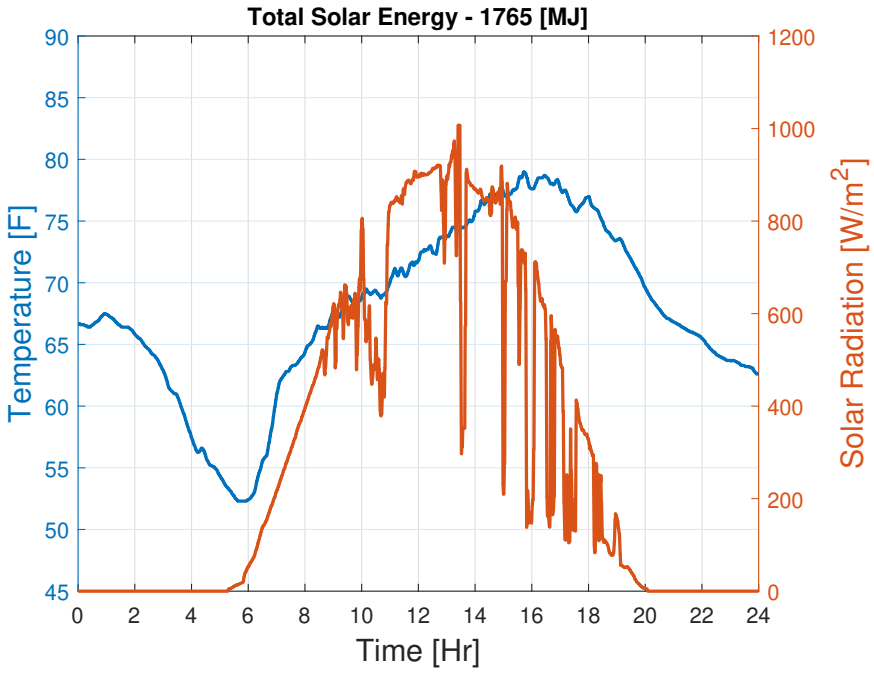

Figure 5.5: The partly cloudy sky solar radiation and temperature time series. The partly cloudy sky solar radiation maintains the Gaussian shape but include random dips representing isolated clouds obscuring direct solar radiation on the surface sensor.

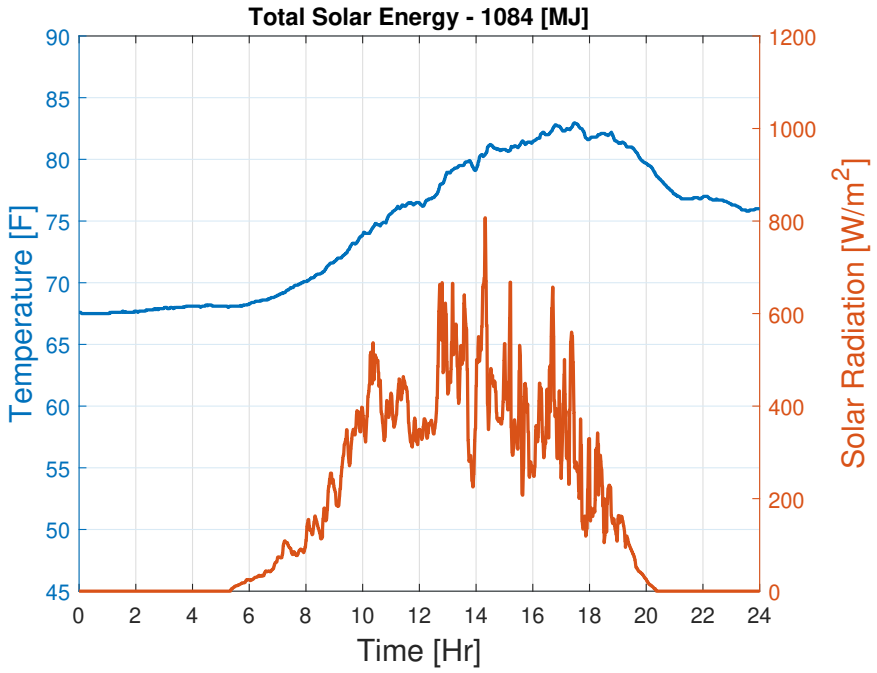

Figure 5.6: The overcast sky solar radiation and temperature time series. The amplitude of the 24 Hr, diurnal Gaussian-type curve is greatly reduced under overcast skies. The higher frequency oscillations within the time series indicate the variety of dense clouds inhibiting the solar radiation transmission reaching the surface sensor, as they traverse the sampling location.

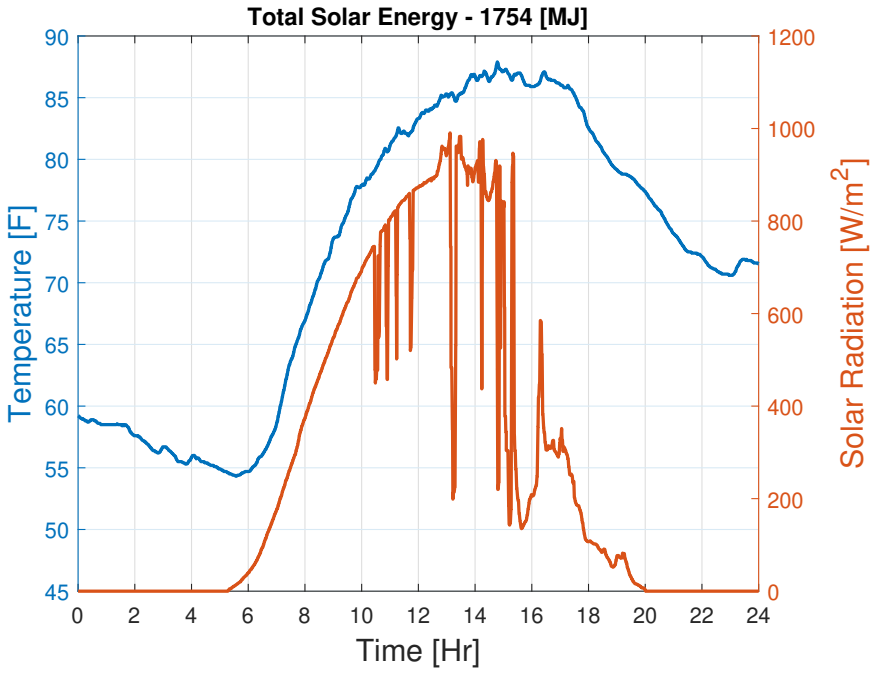

Figure 5.7: The monsoon sky solar radiation and temperature time series. The monsoon sky exhibits clear, partly cloudy and overcast conditions within a 24 Hr period. Here, the solar radiation sampled indicate early morning clear skies; as mid-day approaches, conditions transition to partly cloudy skies; by late afternoon/evening, the sky becomes overcast.

5.4.2 Event Scenario

The event scenario included ten events, the events triggered variable pulse width and height signals to become active or inactive within a shelter. The event schedule was assumed to repeat every 24 hours, and was invariant of the meteorological conditions. The event profile used for the simulation studies is provided in Figure 5.8. Both the wash and dry cycle events impact loads found within a laundry shelter, and the training and briefing events impact loads found within the communications (COM),

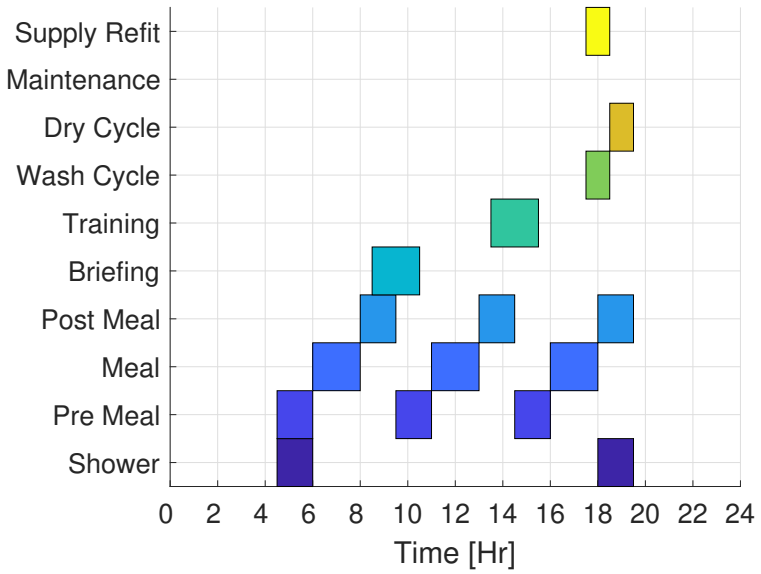

Figure 5.8: The event schedule contains ten different events, different events, which increase the electrical load within a specific shelter.

combat operations center (COC), and office shelters. The shower event impacts loads in the shower and billeting shelters, and the meal events impact loads found within both the kitchen and billeting shelters. Finally, the latrine shelters are invariant of the event schedule and have minimal power requirements.

5.4.3 Electrical Load Scenario

As stated previously, the aggregate electrical load is composed of an equipment electrical load which is invariant of the meteorological conditions, and an HVAC electrical load which is temperature dependent. For the subsequent example, the equipment electrical load was held constant, however because four different atmospheric conditions were used, four dissimilar thermal electrical loads arose, provided in Figure 5.9 -

Figure 5.12. Radiation heat transfer effects were neglected as stated in the microgrid component models of Section 5.2.4, the variable HVAC electrical load then varied from the variable ambient temperature profile.

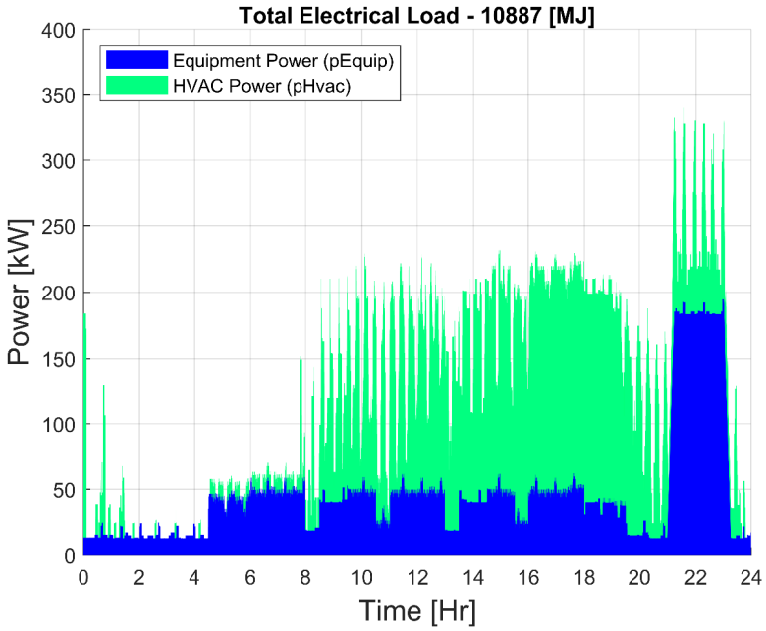

Figure 5.9: The clear sky electrical load.

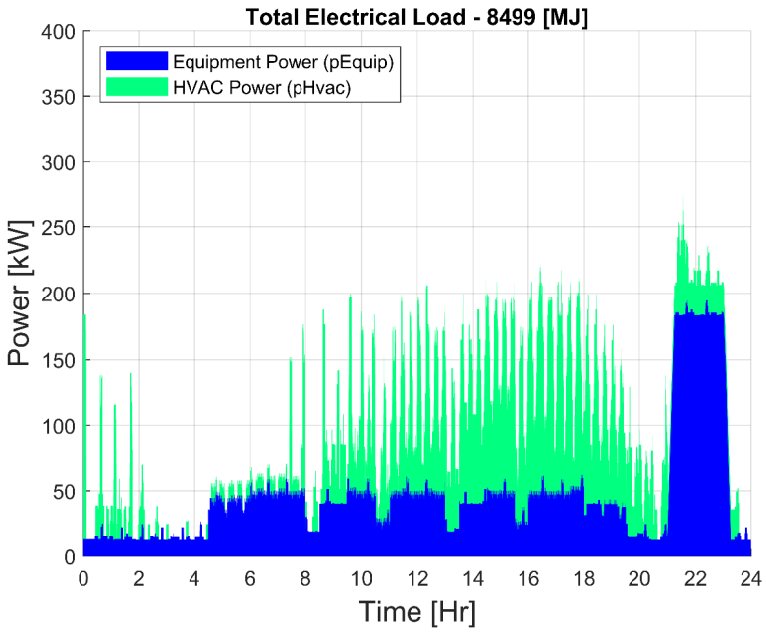

Figure 5.10: The partly cloudy sky electrical load.

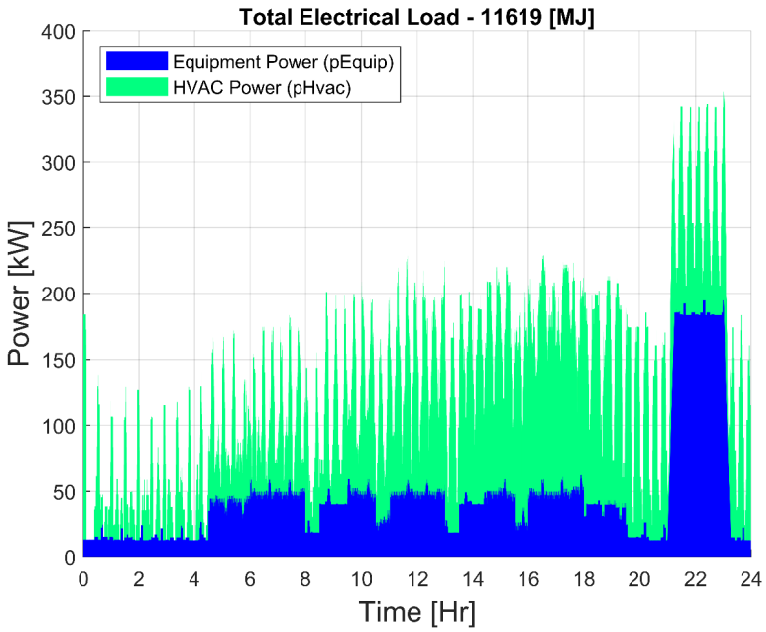

Figure 5.11: [The full overcast sky electrical load.

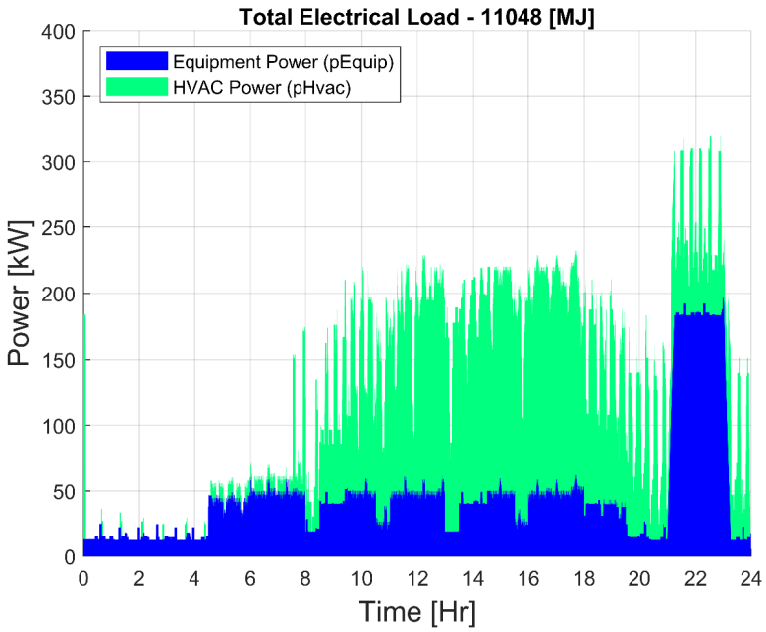

Figure 5.12: The monsoon sky electrical load.

5.4.4 Forecasting Scenario

The LTO's energy management policy required a 24 Hr weather forecast, from which the electrical load and the generated PV power was estimated. A persistent zero-order hold (ZOH) forecast was generated for each of the four meteorological conditions with variable forecast intervals. The meteorological forecast interval refers to the time duration, for which the forecasted solar radiation and temperature values are applicable. Each prediction window (24 Hr) was divided into n evenly spaced periods, based on the forecast interval. For example, a 15 Min interval meant that the forecast was divided into 96 equal-spaced intervals. While a 3 Hr forecast interval meant that

the forecast was divided into 8 equally spaced intervals. To generate a 3 Hr persistent forecast, the first meteorological sample (solar radiation or temperature) was sampled and held constant over the next 3 Hrs. The next measurement is taken 3 Hrs after the first measurement, this value persists for the next 3 Hr period. This process is continued until the full 24 Hr forecast is generated. These forecasts were generated prior to the start of the simulation. Recognizing this predictive method as a baseline, additional atmospheric forecasting techniques are being tested which are anticipated to yield more efficient energy management. Examples of the ZOH persistent forecast are provided in Figure 5.14 and Figure 5.14

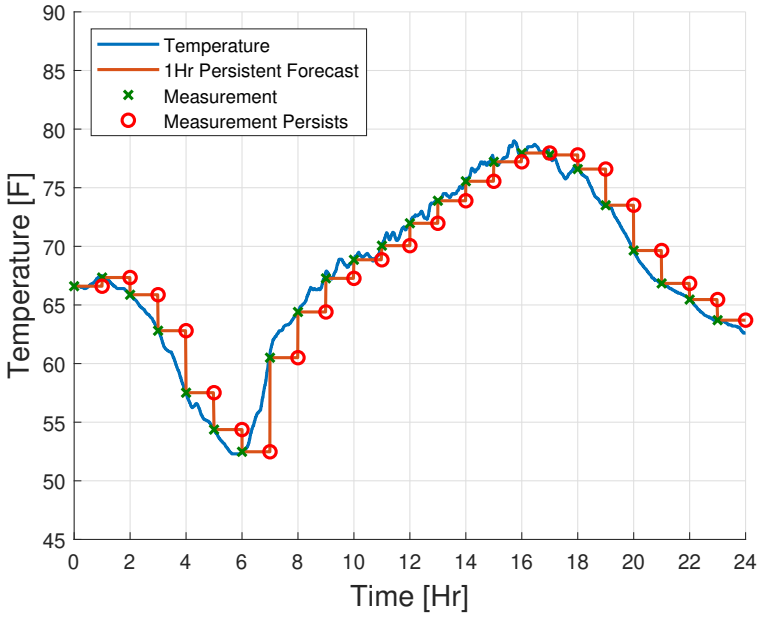

Figure 5.13: A temperature profile sampled at 1 Min, with a 1 Hr persistent forecast. Notice the measurements of the temperature are taken at predefined intervals, and the value persists until another measurement is taken. This process repeats until a 24 Hr forecast exists.

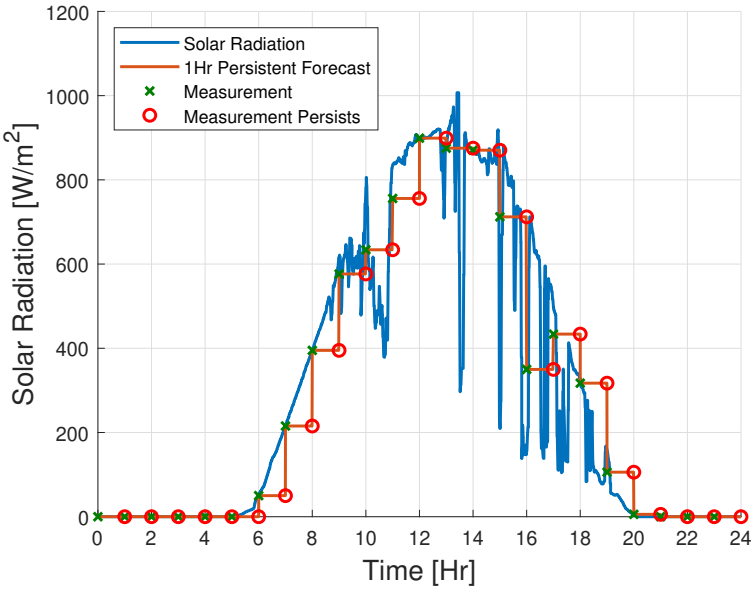

Figure 5.14: A solar radiation profile sampled at 1 Min, with a 1 Hr persistent forecast. Notice the measurements of the solar radiation are taken at predefined intervals, and the value persists until another measurement is taken. This process repeats until a 24 Hr forecast exists.

5.4.5 Electrical Architecture Scenario

The electrical architecture included two 30 kW diesel generators, two 60 kW diesel generators, four 60 kW batteries, four PV arrays each with PV storage, capable of producing 20 kW of power using Maximum Power Point Tracking (MPPT) under standard operating conditions, and eighteen different electrical loads, distributed into four microgrids. Each of the four microgrids had one generator, storage, renewable, and multiple loads. Two of the four microgrid buses had five loads, while the remaining eight loads were evenly distributed among the two remaining microgrid buses. The

microgrid buses were connected within a ring configuration, and the electrical transmission losses were omitted. The electrical architecture is provided in Figure 5.15.

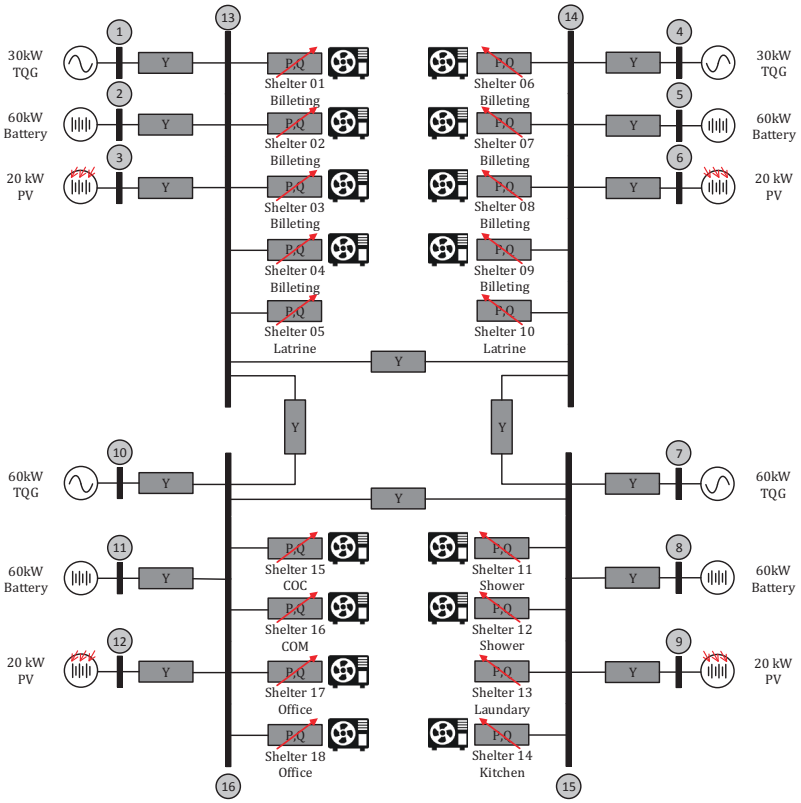

Figure 5.15: The electrical architecture which includes four microgrids, each with a single diesel generator, PV array, electrical storage, and multiple time-varying electrical loads. The presence of an HVAC is denoted using the icon located immediately to the left or right of a shelter.

5.5 Results

The results collected from the four meteorological scenarios were normalized with respect to the total electrical load energy. The resulting normalization results are

provided in Figure 5.16 - Figure 5.17. The fuel consumption results indicate that the overcast sky conditions are the least sensitive to the meteorological conditions, followed by the partly cloudy, clear, and monsoon sky conditions. Dissimilarly to the fuel consumption requirements, the total energy storage capacity results indicate that the overcast sky conditions are the least sensitive to the meteorological conditions, followed by the monsoon, partly cloudy, and clear sky conditions. Similarly to the fuel consumption requirements, the total initial stored energy results indicate that the overcast sky conditions are the least sensitive to the meteorological conditions, followed by the partly cloudy, clear, and monsoon sky conditions.

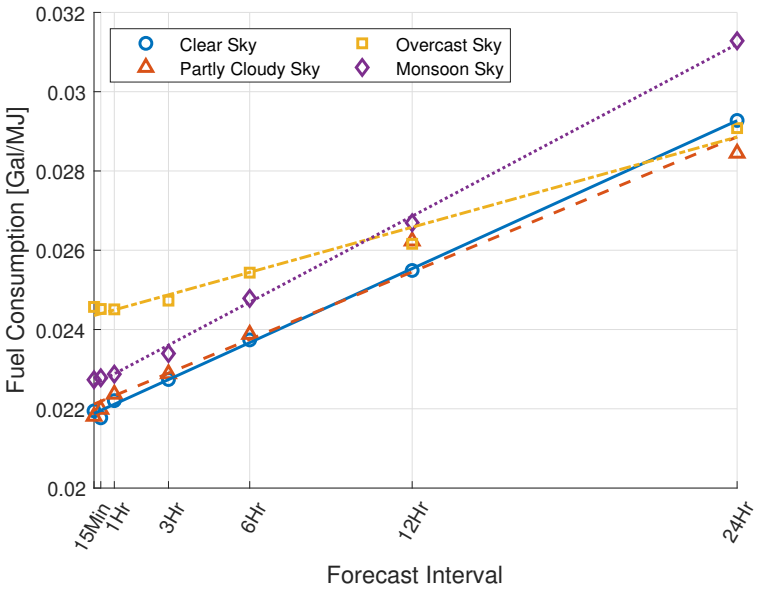

Figure 5.16: The fuel consumed, normalized with respect to the total electrical load provided in Figure 5.9 - Figure 5.12 subject to the four weather scenarios of Figure 5.4 - Figure 5.7.

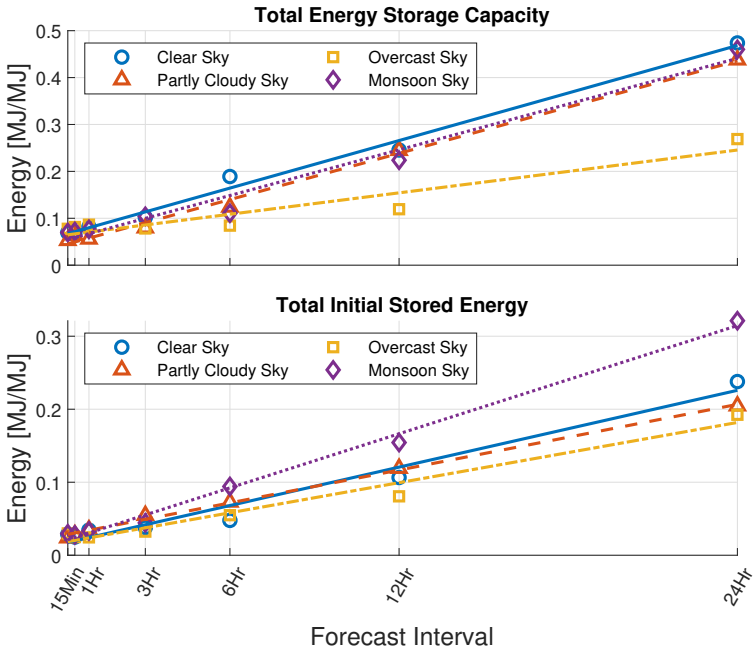

Figure 5.17: The fuel consumed, normalized with respect to the total electrical load provided in Figure 5.9 - Figure 5.12 subject to the four weather scenarios of Figure 5.4 - Figure 5.7.

The normalized figures provided in Figure 5.16 - Figure 5.17 can be used to help size the individual electrical storage requirements in addition to the fuel consumed. For example, consider a separate, alternative microgrid architecture constructed in a dry region having infrequent cloud cover. Let this scenario also include a 5000 MJ electrical load, and 1000 MJ of PV energy, both of which span a 24 Hr period, which includes the ability to provide weather forecasts separated into 3 Hr intervals. Using the clear sky fuel consumption trajectory provided in Figure 5.16, 0.0227 Gal/MJ is consumed per MJ of electrical load. Multiplying this number by the electrical load, an estimated 113.5 gallons are consumed for the 24 Hr period. Similarly, the

energy storage metrics of Figure 5.17 shows that 0.12 MJ/MJ of energy per MJ of the electrical load is required for the total electrical storage capacity, while 0.05 MJ/MJ is required for the total initial stored energy. Multiplying these values by the electrical load of 5000 MJ shows that the electrical storage capacity must be able to store a minimum of 600 MJ, and the electrical storage must contain 250 MJ of energy at the beginning of the 24 hour period. It is important to note that our battery model assumed the battery operated within a region in which the voltage remained linear. These estimates should be appropriately scaled to account for the nonlinearities of a more realistic electrical storage device.

The fuel consumption and energy storage requirements depend heavily on the forecast methodology. For all-sky conditions, as the forecast interval increases, both the fuel consumption and the electrical energy requirements increase linearly. Larger forecast intervals yield progressively less accurate forecasts, the electrical storage discharges/charges more regularly to correct for the degraded forecasts, leading to larger energy storage requirements. Greater utilization of the energy storage leads to greater initial energy storage requirements, increasing the fuel consumed.

Of the four sky conditions, the overcast sky conditions are the least sensitive to the forecast interval, while monsoon sky conditions are the most sensitive, regarding both fuel consumed and initial energy storage requirements. Both partly cloudy and clear sky conditions have approximately the same sensitivity to both metrics.

The results collected from the clear, partly cloudy, and monsoon sky conditions have similar apparent slopes for both the fuel consumption and the total energy storage metrics. This behavior was likely due in part because both the partly cloudy and monsoon sky conditions have discernible Gaussian trends, like the clear sky conditions. The lack of these features within the overcast sky conditions results in a sufficiently different slope and therefore sensitivity to the meteorological conditions.

Further, the selection of the forecast methodology is important for progressively more variable meteorological conditions. The variable meteorological conditions will yield inaccurate forecasts; Conversely, less variable meteorological conditions yield more accurate forecasts. The forecast accuracy degrades the LTO's solutions, requiring greater energy storage utilization, increasing the total storage requirements. If the meteorological conditions are less variable, more efficient operation may arise when an energy management strategy is deployed.

Using a persistent forecasting methodology leads to a reduction in the local energy storage requirements associated with the PV asset. This behavior primarily results because the generated forecasts lag the measurements. The diurnal behavior of the solar irradiance leads to more frequent charging of the PV storage prior to solar noon, after which more frequent discharging occurs. This combination limits the required initial energy storage requirements for the PV's collocated electrical storage.

5.6 Conclusions and Future Work

The primary contribution of this work was to develop; (1) the optimal energy management strategy, and (2) an approach for quantifying the effect of meteorological conditions on fuel and energy storage requirements. The individual results collected from the four distinctly different meteorological weather conditions prior to normalization with respect to the electrical load are provided in Appendix B.

The forecasting methodology and accuracy can greatly impact the performance of an electrical grid if coupled with an energy management strategy. More accurate forecasts will lead to a reduction in fuel consumption and energy storage requirements. Less accurate forecasts require greater electrical storage requirements to accommodate the less fuel optimal operation of the diesel generation assets.

Further, the forecasting methodology has a direct correlation between the meteorological conditions. The sensitivity of the forecast interval increases with an increase in the variability of the twenty-four-hour meteorological conditions. For more variable weather profiles, less optimal performance may arise if inaccurate forecasting strategies are implemented within an energy management strategy. More accurate forecasting methodologies can lead to better performance of the generation assets, yielding more optimal fuel and energy storage requirements.

The results collected illustrated that the overall fuel usage increased with increased weather forecast intervals. This observation was a function of the degraded representation of the meteorological conditions, resulting in an underestimation of the electrical load. Underestimates of the electrical load drove the energy management policy to rely on expensive diesel generators for longer periods of time, increasing the total fuel consumption. The net result was increased fuel consumption, both the maximum energy storage capacity and minimum initial energy storage requirements increased due to the larger forecast intervals.

The case studies mainly focused on the use of persistent forecasts; however, for a more complete set of results, additional forecasts were generated and tested in an alternative study. Both forecast methods were considered to be fixed, and did not include the ability to change throughout the simulation. In practice, while a day ahead forecast can be generated, the forecast would often be updated progressively throughout the day, correcting for the actual conditions. Future work includes a method to incorporate the adaptability of the forecast.

Additionally, we hope to introduce variability in regards to actuating the electrical loads to meet some prescribed minimal energy usage, while trying to further minimize energy usage by altering the HVACs temperature or mode set-point. This strategy would be achieved by harnessing the thermal capabilities of a structure used to maintain the thermal mass at a desired temperature. Energy management coupled with

predictions could enable the electrical loads to be shifted in time to yield more optimal fuel usage or energy storage.

Chapter 6

Blending of Heterogeneous Assets for Cooperative Control

In Chapter 5, an energy management strategy for an AC microgrid using model predictive control was presented. The strategy required future weather predictions, from which future electrical load and electrical generation capacity of the renewable assets were generated. Using these predictions, the energy usage of the generation assets were optimized, leading to minimal fuel consumption and minimal energy storage requirements. In this chapter, all previous research efforts culminate with the development of a method to generate optimal energy management across a set of heterogeneous assets with multiple competing objective functions.

6.1 Model Description

The primary goal of this research effort was to generate a methodology that blends a set of heterogeneous generation assets contained within a tactical microgrid. Previous research endeavors considered the use of diesel generators, vehicles, electrical storage, and PV arrays. Many of the research efforts included optimization strategies to minimize electrical losses, yielding more efficient power flow.

In this research effort, a methodology to blend a set of heterogeneous diesel generators is established in Section 6.1.1. A similar methodology used to blend a set of military grade vehicles follows in Section 6.1.2, intended to simplify the two degree of freedom fuel consumption model to a single degree of freedom fuel consumption model. A methodology to blend a set of heterogeneous diesel fuel based generation assets is provided in Section 6.1.3. Finally, Section 6.1.4 provides a method to maximize the output power of a PV array, consistent for short-term or long-term control.

The remainder of the chapter includes multiple case studies, one which illustrate the blending of the diesel fuel based assets (Section 6.2), followed by a case study to blend the diesel fuel based assets and the renewable based assets in Section 6.3. The final section contains a case study to blend a set of heterogeneous assets, using the long-term optimal energy management policy developed within Chapter 5 in conjunction

with the short-term optimal energy management policy developed in Chapter 4.

6.1.1 Diesel Generator Fuel Blending

Three phase diesel generators are designed to operate at 50 Hz or 60 Hz. The fuel consumption of the diesel generators are directly tied to the operation of the prime mover or engine, however, because of the requirement that the generator must operate at a constant frequency, the typical fuel consumption models have been simplified to a single degree of freedom, relating the output electrical power to a fuel consumption rate. Typical fuel consumption models for a generator are constructed using either a second order polynomial or third order polynomial such as the one provided in Equation 6.1,

$$\dot{q} = a_3 P^3 + a_2 P^2 + a_1 P + a_0 \tag{6.1}$$

where P is electrical power produced in kW, $\dot{q}$ is the fuel consumption rate in Gal/Hr, and a_3, a_2, a_1, and a_0 are coefficients of the polynomial which describe the fuel consumption behavior of the diesel generator. Using data from common military grade diesel generators coupled with the cubic fuel consumption model provided in Equation 6.1, approximate values for the unknown coefficients for a cubic fuel consumption model were generated, provided in Table 6.1.

Type	a_3 $\frac{gal}{Hr \quad kW^3}$	a_2 $\frac{gal}{Hr \quad kW^2}$	a_1 $\frac{gal}{Hr \quad kW}$	a_0 $\frac{gal}{Hr}$
3 kW AMMPS	-1.98e-03	1.90e-02	3.73e-02	1.20e-01
5 kW AMMPS	-1.28e-03	1.19e-02	2.66e-02	2.50e-01
10 kW AMMPS	-5.33e-05	3.09e-03	2.55e-02	3.92e-01
15 kW AMMPS	-1.58e-05	1.27e-03	4.25e-02	5.39e-01
30 kW AMMPS	-7.90e-06	7.75e-04	4.45e-02	7.91e-01
60 kW AMMPS	-5.43e-06	7.08e-04	3.57e-02	1.15e+00
100 kW AMMPS	-1.55e-06	2.15e-04	4.97e-02	1.84e+00
200 kW AMMPS	2.40e-06	-2.58e-04	1.12e-01	2.48e+00
5 kW TQG	-1.71e-03	1.60e-02	1.47e-02	2.60e-01
10 kW TQG	-6.40e-04	1.44e-02	-4.00e-02	5.00e-01
15 kW TQG	-6.32e-05	2.13e-03	4.09e-02	5.30e-01
30 kW TQG	-2.37e-05	1.69e-03	2.87e-02	8.70e-01
60 kW TQG	-2.02e-05	2.42e-03	-2.38e-02	1.74e+00

Table 6.1
Using the third order polynomial curve fit in conjunction with manufacture specifications for military type diesel generators, cubic fuel consumption model coefficients were computed.

Consider an electrical network which requires four 30 kW generators, in this case, assume that there are four 30 kW AMMPS generator variants. Due to manufacturing

differences the fuel models differ by $\pm 5\% - \pm 10\%$. For any given electrical profile, an infinite number of operating points exist which lead to sub-optimal or potentially optimal fuel use. In order to bound the infinite set of operating points, four fuel consumption models were generated, and concatenated to form a discrete fuel consumption trajectory. By concatenating each of the separate fuel consumption models to form a single trajectory, the anticipated fuel consumption of the generators could be estimated per any electrical load not exceeding 120 kW. Further for a set of n diesel generators, there are at most n factorial potential fuel consumption trajectories which could be generated, for the case in which there are four 30 kW AMMPS generators, a total of 24 distinct fuel trajectories exist, provided in Figure 6.1 and Figure 6.2.

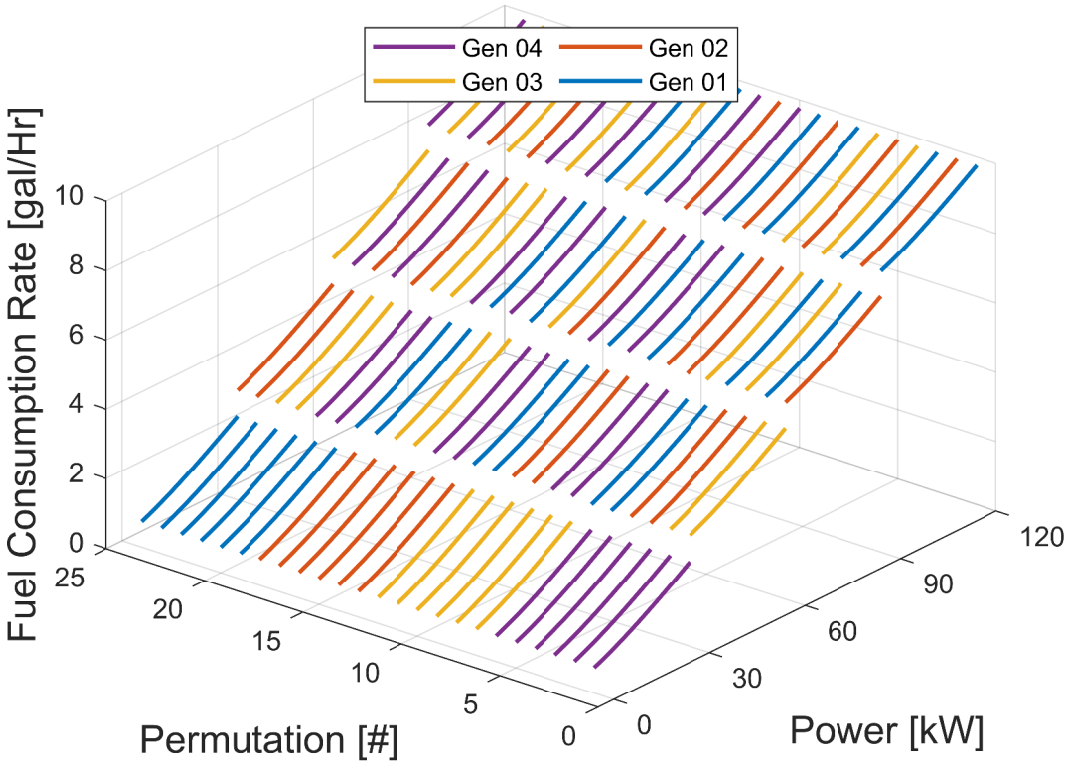

Figure 6.1: Using a permutation vector in addition to the individual fuel consumption curves for a 30 kW AMMPS diesel generator, n distinctly different fuel consumption trajectories were generated. Within the 3D fuel trajectory, the X-Axis is the generator power, the Y-Axis is the generator permutation, and the Z-Axis is the generator fuel consumption.

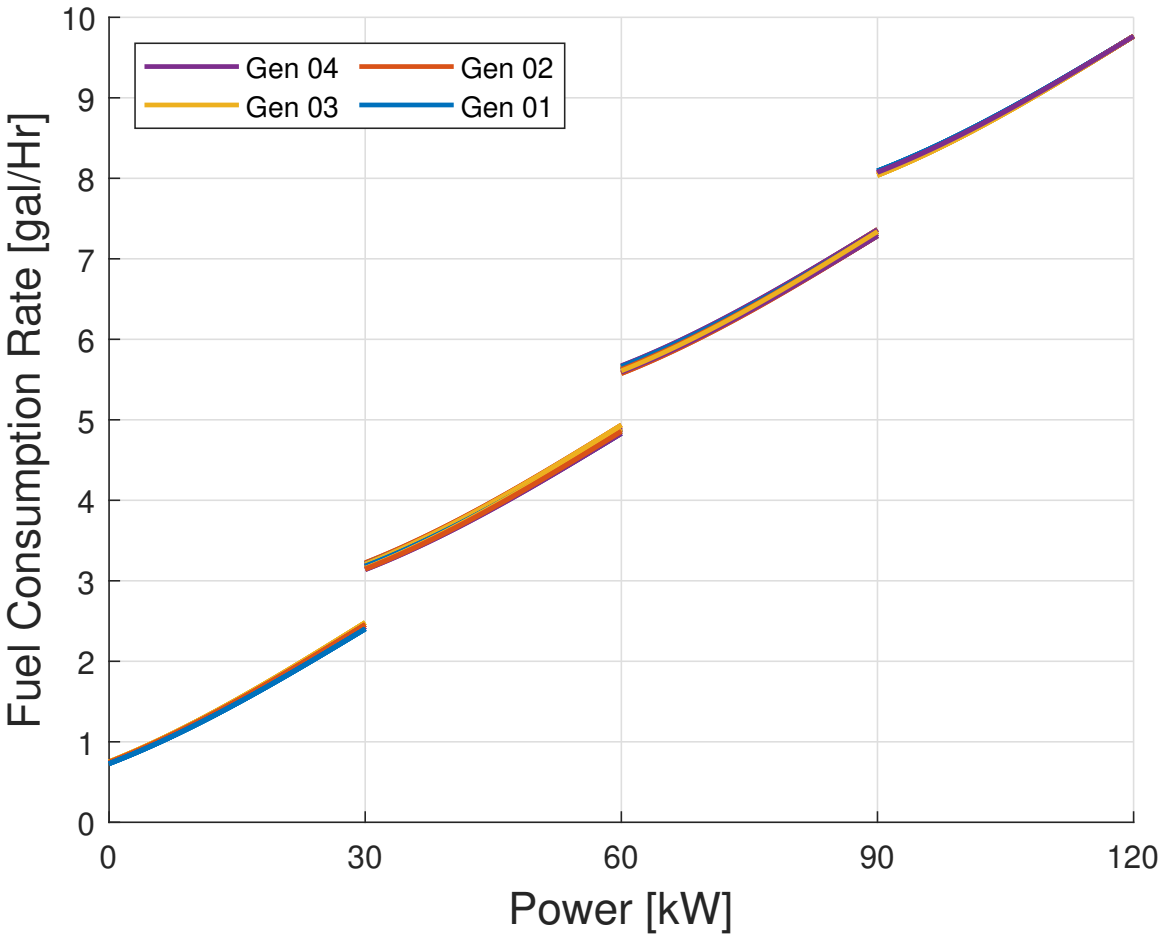

Figure 6.2: Using a permutation vector in addition to the individual fuel consumption curves for a 30 kW AMMPS diesel generator, n distinctly different fuel consumption trajectories were generated, overlaying the fuel curves on a single axes makes it easier to digest and identify the optimal fuel trajectory. The 3D surface was rotated such that you are looking directly down the Y-Axis or the permutation axes.

The fuel consumption trajectories are discontinuous at points in which additional assets must be ramped up/down per the required electrical load, for this case the transition points occur at 30 kW, 60 kW, 90 kW, and 120 kW (multiples of 30). Using the four generator variants, there exists a single fuel trajectory or precedence order

which could yield minimal fuel use. If the electrical load is such that $(0 < P_{lod} \leq 30)$ kW, generator one should be used, if the electrical load was such that $(30 < P_{lod} \leq 60)$ kW, generator one would always be running at maximum rated power, while generator four is varied. Further if the electrical load is such that $(60 < P_{lod} \leq 90)$ kW, both generator one and four should always be running at maximum rated power, while generator two is varied. Finally, for all subsequently higher electrical loads greater than 90 kW, generator one, four, and two should be used, operating at maximum power, while generator three is varied. The postulated fuel curve potentially yields an energy management policy in which minimal fuel is consumed, but is discontinuous at the transition points. At these transition points, additional generation assets must be ramped up/down as the load increases, load deficits are likely to occur during these transitional points. Most microgrid applications include electrical storage for reactive or active power compensation, which support near instantaneous injection of current. The electrical storage should be used during generator transitions to accommodate for potential load deficits and to minimize ramp up/down inefficiencies.

Now consider an electrical network which requires four generators, (1) a 30 kW TQG, (2) a 60 kW TQG, (3) a 30 kW AMMPS, and (4) a $60kW$ AMMPS. By concatenating each of the individual fuel trajectories into a single trajectory and defining a permutation array, Figure 6.3 and Figure 6.4 were generated.

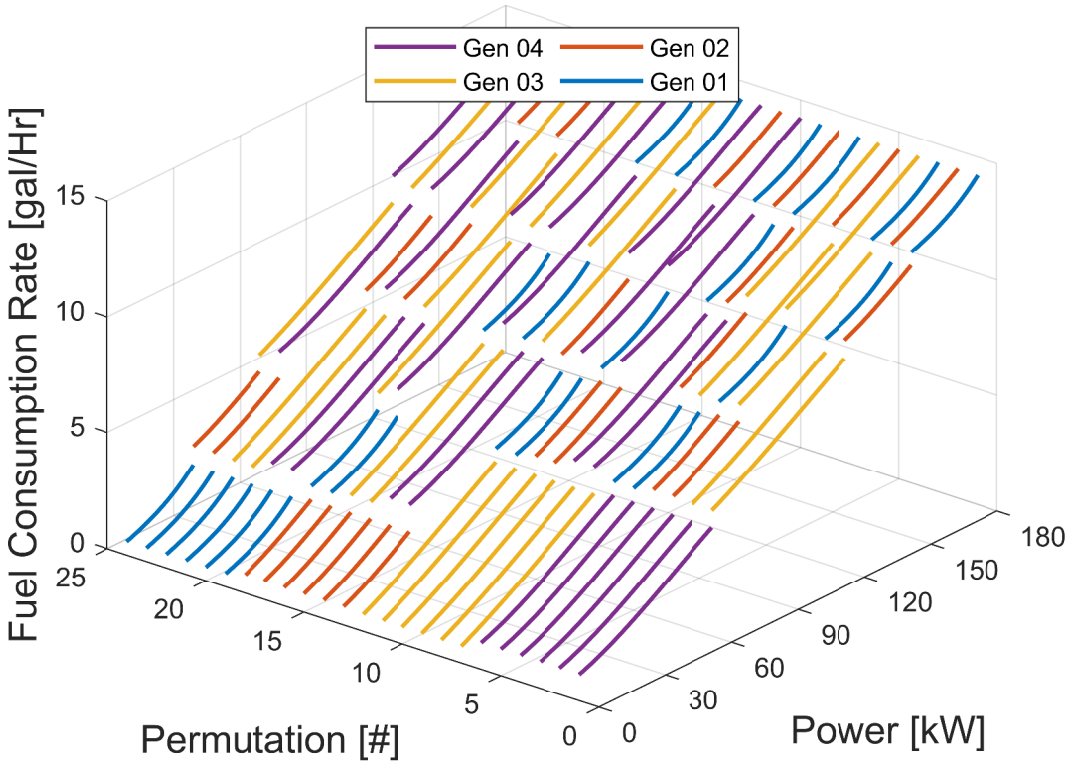

Figure 6.3: Using a permutation vector in addition to the individual fuel consumption curves for two 30 kW and two 60 kW diesel generators, n distinctly different fuel consumption trajectories were generated. Within the 3D fuel trajectory, the X-Axis is the generator power, the Y-Axis is the generator permutation, and the Z-Axis is the generator fuel consumption.

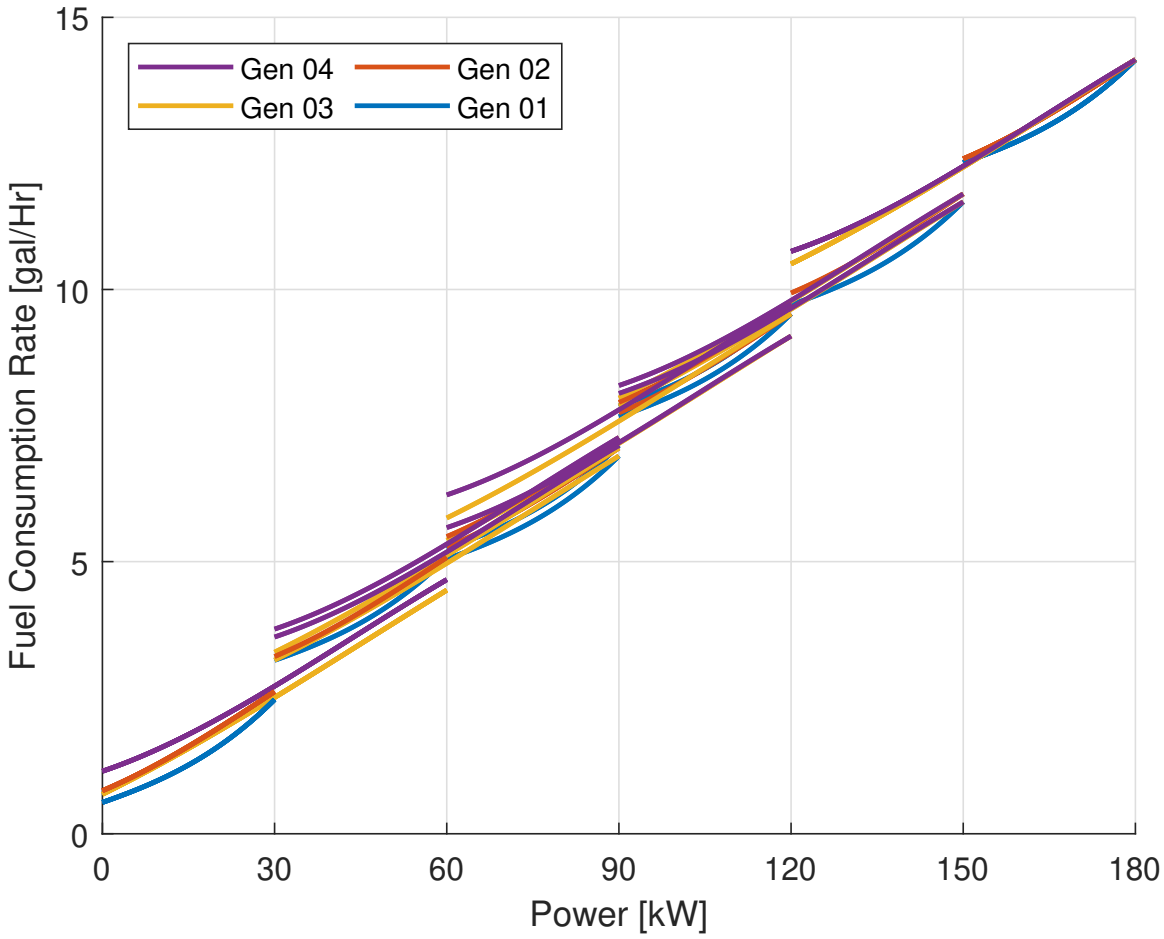

Figure 6.4: Using a permutation vector in addition to the individual fuel consumption curves for two 30 kW and two 60 kW diesel generators, n distinctly different fuel consumption trajectories were generated, overlaying the fuel curves on a single axes makes it easier to digest and identify the optimal fuel trajectory. The 3D surface was rotated such that you are looking directly down the Y-Axis or the permutation axes.

Similarly to the previously constructed fuel trajectories, a single trajectory exists which yields minimal fuel consumption, however, due to the differences regarding the rated electrical power in addition to the different manufacturer variants, the optimal fuel trajectory is difficult to identify. For instance, the transition points are

no longer constrained to occur at multiples of 30 kW or 60 kW, they could occur throughout individual fuel trajectories. One example of this occurs roughly when the electrical load is such that $(35 < P_{lod} \leq 60)$ kW, over this interval, the respective fuel curves indicate that greater efficiency is obtained if generator three is online as opposed to generator four. However, while the use of one generator is preferred for the given electrical load, the requirement that one generator has to be spun up while the other is spun down may result in less efficient fuel consumption. This type of behavior while optimal for extended operation may yield adverse effects if the electrical load continuously changes rapidly. To avoid implementing an energy management policy that would yield this behavior, a single precedence order for the contingent of generators should be selected from any of the n factorial potential trajectories, sized using the anticipated electrical load. If the total electrical load rarely exceeds 60 kW, generator four or three should always be used to established the precedence followed by generator one, the remaining two generators would be added to precedence order following generator one and three.

The optimal fuel trajectory would require multiple assets to be turned on and off simultaneously, this assumes the assets can be autonomously controlled by a supervisory controller, in reality, this is not the case, and the inability to operate the assets autonomously could lead to less optimal operation of the assets. This type of behavior could greatly affect the operation of the energy management strategy and requires additional investigation.

6.1.2 Military Vehicle Blending

Similar to diesel generators, military vehicle variants such as the MRAP, the HMMWV, or the JLTV have the ability to generate electrical power through the use of an ISG. Unlike a diesel generator that is designed to operate at a fixed speed of 50 Hz or 60 Hz with a variable torque/power, vehicles may operate with variable speed and torque, resulting in a two degree of freedom fuel consumption model. The main goal of this section was to reduce the two degree of freedom fuel consumption model to a more manageable single degree of freedom approximation. Example fuel consumption maps which vary as a function of both engine speed and torque are shown in Figure 6.5 and Figure 6.6.

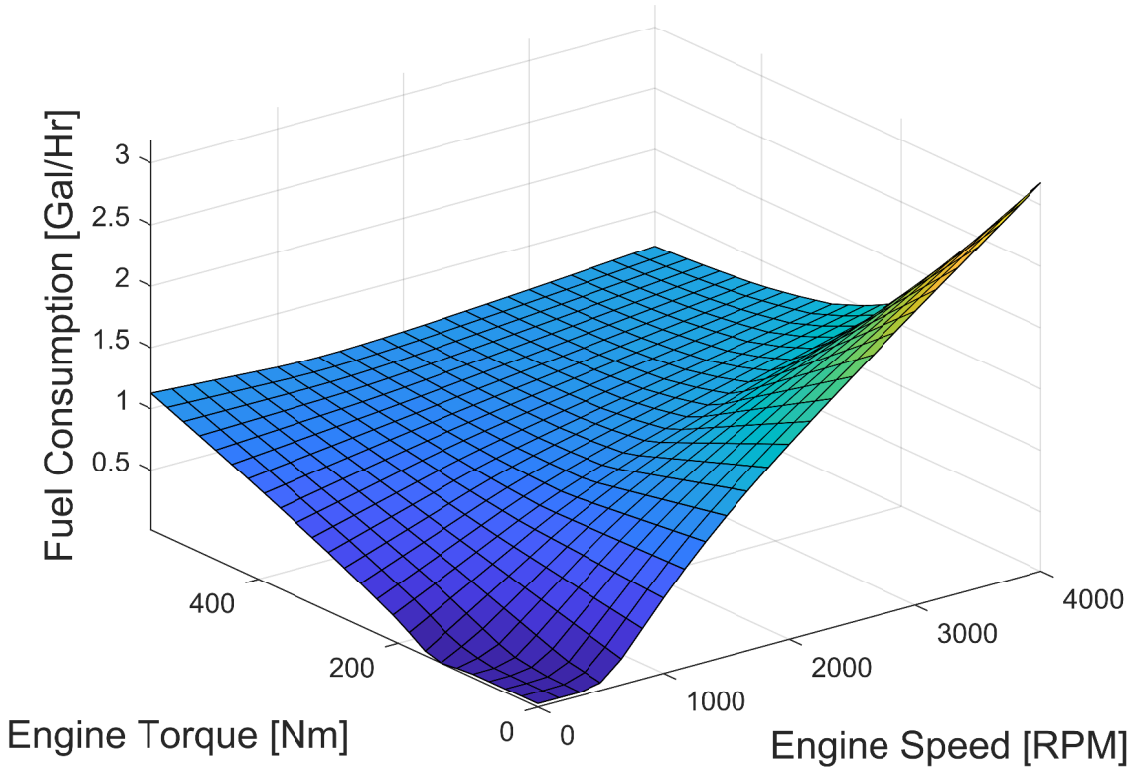

Figure 6.5: The fuel consumption for the HMMWV which uses a GEP 6.5 L 205 HP engine.

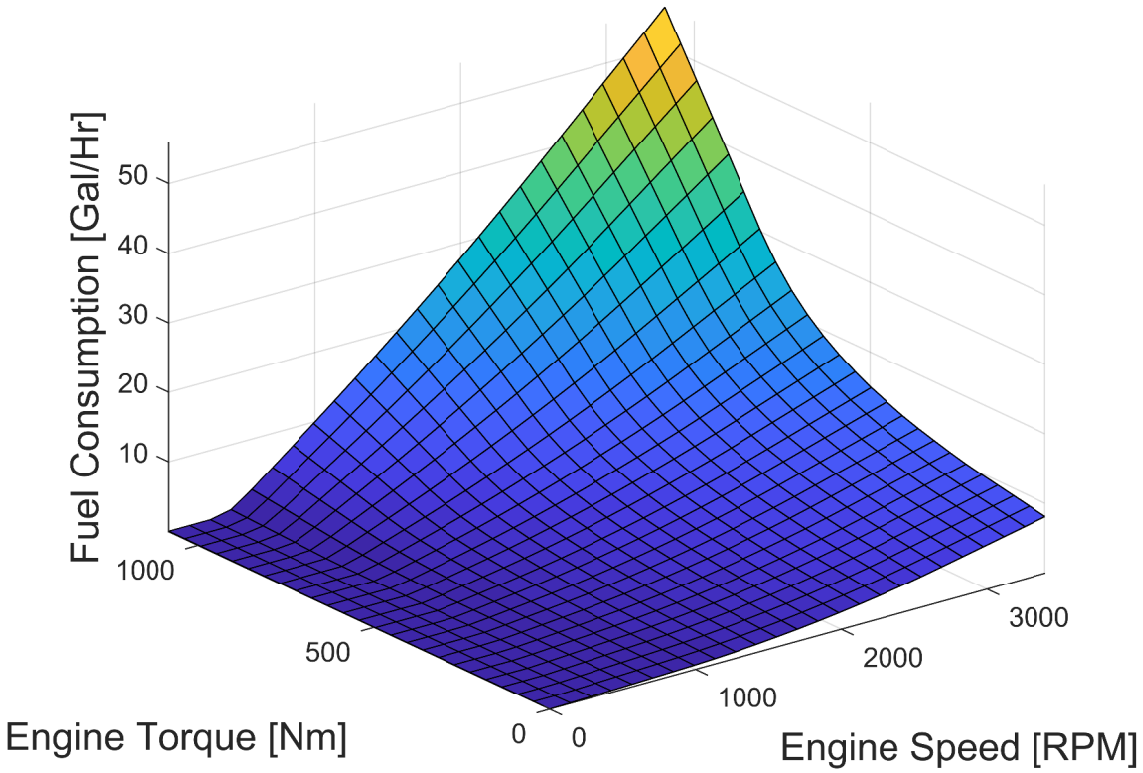

Figure 6.6: The fuel consumption for the MRAP which uses a CAT C7 350 HP engine.

The amount of fuel consumed by a vehicle is a result of the variable speed and torque required to operate the vehicle during a maneuver. If the intent is to harness the vehicle's hardware to generate electrical power, the ISG or alternator must be active. Military vehicle variants such as the HMMWV and the MRAP are capable of exporting 30 kW or 125 kW of electrical power respectively. Typical output electrical power and load torque curves for military grade alternators are provided in Figure 6.7.

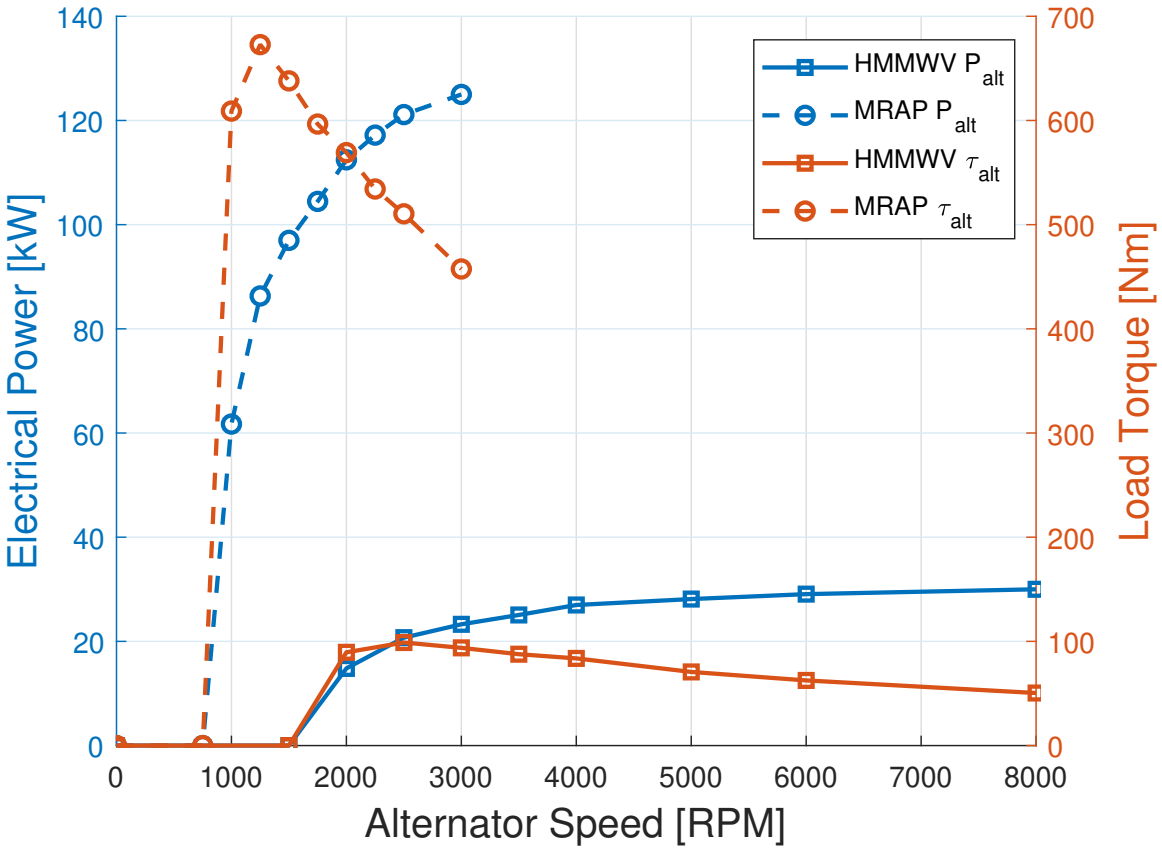

Figure 6.7: Typical alternator output electrical power and load torque as a function of speed for the HMMWV and MRAP vehicle variants.

Depending on the vehicle variant, the alternator may operate at abnormally high speeds, the likely cause of this type of behavior results from the connection between the engine (prime mover) and the alternator. Common practices used for civilian-based vehicles is to drive the alternator off the serpentine belt, this would result in a speed reduction/amplification leading to a torque amplification/reduction, and this behavior is likely to be found within an HMMWV. Dissimilar to the HMMWV, MRAP's have transmission ISGs, meaning, the engine speed is also the drive speed

of the alternator. It was assumed that the alternator's speed/torque/power (states) can be related to the engine states by Equation 6.2 and Equation 6.3,

$$\omega_{alt} = N_e \omega_{eng} \tag{6.2}$$

$$\tau_{alt} = \eta \frac{\tau_{eng}}{N_e} \tag{6.3}$$

where τ_{alt} is the load torque of the alternator in Nm, ω_{alt} is the alternator speed in RPM, τ_{eng} is the engine torque in Nm, ω_{eng} is the engine speed RPM, η is the transmitted torque efficiency which is dimensionless, and N_e is the turn ratio between the engine output and the alternator input. Using Equation 6.2 and Equation 6.3, the engine states can be represented in terms of the alternators states, this process will allow the output of the engine to be converted to the input of the alternator, which enables the output of the alternator to be approximated with regards to fuel consumption of the engine.

The power generated via the alternator is ultimately generated via the engine and transferred through the serpentine belt or output shaft of the engine to a transmission's ISG. In order to reduce the two degree of freedom fuel consumption problem to a single degree of freedom fuel consumption problem, the engine limitations must also be considered. It is common practice for vehicle or engine manufacturers to provide engine power and torque curves for wide open throttle (WOT) conditions. Provided in Figure 6.8 are approximate WOT power and torque curves for the

HMMWV and MRAP [1].

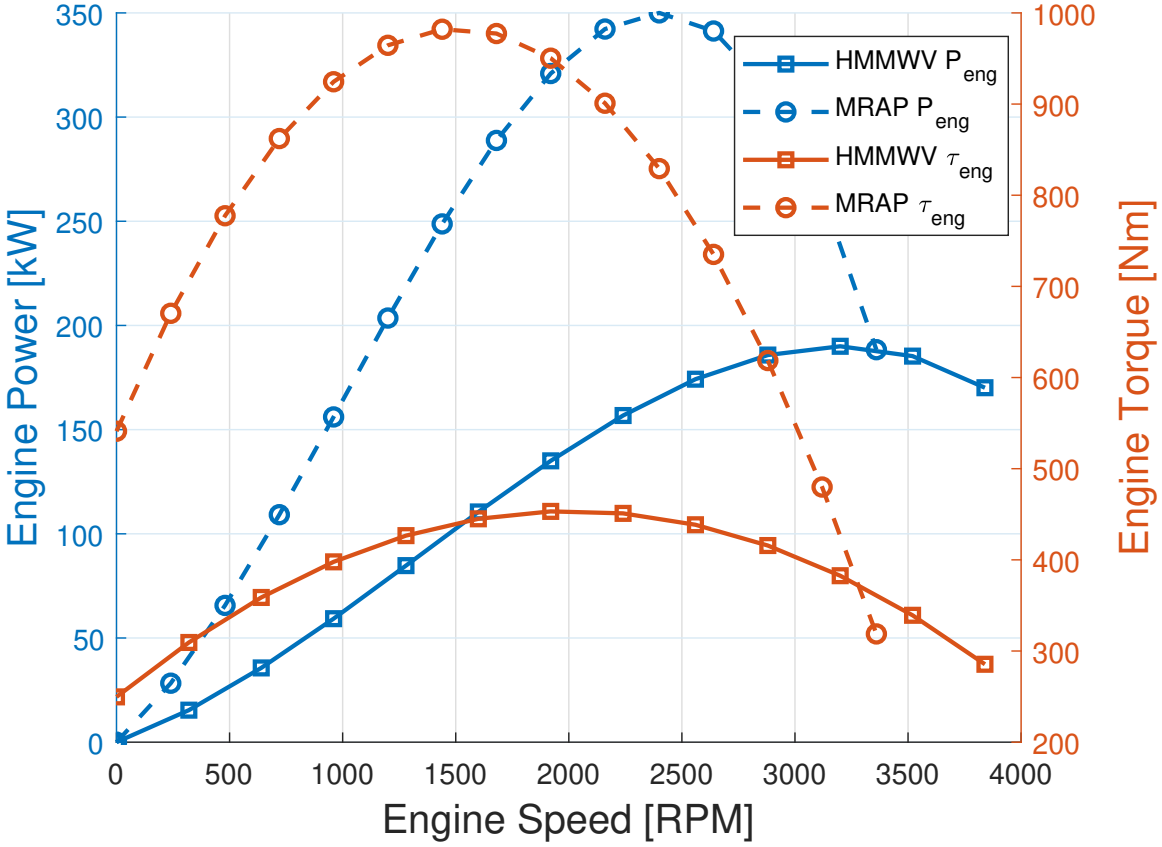

Figure 6.8: Typical engine power and torque curves at wide open throttle conditions for the HMMWV and MRAP vehicle variants.

Using the individual fuel maps shown in Figure 6.5 and Figure 6.6, a fuel fit for each of the fuel consumption maps was generated. Using the same curve fitting functionalities in *MATLAB*, WOT engine torque and power curves in addition to alternator load torque and output electrical power curves were generated. Applying Equation 6.2 and

[1]The base engine output power was scaled, manufactures specifications resulted in a WOT curve which yielded insufficient power/torque to provide 125 kW, military vehicle variants such as the MRAP may have turbochargers integrated within the respective platform to boost the available engine power/torque

Equation 6.3 to the respective curve fits and overlaying them on fuel maps, results in Figure 6.9 and Figure 6.10.

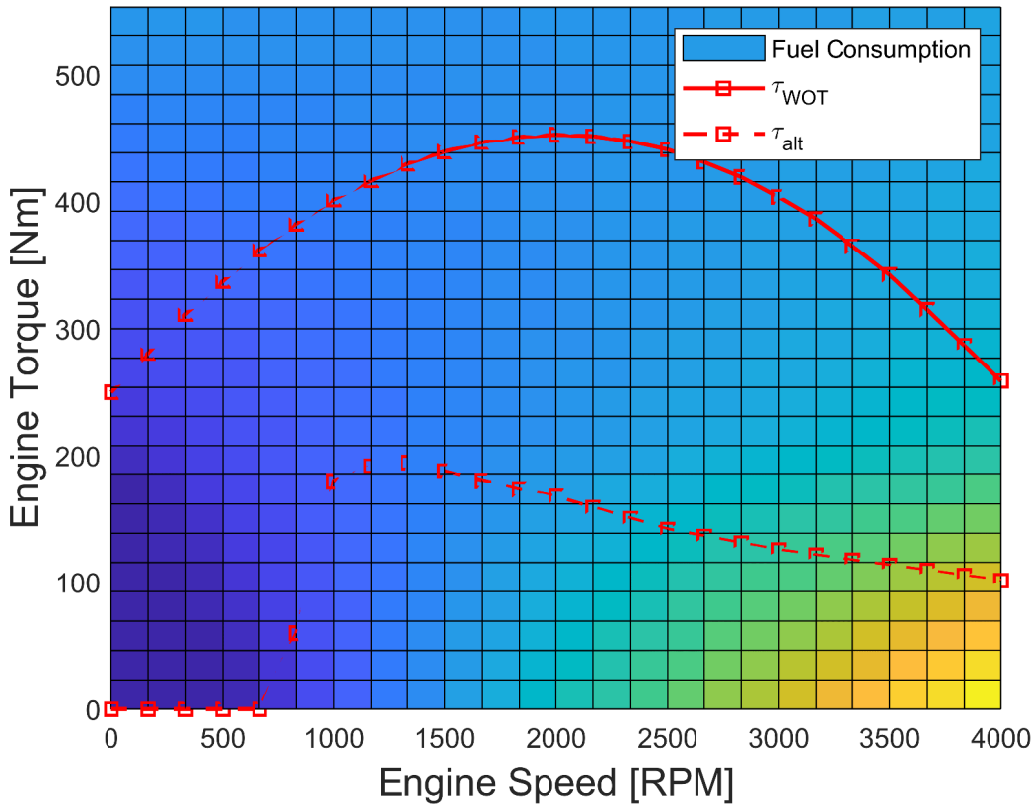

Figure 6.9: The fuel consumption map overlaid with the WOT torque and alternator load torque for the HMMWV.

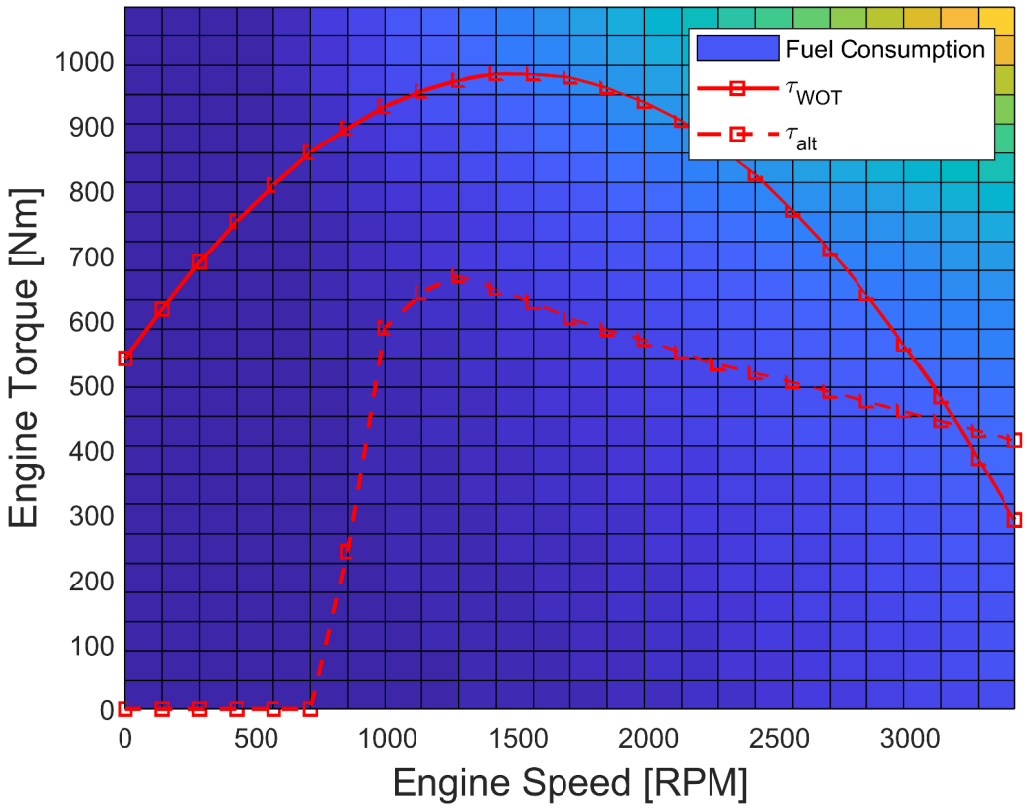

Figure 6.10: The fuel consumption map overlaid with the WOT torque and alternator load torque for the MRAP.

Similar to the diesel generators, the fuel consumption rate of the vehicle was approximated as a function of the output electrical power. The concatenation of the vehicle fuel consumption curves was arranged with a single HMMWV followed by a single MRAP provided in Figure 6.11.

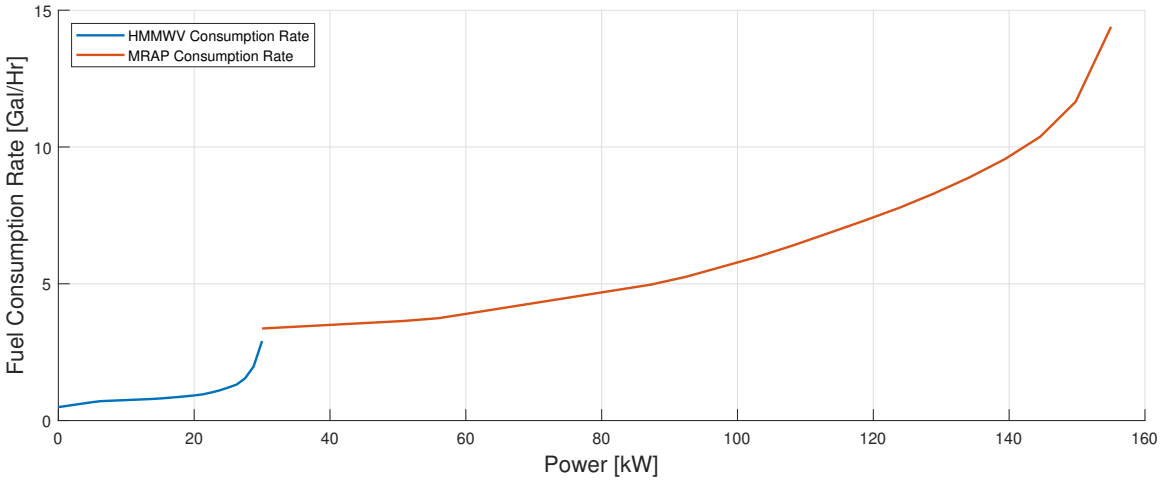

Figure 6.11: The concatenation of the HMMWV and MRAP fuel consumption rate characteristics.

Similarly to the methodology used to blend a set of heterogeneous diesel generator assets, the same principles presented in Section 6.1.1 could be applied to the fuel curves for the military type vehicles, from which sub-optimal or optimal fuel consumption could be achieved. Because this information was provided previously it is not repeated within this section.

Military vehicle variants require that the electrical power generated via the alternator or ISG be converted from AC to DC, enabling the vehicle's on-board weapon or sensor suites to be operated. This could also include the ability to charge any on-board electrical storage. Power transferred from the engine to the DC electrical system could be exported to an AC electrical network using a DC/AC converter. For the subsequent simulation studies, the vehicle platform was assumed to be made up of five components including (1) a diesel engine, (2) an alternator or ISG connected to six

phase self-rectifying circuit enabling the AC output to be directly converted to a DC voltage and current, (3) a nonlinear dynamic battery model, (4) multiple DC/DC converters to facilitate the flow of power between the alternator and the electrical storage, and (5) a DC/AC converter which enables the DC power to be exported to an AC electrical distribution network. The basic electrical circuit diagram used to construct the vehicle asset is shown in Figure 6.12. Information from the previous sections and chapters were used to construct the vehicle model.

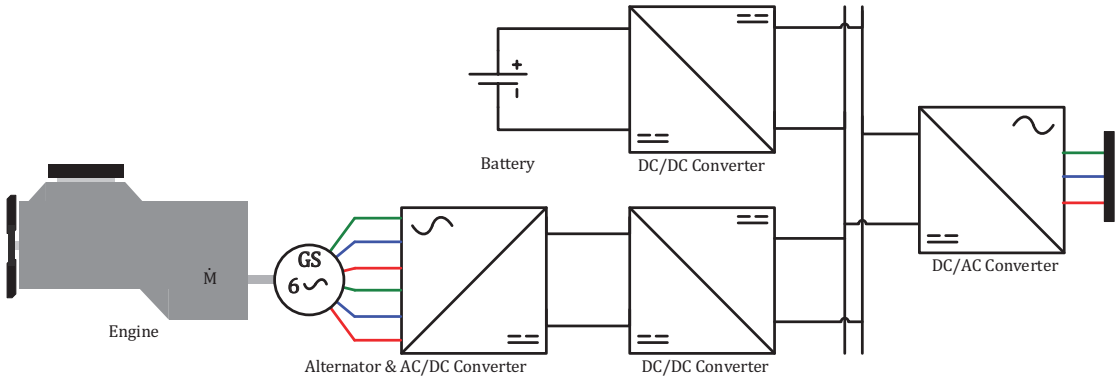

Figure 6.12: The electrical circuit diagram used to model the electrical vehicle asset.

The electrical architecture of the vehicle includes collocated electrical storage. This storage is important in order to always ensure sufficient power was provided by the vehicle asset when requested. If the vehicle asset was inactive, however, was required to export electrical power, the electrical storage must discharge until the engine was brought online and controlled to achieve the desired electrical output power of the ISG to accommodate the required electrical load. Without this electrical storage asset,

there would be unnecessary power deficits which would occur during load increases or decreases.

6.1.3 Blending of Diesel Fuel Based Assets

In Section 6.1.1 the fuel consumption characteristics for a three-phase AC diesel generator was provided as a function of electrical power. In Section 6.1.2 the two degree of freedom fuel consumption models of a vehicle were provided, using information regarding the typical behavior of an alternator, the two degree of freedom fuel consumption model can be approximated as a single degree of freedom fuel consumption model. Similar to the diesel generators, the fuel consumption rate of the vehicle were approximated as a function of output electrical power. In the previous sections, two different vehicle variants were presented, capable of exporting 30 kW or 125 kW of electrical power via the alternator or ISG. For this reason, two different generator variants that have commensurate generation capacity are used to generate a methodology to blend a set of diesel fuel based assets. The selected diesel generator variants include a 30 kW and a 200 kW AMMPS generator. Using the two diesel generator fuel curves and assuming a single precedence order of the 30 kW and the 200 kW diesel generator, a fuel trajectory was computed, and is shown in Figure 6.13. Similarly, using two different vehicle variant fuel curves and assuming a single precedence order of the HMMWV and the MRAP a second fuel trajectory

was constructed and also shown in Figure 6.13.

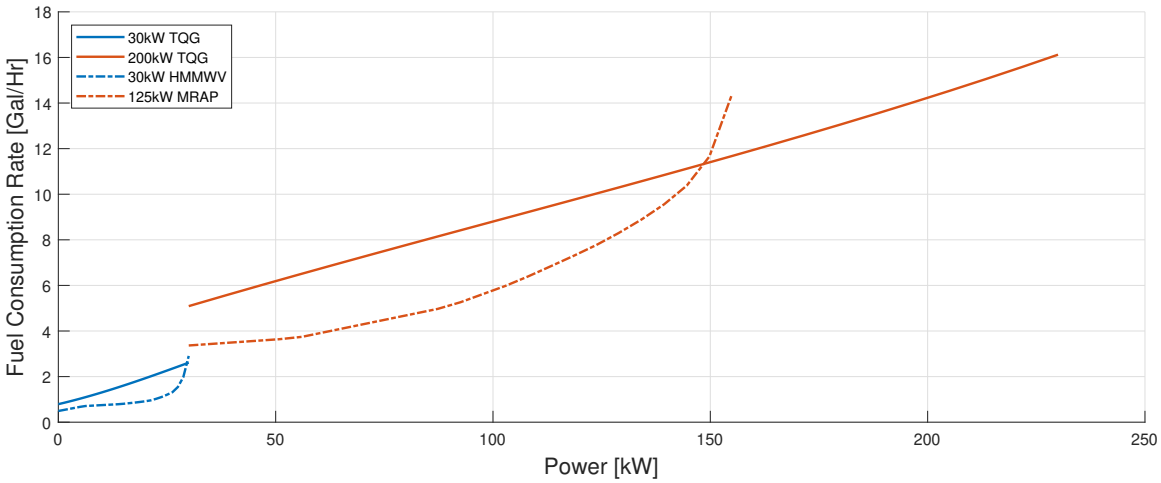

Figure 6.13: The concatenated HMMWV and MRAP fuel consumption characteristics overlaid with 30 kW and 200 kW TQG fuel consumption trajectories.

Based on Figure 6.13 for any electrical load profile which does not exceed 155 kW (the maximum rated capacity for the two vehicles) it is always more fuel efficient to use the two vehicles as opposed to the two diesel generators. While the fuel consumption curves indicated minimum fuel usage could be obtained by using the vehicles, the consumption characteristics of the vehicles do not incorporate additional losses within the electrical architecture or added inefficiencies within the engine. The output electrical power for the ISG assumes a maximum of 30 kW or 125 kW can be generated, by varying the speed and torque of the engine. This does not include additional electrical losses within the vehicle platform. Electrical power generated via the

alternator must be transferred to a DC electrical bus, with connections to the electrical storage, and a DC/AC converter. These additional losses are not incorporated and may result in additional energy usage not included within the fuel consumption trajectory of the single degree of freedom fuel consumption model.

For example, assume the HMMWV must provide 30 kW of electrical power. To achieve this, the engine must be operable, and adjust its speed and torque accordingly to enable the alternator to generate 30 kW of electrical power, rectified using an AC/DC converter. To flow power from the AC/DC converter to the DC bus, power is passed through a DC/DC converter, assuming a non-ideal power transfer, $P_{alt} = \eta P_{alt_{dc/dc}}$ where $P_{alt_{dc/dc}} < 30$ kW. To export 30 kW of electrical power to an AC network, the power into the DC/AC inverter from the DC bus must then be $P_{dc/ac} = \eta P_{ac}$ where $P_{dc/ac} > 30$ kW. This means additional power must be injected via the vehicle's onboard electrical storage to account for dissipative losses within the DC electrical system. The same type of behavior would affect the MRAP or any other vehicle variant which has similar electrical architecture. Finally, there are periods of time in which the load increases or decreases. When the load increases, the engine would lag and produce insufficient electrical power to accommodate the electrical load, additional power should be injected from the vehicle's onboard electrical storage until the engine torque and speed are increased to satisfy the electrical load requirements. If however, the load decreased, the alternator would overproduce electrical power, the excess electrical power would then be transferred from the alternator to the onboard

electrical storage.

For the subsequent simulation studies, multiple fuel consumption trajectories or precedence orders were developed. Each precedence order used for the simulation studies have been provided within the corresponding sections. To conclude the blending of the diesel fuel based assets, consider a fuel trajectory that requires the concatenation of the 30 kW and a 200 kW diesel generator, followed by concatenating the HMMWV and the MRAP. Inverting the previous fuel consumption trajectory would lead to a different fuel consumption trajectory, both fuel trajectories are provided in Figure 6.14.

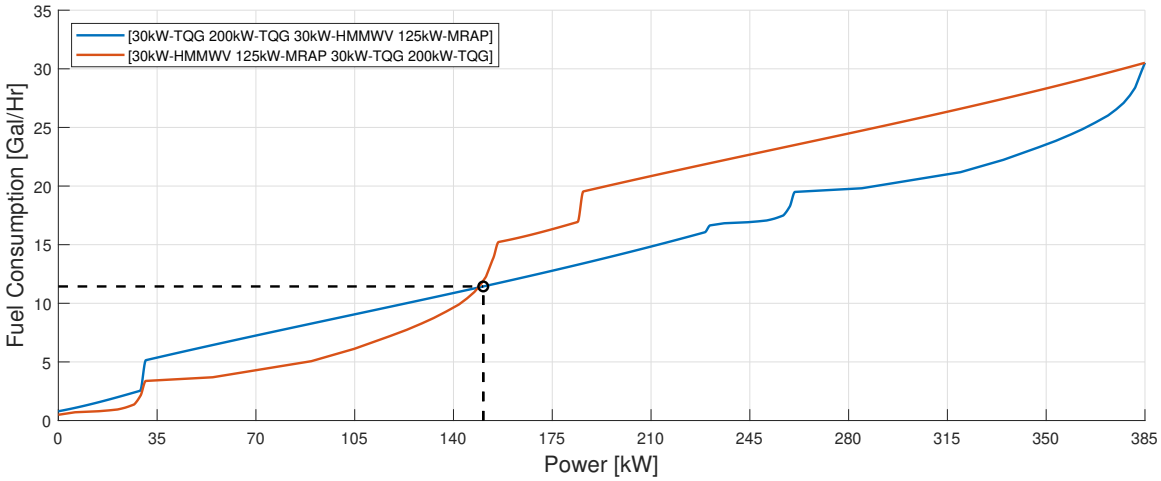

Figure 6.14: The fuel characteristics for the diesel generators and military vehicles, using two different concatenation orders, yielding two separate power apportionment strategies.

Analysis of the two fuel trajectories would indicate that the optimal fuel usage of the

diesel assets could be achieved if the HMMWV is active when the electrical load is such that $(0 < P_{lod} \leq 30)$ kW, if the electrical load is then such that $(30 < P_{lod} \leq 120)$ kW, the HMMWV should be maxed out, and the MRAP should export a variable amount of electrical power. If the electrical load exceeds 120 kW, it becomes more fuel efficient to operate the 30 kW generator followed by the 200 kW generator. For progressively larger electrical loads the HMMWV, and the MRAP should be brought online respectively. For these two fuel trajectories, an inflection point was observed to occur at 120 kW. At this point, more fuel optimal operation could be achieved by switching between the two fuel trajectories. Again the use of the concatenated fuel trajectories assumes that the individual assets can be turned on or off by a supervisory controller autonomously.

6.1.4 Photovoltaic Array Modeling with Maximum Power Point Tracking

In the previous sections, assets that require the use of expensive diesel fuel were considered and analyzed to obtain a methodology to blend all diesel-based generation assets. In practice, however, military microgrids may also possess electrical storage or renewable-based generation assets which could generate electrical power by harnessing various forms of energy. In this section, renewable based assets are considered, more specifically a method to maximize the output power of a PV array was developed.

Renewable power generation devices are fundamentally different than traditional power generation sources that consume fossil fuel to generate electrical power. These devices are incapable of producing reliable power due to the intermittent nature of the hydrological or meteorological conditions. Additionally, renewable devices are coupled with electrical storage assets to provide more reliable power generation. In order to maximize the output power of a PV array, the orientation of the array may be altered to maximize the output electrical power for variable conditions. Further, the power electronics incorporated within the hardware may also be modulated to further maximize the generated electrical power. Two main methods are typically used to modulate the output voltage of a PV array, sometimes in combination with each other including, (1) the perturb and observe methodology, and (2) using known characteristics of the PV array and known operating conditions to estimate the output voltage. Both methods are used to modulate the PV arrays output voltage, resulting in an MPPT control strategy. The perturb and observe method works for real-time control and is not easily applied for long-term energy management, however, the second methodology could be used for both real-time control, and long-term energy management. The remainder of this section provides more detailed information regarding generating an MPPT algorithm using known characteristics of the PV array.

The governing equations for a photovoltaic array are based on the published research paper [1], which proposes constructing a mathematical model of a PV array based

on information commonly available within the equipment datasheets for a PV panel. The purpose of using this model is that the parameters needed are readily available or could be easily ascertained. The output current I_{pv} of the PV cell is,

$$I_{pv} = \left(1 + \frac{R_s}{R_{sh}}\right)^{-1} \left(G_{pu}(I_{sc}^0 + \alpha_{Isc}\Delta T) - \beta e^{\gamma(V_{pv} + \alpha_{V_{oc}}\Delta T - V_{oc}^0)} - \frac{V_{pv}}{R_{sh}}\right) \tag{6.4}$$

where R_s is the series resistance, R_{sh} is the shunt resistance, $G_{pu} = G_{amb}/1000$ which is the relative solar irradiance, G_{amb} is the ambient solar irradiance, I_{sc} is the short circuit current, $\Delta T = T_{amb} - 25$, T_{amb} is the ambient temperature, β and γ are time varying coefficients governing the nonlinear behavior of the PV array, V_{pv} is the PV cell voltage, and V_{oc} is the open circuit voltage. The shunt resistance is then defined as,

$$R_{sh} = \frac{V_{mpp}^0 - \alpha_{V_{oc}}\Delta T}{G_{pu}\frac{I_{sc}^0 - I_{mpp}^0}{2}} = \frac{V_{sh}}{I_{sh}}. \tag{6.5}$$

where R_{sh} is the shunt resistance, V_{mpp}^0 and I_{mpp}^0 are the maximum power point voltage and current, I_{sc}^0 is the short circuit current, $\alpha_{V_{oc}}$ is a coefficient which accounts for voltage degradation as a function of temperature variation, V_{sh} is the shunt resistance voltage drop, and I_{sh} is the shunt resistance current. Parameters V_{mpp}^0, I_{mpp}^0, and I_{sc}^0 are parameters which are observed at standard test conditions (STC). Henceforth, any parameter raised to the zeroth power indicates the parameter was observed at

STC. The series resistance is then defined as,

$$R_s = \frac{\frac{V_{oc}^0 - V_{mpp}^0}{4}}{G_{pu}\left(I_{mpp}^0 + \alpha_{I_{sc}}\Delta T\right)} = \frac{V_s}{I_s}. \tag{6.6}$$

where R_s is the series resistance, V_s and I_s is the voltage and current across the series resistor. The voltage at the terminals of the PV cell is then,

$$V_{pv} = V_{sh} - V_s \tag{6.7}$$

The shunt voltage and series voltage inferred from the previous equations are then $V_{sh} = \left(V_{mpp}^0 - \alpha_{V_{oc}}\Delta T\right)$ and $V_s = \left(\frac{V_{oc}^0 - V_{mpp}^0}{4}\right)$ respectively. As discussed in [1], evaluating β and α necessitates that certain constraints be imposed to sufficiently model the behavior of a PV array. These constraints are imposed at three important operating conditions, (1) the open circuit voltage V_{oc} is zero when the short circuit current $I_{pv} = I_{sc}$, (2) the short circuit current I_{sc} is zero when the open circuit voltage is $V_{pv} = V_{oc}$, and (3) the maximum power point voltage $V = V_{mpp}$. This can be stated as,

$$I = I_{sc} \text{ for } V_{sc} = 0, \tag{6.8}$$

$$I_{sc} = 0 \text{ for } V = V_{oc}, \tag{6.9}$$

$$\frac{dP}{dV} = 0 \text{ for } V = V_{mpp}. \tag{6.10}$$

Solving Equation 6.8 - Equation 6.10 yields

$$I_{sc} = p\left[G_{pu}\left(I_{sc}^{0} + \alpha_{I_{sc}}\Delta T\right)\right] \tag{6.11}$$

$$\beta = G_{pu}\left(I_{sc}^{0} + \alpha_{I_{sc}}\Delta T\right) - \frac{V_{oc}^{0} - \alpha_{V_{oc}}\Delta T}{R_{sh}} \tag{6.12}$$

$$\gamma = \frac{1}{V_{mpp}^{0} - V_{oc}^{0}} \ln\left(\frac{G_{pu}\left(pI_{sc}^{0} - I_{mpp}^{0}\right) - (1-p)\alpha_{I_{sc}}\Delta T - \frac{p(V_{mpp}^{0}) - \alpha_{V_{oc}}}{R_{sh}}}{p\left(G_{pu}\left(I_{sc}^{0} + \alpha_{I_{sc}}\Delta T\right) - \frac{V_{oc} - \alpha_{V_{oc}}\Delta T}{R_{sh}}\right)}\right) \tag{6.13}$$

where

$$p = \frac{R_{sh}}{R_s + R_{sh}}. \tag{6.14}$$

The parameters β and γ now depend on the data commonly available provided by the manufacturer [1]. The cell temperature $T_c(^oC)$ is related to the ambient temperature $T_{amb}(^oC)$ by,

$$T_c = T_{amb} + \frac{G_{amb}}{800}(T_{notc} - 20), \tag{6.15}$$

where $T_{notc}(^oC)$ is the nominal operating cell temperature (NOCT). The cell voltage V_{cell} and current I_{cell} are related to the module voltage V_{pv} and current I_{pv} by

$$V_{cell} = \frac{V_{pv}}{N_s} \tag{6.16}$$

$$I_{cell} = \frac{I_{pv}}{N_p} \tag{6.17}$$

where N_s and N_p are the number of cells in series and the number of parallel groups of cells respectively. As stated in [1], the open circuit voltage V_{oc} is directly linked to

the cell temperature by the subsequent equation,

$$V_{oc} = V_{oc}^{0} - \alpha_{V_{oc}} \Delta T \tag{6.18}$$

Using Equation 6.18 the approximate maximum open circuit voltage for the solar panel could be computed provided the cell temperature is known, which can be computed using Equation 6.15. All other previously mentioned equations enable a model to be constructed estimating the operation of a PV array. These equations were extended to construct a MPPT algorithm to estimate the required operating voltage for the PV array to maximize the generated power. Assuming that the current operating conditions yield $G_{amb} = 500\ W/m^2$, and $T_{amb} = 20^o$ C and the parameters used to model the PV array are those provided in Table 6.2, the VI and VP curves for a solar array were computed, and provided in Figure 6.15.

Symbol	Description	Unit	Value
P_s	Cell series resistance	W	180
V_{oc}^0	Open Circuit Voltage at STC	V	45
I_{sc}^0	Short Circuit Current at STC	A	5.25
V_{mpp}^0	Voltage at Maximum Power at STC	A	36.8
I_{mpp}^0	Current at Maximum Power at STC	A	4.87
$NOCT$	Nominal Operating Cell Temperature	^oC	40
$\alpha_{I_{sc}}$	Short Circuit Current Temperature Coefficient	$\%/^oC$	0.1
$\alpha_{V_{oc}}$	Open Circuit Voltage Temperature Coefficient	$\%/^oC$	-0.37
N_s	Number of Series Cells	#	10
N_p	Number of Parallel Cells	#	40

Table 6.2
PV parameters used to construct a PV array and the MPPT algorithm.

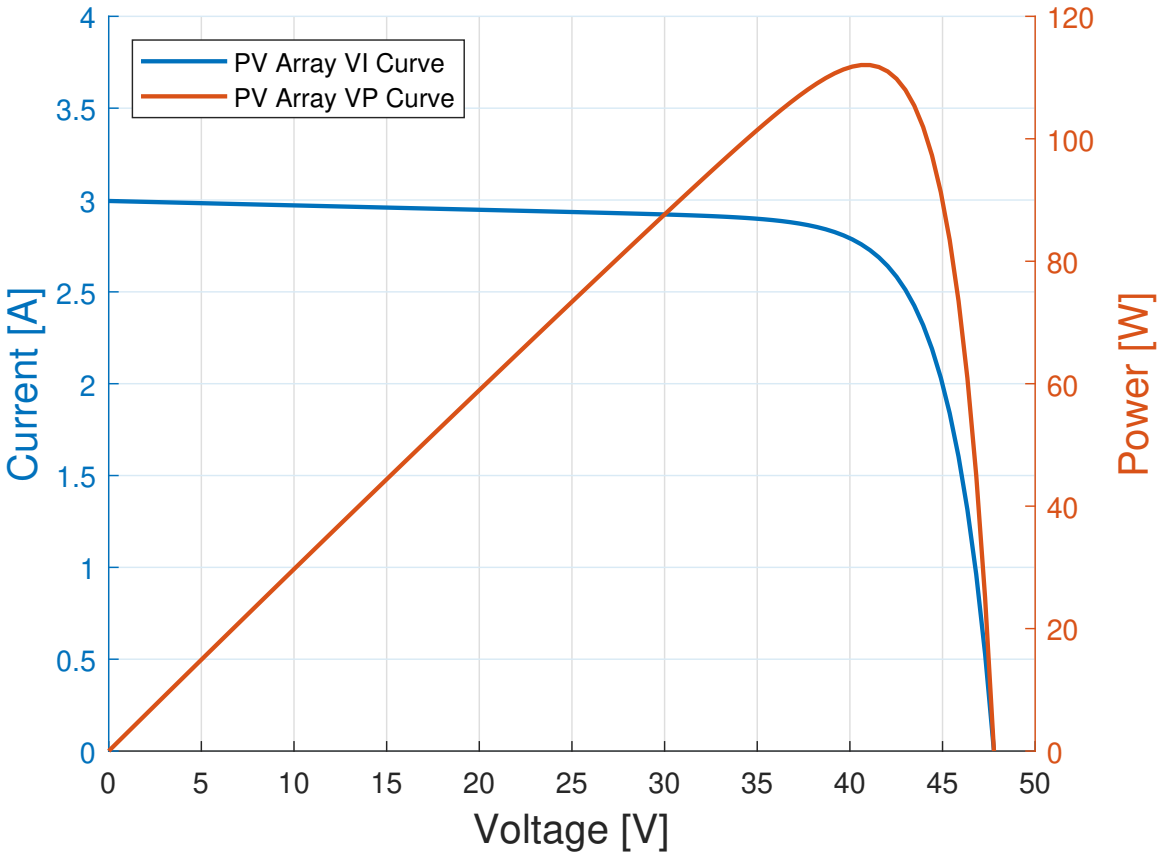

Figure 6.15: The PV array's VI and VP curve with for the given set of operating conditions.

Analysis of Figure 6.15 would indicate that the maximum output power of the PV array could be obtained by modulating the PV array's output voltage to be $V_{pv} = 40.95$ V, yielding approximately 112 W (using similar parameters defined in [1]). Now consider a vector of solar radiation and temperature points such as those provided in Figure 6.16, passing these trajectories to the MPPT algorithm enables the modulated voltage to be computed, yielding maximum power generation of the PV array.

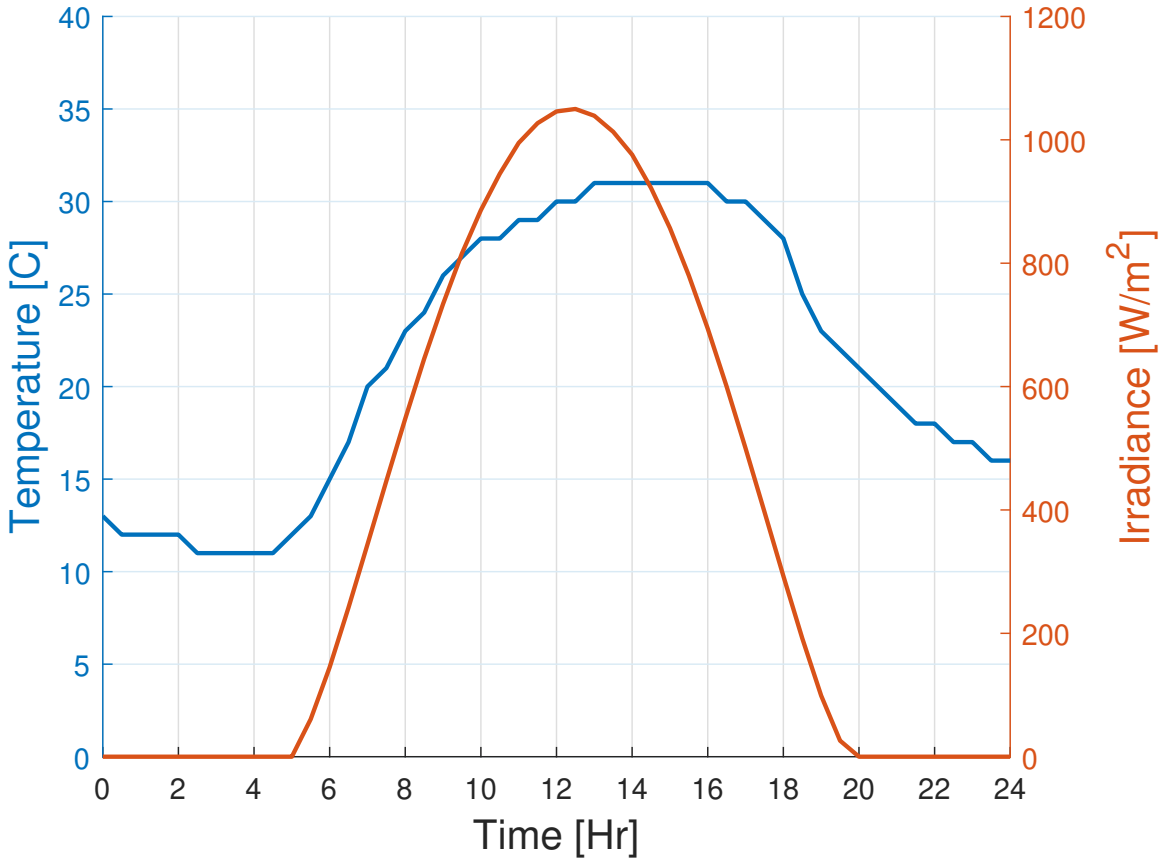

Figure 6.16: Example of common solar radiation and ambient temperature profiles required to estimate the output power of a PV array.

Using the temperature and solar radiation profiles provided in Figure 6.16 in addition to the equations provided previously, the required voltage to obtain the maximum power in addition to the resulting output power have been provided in Figure 6.17.

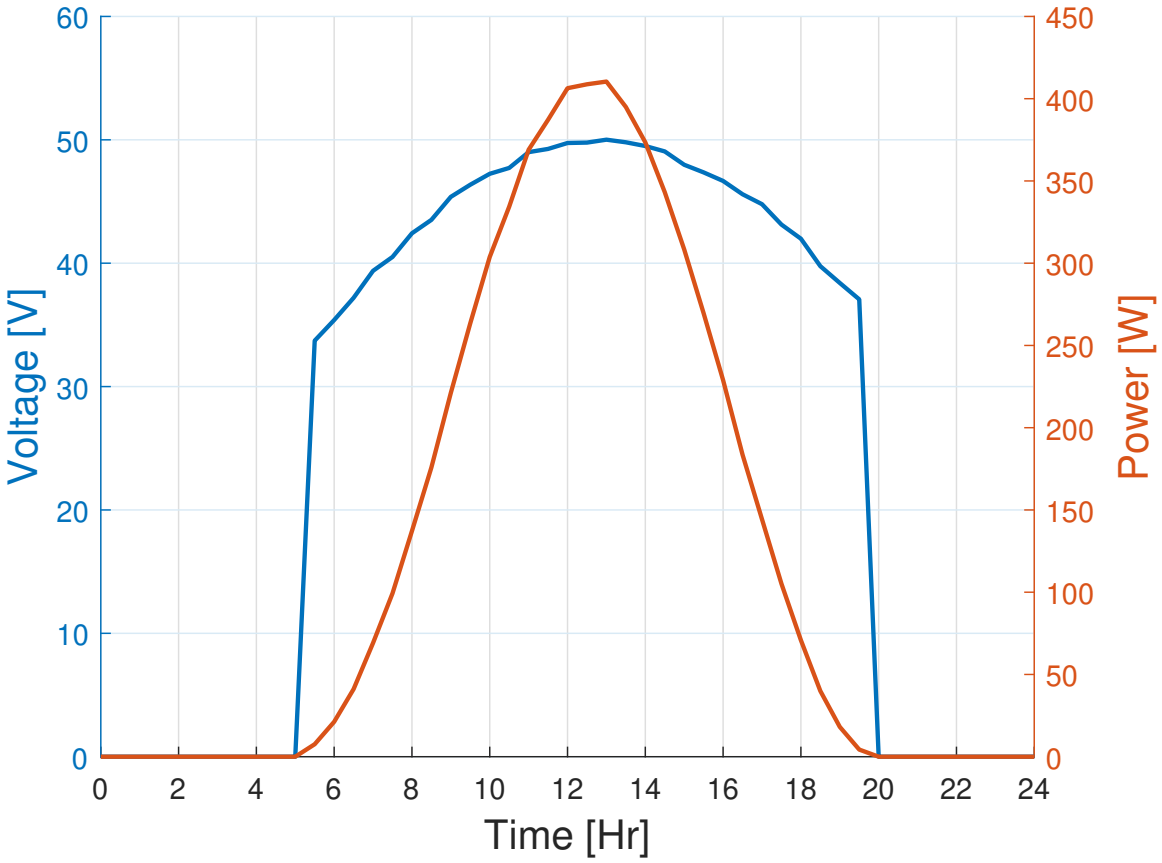

Figure 6.17: Example of common solar radiation and ambient temperature profiles required to estimate the output power of a PV array.

Similar to the vehicle asset, renewable based power generation assets are usually coupled with electrical storage. For the subsequent simulation studies to follow, the renewable asset was assumed to be made up of four components including (1) a PV array, (2) a nonlinear dynamic battery model, (3) multiple DC/DC converters to facilitate the flow of power between the PV array and the electrical storage, and (4) a DC/AC converter which enables the DC power to be exported to an AC electrical distribution network. The basic electrical circuit diagram used to construct the

renewable asset is presented in Figure 6.18. Information from the previous sections and chapters were used to construct the renewable model.

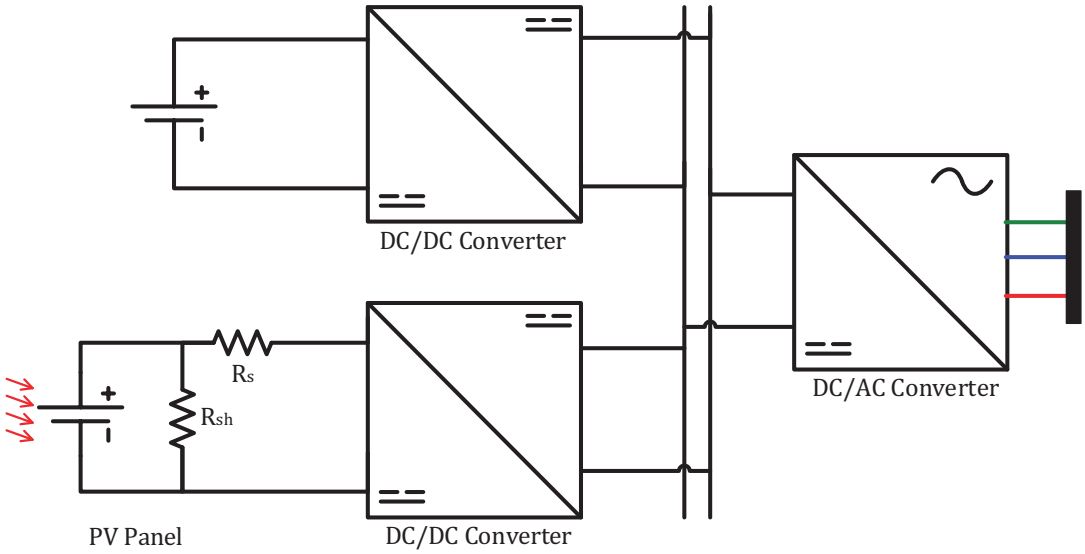

Figure 6.18: The electrical circuit diagram used to model the electrical renewable asset.

6.2 Blending of Diesel Fuel Based Assets

This section is subdivided into three subsections, with the first providing information regarding the selected scenario including the electrical architecture and the time-varying electrical load. The second section contains information regarding the power apportionment strategies, and the final section presents the results.

6.2.1 Scenario Description

Consider an electrical grid with three generation assets, including (1) a 200 kW TQG, (2) a single MRAP capable of exporting 125 kW of electrical power, and (3) a single electrical storage asset directly connected to an AC electrical bus. In addition to the three electrical generation assets, there are three time-varying complex electrical loads. All of the generation and load assets are connected directly to the main AC electrical distribution bus through a RL transmission line. The corresponding electrical architecture is shown in Figure 6.19.

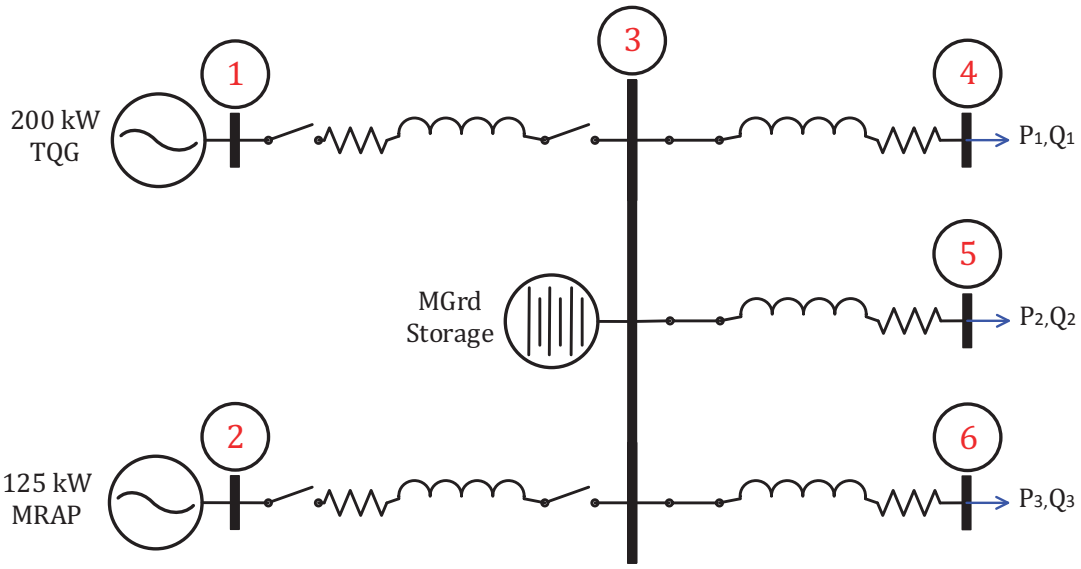

Figure 6.19: The electrical architecture with a single diesel generator, an electrical storage, a military vehicle, and three time varying electrical loads.

Further the electrical load is provided in Figure 6.20. The electrical load was equally separated across the three load buses.

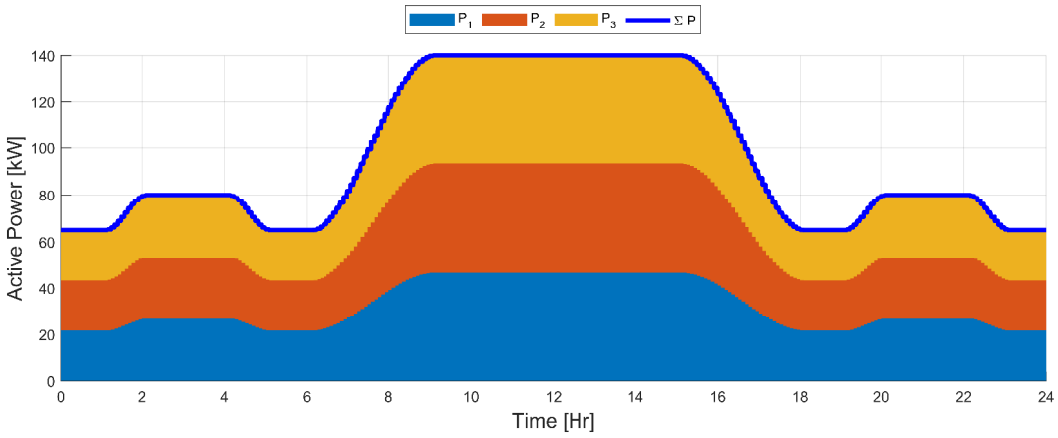

(a) The aggregate active power electrical load was evenly divided among the three load buses.

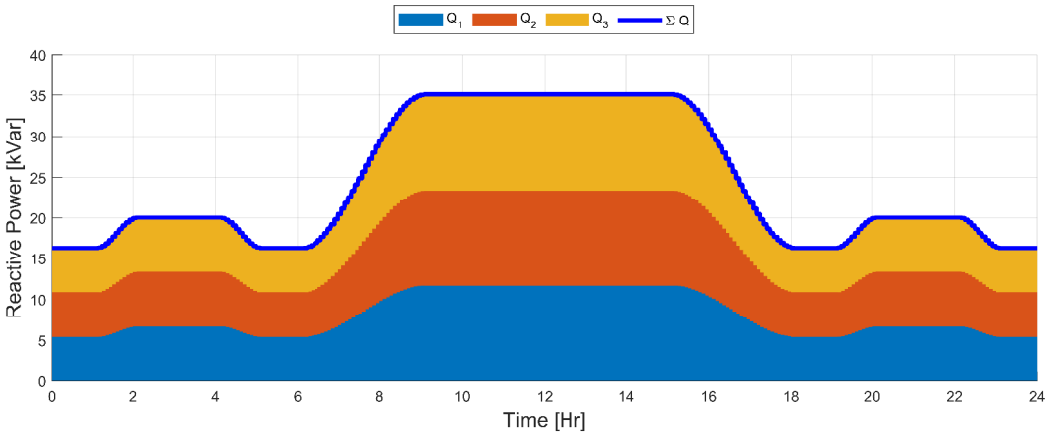

(b) The aggregate reactive power electrical load was evenly divided among the three load buses.

Figure 6.20: The complex electrical load for each of the three load buses for the duration of the simulation epoch.

6.2.2 Energy Management Policy

The energy management policies require blending of a single 200 kW TQG diesel generator and a single MRAP capable of exporting 125 kW of electrical power. For the selected set of generation assets, there exists exactly four distinctly different fuel trajectories which can be generated using the concatenation methodology provided earlier. For these case studies however, each of the individual fuel trajectory curves for each assets were used independently for the generator and vehicle only cases. A third case study was simulated which used the more optimal combination of the two fuel trajectories. The fuel trajectories used for the simulation studies are provided in Figure 6.21.

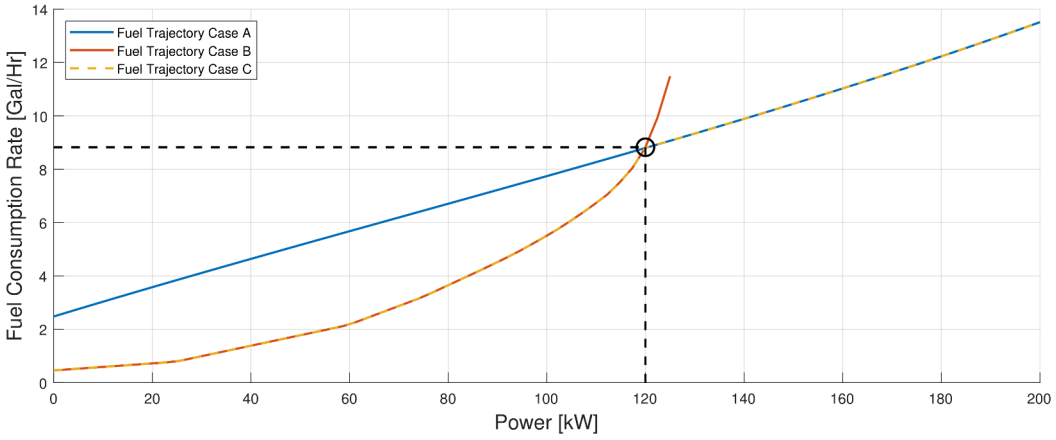

Figure 6.21: The energy management's fuel trajectories used within the subsequent simulation studies.

Three separate simulation studies were conducted using the three different fuel trajectories provided in Figure 6.21. For the first case study (Case A), the 200 kW TQG is assumed to be the primary power generation asset, while the storage is considered to be the secondary power generation asset. Similarly, for the second case study (Case B), the 125 kW MRAP is assumed to be the primary power generation asset, while the storage is considered to be the secondary power generation asset. For the third and final case study (Case C) both the 200 kW TQG and the 125 kW MRAP were considered to be the primary power generation assets, while the storage is the secondary power generation asset. Dissimilarly with the previous case studies, the MRAP was active assuming the electrical load is such that $(0 < P_{lod} \leq 120)$ kW. If the electrical load exceeds 120 kW the TQG is brought online, and the vehicle was taken offline, the inverse is also true if the electrical load decreases. For near instantaneous power imbalances, the electrical storage associated with the AC microgrid distribution bus injects sufficient current to achieve desired power flow. The fuel trajectories are used to compute the power generation commands for each diesel fuel-based asset, these commands were passed to an optimal power flow agent (Section 4.3.4), which computed the optimal complex voltage for each bus within the electrical architecture, that yielded sufficient electrical load. The voltage commands were then used in conjunction with the complex nodal admittance matrix to simulate the electrical network. The results collected from each of the three cases are provided within the subsequent section.

6.2.3 Case Studies

The results from the three different case studies are provided in Figure 6.22 - Figure 6.27. The individual contributions from the three generation assets are shown in Figure 6.22 - Figure 6.24 for all three case studies. As expected the contingent of generation assets have sufficient generation capacity, such that the electrical load could be satisfied by either primary asset or some combination of the two. This assumes that the electrical storage capabilities of the vehicle platform were sufficient to accommodate an electrical load that exceeds the rated capacity of the alternator or ISG. Instantaneous current injection was used to correct power imbalances after the new optimal voltage magnitude and angle set points were computed via the power flow control agent. While not shown, the generation assets must also provide sufficient reactive power to meet the required reactive load. The reactive power contributions would look similar to the active power contributions when electrical losses are considered.

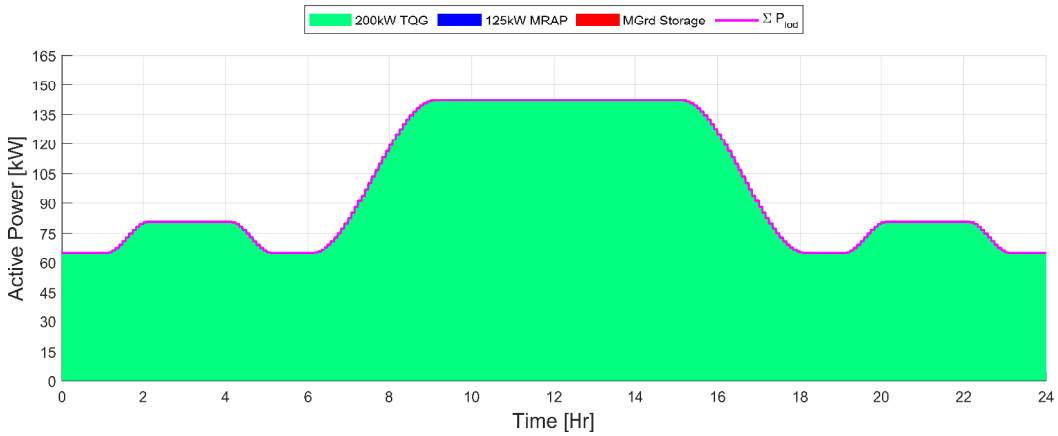

Figure 6.22: Case A - The active power contributions for each asset, instantaneous power was injected via the electrical storage, the bulk of the power was provided by the diesel generator.

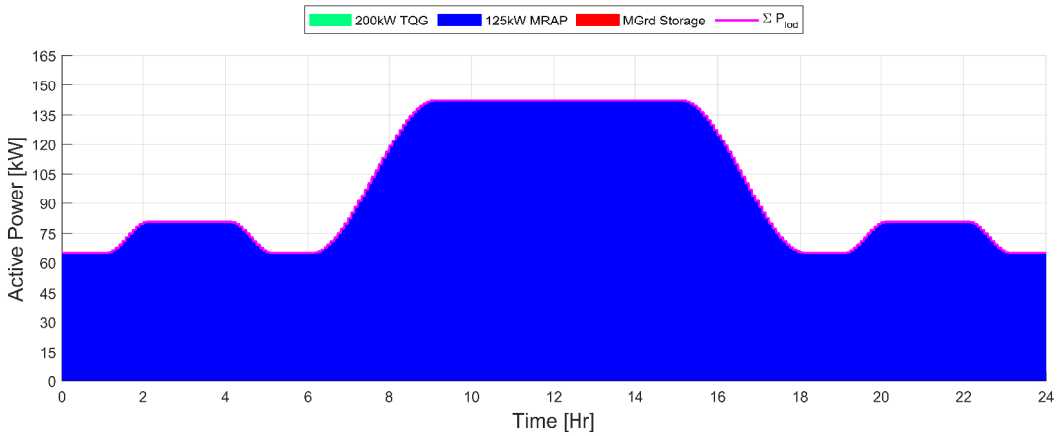

Figure 6.23: Case B - The active power contributions for each asset, instantaneous power was injected via the electrical storage, the bulk of the power was provided by the military vehicle.

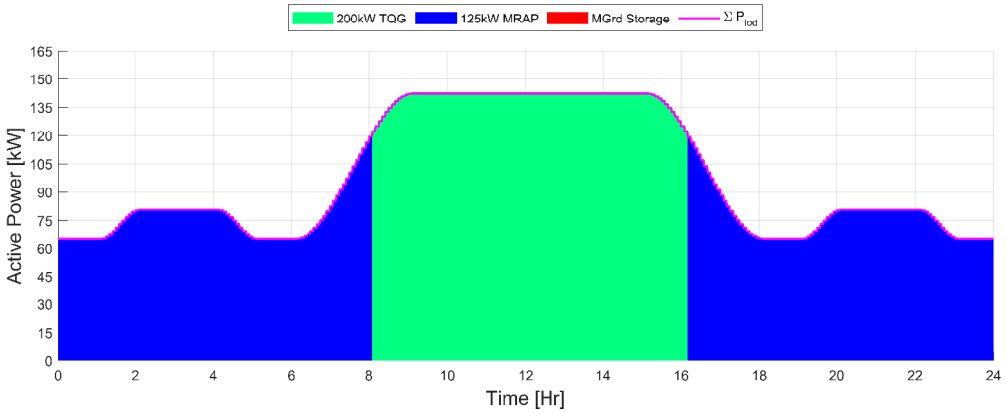

Figure 6.24: Case C - The active power contributions for each asset, instantaneous power was injected via the electrical storage, the bulk of the power was provided by the military vehicle or diesel generator depending on the required electrical load.

Now consider the use of bus storage, and the collocated storage within the military vehicle provided in Figure 6.25 - Figure 6.26. The energy storage requirements for the bus storage asset (Figure 6.25) of Case A and B were roughly equivalent, due to symmetric loading. Any energy which was discharged over the first 12 Hrs was recovered over the remaining 12 Hr period. For both Case A and B, the electrical storage asset requires that the electrical storage be fully charged, with roughly 278 kJ of energy available to accommodate the power apportionment policies resulting from the different fuel trajectories. Similarly to Case A and B, Case C also requires that the electrical storage asset be fully charged, dissimilarly, however, the electrical storage must contain 1.06 MJ of electrical energy to accommodate the power apportionment policy. Further, the final energy storage state was lower than the initial energy storage state.

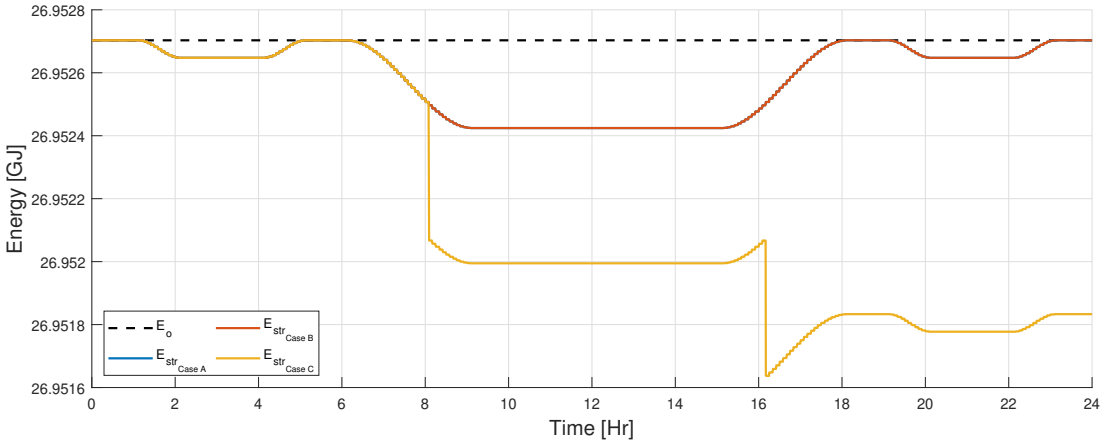

Figure 6.25: The electrical storage asset's energy usage throughout across the three case studies throughout simulation epoch.

Now consider the collocated electrical storage within the vehicle platform provided in Figure 6.26. For Case A, there was no deviation from the initial energy storage state for the vehicle, this is consistent with the vehicle asset being inoperable. For Case B, the vehicle platform requires approximately 632 MJ of energy to accommodate the power apportionment policy. This type of result was expected because the electrical load exceeds the rated output power of the vehicle's alternator or ISG, indicating the remaining electrical power must either come from the electrical storage associated with the AC bus, or from the collocated electrical storage within the vehicle. Further, the final energy storage state was lower than the initial energy storage state, this type of behavior could be problematic for the vehicle assets, as it would require the engine to be operable for a greater period of time to charge the onboard storage. This may inhibit the ability of the vehicle to participate in silent watch operations should the need arise. Finally, for Case C, the electrical storage must now be able

to provide 10.78 MJ of electrical energy. Again the final energy state for the vehicle was lower than the initial, however, there was roughly a 60% decrease in the total amount of energy required when compared to Case B.

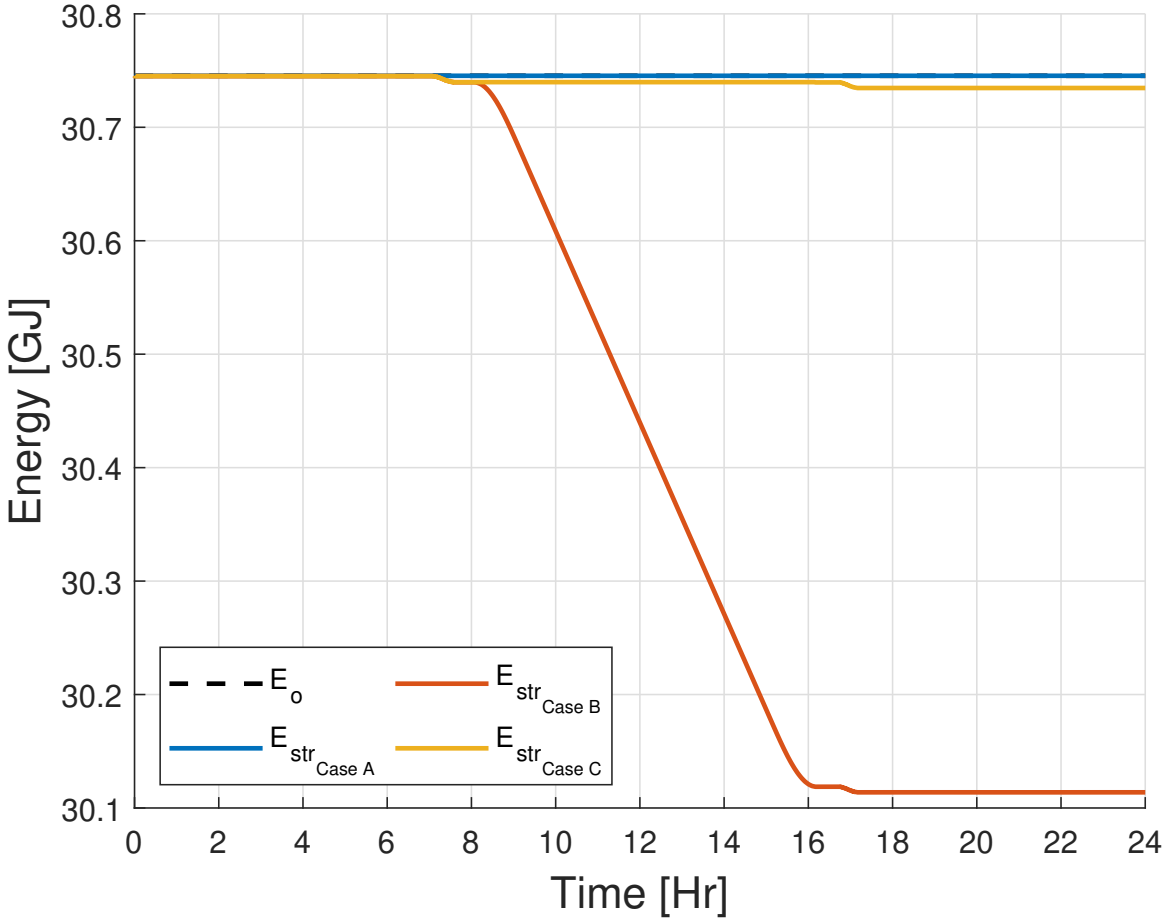

Figure 6.26: The vehicle's electrical storage energy use throughout across the three case studies throughout simulation epoch.

Now consider the fuel consumed by the diesel assets. Based on the fuel consumption characteristics of the generator and vehicle, it was determined that the vehicle operated more efficiently as long as the electrical load did not exceed 120 kW. For

substantially higher electrical loads exceeding 120 kW, the diesel generator operates more fuel efficiently. This type of behavior could be inferred from analysis of the fuel trajectories presented in Figure 6.27. For the first eight hours, the rate of fuel used via the vehicle was less than the generator for both Case A and C, resulting in less fuel consumed via the vehicle. Eight hours after the simulation began, the total electrical load reaches 120 kW, at this point, the vehicle's alternator was likely required to begin operating at or near its maximum rated output of 125 kW. To accommodate electrical loads that exceed 120 kW, the MRAP was pushed toward a less fuel optimal operating point when compared to the diesel generator, additionally, the electrical storage associated with the vehicle must now discharge to accommodate a higher electrical load. Approximately two hours past this point the fuel consumption of Case B exceeds the fuel consumption of the generator shown in Case A. Dissimilarly for Case C, the vehicle platform was ramped down, and the diesel generator was ramped up, consuming less diesel fuel than both Case A and B. Sometime later within the simulation when the electrical load drops below 120 kW, the vehicle asset would begin operating more efficiently, however, the large duration in which the vehicle was required to operate inefficiently drives Case B to use the most fuel. For Case A, the diesel generator consumed approximately 185 gallons, while the vehicle consumed 208 gallons for Case B, and finally, as one might expect, the use of both the vehicle and the generator consumed approximately 160 gallons for Case C.

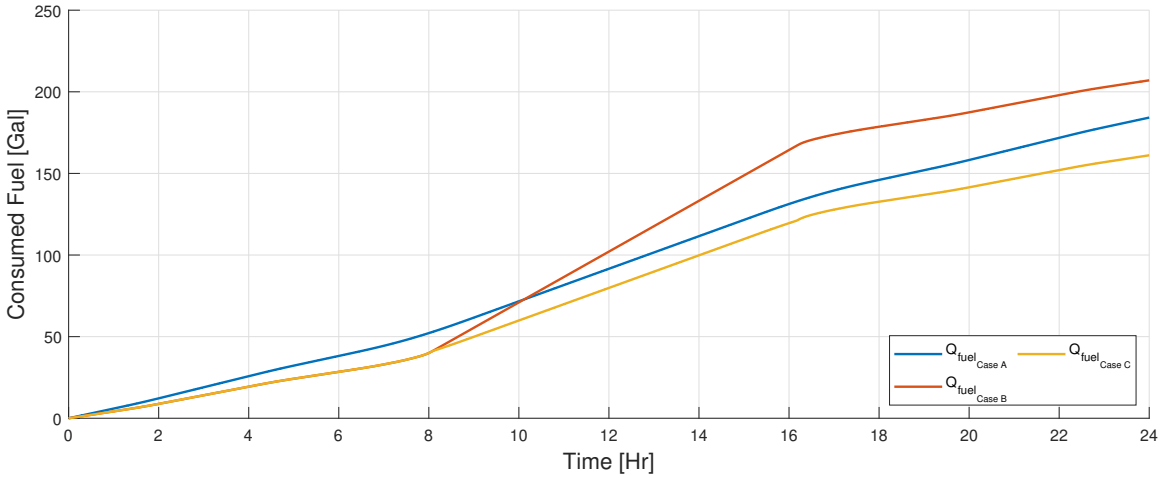

Figure 6.27: The combined fuel consumed by the contingent of the diesel generators and military type vehicles.

For the given power apportionment strategies, it was determined that a 227300% increase in electrical storage capacity yielded approximately a 12% increase in fuel consumption using the apportionment strategy of Case B over Case A, conversely, it was also determined that approximately a 4170% increase in energy storage capacity yielded a 13% decrease in fuel consumption when the apportionment strategy of Case C was used instead of Case A. More fuel optimal behavior was achieved using Case C's power apportionment strategy, but at the cost of requiring greater electrical storage.

While it is apparent which of the three case studies yielded the most optimal fuel use, it is less apparent which of the three cases yielded more optimal energy use. In order to assess the complete energy used throughout the simulation, the equivalent fuel consumption should be considered. The equivalent fuel consumption considers the contribution of all diesel-based fuel assets, in addition to the energy stored within

the electrical assets. To compute the equivalent fuel consumption, two separate energy states were considered regarding the total electrical storage, (1) the amount of energy required within the electrical storage asset at the beginning of the simulation, and (2) the difference between the initial energy state and the final energy state. The second metric was important because the optimal fuel usage policy would be to drain all electrical energy reserves to service the electrical load. When the electrical energy was depleted, the remainder of the electrical load would be serviced by the diesel generation assets. This solution would be problematic for military operations, especially considering the vehicle platform cannot operate without external stimuli to charge the electrical storage. The first energy metric always yields an added fuel cost, while the second energy metric could result in either an addition or reduction of fuel as a result of the difference between the initial energy state and the final energy state. If the final energy state was lower than the initial energy state, the equivalent fuel consumption increases, while the inverse would lead to a decrease. Finally, Equation 6.19 - Equation 6.20 are applied to the storage metrics to compute the added fuel consumption metrics.

$$q_{min} = \frac{|E_{min}|}{3600(P_{rated})}\dot{q}_{P_{rated}} \tag{6.19}$$

$$q_{add} = \frac{E_{int} - E_{fin}}{3600(P_{rated})}\dot{q}_{P_{rated}} \tag{6.20}$$

In Equation 6.19 - Equation 6.20, E_{min} is the minimum energy required in Joules,

E_{int} is the initial energy state in Joules, E_{fin} is the final energy state in Joules, P_{rated} is the maximum rated electrical power of the respective generation asset in W, and $\dot{q}$ is the fuel consumption rate at maximum rated electrical power in Gal/Hr. Using both Equation 6.19 and Equation 6.20 the additional fuel costs was computed for each case and added to the original fuel consumption metric, resulting in the equivalent fuel consumption trajectory of Figure 6.28.

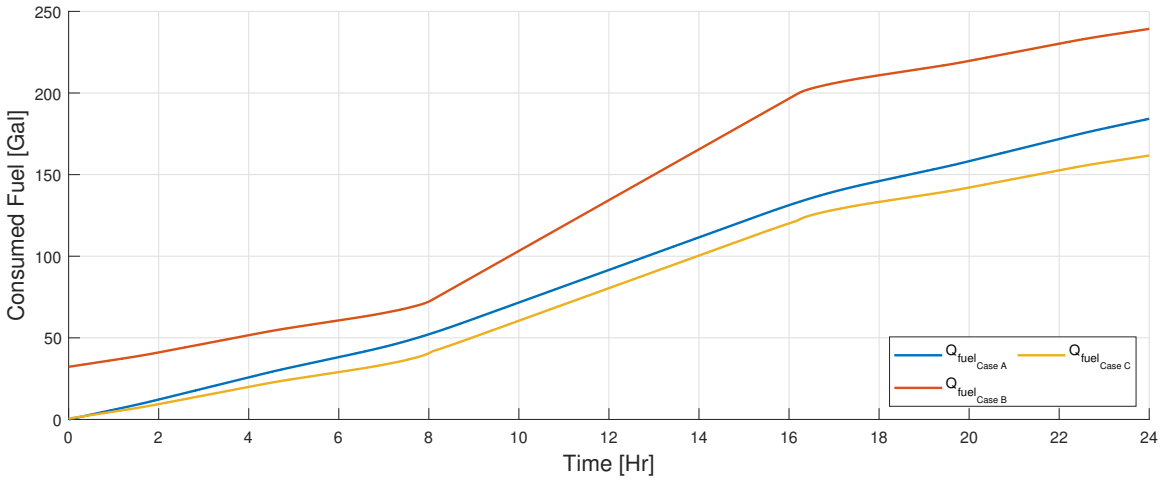

Figure 6.28: The equivalent fuel consumption for each of the three case studies.

The equivalent fuel consumption which incorporates the electrical storage requirements indicates that Case B yields the least efficient solution, primarily due to the minimum storage requirement and the fact that the final energy state was sufficiently smaller than the initial energy storage state. Alternatively there was not much difference between the equivalent fuel consumption for Case A and Case C when compared to Figure 6.27. This indicates that the most optimal energy management policy of

the three simulated case studies was that of Case C, followed by Case A.

6.3 Blending of Diesel Fuel and Renewable Assets

This section is also subdivided into three subsections, with the first providing information regarding the selected scenario including the electrical architecture, the selected event schedule, and the meteorological weather conditions, which govern the time varying electrical load. The second section contains information regarding the power apportionment strategies, and the final section presents the results.

6.3.1 Scenario Description

Consider an electrical grid with six generation assets, including (1) a 30 kW TQG, (2) a 200 kW TQG, (3) a 30 kW HMMWV, (4) a 125 kW MRAP, (5) a single PV array capable of generating 125 kW of electrical power using MPPT, and (6) a single electrical storage asset directly connected to an AC electrical bus. In addition to the six electrical generation assets, there were eighteen time-varying complex electrical loads. Both the active and reactive electrical load was subdivided into two components, (1) an equipment electrical load which varies as a function of a prescribed event schedule and rather invariant to the current meteorological conditions, and (2) an HVAC load

which varies as a function of the current meteorological conditions. All of the generation and load assets were connected directly to the main AC electrical distribution bus through an RL transmission line. The corresponding electrical architecture are provided in Figure 6.29.

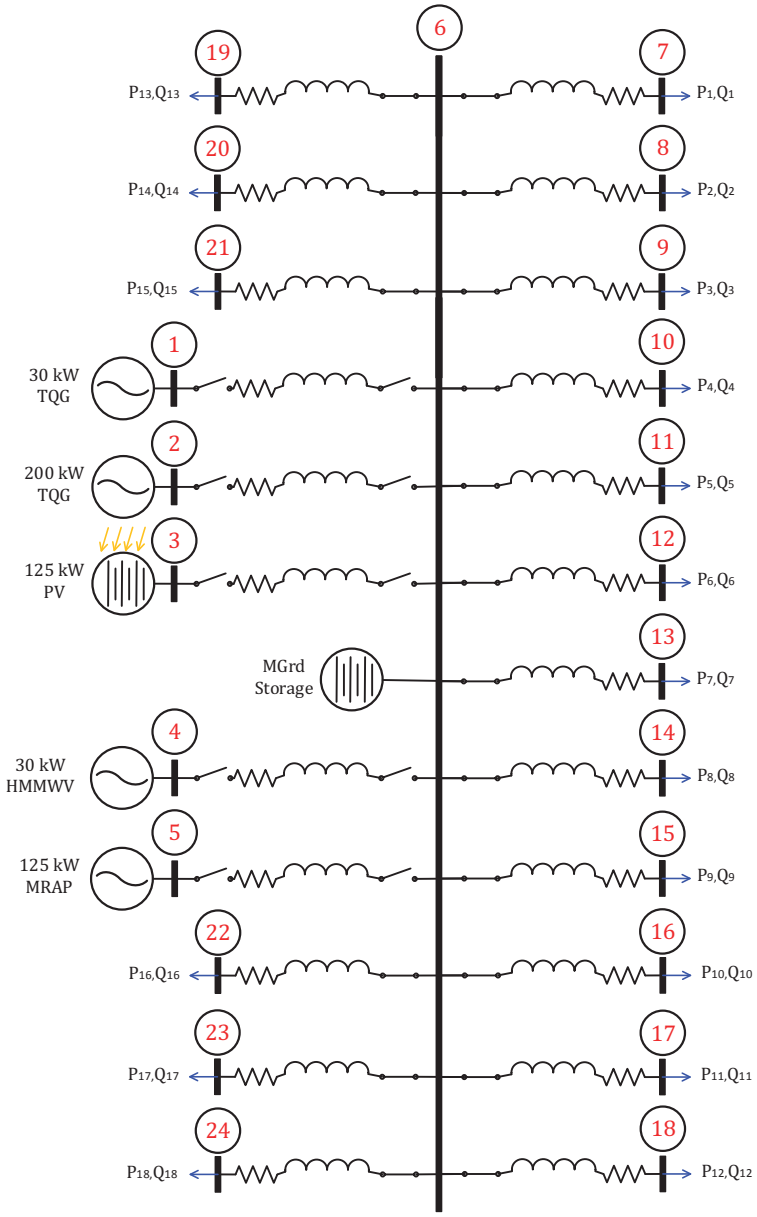

Figure 6.29: The electrical architecture with two diesel generators, two military grade vehicles, a PV array, an electrical storage assets, and eighteen electrical loads.

In order for the electrical load to be computed, an event schedule which governs the

equipment electrical load, in addition to a set of meteorological conditions must first be defined. The event schedule used to generate the electrical load is displayed in Figure 6.30, and the selected meteorological conditions used for the case studies are presented in Figure 6.31.

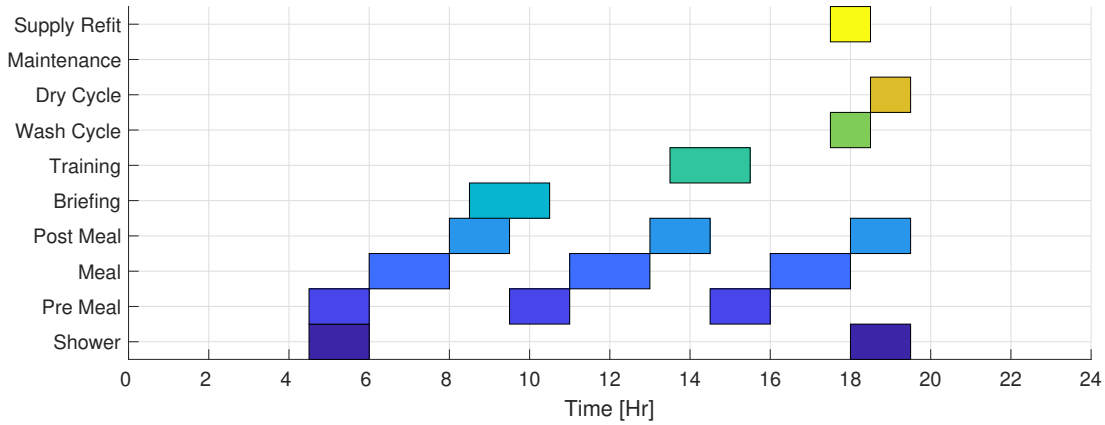

Figure 6.30: The selected event schedule includes events that cause the equipment electrical load to increase or decrease as a function of an event occurring within a specific shelter, based on load designations (not provided).

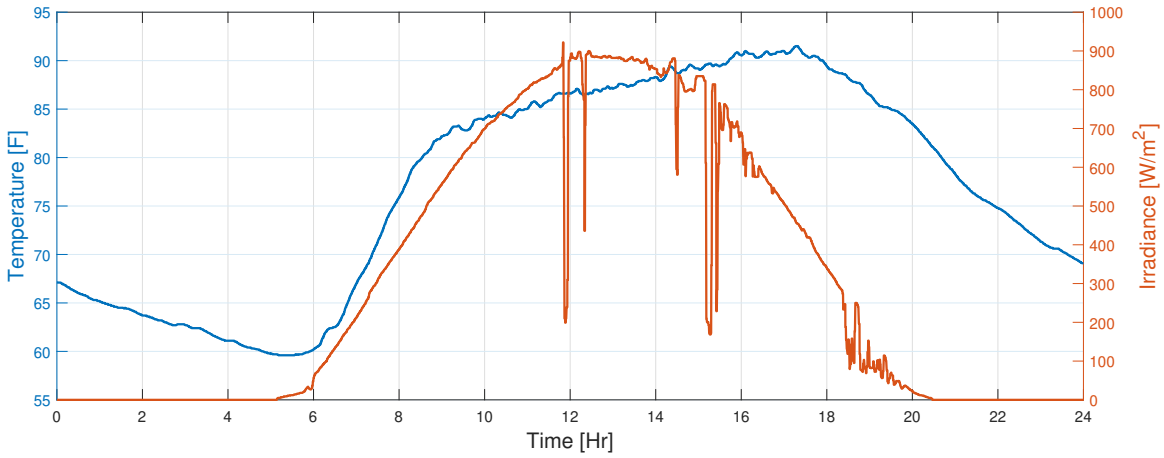

Figure 6.31: The selected meteorological conditions used for the simulation studies includes the ambient temperature and solar irradiance. The temperature profile is directly linked to the HVAC electrical load.

Using the event schedule in addition to the meteorological conditions provided, the corresponding time-varying electrical load was generated as shown in Figure 6.32.

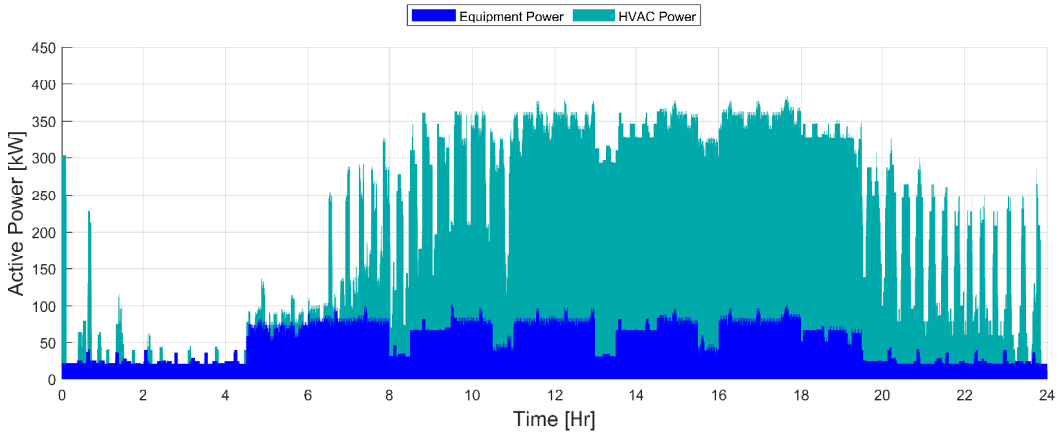

(a) The individual active power contributions from the equipment and HVAC electrical load.

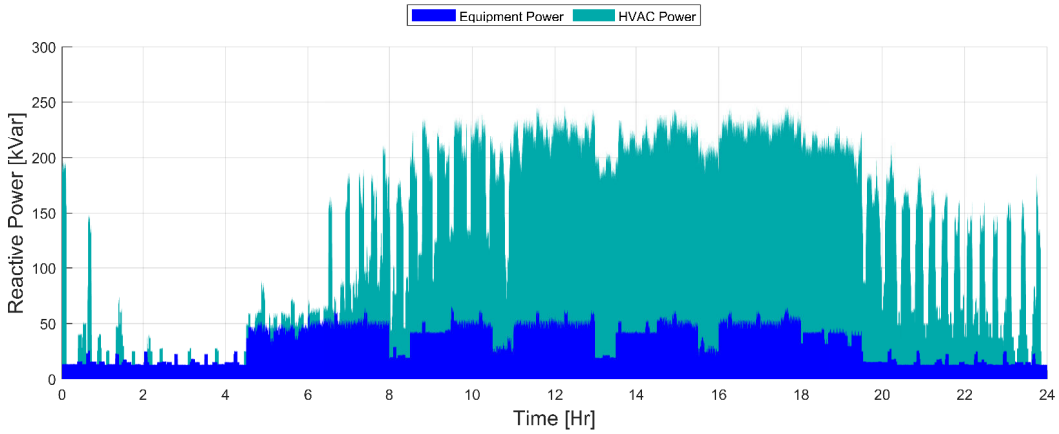

(b) The individual reactive power contributions from the equipment and HVAC electrical load.

Figure 6.32: The complex electrical load distributed across the eighteen load buses.

6.3.2 Energy Management Policy

The energy management policy requires blending of two diesel generators (30 kW TQG and 200 kW TQG), and two military type vehicles (30 kW HMMWV and 125 kW MRAP). For the selected set of generation assets, there exists exactly twenty-four distinctly different fuel trajectories that can be generated using the concatenation methodology provided earlier within this chapter. For the subsequent case studies, three different precedence orders were used, provided in Figure 6.33.

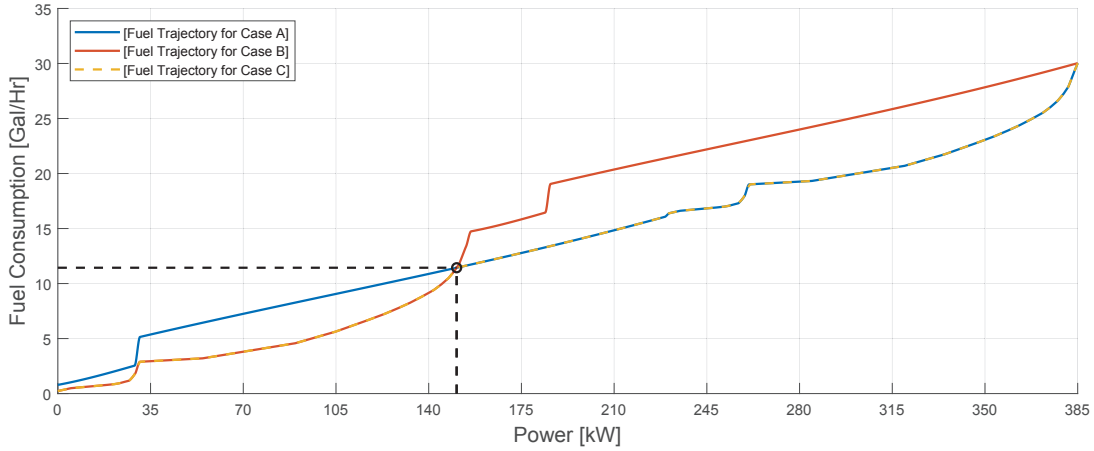

Figure 6.33: The energy management's fuel trajectories used within the subsequent simulation studies.

Three separate simulation studies were conducted using the three different fuel trajectories provided in Figure 6.33. For the first case study (Case A), all four diesel-based generation assets were used, the precedence order requires the use of the 30 kW TQG,

followed by the 200 kW TQG, 30 kW HMMWV, and finally the 125 kW MRAP. For the second case study (Case B), the precedence order of Case A was reversed. The third and final case study includes a combination of both Case A and Case B's fuel trajectories. If the electrical load was such that $(0 < P_{lod} \leq 150)$ kW the precedence order used was that of Case B's fuel trajectory, if however, the electrical load exceeds 150 kW, the precedence order defined by the fuel trajectory for Case A was used. It is expected that the use of Case C's fuel trajectory will yield the most fuel efficient operation.

For the subsequent case studies, a single PV array capable of generating 125 kW of electrical power using an MPPT algorithm was utilized. Similar to Section 6.2 energy management strategy, the fuel trajectories are used to compute the power generation commands for each diesel fuel-based assets. The MPPT was used to generate the PV's power generation commands. All power generation commands were passed to an optimal power flow agent (Section 4.3.4), which computed the optimal complex voltage for each bus within the electrical architecture, which yielded sufficient power flow to accommodate the desired electrical load. The voltage commands were then used in conjunction with the complex nodal admittance matrix to simulate the electrical network. The results collected from each of the three cases are provided in the subsequent section.

6.3.3 Case Studies

The results from the three different case studies are provided in Figure 6.34 - Figure 6.40. Provided in Figure 6.34 - Figure 6.36 include the individual active power contributions required to satisfy the aggregate electrical load, distributed across the eighteen different microgrid buses. The aggregate electrical power was less than the total electrical generation capacity of the diesel fuel based assets (385 kW). In addition to the diesel fuel based assets, there was also a PV array capable of exporting an estimated 125 kW of electrical power using MPPT, in addition to a microgrid electrical storage asset. Regardless of the power apportionment strategy defined previously, there was sufficient generation capacity to satisfy the prescribed electrical load.

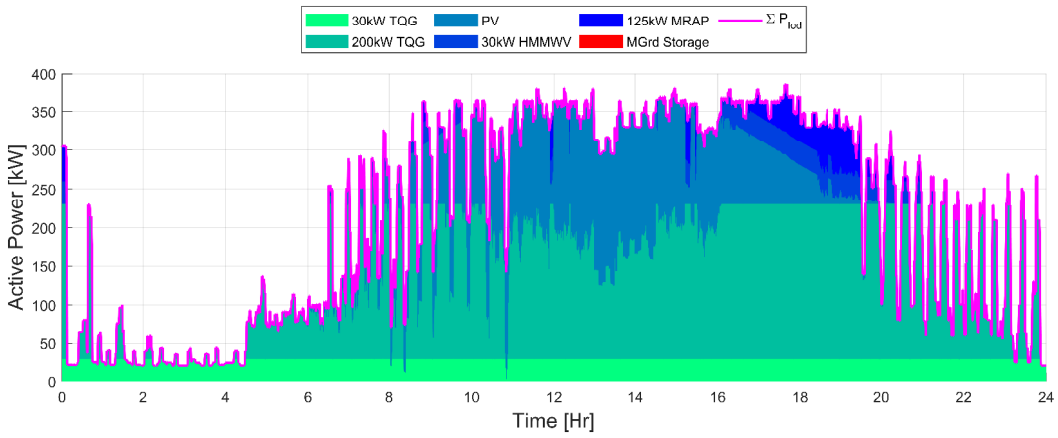

Figure 6.34: Case A - The active power contributions for each asset, instantaneous power was injected via the electrical storage, the bulk of the power was provided by the diesel generators followed by the military type vehicles.

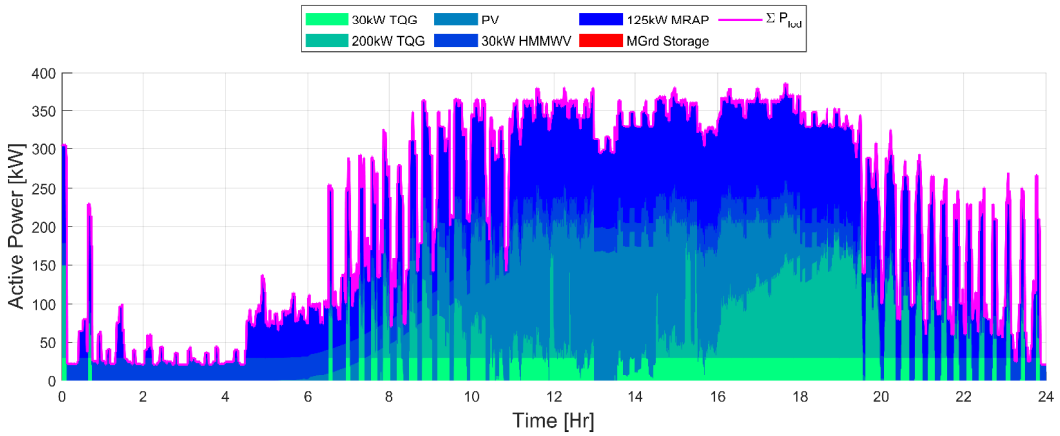

Figure 6.35: Case B - The active power contributions for each asset, instantaneous power was injected via the electrical storage, the bulk of the power was provided by the military type vehicles followed by the diesel generators.

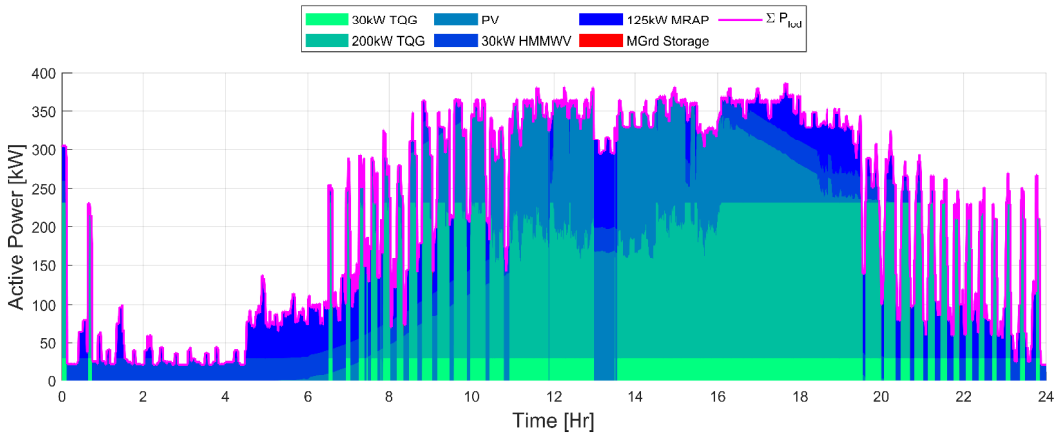

Figure 6.36: Case C - The active power contributions for each asset, instantaneous power was injected via the electrical storage. Depending on the electrical load, the precedence order switches throughout the simulation to yield more fuel efficient behavior.

Now consider the use of bus storage, and the collocated storage within the both the military vehicles and the renewable asset provided in Figure 6.37 - Figure 6.39. The bus storage asset (Figure 6.37) utilizes a different amount of electrical storage

for Case A, B, and C, which results from the optimal power flow agent attempting to minimize electrical losses incurred due to the flow of power throughout the AC electrical architecture. Due to the variable electrical load which increases or decreases beyond 150 kW, it was determined that Case A and B which have fixed precedence orders used minimal energy storage requirements to achieve sufficient power flow when compared to Case C which requires more electrical storage. For all three power apportionment policies, the final electrical storage state was lower than the initial, resulting from non-symmetric loading, and the absence of feedback controls to drive the electrical storage back to the initial energy storage value. For the given power apportionment strategies, it was determined that the electrical storage assets for Case A, B, and C must be fully charged when the simulation starts to accommodate the power apportionment strategies. Further, the electrical storage asset must be sized appropriately, requiring roughly 7.23 MJ, 10.50 MJ, and 36.61 MJ of electrical storage to accommodate the three separate apportionment strategies of Case A, B, and C respectively.

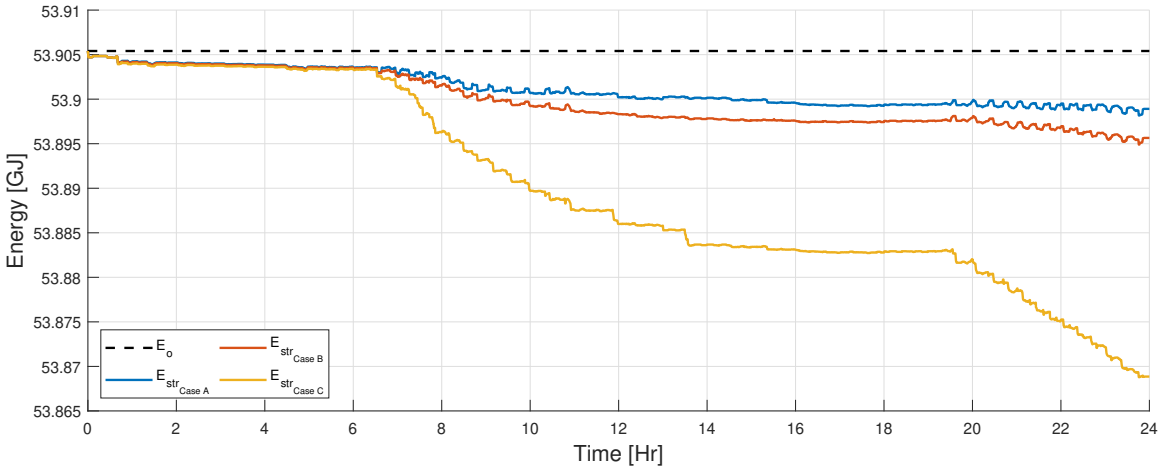

Figure 6.37: The electrical storage asset's energy usage throughout across the three case studies throughout simulation epoch.

Similarly, the collocated electrical storage associated with the renewable asset (Figure 6.38) utilizes a different amount of electrical storage for Case A, B, and C, which results from the optimal power flow attempting to minimize electrical losses. The amount of electrical energy charged or discharged to the electrical storage behaves similarly to the irradiance profile. For all three power apportionment policies, the final electrical storage state was lower than the initial, resulting from non-symmetric loading, and the absence of feedback controls to drive the electrical storage back to the initial energy storage value. Dissimilarly to the electrical storage asset, the final energy state of the renewable's collocated electrical storage increases following an increase in the irradiance, and decreases following a decrease in irradiance. If this had been a clear sky case, the difference between the final energy state and the initial energy state would be reduced when compared to the results provided within

this section. For the given power apportionment strategy, it was concluded that the renewable's electrical storage asset for Case A, B, and C require that the storage contain roughly one-third the total rated energy capacity of the storage asset at the beginning of the 24 Hr period, to accommodate the power apportionment strategy. Further, the electrical storage asset must be sized appropriately requiring roughly 800 kJ, 820 kJ, and 850 kJ of electrical storage for Case A, B, and C respectively.

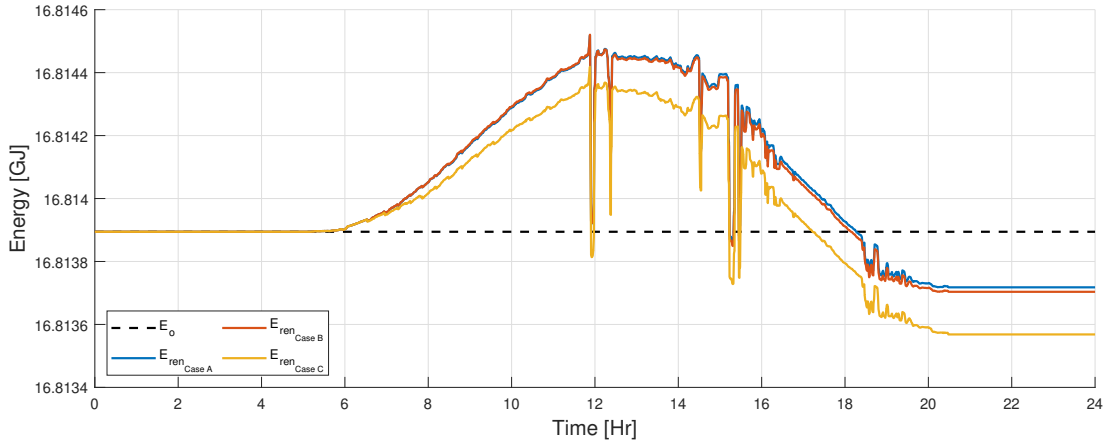

Figure 6.38: The electrical storage energy for the renewable's collocated electrical storage asset for each of the three case studies.

Similarly, the collocated electrical storage associated with the vehicle asset (Figure 6.39) utilizes a different amount of electrical storage for Case A, B, and C. For all three power apportionment policies, the final electrical storage state was lower than the initial, resulting from non-symmetric loading, and the absence of feedback controls. For the given power apportionment strategy, it was determined that the vehicle's electrical storage asset must be sized appropriately requiring

roughly 23.56 MJ, 375.36 MJ, and 77.44 MJ of electrical storage to accommodate the apportionment strategies of Case A, B, and C respectively.

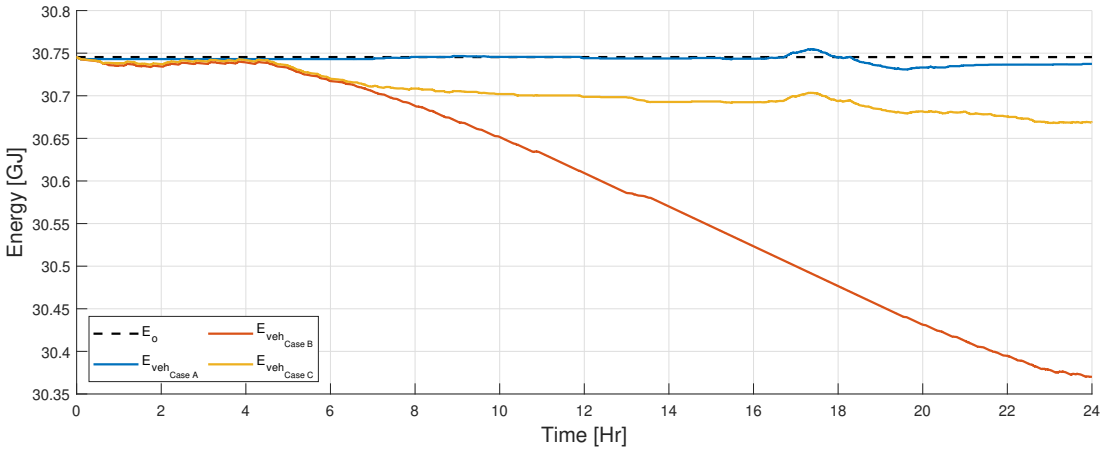

Figure 6.39: The electrical storage energy for the vehicle's collocated electrical storage asset for each of the three case studies.

Now consider the fuel consumed by all diesel fuel based assets. Based on the fuel consumption characteristics of the generators and vehicles, it was determined that the vehicles operate more fuel efficiently as long as the electrical load does not exceed 150 kW. For substantially higher electrical loads exceeding 150 kW, the diesel generators operate more fuel efficiently. This type of behavior was inferred from Figure 6.40. For the first six hours, the fuel consumption rate of the vehicles was less than the generators for both Case B and C, resulting in less fuel consumed. Approximately six and a half hours after the simulation began, the total electrical load continually achieves an electrical load which requires the vehicle's alternators to begin operating at or near its maximum rated output of 30 kW and 125 kW for Case B. Approximately nine

hours into the simulation, the use of the precedence order of Case B consumes more fuel than the precedence order of case A. Conversely, between six and eight hours into the simulation, the electrical load increases such that the use of the variable precedence order of Case C yields more fuel optimal behavior for the entire duration of the simulation epoch, when compared to Case A and Case B fuel trajectories. For Case A, the diesel fuel based assets consumed approximately 290 gallons, while the same diesel fuel based assets consumed approximately 388 gallons for Case B. Finally as one might expect based on the power apportionment policies, the use of both the vehicle and the generator consumed approximately 270 gallons for Case C.

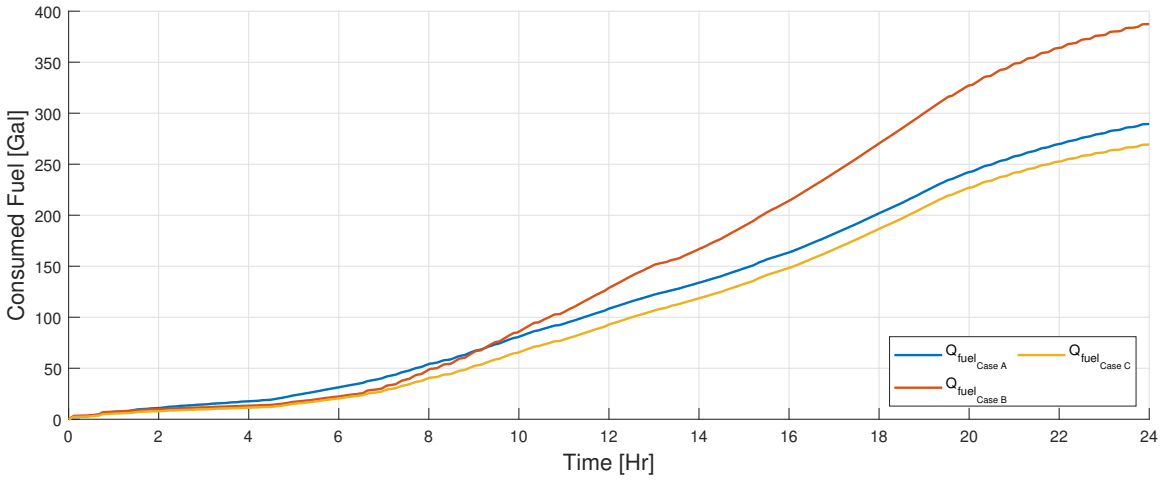

Figure 6.40: The combined fuel consumed by the contingent of the diesel generators and military type vehicles.

For the given power apportionment strategies, it was determined that a 1124% increase in electrical storage capacity yielded approximately a 34% increase in fuel

consumption using the apportionment strategy of Case B over Case A, conversely, it was also determined that approximately a 264% increase in energy storage capacity yielded a 7% decrease in fuel consumption when the apportionment strategy of Case C was used instead of Case A. More fuel optimal behavior was achieved using Case C's power apportionment strategy, but at the cost of requiring greater electrical storage requirements.

In order to assess the optimality of the energy management policies, the equivalent fuel consumption must again be computed. Using both Equation 6.19 and Equation 6.20 the additional fuel costs were computed for each case and added to the original fuel consumption metric, resulting in the equivalent fuel consumption trajectories of Figure 6.41.

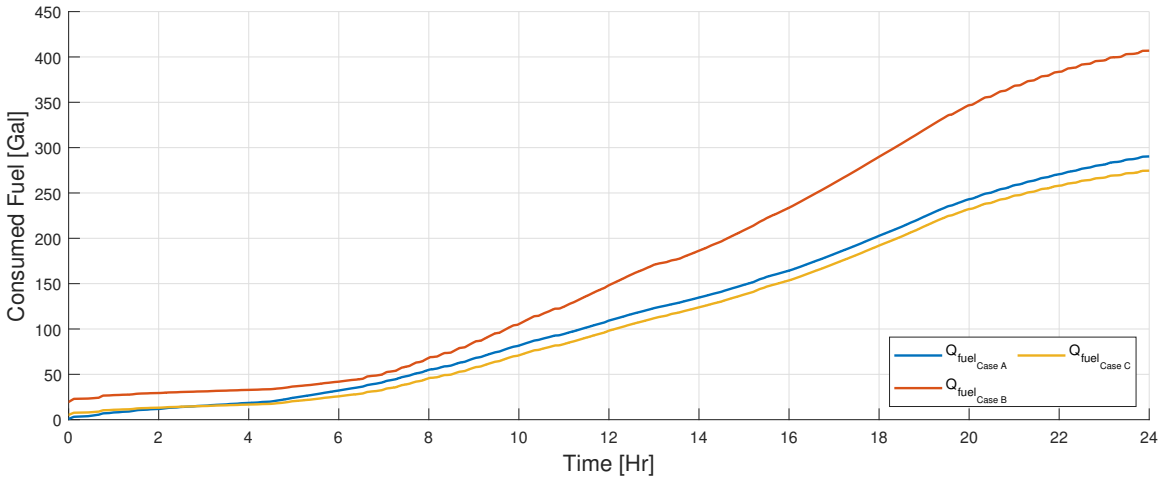

Figure 6.41: The equivalent fuel consumption for each of the three case studies.

The equivalent fuel consumption which incorporates the electrical storage requirements indicates that Case B again yields the least optimal equivalent fuel consumption, primarily due to the minimum storage requirement and the fact that the final energy state was sufficiently smaller than the initial energy storage state. Alternatively there was little difference between the equivalent fuel consumption for Case A and Case C when compared to Figure 6.41. This indicates that the most optimal energy management policy of the three simulated case studies was that of Case C, followed by Case A.

6.4 Blending of Heterogeneous Assets

This section is also subdivided into three subsections, with the first providing information regarding the selected scenario including the electrical architecture, the selected event schedule, and the meteorological weather conditions overlaid with a realistic forecasting methodology, which governs the time varying electrical load. The second section contains information regarding the power apportionment strategies, and the final section presents the results.

6.4.1 Scenario Description

Finally, consider an electrical grid with seven generation assets, including (1) a 30 kW TQG, (2) a 200 kW TQG, (3) a 30 kW HMMWV, (4) a 125 kW MRAP, (5) a single PV array capable of generating 125 kW of electrical power using MPPT, (6) a 60 kW RESCU electrical storage, and (7) a single electrical storage asset directly connected to an AC electrical bus. The 60 kW electrical storage asset could export 60 kW of electrical power for an hour assuming maximum state of charge, after which the asset would be depleted. In addition to the seven electrical generation assets, there were eighteen time-varying complex electrical loads. All of the generation and load assets were connected directly to the main AC electrical distribution bus through an RL transmission line. The corresponding electrical architecture is shown in Figure 6.42.

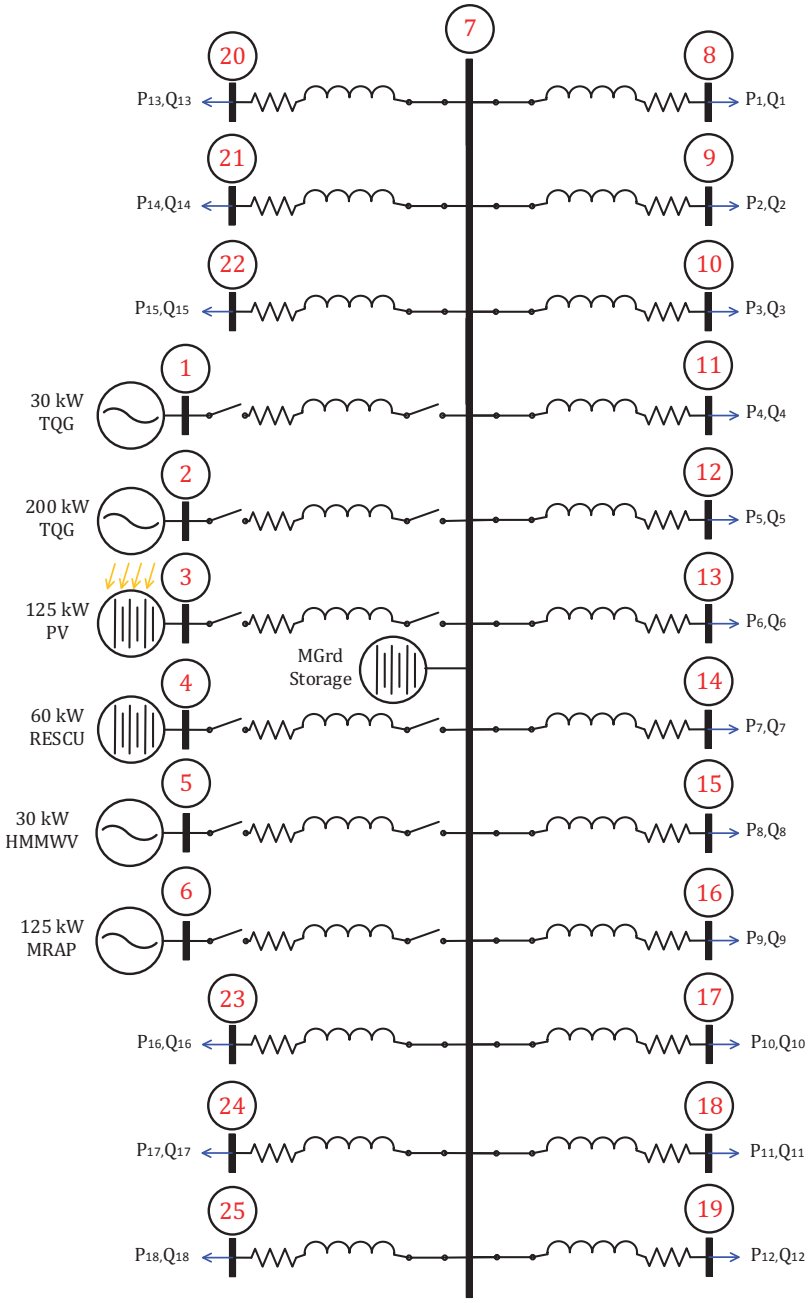

Figure 6.42: The electrical architecture used for the subsequent simulation studies, contains two diesel generators, two military-grade vehicles, a PV array, two electrical storage assets (one general asset, and one directly connected to the AC bus), and eighteen electrical loads.

Both the event schedule and the meteorological weather conditions provided in Figure 6.30 and Figure 6.31 remain unchanged, resulting in the same complex power displayed in Figure 6.32. The only major difference for the subsequent simulation studies include a methodology used to generate the power generation commands. The energy management strategy of Chapter 5 was used, which required meteorological weather forecasts, from which the electrical load associated with the HVAC could be estimated. The event schedule was assumed to repeat every 24 Hrs, this means that the electrical equipment load could be estimated with a high degree of accuracy. A 15 Min persistent forecast was used for the simulation studies, a 1 Hr persistent forecast has been overlaid with the corresponding meteorological weather conditions as a reference to illustrate the persistent forecasting methodology, presented in Figure 6.43.

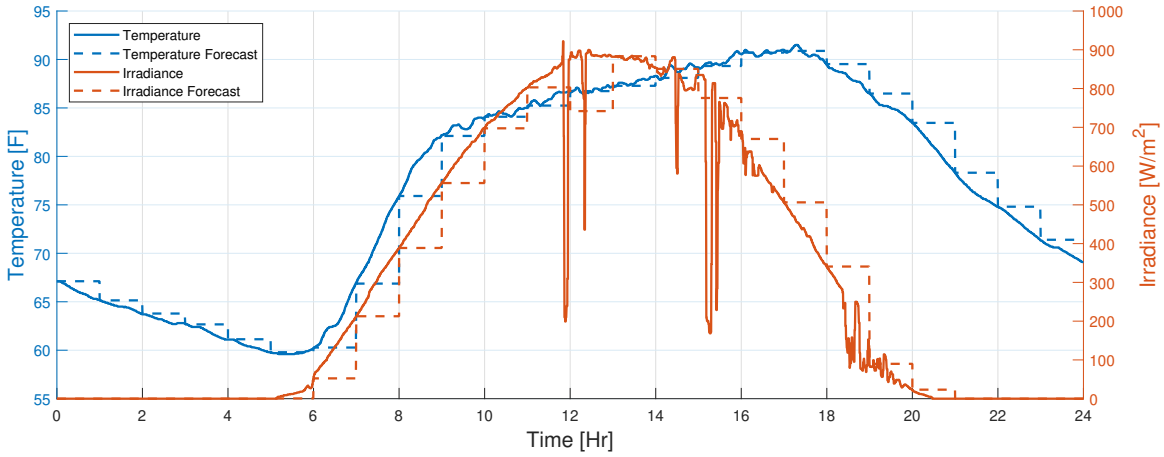

Figure 6.43: The selected meteorological conditions used for the simulation studies include, the ambient temperature and solar irradiance. The temperature profile is directly linked to the HVAC electrical load. The persistent forecasts have been included.

6.4.2 Energy Management Policy

The energy management policy requires blending of two diesel generators (30 kW TQG and 200 kW TQG), and two military type vehicles (30 kW HMMWV and 125 kW MRAP). The same three energy management or precedence orders used within Section 6.3.2 were again used.

For the subsequent case studies, the PV array was capable of generating 125 kW of electrical power using an MPPT algorithm. Unlike the previous simulation case studies, the precedence orders were used in conjunction with the LTO's energy management strategy of Section 5.3 corrected to include vehicle assets and the three different precedence orders of Section 6.3.2. The output of the LTO was then passed to an optimal power flow agent (Section 4.3.4) to minimize line loses resulting from the transfer of power between the individual AC buses and the main microgrid bus, simulated using the complex nodal admittance matrix.

6.4.3 Case Studies

The results from the three different case studies are provided in Figure 6.44 - Figure 6.53. Shown in Figure 6.44 - Figure 6.49 include the individual active power contributions required to satisfy the aggregate electrical load, distributed across the

eighteen different microgrid buses.

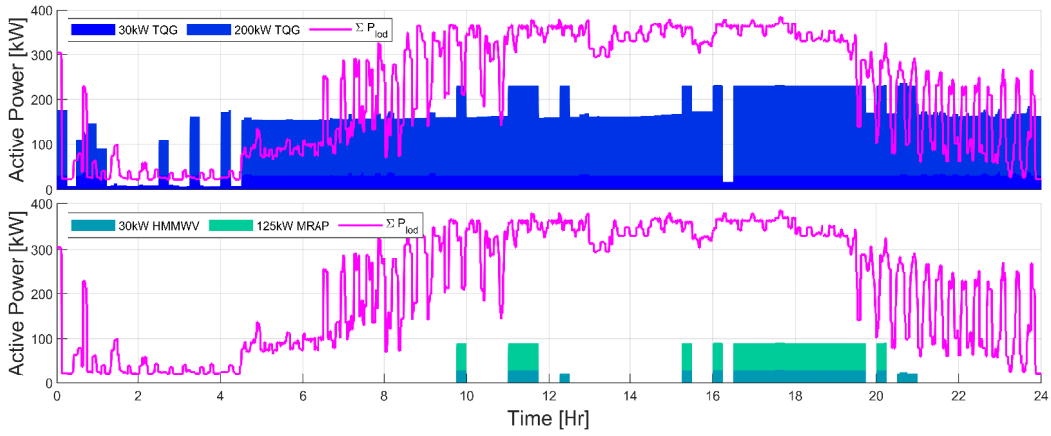

Figure 6.44: Case A - Diesel Fuel Based Asset Electrical Power Contribution compared to the Aggregate Electrical Load

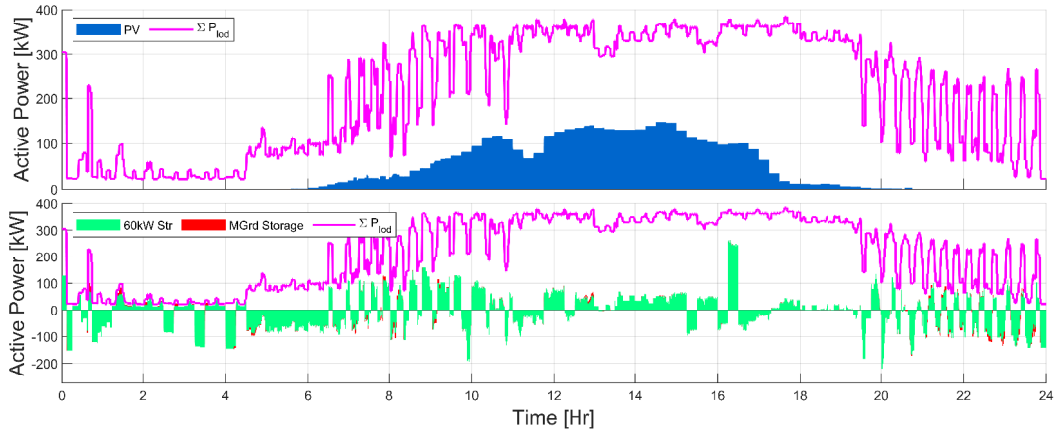

Figure 6.45: Case A - Electrical Storage Based Asset Electrical Power Contribution compared to the Aggregate Electrical Load

Similarly to the results presented in Section 6.3, there was sufficient electrical generation to accommodate all three power apportionment strategies. Unfortunately, due to the added contribution of the dedicated 60 kW electrical storage, the individual electrical power contributions for each asset cannot be readily plotted on a single figure. Requiring each of the individual power contributions to be separated among two

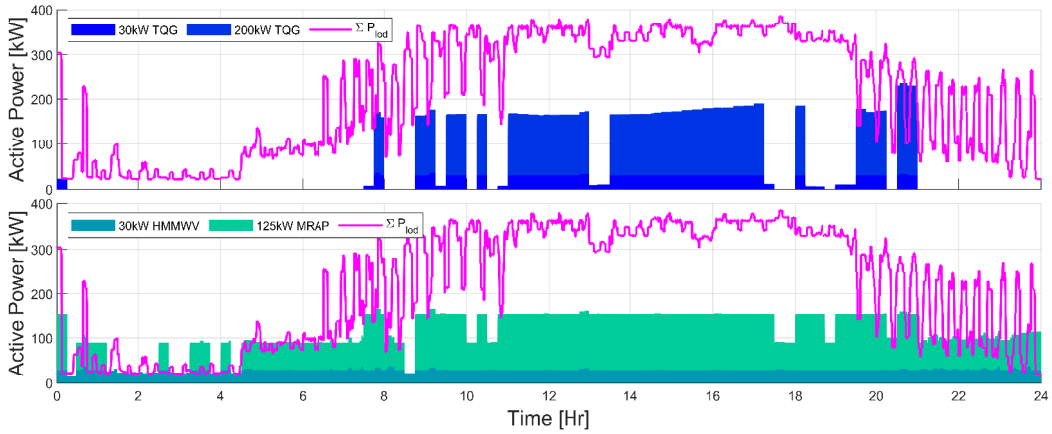

Figure 6.46: Case B - Diesel Fuel Based Asset Electrical Power Contribution compared to the Aggregate Electrical Load

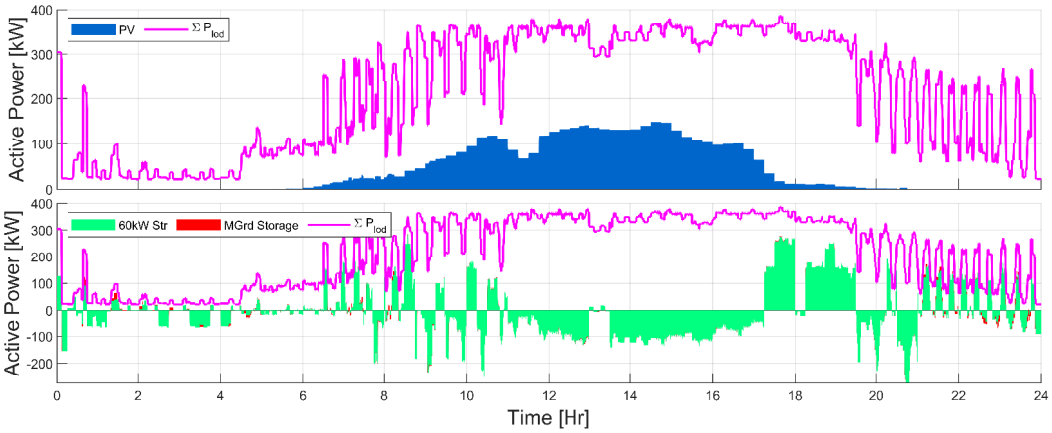

Figure 6.47: Case B - Electrical Storage Based Asset Electrical Power Contribution compared to the Aggregate Electrical Load

separate figures for each of the three case studies. Figure 6.44 - Figure 6.45 contain the individual power contributions for the power apportionment strategy of Case A. When the active power contributions are summed for each asset, they yield the total aggregate electrical load. Notice that when adding the diesel fuel based contributions with the PV contributions the total generated electrical load may be higher than the aggregate electrical load. If this was the case, the dedicated electrical storage charged

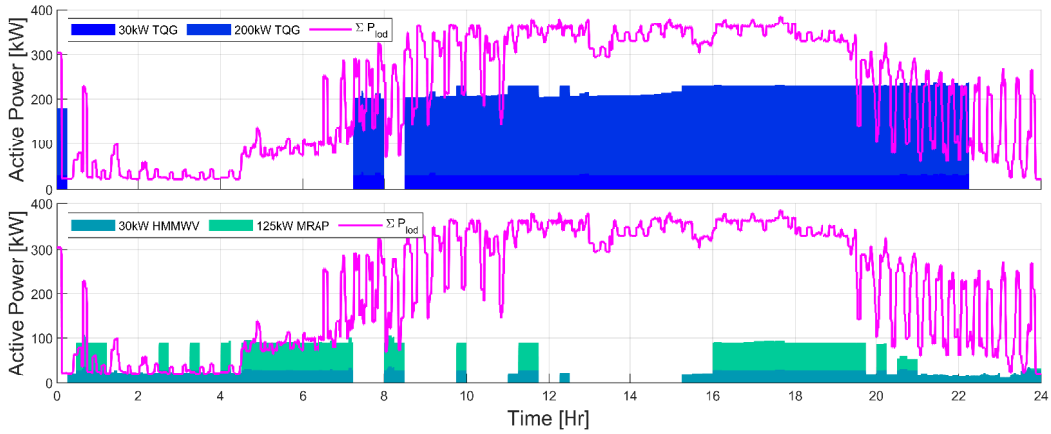

Figure 6.48: Case C - Diesel Fuel Based Asset Electrical Power Contribution compared to the Aggregate Electrical Load

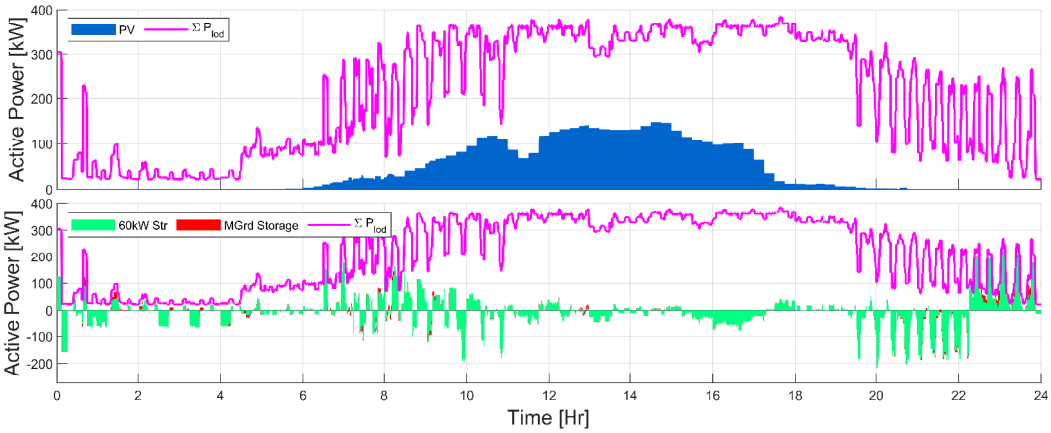

Figure 6.49: Case C - Electrical Storage Based Asset Electrical Power Contribution compared to the Aggregate Electrical Load

to track the electrical load. If the added contributions are less than the electrical load, the electrical storage discharged to satisfy the prescribed electrical load. Similar behavior was also observed within Figure 6.46 - Figure 6.47, and Figure 6.48 - Figure 6.49 for Case B, and C.

Now consider the use of electrical storage, and the collocated storage within the both

the military vehicles and the renewable asset provided in Figure 6.50 - Figure 6.52. The combination of bus storage and the 60 kW RESCU electrical storage asset (Figure 6.50) utilizes a different amount of electrical storage for Case A, B, and C, again resulting from the optimal power flow agent, dissimilarly the LTO's energy management solution also contributes to additional differences. Unlike the previous case studies, the inclusion of the energy management policies within the LTO enables, the LTO's energy management solution to correct for differences between the predicted and measured operating conditions. This allows the LTO to try and manage the electrical storage assets to drive the final energy state toward the initial energy state. Additionally, the combination of the bus storage and the 60 kW RESCU mirrored the aggregate electrical storage of the vehicle and renewable assets. This will most likely never be achieved as added electrical losses within the AC and DC electrical architectures are not included within the LTO's formulation. For the given power apportionment strategies, it has been determined that the electrical storage assets for Case A, B, and C must contain an estimated 203.59 MJ, 204.95 MJ, and 171.41 MJ at the beginning of the simulation. The combined electrical storage capacity of the bus storage and the 60 kW RESCU must then be 1.20 GJ, 2.12 GJ, and 1.27 GJ to accommodate the three separate apportionment strategies of Case A, B, and C respectively. Similarly, the collocated electrical storage associated with the renewable asset (Figure 6.51) also utilizes a different amount of electrical storage for Case A, B, and C. For all three power apportionment policies, the final

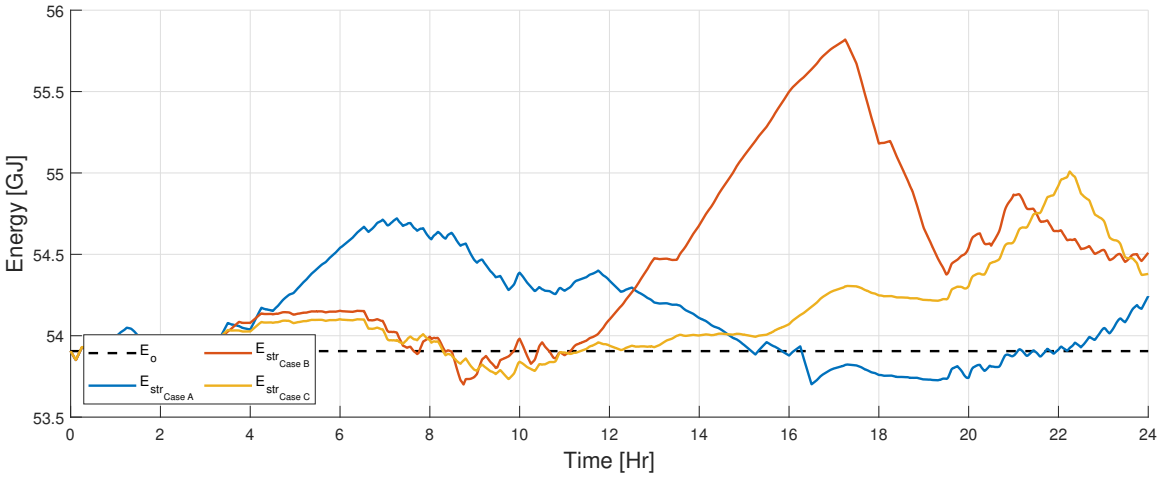

Figure 6.50: The electrical storage asset's energy usage throughout across the three case studies throughout simulation epoch.

electrical storage state was lower than the initial, resulting from non-symmetric loading, and the absence of specific feedback controls to drive the electrical storage back to the initial energy storage value. While there are no specific feedback controls to make sure the renewable's energy state ends where it began, there was a combined final energy state constraint which considers all electrical storage assets. Recall that the combination of both the bus storage and the 60 kW RESCU electrical storage resulted in a final energy state which was higher than the initial energy state. To ensure the final energy state was roughly equal to the initial energy state (aggregate electrical storage) within the LTO's optimization routine, the renewable energy state ends at a lower energy state than the initial energy state, offsetting the bus storage and the 60 kW RECU's electrical storage state. For the given power apportionment strategies, it has been determined that the renewable's electrical storage asset for Case A, B, and C must contain an estimated 371.91 MJ, 371.78 MJ, and 371.90 MJ at the beginning of the simulation. The PV's collocated electrical storage must

then be 438.90 MJ, 438.82 MJ, and 438.87 MJ to accommodate the three separate apportionment strategies of Case A, B, and C respectively.

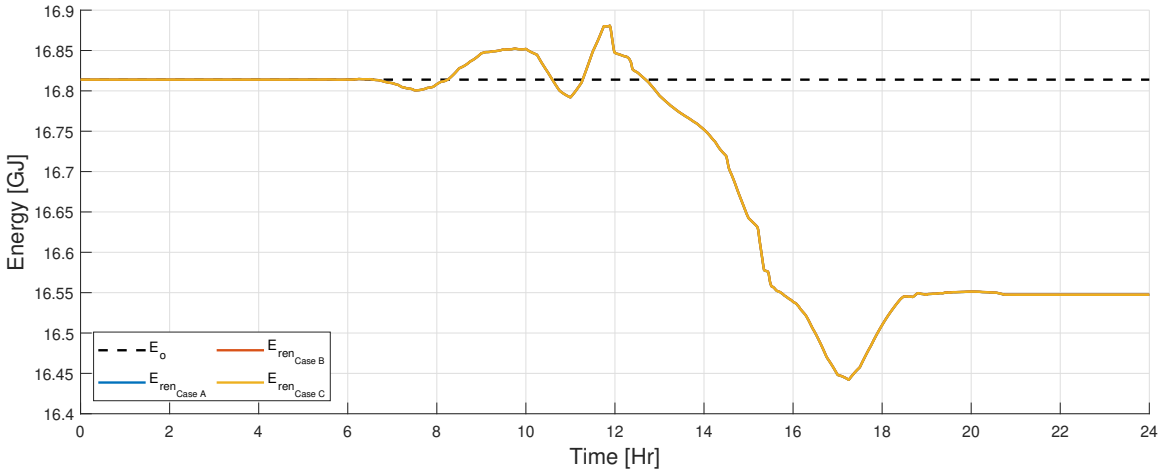

Figure 6.51: The electrical storage energy for the renewable's collocated electrical storage asset for each of the three case studies.

Now consider the collocated electrical storage associated with the vehicle assets (Figure 6.52). Recall that the combination of both the bus storage and the 60 kW RESCU electrical storage resulted in a final energy state which was higher than the initial energy state. If the contribution from renewable asset was added to the combined electrical assets, the final energy state would still be higher than the initial energy storage state. To satisfy the end storage constraint within the LTO's optimization routine, the vehicle's energy storage must end at a lower energy state to accommodate the use of the other electrical storage assets. For the given power apportionment strategies, it was determined that the vehicle's electrical storage asset for Case A, B, and C must contain an estimated 30.63 MJ, 395.40 MJ, and 97.58 MJ

at the beginning of the simulation. The vehicle's collocated electrical storage must then be 30.63 MJ, 395.40 MJ, and 97.58 MJ to accommodate the three separate apportionment strategies of Case A, B, and C respectively.

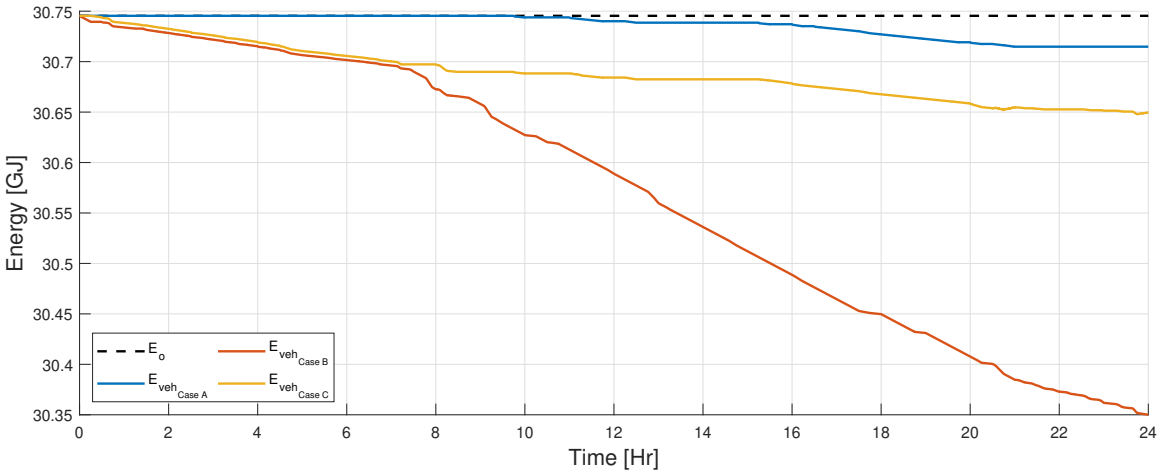

Figure 6.52: The electrical storage energy for the vehicle's collocated electrical storage asset for each of the three case studies.

Now consider the fuel consumed by all diesel fuel based assets. Based on the fuel consumption characteristics of the generators and vehicles, it was determined that the vehicles operate more fuel efficiently as long as the electrical load does not exceed 150 kW. For substantially higher electrical loads exceeding 150 kW, the diesel generators will operate more fuel efficiently. This type of behavior was inferred from Figure 6.53. For Case A, the diesel fuel based assets consumed approximately 312 gallons, while the same diesel fuel based assets consumed approximately 390 gallons for Case B. Finally as one might expect based on the power apportionment policies, the use of Case C's fuel trajectory resulted in approximately 300 gallons of fuel consumed. For

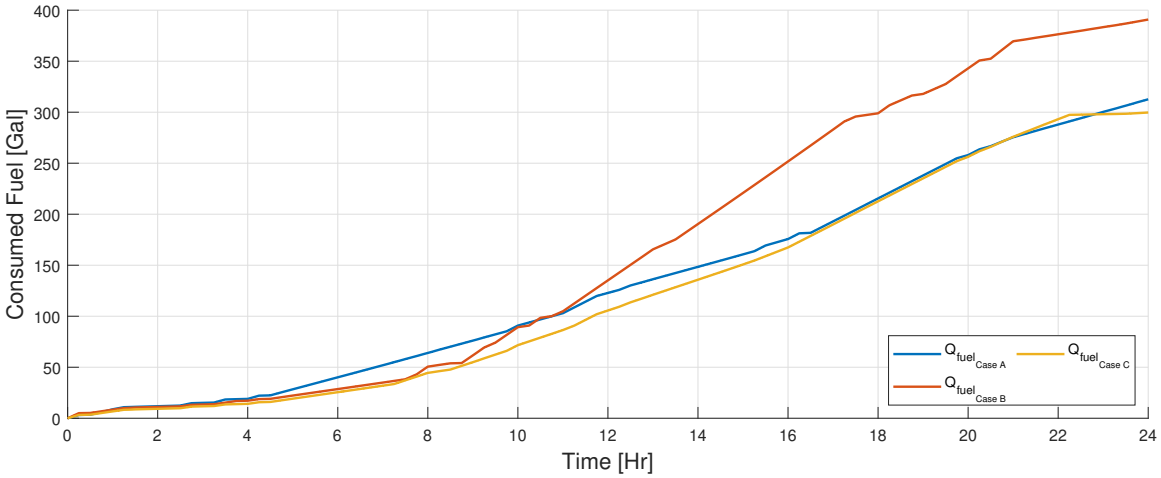

Figure 6.53: The combined fuel consumed by the contingent of the diesel generators and military type vehicles.

the given power apportionment strategies, it was determined that a 98% increase in electrical storage capacity yielded approximately a 25% increase in fuel consumption using the apportionment strategy of Case B over Case A, conversely, it was also determined that approximately a 22% increase in energy storage capacity yielded a 4% decrease in fuel consumption when the apportionment strategy of Case C was used instead of Case A. More fuel optimal behavior could be achieved using Case C's power apportionment strategy, but at the cost of requiring greater electrical storage requirements.

In order to assess the optimality of the energy management policies, the equivalent fuel consumption must again be computed. Using both Equation 6.19 and Equation 6.20 the additional fuel costs were computed for each case and added to the original fuel consumption, resulting in the equivalent fuel consumption provided in Figure 6.54. The equivalent fuel consumption which incorporates the electrical stor-

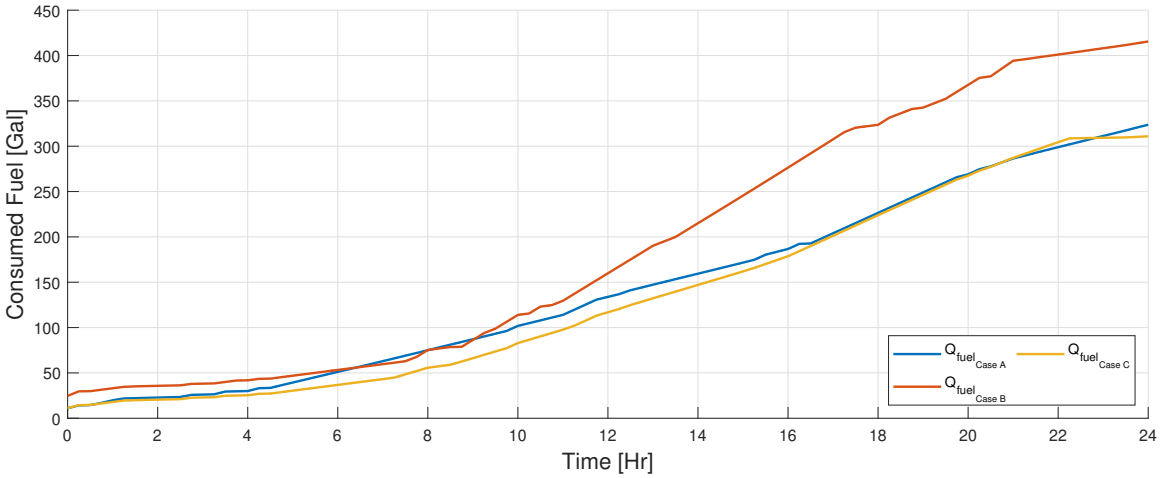

Figure 6.54: The equivalent fuel consumption for each of the three case studies.

age requirements indicates that Case B again yields the least optimal equivalent fuel consumption, primarily due to the minimum storage requirement and the fact that the final energy state was sufficiently smaller than the initial energy storage state. Alternatively there was not much difference between the equivalent fuel consumption for Case A and Case C when compared to Figure 6.54. This indicates that the most optimal energy management policy of the three simulated case studies was that of Case C, followed by Case A.

6.5 Conclusions

The results collected from the three previously provided case studies indicated that using known characteristics of a vehicles alternator or ISG in addition to the engine power and torque curves, and a variable speed and torque fuel map for a vehicle,

the two degree of freedom fuel consumption model of a vehicle was approximated as a single degree of freedom fuel consumption model. The approximate fuel consumption models of the vehicles are similar to traditional diesel generator fuel consumption models, this enables blending of the diesel fuel based assets, resulting in a power apportionment strategy. Using the concatenation methodology described in Section 6.1.1 in addition to a permutation vector, the infinite solution space could be bounded, and the most optimal power apportionment strategy identified. The optimal strategy may require generation assets to be continuously brought online or taken offline. If there are no electrical storage assets that permit near instantaneous injection of power to accommodate load imbalances, roughly double the fuel consumption may be observed around these transitional points, to switch between more or less optimal power apportionment strategies.

Complete blending of renewable and diesel fuel based assets was achieved using a power apportionment strategy to blend the diesel fuel based assets. This apportionment strategy was then coupled with an MPPT algorithm to blend both the diesel fuel based assets in addition to the renewable assets. Using the combination of the two, more optimal fuel consumption was observed, leading to more optimal energy management of the generation assets.

Finally, incorporation of both the blending policy used for diesel fuel based assets,

the MPPT algorithm, and the LTO's energy management strategy, and the adaptive leader election short-term optimal energy management strategy, a diverse set of heterogeneous assets could be managed and controlled. The inclusion of the LTO's energy management strategy enables long-term optimization to be performed, which may yield more optimal energy usage for a given scenario. Among the scenarios presented within the chapter, the results collected using the LTO provided in Section 6.4 were sub-optimal when compared to the results collected from Section 6.3. There are multiple reasons why this could potentially occur. In order for the LTO to operate, it requires meteorological forecasts, if the forecasts are incorrect, the LTO accounts for this, and tries to obtain the most fuel efficient behavior. If the error within the forecasts were reduced, the operation of the LTO may converge toward the solution obtained in Section 6.3.

Let it also be known that more optimal energy solutions may not be obtained using the LTO's energy management solution due to the use of an additional electrical storage asset. The LTO's energy management solution will attempt to minimize fuel consumption, energy storage may be used more extensively to minimize fuel consumption over the twenty-four hour epoch. Further the electrical storage was designated as a slack asset within the energy management strategy. This ultimately means that the asset was required to inject additional current to ensure sufficient power flow. This likely means the electrical storage will be operating at higher electrical loads when compared to the loads of Section 6.3, meaning greater electrical losses. This

potentially means that the use of the energy management strategy may be unable to reduce electrical losses and fuel consumption to the point in which more optimal energy solutions are obtained, when compared to the results collected in Section 6.3.

The LTO's optimal solution policy also enables long term forecasting. While not shown, the results collected within Section 6.3 could lead to potential load deficits, if the electrical load exceeds the rated electrical generation capacity. If this happens, load shedding must be completed to maintain grid stability. Using the long-term forecasting capabilities of the LTO, these types of situations could be avoided by charging the various electrical storage assets prior to conditions in which load deficits may occur. During the load deficits, the various electrical storage assets would discharge enabling no or minimal load shedding to occur. Additional runs were completed and provided in Appendix C to test the hypothesis that decreasing the forecast interval and increasing the execution frequency of the LTO could enable more optimal solutions to be obtained similar to those provided in Section 6.3. Continuous versus discrete optimization of the LTO was also considered.

Chapter 7

Summary and Conclusions

In Chapter 6 a methodology to blend a set of heterogeneous assets with competing objective functions was provided, which built on all previously presented material within Chapter 1 - Chapter 5 regarding modeling and simulating AC electrical grids, coupled with various control or energy management strategies. Within this final chapter, the main results and conclusions from the proceeding research efforts are presented, followed by future further research efforts. The chapter concludes with a complete list of the current and future list of publications generated.

7.1 Conclusions

In Chapter 3, optimal power management of vehicle sourced military outposts was considered, with diesel generators, electrical storage, and military type vehicles during a 72 Hr build-up phase of the outpost. Two different scenarios were simulated, one considered continuous uninterrupted construction of the outpost, while the second includes discontinuous interrupted construction of the outpost which yielded insufficient generation capacity throughout the buildup phase. The electrical assets were controlled assuming a centralized control architecture, configured to use minimal fuel provided the availability of the assets was defined by an event schedule. The results indicated that military vehicle's such as an MRAP or HMMWV could be used in addition to ordinary generation equipment (diesel generators and electrical storage) to meet a time-varying electrical load. Military vehicles such as the MRAP or JLTV possess the ability to export electrical power commensurate with typical military grade diesel generators. Conversely, integration of the vehicle assets could lead to potential load deficits if insufficient electrical generation equipment was absence from the asset pool. Insufficient electrical generation capabilities require load shedding, without which, grid instability may occur. To aid in the decision to shed electrical loads, the time-varying electrical load was divided into three prioritized electrical loads, which were further subdivided into multiple shelters. Shelters are physical structures which contain electrical equipment, common shelter designations

include laundry, billeting (general living quarters), combat operations centers (COC), and chow hall. Using shelter designations in addition to a prioritized electrical load, lower prioritized electrical loads could be shed, during or proceeding anticipated load deficits mitigating potential grid instabilities. To avoid this type of behavior, enough stationary electrical power generation equipment should be delivered to the outpost during the build-up phase of the electrical grid. If however the logistical supply chain was interrupted, or requires simplification, military-type vehicles could be used to aid in the construction or operation of a microgrid. It was postulated that more optimal fuel usage or energy usage could be obtained if additional information was provided to a supervisory control agent regarding the availability of the assets. Further, the centralized control strategy implemented requires large communication throughput, which limits the scalability and extensibility of the control algorithms.

Then in Chapter 4, a centralized electrical control structure was again applied to control an AC electrical microgrid containing diesel generators and military type vehicles similar to the research effort provided in Chapter 3. Dissimilarly, the centralized control was modularized and disseminated among all electrical generation assets, forming a distributed control architecture which was less susceptible to a single point of failure due to the control architecture. Each generation asset had the ability to compute an optimal power apportionment strategy and implement $frac1N^{th}$ of a solution to control the AC grid. Due to the presumed manufacturing differences in addition to unknown communication delays, the use of each apportionment strategy

independently to control the AC grid would likely lead to grid instability. To manage the contingent of assets, an adaptive leader election protocol was introduced which used time-varying leader desirability criteria to elect both a primary and secondary leader. The measurements used to compute the desirability to lead were based on the longevity of the availability of the assets to provide electrical power such as rated electrical power, fuel consumption rate, remaining fuel capacity, current availability, and future availability limited to a fifteen-minute look ahead. Using this type of criteria, the assets with the greatest longevity were always elected to lead, and deterministic events such as maintenance or insufficient fuel consumption were less likely to affect the stability of the electrical grid. Assets with diminishing longevity were less likely to be elected leader and ramped down or up proceeding or following scheduled topology changes, which could be extended to include diminishing fuel capacity. The inclusion of the leader election protocol enables a single AC power apportionment policy to be generated via cooperative negotiation, yielding a single power flow solution which enables control of the grid. The leader election protocol used two different types of communication forwarding strategies including, (1) the nearest neighbor algorithm, used to conduct the leader election, and (2) bidirectional communication, used to report the current measurements of each asset and to implement the control commands. The resulting communication forwarding strategies resulted in a communication complexity of at most $2N$, in contrast, a fully connected communication system requires N^2, this improves the scalability and extensibility of

implementing a centralized control architecture for an AC electrical grid. This research effort focused more on the implementation of an apportionment policy with optimal power flow, minimizing dissipative electrical losses. In subsequent studies, more optimal fuel usage behavior was achieved for a diverse set of generation assets.

The previous research endeavors required continuous periodic optimization for short term optimal control to minimize fuel consumed or dissipative energy losses. In Chapter 5, a long-term optimal energy management strategy was derived for control of an AC electrical network, which used a model predictive control (MPC) methodology to provide optimal energy use with regards to both fuel consumption and energy charged or discharged via an electrical storage device. The fuel consumption characteristics for each diesel generator were concatenated to form a complete fuel consumption trajectory, enabling fuel consumption for the diesel generators to be estimated, also providing a power apportionment strategy specific to the diesel generators simplifying the subsequent optimal energy management policy. Multiple forecasting methods were generated and applied to predict future operating conditions which affect both the electrical load and the generation assets. In particular, the ambient temperature and solar radiation forecast were generated. From the forecasts, the anticipated maximum electrical power generated via a photovoltaic array could be predicted, in addition to the electrical load. The electrical load was subdivided into two components; (1) an equipment power, invariant of the weather conditions, and (2) the HVAC power, which varies as a function of temperature. The equipment power was driven

by an event schedule which was presumed to be repetitive for a 24 Hr epoch. Using the predicted electrical load, fuel consumption characteristics of the diesel generators, and electrical storage measurements for all electrical storage assets throughout the AC electrical grid (distributed electrical storage at each microgrid bus, in addition to electrical storage collocated at a PV array, termed the PV storage), a long-term optimal energy management solution could be computed and implemented to yield more optimal energy use. Multiple forecast intervals were studied, using variable meteorological conditions considering clear sky, partly cloudy sky, full overcast sky, and monsoon sky conditions. The results indicated, that more optimal energy usage occurred for smaller forecast intervals, and as the forecast interval increased, the fuel consumed increased linearly. The estimated electrical storage requirements were also tracked which followed a similar linearly increasing trend as forecast interval increased for all sky conditions. The research effort yielded considerable insight regarding long-term optimal energy management of an AC electrical grid containing stationary diesel generators, distributed electrical storage, and renewable power generation assets. Capabilities and methodologies created and implemented within the research effort could be extended to include a more diverse set of generation assets.

Finally, in Chapter 6, a methodology to blend a set of heterogeneous assets with competing objective functions was established. First fuel consumption characteristics for multiple diesel generators were considered, which include a single degree of freedom (output electrical power vs fuel consumption rate). A methodology to blend a set of

diesel generators was then provided, however, the methodology that yielded optimal fuel usage was problematic. The optimal fuel usage policy could potentially include more than N transition points, for N diesel generators. At a transition point, multiple assets must be ramped up or down simultaneously to achieve more fuel optimal operation. During a transition, roughly double the fuel consumption may be consumed. This behavior could be mitigated if coupled with electrical storage, capable of handling high-speed transient current injections, correcting for momentary power imbalances. Further, if the electrical load was continuously requiring assets to be turned on or off rapidly in accordance with the optimal fuel trajectory, degradation of the asset is expected. As such, it was identified the most optimal behavior of the generators was best obtained by concatenating the diesel generators fuel consumption based on the anticipated electrical load. Military type vehicles were then considered, dissimilar to the generators, the vehicle's fuel consumption varies as a function of the speed and torque of the engine. This results in a two degree of freedom fuel consumption model as opposed to a single degree of freedom fuel consumption model when compared to traditional diesel generators. This makes the blending of diesel-fuel based assets challenging. Using characteristics relating to the physical components within the vehicle platform including the engine and an alternator or ISG, a similar methodology used for the generators could be constructed for the vehicles which reduced the two degree of freedom fuel consumption model, to an approximate single

degree of freedom model. This approximate fuel consumption model enables blending of diesel-fuel based assets. Proceeding the blending of diesel-fuel based assets, a methodology to obtain maximum power generation of a PV array was provided. The three different policies were then combined and simulated, resulting in three different case studies; (1) considering diesel fuel based assets, (2) considering diesel fuel based assets in addition to renewables, and (3) one which considered diesel fuel assets, renewables, and electrical storage. The third case study was coupled with the energy management policy provided in Chapter 5, this results in a complete methodology to blend a diverse set of generation assets. The methodology provided within Chapter 6 could be extended to include a more diverse set of electrical assets or applied to a more general energy network.

To conclude, the previous research efforts focused on modeling various power generation devices found within a hybrid electrical network with a set of diverse heterogeneous assets. Coupled with realistic deterministic events and meteorological data, variable electrical loads were generated forming an operational scenario. Centralized control strategies were applied to the selected electrical architectures, from which various energy management policies capable of minimizing value stream impacts such as fuel consumed or dissipative energy losses were developed. The studies indicated that a reduction of fuel consumption could be obtained, however, a significant reduction in fuel consumption typically requires excessive electrical storage requirements, which could lead to suboptimal energy management. Careful moderation of the grid's

assets was required to obtain more energy efficient operation, potentially simplifying the logistical support requirements and boosting the capabilities of an electrical grid, leading to improved resiliency, reliability, and security. The primary application area revolved around military operations, however, the capabilities developed could be extended for disaster relief operations and more general civilian-based electrical grids.

7.2 Future Work

To conclude, the previous research efforts focused on modeling various power generation devices found within a hybrid electrical network with a set of diverse heterogeneous assets. Coupled with realistic deterministic events and meteorological data, variable electrical loads were generated forming an operational scenario. Centralized control strategies were applied to the selected electrical architectures, from which various energy management policies capable of minimizing value stream impacts such as fuel consumed or dissipative energy losses were developed. The studies indicated that a reduction of fuel consumption could be obtained, however, a significant reduction in fuel consumption typically requires excessive electrical storage requirements, which could lead to suboptimal energy management. Careful moderation of the grid's assets was required to obtain more energy efficient operation, potentially simplifying the logistical support requirements and boosting the capabilities of an electrical grid, leading to improved resiliency, reliability, and security. The primary application area

revolved around military operations, however, the capabilities developed could be extended for disaster relief operations and more general civilian-based electrical grids.

The previous research endeavors considered stationary electrical networks, some of which contained transient assets. Future military applications likely include a more diverse set of assets which are dynamic and should be considered as more general energy networks, with variable power generation, storage, and computational capabilities. Such a set of diverse assets require extensible power apportionment and control policies coupled with high-speed secure communication in order to effectively operate and support future operations.

Future work should include the development of higher fidelity models that support integration for hardware-in-the-loop (HIL) or software-in-the-loop (SIL) modeling and simulation, compatible for use on real-time simulators. The higher fidelity models would enable more complex dynamics to be modeled, which could greatly affect the development of energy management policies to control an energy network. The use of a real-time simulator would require software which is closer to field deployable and could aid in the development of new hardware or software.

Current technological capabilities have resulted in relatively cheap and extensive computational hardware and software, including the OPAL real-time simulator, real-time digital power systems simulator (RTDS), HIL Typhoon, PC 104, Raspberry PI, and Arduino which could be used to develop and implement variable control algorithms

for a variety of applications. One such research effort currently being pursued is the use of the long-term energy management strategy applied to a DC electrical network. The initial deployment of the energy management strategy will likely include the use of an ordinary laptop computer communicating in near real-time through UDP, or deployment directly to a Raspberry PI. The algorithm would be tested within a simulation prior to integration within physical hardware.

Aside from physical hardware, additional research endeavors are currently underway to further develop the long-term energy management policy with integration to consider exergy. Specifically, exergy principles were integrated with a time-varying electrical load generated using energy-based mathematical models. Some of which are relatively invariant to the changing meteorological weather conditions, while some are highly dependent on the current and future conditions. Using the principles of exergy, the electrical load may be altered to obtain more optimal use of the resources, providing greater insight regarding optimal energy management of the electrical assets.

In the fall of 2017 a research project termed the Autonomous Agile Microgrid (AAM) concluded, the main goal of the project was to develop a platform for advanced agent-based control of an electrical grid. The AAM's control architecture was such that the simulation environment could report various value stream impacts within the complete electrical architecture, in addition to a host of communication-based signals and performance criteria contained within a compiled data set. Given recent

technological advancements regarding open source software, artificial intelligence, and machine learning algorithms, components of the AAM will likely be leveraged and extended through the use of machine learning to develop more diverse, complex, and exotic control architectures and algorithms for control of energy networks.

Finally, many if not all energy management strategies developed assumed the individual generation assets could be programmatically turned on or off, in doing so more optimal operation of the assets lead to decreased fuel consumption or energy storage requirements. In reality, the "autonomous" operation of the assets is not currently supported, and would ultimately impact the EMS. Investigation of the non-autonomous and autonomous operation is an area which requires additional research, this would help identify the effect the operation of the assets has on the EMS. Further, this effort would help to drive the need to further development and implementation of distributed controls which enable generation assets to be remotely controlled, enabling more efficient operation of the assets.

References

[1] S. Vergura, "A complete and simplified datasheet-based model of pv cells in variable environmental conditions for circuit simulation," *Energies*, vol. 9, no. 5, 2016. [Online]. Available: http://www.mdpi.com/1996-1073/9/5/326

[2] S. J. Matthews, "Small tactical electric power - technology advancement - application - transition," https://arpa-e.energy.gov/sites/default/files/Matthews_CERDEC_GENSETS_v2.pdf, U.S. Army RDECOM - CERDEC CPI Power Division, accessed: 2017.

[3] IHS, "Silent watch: Vetronics technology creates new vehicle roles," http://www.janes360.com/images/assets/583/67583/Silent_watch_Vetronics_technology_creates_new_vehicle_roles_edit.pdf, U.S. Army RDECOM - CERDEC CPI Power Division, accessed: 2017.

[4] J. Hancock, S. W. Kolhoff, D. Z. McGrew, M. A. M. Ph.D., A. G. Skowronska,

J. Vandiver, J. Gatherer, J. Palmer, R. Wood, P. Curtiss, and M. Dorflinger, "Tactical vehicle to grid and vehicle," 2016.

[5] R. Langner, "Stuxnet: Dissecting a cyberwarfare weapon," *IEEE Security & Privacy*, vol. 9, no. 3, pp. 49–51, 2011.

[6] W. Kempton and J. Tomić, "Vehicle-to-grid power fundamentals: calculating capacity and net revenue," *Journal of power sources*, vol. 144, no. 1, pp. 268–279, 2005.

[7] S. Han, S. Han, and K. Sezaki, "Development of an optimal vehicle-to-grid aggregator for frequency regulation," *IEEE Transactions on smart grid*, vol. 1, no. 1, pp. 65–72, 2010.

[8] Y. Ota, H. Taniguchi, T. Nakajima, K. M. Liyanage, and A. Yokoyama, "An autonomous distributed vehicle-to-grid control of grid-connected electric vehicle," in *Industrial and Information Systems (ICIIS), 2009 International Conference on*. IEEE, 2009, pp. 414–418.

[9] C. Battistelli, L. Baringo, and A. Conejo, "Optimal energy management of small electric energy systems including v2g facilities and renewable energy sources," *Electric Power Systems Research*, vol. 92, pp. 50–59, 2012.

[10] S. Vachirasricirikul and I. Ngamroo, "Robust lfc in a smart grid with wind power penetration by coordinated v2g control and frequency controller," *IEEE Transactions on Smart Grid*, vol. 5, no. 1, pp. 371–380, 2014.

[11] M. C. Kisacikoglu, B. Ozpineci, and L. M. Tolbert, "Examination of a phev bidirectional charger system for v2g reactive power compensation," in *2010 Twenty-Fifth Annual IEEE Applied Power Electronics Conference and Exposition (APEC)*. IEEE, 2010, pp. 458–465.

[12] H. Khayyam, H. Ranjbarzadeh, and V. Marano, "Intelligent control of vehicle to grid power," *Journal of Power Sources*, vol. 201, pp. 1–9, 2012.

[13] D. M. Rizzo and G. G. Parker, "State of charge optimization for military hybrid vehicle microgrids," in *Innovative Smart Grid Technologies (ISGT), 2013 IEEE PES*, Feb 2013, pp. 1–6.

[14] D. M. Rizzo, "Military vehicle optimization and control," *Michigan Technological Unicersity Digitial Commons*, 2014.

[15] S. Fish and T. B. Savoie, "Simulation-based optimal sizing of hybrid electric vehicle components for specific combat missions," *IEEE Transactions on Magnetics*, vol. 37, no. 1, pp. 485–488, Jan 2001.

[16] W. Smith and P. Nunez, "Power and energy computational models for the design and simulation of hybrid-electric combat vehicles," in *Enabling Technologies for Simulation Science IX*, vol. 5805. International Society for Optics and Photonics, 2005, pp. 13–24.

[17] G. Rizzoni, J. R. Josephson, A. Soliman, C. Hubert, C.-G. Cantemir, N. Dembski, P. Pisu, D. Mikesell, L. Serrao, J. Russell *et al.*, "Modeling, simulation,

and concept design for hybrid-electric medium-size military trucks," in *Enabling Technologies for Simulation Science IX*, vol. 5805. International Society for Optics and Photonics, 2005, pp. 1–13.

[18] T. Ersal, C. Ahn, I. A. Hiskens, H. Peng, and J. L. Stein, "Impact of controlled plug-in evs on microgrids: A military microgrid example," in *Power and Energy Society General Meeting, 2011 IEEE*. IEEE, 2011, pp. 1–7.

[19] R. Jane, G. G. Parker, W. Weaver, R. Matthews, D. Rizzo, and M. Cook, "Optimal power management of vehicle sourced military outposts," *SAE International Journal of Commercial Vehicles*, vol. 10, no. 1, pp. 132–143, mar 2017. [Online]. Available: https://doi.org/10.4271/2017-01-0271

[20] Y. Levron, J. M. Guerrero, and Y. Beck, "Optimal power flow in microgrids with energy storage," *IEEE Transactions on Power Systems*, vol. 28, no. 3, pp. 3226–3234, 2013.

[21] P. Malysz, S. Sirouspour, and A. Emadi, "An optimal energy storage control strategy for grid-connected microgrids," *IEEE Transactions on Smart Grid*, vol. 5, no. 4, pp. 1785–1796, 2014.

[22] M.-H. Khooban, T. Dragicevic, F. Blaabjerg, and M. Delimar, "Shipboard microgrids: A novel approach to load frequency control," *IEEE Transactions on Sustainable Energy*, vol. 9, no. 2, pp. 843–852, 2017.

[23] R. S. Jane, G. G. Parker, W. Weaver, and D. M. Rizzo, "Fuel-optimal strategies for vehicle supported military microgrids," SAE Technical Paper, Tech. Rep., 2016.

[24] T. Ersal, C. Ahn, I. A. Hiskens, H. Peng, A. Stefanopoulou, and J. L. Stein, "On the effect of dc source voltage on inverter-based frequency and voltage regulation in a military microgrid," in *2012 American Control Conference (ACC)*. IEEE, 2012, pp. 2965–2971.

[25] J. Wu and X. Guan, "Coordinated multi-microgrids optimal control algorithm for smart distribution management system," *IEEE Transactions on Smart Grid*, vol. 4, no. 4, pp. 2174–2181, 2013.

[26] M. Jun and A. J. Markel, "Simulation and analysis of vehicle-to-grid operations in microgrid," in *2012 IEEE Power and Energy Society General Meeting*. IEEE, 2012, pp. 1–5.

[27] J. Stamp, "The spiders project-smart power infrastructure demonstration for energy reliability and security at us military facilities," in *2012 IEEE PES Innovative Smart Grid Technologies (ISGT)*. IEEE, 2012, pp. 1–1.

[28] S. Martinenas, M. Marinelli, P. B. Andersen, and C. Træholt, "Implementation and demonstration of grid frequency support by v2g enabled electric vehicle," in *2014 49th International universities power engineering conference (UPEC)*. IEEE, 2014, pp. 1–6.

[29] X. Wang, K. Huang, S. Yan, and B. Xu, "Simulation of three-phase voltage source pwm rectifier based on direct current control," in *2008 Congress on Image and Signal Processing*, vol. 5. IEEE, 2008, pp. 194–198.

[30] T. H. Inc., "Battery-modeling and application," Typhoon HIL Inc., Tech. Rep., 2013.

[31] D. of Defense (DoD), "Handbook for mobile electric power engine generator standard family general characteristics," Website, Tech. Rep., 2016.

[32] I. E. Commission *et al.*, "Microgrids for disaster preparedness and recovery: with electricity continuity plans and systems," *Geneva Switzerland: IEC 2014*, pp. 41–45, 2014.

[33] C. Abbey, D. Cornforth, N. Hatziargyriou, K. Hirose, A. Kwasinski, E. Kyriakides, G. Platt, L. Reyes, and S. Suryanarayanan, "Powering through the storm: Microgrids operation for more efficient disaster recovery," *IEEE Power and Energy Magazine*, vol. 12, no. 3, pp. 67–76, 2014.

[34] W. Fokkink, *Distributed Algorithms: An Intuitive Approach*. The MIT Press, 2013.

[35] Z. Gao, L. Wang, M. Yang, and X. Yang, "Cnpgsdp: An efficient group-based service discovery protocol for manets," *Computer Networks*, vol. 50, no. 16, pp. 3165 – 3182, 2006. [Online]. Available: http://www.sciencedirect.com/science/article/pii/S1389128605004123

[36] S. Yousefi, M. S. Mousavi, and M. Fathy, "Vehicular ad hoc networks (vanets): challenges and perspectives," in *ITS Telecommunications Proceedings, 2006 6th International Conference on.* IEEE, 2006, pp. 761–766.

[37] N. Malpani, J. L. Welch, and N. Vaidya, "Leader election algorithms for mobile ad hoc networks," in *Proceedings of the 4th International Workshop on Discrete Algorithms and Methods for Mobile Computing and Communications*, ser. DIALM '00. New York, NY, USA: ACM, 2000, pp. 96–103. [Online]. Available: http://doi.acm.org/10.1145/345848.345871

[38] M. Jayne and C. Morgan, "A new mathematical model of a lead acid battery for electric vehicles," Eighth Int'l Electric Vehicle Conference, Tech. Rep., 10 1986.

[39] S. Chriscoe, "Manufacture specifications for military grade alternators," Private Communication, 2014.

[40] Caterpillar. (2014) Industrial diesel engines - lesser regulated and non-regulated c9 acert. [Online]. Available: http://www.cat.com/en_US/products/new/power-systems/industrial-oem/industrial-diesel-engines-lesser-regulated-non-regulated/18396452.html

[41] J. McCalley and L. Tesfatsion, "The power flow equations," 2011. [Online]. Available: http://home.eng.iastate.edu/~jdm/ee553/DCPowerFlowEquations.pdf

[42] S. Balhara and K. Khanna, "Leader election algorithms in distributed systems," *Journal of Computer Science and Information Technology, IJCSMC*, vol. 3, no. 6, pp. 374–379, 2014.

[43] S. Degelia and D. Mueller, "Potential availability and stability of solar power in oklahoma white paper," 2014.

[44] S. Blumsack and K. Richardson, "Cost and emissions implications of coupling wind and solar power," *Smart Grid and Renewable Energy*, vol. 3, no. 04, p. 308, 2012.

[45] G. Reikard, "Predicting solar radiation at high resolutions: A comparison of time series forecasts," *Solar Energy*, vol. 83, no. 3, pp. 342 – 349, 2009. [Online]. Available: http://www.sciencedirect.com/science/article/pii/S0038092X08002107

[46] C. W. Chow, B. Urquhart, M. Lave, A. Dominguez, J. Kleissl, J. Shields, and B. Washom, "Intra-hour forecasting with a total sky imager at the uc san diego solar energy testbed," *Solar Energy*, vol. 85, no. 11, pp. 2881 – 2893, 2011. [Online]. Available: http://www.sciencedirect.com/science/article/pii/S0038092X11002982

[47] R. Abdel-Aal, "Hourly temperature forecasting using abductive networks," *Engineering Applications of Artificial Intelligence*, vol. 17, no. 5, pp. 543–556, 2004.

[48] Ö. A. Dombaycı and M. Gölcü, "Daily means ambient temperature prediction using artificial neural network method: A case study of turkey," *Renewable Energy*, vol. 34, no. 4, pp. 1158–1161, 2009.

[49] J. Shi, W. Lee, Y. Liu, Y. Yang, and P. Wang, "Forecasting power output of photovoltaic systems based on weather classification and support vector machines," *IEEE Transactions on Industry Applications*, vol. 48, no. 3, pp. 1064–1069, May 2012.

[50] C. Tao, D. Shanxu, and C. Changsong, "Forecasting power output for grid-connected photovoltaic power system without using solar radiation measurement," in *The 2nd International Symposium on Power Electronics for Distributed Generation Systems*, June 2010, pp. 773–777.

[51] A. Islahi, S. Shakil, and M. Hamed, "Hottel's clear day model for a typical arid city-jeddah," *International J. Engineer. Sci. Invent*, vol. 4, no. 6, pp. 32–37, 2015.

[52] H.-T. Yang, C.-M. Huang, Y.-C. Huang, Y.-S. Pai *et al.*, "A weather-based hybrid method for 1-day ahead hourly forecasting of pv power output," *IEEE Trans. Sustain. Energy*, vol. 5, no. 3, pp. 917–926, 2014.

[53] M. Bouzerdoum, A. Mellit, and A. M. Pavan, "A hybrid model (sarima–svm) for short-term power forecasting of a small-scale grid-connected photovoltaic plant," *Solar Energy*, vol. 98, pp. 226–235, 2013.

[54] T. Hong, J. Wilson, and J. Xie, "Long term probabilistic load forecasting and normalization with hourly information," *IEEE Transactions on Smart Grid*, vol. 5, no. 1, pp. 456–462, Jan 2014.

[55] L. Hernandez, C. Baladron, J. M. Aguiar, B. Carro, A. J. Sanchez-Esguevillas, J. Lloret, and J. Massana, "A survey on electric power demand forecasting: future trends in smart grids, microgrids and smart buildings," *IEEE Communications Surveys & Tutorials*, vol. 16, no. 3, pp. 1460–1495, 2014.

[56] H. Zhou, T. Bhattacharya, D. Tran, T. S. T. Siew, and A. M. Khambadkone, "Composite energy storage system involving battery and ultracapacitor with dynamic energy management in microgrid applications," *IEEE Transactions on Power Electronics*, vol. 26, no. 3, pp. 923–930, March 2011.

[57] D. Lu and B. Francois, "Strategic framework of an energy management of a microgrid with a photovoltaic-based active generator," in *Advanced Electromechanical Motion Systems & Electric Drives Joint Symposium, 2009. ELECTROMOTION 2009. 8th International Symposium on.* IEEE, 2009, pp. 1–6.

[58] W. Shi, X. Xie, C.-C. P. Chu, and R. Gadh, "Distributed optimal energy management in microgrids." *IEEE Trans. Smart Grid*, vol. 6, no. 3, pp. 1137–1146, 2015.

[59] GlobalSecurity.org, "Tactical quiet generators." [Online]. Available: https://www.globalsecurity.org/military/systems/ground/mep-tqg.htm

[60] D. M. Rizzo, Private Communication, 2016.

[61] N. T. Eichenberg, A. S. Leger, and J. Spruce, "Impacts of thermally efficient structures and photovoltaic sources in military microgrids," in *2016 Clemson University Power Systems Conference (PSC)*, March 2016, pp. 1–5.

[62] D. M. Smith, A. S. Leger, and B. Severson, "Automated demand response of thermal load with a photovoltaic source for military microgrids," in *2015 Clemson University Power Systems Conference (PSC)*, March 2015, pp. 1–8.

[63] R. S. Jane, G. G. Parker, W. W. Weaver, and S. Y. Goldsmith, "Simulation for vehicle-to-vehicle and vehicle-to-grid resource sharing analysis," in *Ground Vehicle Systems Engineering and Technology Symposium (GVSETS)*. GVSETS, 2014.

[64] M. D. The Mathworks, "Design time series narx feedback neural networks," 2019.

[65] M. Lange, U. Focken, R. Meyer, M. Denhardt, B. Ernst, and F. Berster, "Optimal combination of different numerical weather models for improved wind power predictions," in *6th International Workshop on Large-Scale Integration of Wind Power and Transmission Networks for Offshore Wind Farms, Delft*, 2006.

[66] M. Lange and H.-P. Waldl, "Assessing the uncertainty of wind power predictions

with regard to specific weather situations," in *Proceedings of the European Wind Energy Conference, Copenhagen, Denmark*, 2001, pp. 695–698.

[67] E. Barklund, N. Pogaku, M. Prodanovic, C. Hernandez-Aramburo, and T. C. Green, "Energy management in autonomous microgrid using stability-constrained droop control of inverters," *IEEE Transactions on Power Electronics*, vol. 23, no. 5, pp. 2346–2352, 2008.

[68] E. Kuznetsova, Y.-F. Li, C. Ruiz, and E. Zio, "An integrated framework of agent-based modelling and robust optimization for microgrid energy management," *Applied Energy*, vol. 129, pp. 70–88, 2014.

[69] T. Zhou and B. François, "Energy management and power control of a hybrid active wind generator for distributed power generation and grid integration," *IEEE Transactions on industrial electronics*, vol. 58, no. 1, pp. 95–104, 2011.

[70] J. Jimeno, J. Anduaga, J. Oyarzabal, and A. G. de Muro, "Architecture of a microgrid energy management system," *European Transactions on Electrical Power*, vol. 21, no. 2, pp. 1142–1158, 2011.

[71] P. T. Baboli, M. Shahparasti, M. P. Moghaddam, M. R. Haghifam, and M. Mohamadian, "Energy management and operation modelling of hybrid ac–dc microgrid," *IET Generation, Transmission & Distribution*, vol. 8, no. 10, pp. 1700–1711, 2014.

[72] O. Tremblay, L.-A. Dessaint, and A.-I. Dekkiche, "A generic battery model for the dynamic simulation of hybrid electric vehicles," in *2007 IEEE Vehicle Power and Propulsion Conference*. Ieee, 2007, pp. 284–289.

[73] P. Krause, O. Wasynczuk, S. D. Sudhoff, and S. Pekarek, *Analysis of electric machinery and drive systems*. John Wiley & Sons, 2013, vol. 75.

[74] P. Pejovic, *Three-phase diode rectifiers with low harmonics: current injection methods*. Springer Science & Business Media, 2007.

[75] S. Vasudevan, J. Kurose, and D. Towsley, "Design and analysis of a leader election algorithm for mobile ad hoc networks," Oct 2004, pp. 350–360.

[76] C. Guille and G. Gross, "A conceptual framework for the vehicle-to-grid (v2g) implementation," *Energy policy*, vol. 37, no. 11, pp. 4379–4390, 2009.

[77] J. Santa, A. F. Gómez-Skarmeta, and M. Sánchez-Artigas, "Architecture and evaluation of a unified v2v and v2i communication system based on cellular networks," *Computer Communications*, vol. 31, no. 12, pp. 2850–2861, 2008.

[78] C. Guille and G. Gross, "Design of a conceptual framework for the v2g implementation," in *2008 IEEE Energy 2030 Conference*. IEEE, 2008, pp. 1–3.

[79] L. Rizzo, "Effective erasure codes for reliable computer communication protocols," *ACM SIGCOMM computer communication review*, vol. 27, no. 2, pp. 24–36, 1997.

[80] M. Jerbi, P. Marlier, and S. M. Senouci, "Experimental assessment of v2v and i2v communications," in *2007 IEEE International Conference on Mobile Adhoc and Sensor Systems*. IEEE, 2007, pp. 1–6.

[81] K. Koscher, A. Czeskis, F. Roesner, S. Patel, T. Kohno, S. Checkoway, D. McCoy, B. Kantor, D. Anderson, H. Shacham *et al.*, "Experimental security analysis of a modern automobile," in *2010 IEEE Symposium on Security and Privacy*. IEEE, 2010, pp. 447–462.

[82] H. Conceição, L. Damas, M. Ferreira, and J. Barros, "Large-scale simulation of v2v environments," in *Proceedings of the 2008 ACM symposium on Applied computing*. ACM, 2008, pp. 28–33.

[83] U. E. Larson and D. K. Nilsson, "Securing vehicles against cyber attacks," in *Proceedings of the 4th annual workshop on Cyber security and information intelligence research: developing strategies to meet the cyber security and information intelligence challenges ahead*. ACM, 2008, p. 30.

[84] S. M. Bellovin, "Security problems in the tcp/ip protocol suite," *ACM SIGCOMM Computer Communication Review*, vol. 19, no. 2, pp. 32–48, 1989.

[85] J. Postel and J. K. Reynolds, "Telnet protocol specification," 1983.

[86] L. Almeida, P. Pedreiras, and J. A. G. Fonseca, "The ftt-can protocol: Why and how," *Industrial Electronics, IEEE Transactions on*, vol. 49, no. 6, pp. 1189–1201, 2002.

[87] L.-A. Larzon, M. Degermark, and S. Pink, *UDP lite for real time multimedia applications*. Hewlett-Packard Laboratories, 1999.

[88] J. Tomić and W. Kempton, "Using fleets of electric-drive vehicles for grid support," *Journal of Power Sources*, vol. 168, no. 2, pp. 459–468, 2007.

[89] W. Kempton and J. Tomić, "Vehicle-to-grid power implementation: From stabilizing the grid to supporting large-scale renewable energy," *Journal of Power Sources*, vol. 144, no. 1, pp. 280–294, 2005.

[90] S. Biswas, R. Tatchikou, and F. Dion, "Vehicle-to-vehicle wireless communication protocols for enhancing highway traffic safety," *Communications Magazine, IEEE*, vol. 44, no. 1, pp. 74–82, 2006.

[91] J. Peas Lopes, C. Moreira, and A. Madureira, "Defining control strategies for microgrids islanded operation," *Power Systems, IEEE Transactions on*, vol. 21, no. 2, pp. 916–924, 2006.

[92] M. Pipattanasomporn, H. Feroze, and S. Rahman, "Multi-agent systems in a distributed smart grid: Design and implementation," in *Power Systems Conference and Exposition, 2009. PSCE 09. IEEE/PES*, March 2009, pp. 1–8.

[93] E. M. Schooler, "The connection control protocol: Specification," 1992.

[94] S. Helal, N. Desai, V. Verma, and C. Lee, "Konark-a service discovery and

delivery protocol for ad-hoc networks," in *Wireless Communications and Networking, 2003. WCNC 2003. 2003 IEEE*, vol. 3. IEEE, 2003, pp. 2107–2113.

[95] C. Lee and S. Helal, "Protocols for service discovery in dynamic and mobile networks," *International Journal of Computer Research*, vol. 11, no. 1, pp. 1–12, 2002.

[96] K. Pazul, "Controller area network (can) basics," *Microchip Technology Inc*, p. 1, 1999.

[97] A. Dunkels, "Full tcp/ip for 8-bit architectures," in *Proceedings of the 1st International Conference on Mobile Systems, Applications and Services*, ser. MobiSys '03. New York, NY, USA: ACM, 2003, pp. 85–98. [Online]. Available: http://doi.acm.org/10.1145/1066116.1066118

[98] S. Helal, "Standards for service discovery and delivery," *Pervasive Computing, IEEE*, vol. 1, no. 3, pp. 95–100, 2002.

[99] K. Abrougui, "Design and performance evaluation of service discovery protocols for vehicular networks," Ph.D. dissertation, University of Ottawa, 2011.

[100] R. Patzke, "Fieldbus basics," *Computer Standards & Interfaces*, vol. 19, pp. 275 – 293, 1998. [Online]. Available: http://www.sciencedirect.com/science/article/pii/S0920548998000282

[101] J. Peas Lopes, C. Moreira, and A. Madureira, "Defining control strategies for microgrids islanded operation," *Power Systems, IEEE Transactions on*, vol. 21, no. 2, pp. 916–924, May 2006.

[102] L. H.-J. Kim Jong-Yul, Park June Ho, "Coordinate control strategy for microgrid in grid-connected and islanded operation," *Preprints of the 18th IFAC World Congress*, pp. 14 767–14 771, September 2011.

[103] C. .Inc. (2014) Electric power generation - diesel generator sets. [Online]. Available: http://www.cat.com/en_US/products/new/power-systems/electric-power-generation/diesel-generator-sets.html

[104] J. D. Glover, M. S. Sarma, and T. Overbye, *Power System Analysis and Design*. Stamford, Connecticut: Cengage Learning, 2011.

[105] L. Martin. (2014) Jltv capabilities. [Online]. Available: http://www.lockheedmartin.com/us/products/jltv/JLTV-capabilities.html

[106] K. I. Limited. (2014) Caiman mrap multi-theatre vehicle, united states of america. [Online]. Available: http://www.army-technology.com/projects/caimanmtvusa/

[107] T. MathWorks. (2014) Search r2014a documentation: Matlab - gui building - component selection - gui controls and indicators : uitable. [Online]. Available: http://www.mathworks.com/help/matlab/ref/uitable.html

[108] ——. (2014) Search r2014a documentation: Simulink - simulink examples - variant subsytems. [Online]. Available: http://www.mathworks.com/help/simulink/examples/variant-subsystems.html

[109] J. L. Cebula and L. R. Young, "A taxonomy of operational cyber security risks," DTIC Document, Tech. Rep., 2010.

[110] K. H. Johansson, M. Törngren, and L. Nielsen, "Vehicle applications of controller area network," in *Handbook of networked and embedded control systems*. Springer, 2005, pp. 741–765.

[111] R. B. G. 2011, "Introduction to automotive bus systems," October 2011.

[112] J. Axelsson, J. Fröberg, H. Hansson, C. Norström, K. Sandström, and B. Villing, "A comparative case study of distributed network architectures for different automotive applications." 2005.

[113] E. M. Vector, "Serial bus systems in automobiles," DTIC Document, Tech. Rep., 2006.

[114] M. Broy, I. H. Kruger, A. Pretschner, and C. Salzmann, "Engineering automotive software," *Proceedings of the IEEE*, vol. 95, no. 2, pp. 356–373, 2007.

[115] S. Schulze, M. Pukall, and T. Hoppe, "It security in automotive software development," *GI Softwaretechnik-Trends*, vol. 29, no. 3, pp. 23–28, 2009.

[116] M. Wolf, A. Weimerskirch, and C. Paar, "Security in automotive bus systems," in *Workshop on Embedded Security in Cars*, 2004.

[117] S. Checkoway, D. McCoy, B. Kantor, D. Anderson, H. Shacham, S. Savage, K. Koscher, A. Czeskis, F. Roesner, T. Kohno *et al.*, "Comprehensive experimental analyses of automotive attack surfaces." in *USENIX Security Symposium*. San Francisco, 2011.

[118] C. Miller and C. Valasek, "Adventures in automotive networks and control units," in *DEF CON 21 Hacking Conference. Las Vegas, NV: DEF CON*, 2013.

[119] I. Studnia, V. Nicomette, E. Alata, Y. Deswarte, M. Kaâniche, and Y. Laarouchi, "Survey on security threats and protection mechanisms in embedded automotive networks," in *Dependable Systems and Networks Workshop (DSN-W), 2013 43rd Annual IEEE/IFIP Conference on*. IEEE, 2013, pp. 1–12.

[120] D. K. Nilsson, P. H. Phung, and U. E. Larson, "Vehicle ecu classification based on safety-security characteristics," 2008.

[121] V. Verendel, D. K. Nilsson, U. E. Larson, and E. Jonsson, "An approach to using honeypots in in-vehicle networks," in *Vehicular Technology Conference, 2008. VTC 2008-Fall. IEEE 68th*. IEEE, 2008, pp. 1–5.

[122] P. Papadimitratos, A. La Fortelle, K. Evenssen, R. Brignolo, and S. Cosenza, "Vehicular communication systems: Enabling technologies, applications, and

future outlook on intelligent transportation," *Communications Magazine, IEEE*, vol. 47, no. 11, pp. 84–95, 2009.

[123] R. van der Heijden, "Security architectures in v2v and v2i communication," 2010.

[124] X. Yang, J. Liu, N. H. Vaidya, and F. Zhao, "A vehicle-to-vehicle communication protocol for cooperative collision warning," in *Mobile and Ubiquitous Systems: Networking and Services, 2004. MOBIQUITOUS 2004. The First Annual International Conference on.* IEEE, 2004, pp. 114–123.

[125] F. Kargl, P. Papadimitratos, L. Buttyan, M. Muter, E. Schoch, B. Wiedersheim, T.-V. Thong, G. Calandriello, A. Held, A. Kung *et al.*, "Secure vehicular communication systems: implementation, performance, and research challenges," *Communications Magazine, IEEE*, vol. 46, no. 11, pp. 110–118, 2008.

[126] MATLAB, "Vehicle network toolbox," October 2015, mATLAB.

[127] M. Mateski, C. M. Trevino, C. K. Veitch, J. Michalski, J. M. Harris, S. Maruoka, and J. Frye, *Cyber threat metrics.* Sandia National Laboratories, 2012.

[128] D. P. Duggan, *Generic threat profiles.* United States. Department of Energy, 2005.

[129] D. P. Duggan, S. R. Thomas, C. K. Veitch, and L. Woodard, "Categorizing threat."

[130] W. Inc., "What is social engineering," December 2015, website.

[131] I. FireEye, "Zero-dat exploit," Dec. 17 2015, website.

[132] P. McDaniel and S. McLaughlin, "Security and privacy challenges in the smart grid," *IEEE Security Privacy*, vol. 7, no. 3, pp. 75–77, May 2009.

[133] S. Chakraborty, M. D. Weiss, and M. G. Simoes, "Distributed intelligent energy management system for a single-phase high-frequency ac microgrid," *IEEE Transactions on Industrial Electronics*, vol. 54, no. 1, pp. 97–109, Feb 2007.

[134] D. E. Olivares, C. A. Cañizares, and M. Kazerani, "A centralized energy management system for isolated microgrids." *IEEE Trans. Smart Grid*, vol. 5, no. 4, pp. 1864–1875, 2014.

[135] Y.-K. Chen, Y.-C. Wu, C.-C. Song, and Y.-S. Chen, "Design and implementation of energy management system with fuzzy control for dc microgrid systems," *IEEE Transactions on Power Electronics*, vol. 28, no. 4, pp. 1563–1570, 2013.

[136] F. Katiraei, R. Iravani, N. Hatziargyriou, and A. Dimeas, "Microgrids management," *IEEE power and energy magazine*, vol. 6, no. 3, 2008.

[137] Z. Wang, B. Chen, J. Wang, M. M. Begovic, and C. Chen, "Coordinated energy management of networked microgrids in distribution systems," *IEEE Transactions on Smart Grid*, vol. 6, no. 1, pp. 45–53, 2015.

[138] E. R. Sanseverino, M. L. Di Silvestre, M. G. Ippolito, A. De Paola, and G. L. Re, "An execution, monitoring and replanning approach for optimal energy management in microgrids," *Energy*, vol. 36, no. 5, pp. 3429–3436, 2011.

[139] M. Mao, P. Jin, N. D. Hatziargyriou, and L. Chang, "Multiagent-based hybrid energy management system for microgrids," *IEEE Transactions on Sustainable Energy*, vol. 5, no. 3, pp. 938–946, July 2014.

[140] MATLAB, "Matlab documentation: View," May 19 2019, website.

Appendix A

Scenario Rich Environment

A scenario rich environment was developed using a series of graphical user interfaces (GUIs) termed the scenario generator, which was originally developed over the course of the Autonomous Agile Microgrid (AAM) project. The scenario generator enabled creation of a time varying electrical load, governed by a scenario. A scenario defines (1) the complete electrical architecture including the number of generation, load, and power distribution assets (microgrids), (2) meteorological weather profiles, (3) a predefined U.S. Army relevant event schedule, and (4) a shelter equipment list. The combination of the four separate components drives a more realistic energy grid model, capable of modeling a complex electrical load which varies as a function of the meteorological weather conditions and an event schedule, well suited for military microgrid studies. The remainder of this appendix is separated into five sections, Section A.1

contains more detailed information regarding the electrical architecture, Section A.2 provides additional information regarding the shelter equipment list, Section A.3 describes the required set of meteorological weather profiles, Section A.4 discusses the U.S. Army relevant event schedule, and Section A.5 presents the resulting energy grid model. Most case studies provided in the dissertation utilize scenario-specific information derived from the scenario generator.

A.1 Electrical Architecture

The electrical architecture is the foundation of a scenario, it describes the total number of power generation, load, and distribution assets (microgrids). It also describes the assets type, rated electrical power, and the orientation within the complete electrical architecture. Consider an electrical grid with four main power distribution buses. For every power distribution bus, there is a microgrid, each microgrid has four power generation assets including, a single diesel generator, single electrical storage, a single PV array, and a single vehicle. The microgrid buses are interconnected to each other assuming a ring configuration. Two of the four microgrids have five, variable electrical loads, while the remaining two microgrids have four, variable, electrical loads. The resulting electrical architecture for the postulated electrical grid was provided in Figure A.1.

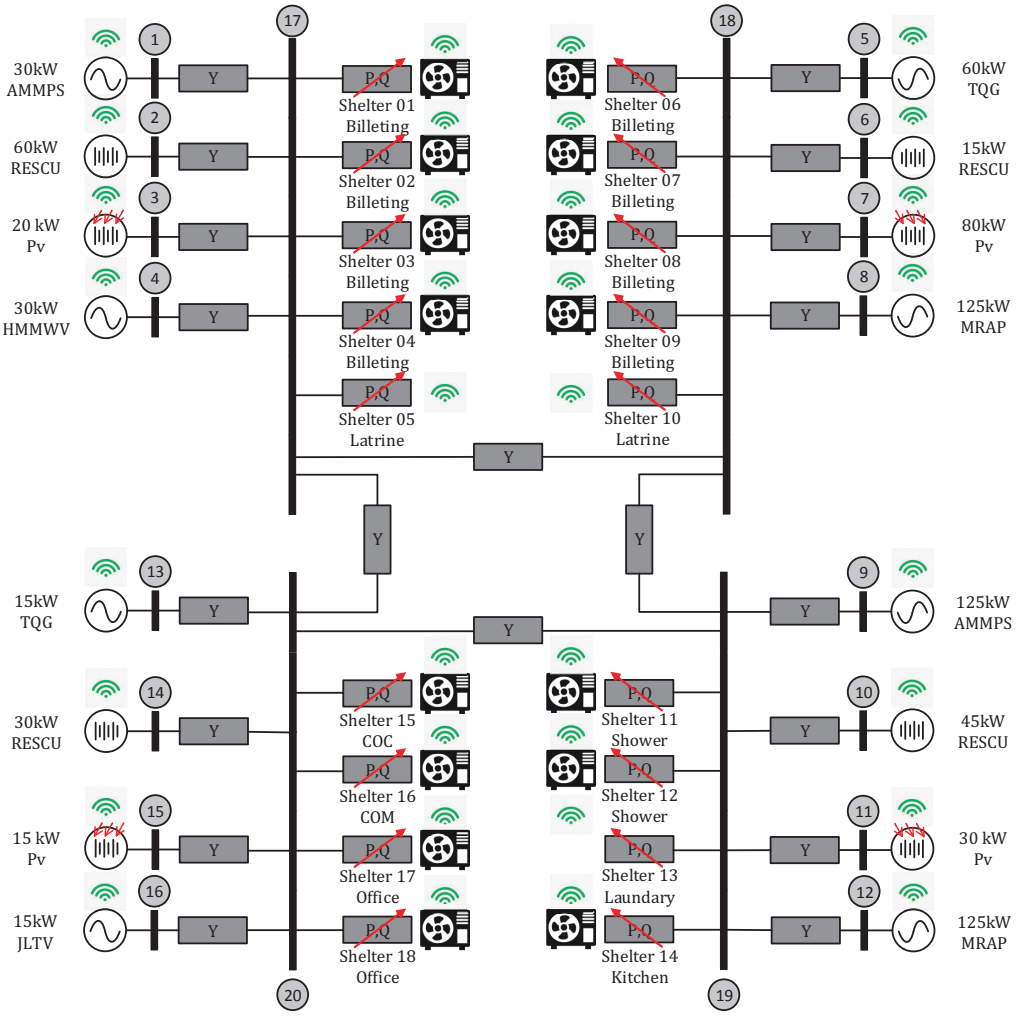

Figure A.1: The example electrical grid architecture.

The electrical architecture and all information that describe the individual generation, load, and distribution assets are contained within a configuration file. Using a *MATLAB* function, a configuration file was parsed, and used to form a configuration file, which constructs a data structure. An example of the derived data structure is provided in Listing 50.

```
%Define Total Number of Assets  [N/A]
config.tgen  = 4;                          %Total Number of Generator Assets
config.tstr  = 4;                          %Total Number of Storage Assets
config.tren  = 4;                          %Total Number of Renewable Assets
config.tveh  = 4;                          %Total Number of Vehicle Assets
config.tmgrd = 4;                          %Total Number of Microgrid Assets
config.tlod  = 18;                         %Total Number of Load Assets

%Define Total Number of Assets Per Microgrid  [N/A]
config.ngen  = [1 ; 1 ; 1 ; 1];         %Number of Generator Assets Per Microgrid
config.nstr  = [1 ; 1 ; 1 ; 1];         %Number of Storage Assets Per Microgrid
config.nren  = [1 ; 1 ; 1 ; 1];         %Number of Renewable Assets Per Microgrid
config.nveh  = [1 ; 1 ; 1 ; 1];         %Number of Vehicle Assets Per Microgrid
config.nmgrd = [1 ; 1 ; 1 ; 1];         %Number of Microgrid Assets Per Microgrid
config.nlod  = [5 ; 5 ; 4 ; 4];         %Number of Load Assets Per Microgrid

%Define Asset Architecture Indices  [N/A]
config.gen_arc_idx  = [1 ; 5 ; 9  ; 13];  %Generator Architecture Indices
config.str_arc_idx  = [2 ; 6 ; 10 ; 14];  %Storage Architecture Indices
config.ren_arc_idx  = [3 ; 7 ; 11 ; 15];  %Renewable Architecture Indices
config.veh_arc_idx  = [4 ; 8 ; 12 ; 16];  %Vehicle Architecture Indices
config.mgrd_arc_idx = [17 ; 18 ; 19 ; 20];%Microgrid Architecture Indices
config.lod_arc_idx  = [21 ; 22 ; 23 ; 24 ; 25 ; 26 ; 27 ; 28 ; 29 ;...
    30 ; 31 ; 32 ; 33 ; 34 ; 35 ; 36 ; 37 ; 38]; %Load Architecture Indices

%Define Microgrid Architecture Indices  [N/A]
config.gen_mgrd_idx  = [1 ; 1 ; 1 ; 1];  %Generator Microgrid Indices
config.str_mgrd_idx  = [1 ; 1 ; 1 ; 1];  %Storage Microgrid Indices
config.ren_mgrd_idx  = [1 ; 1 ; 1 ; 1];  %Renewable Microgrid Indices
config.veh_mgrd_idx  = [1 ; 1 ; 1 ; 1];  %Vehicle Microgrid Indices
config.mgrd_mgrd_idx = [1 ; 1 ; 1 ; 1];  %Microgrid Microgrid Indices
config.lod_mgrd_idx  = [1 ; 1 ; 1 ; 1 ; 1 ; 2 ; 2 ; 2 ; 2 ; 2 ; 3 ; ...
    3 ; 3 ; 3 ; 4 ; 4 ; 4 ; 4];          %Load Microgrid Indices

%Define Rated Acitve Power for Generation Assets [kW]
config.gen_prated = [30 ; 60  ; 125 ; 15];    %Generator Assets Rated Power
config.str_prated = [60 ; 15  ;  45 ; 30];    %Storage Assets Rated Power
config.ren_prated = [20 ; 80  ;  30 ; 15];    %Renewable Assets Rated Power
config.veh_prated = [30 ; 125 ; 125 ; 15];    %Vehicle Assets Rated Power

%Define Rated Reacitve Power for Generation Assets [kVar]
config.gen_qrated = [30 ; 60  ; 125 ; 15];    %Generator Assets Rated Power
config.str_qrated = [60 ; 15  ;  45 ; 30];    %Storage Assets Rated Power
config.ren_qrated = [20 ; 80  ;  30 ; 15];    %Renewable Assets Rated Power
config.veh_qrated = [30 ; 125 ; 125 ; 15];    %Vehicle Assets Rated Power

%Define Topology Matrix
config.top_mat = [0 1 0 1 ; 1 0 1 0 ; ...
                  0 1 0 1 ; 1 0 1 0]; %Microgrid Connections (Topology Matrix)
```

Listing A.1: Example Configuration Data Structure

A.2 Shelter Equipment List

Concurrently to generating the configuration data structure, the data structure would be amended to include a list of equipment contained within a shelter. The shelter equipment list was defined using an Excel document, separated into eleven sheets, sheet one contains parameters specific to an HVAC, and sheet two contains parameters specific to the physical shelter in which the electrical loads are contained. Sheets three through eleven contains parameters specific to a washing machine, drying machine, oven, electric warmer, freezer, dishwasher, water heater, ancillary components, and lights. Each sheet was set up, to enable any shelter to possess any of the predefined electrical assets, each of the eleven sheets, are provided in Figure A.2 - Figure A.12. Using *MATLAB* functions, the configuration data structure was amended to include the shelter equipment list by reading in data contained within the excel document. The amended configuration data structure was subsequently passed to additional *MATLAB* functions or files to generate a complete scenario.

The shelter equipment list was generated in response to data obtained from the Base Camp Integration Laboratory (BCIL) 2016 demo. The data collected provided a base set of shelter designations and insight regarding potential electrical components that may be found within the various shelters. This information was ultimately used to construct the shelter equipment list, the U.S. Army-relevant event schedule, and the

energy grid model, resulting in a scenario rich environment well suited for military microgrid studies.

Shelter		Configuration		Cooling Parameters			Heating Parameters			Fan		Controller		Tier Parameters							
Name	Number	Included	Circuit	Volumetric Flow Rate [m^3/Hr]	Capacity [kW]	COP	Volumetric Flow Rate [m^3/Hr]	Capacity [kW]	COP	Volumetric Flow Rate [m^3/Hr]	Capacity [kW]	COP	Mode	Hysteresis [F]	Tier 01 Allocation [%]	Tier 02 Allocation [%]	Tier 03 Allocation [%]	Tier 04 Allocation [%]	Tier 05 Allocation [%]	Tier 06 Allocation [%]
Billeting	1	1	1	3229	17	1.5	5097.5	10	1.8	5900	6	2	2	5	0	1	0	0	0	0
Billeting	2	1	1	3229	17	1.5	5097.5	10	1.8	5900	6	2	2	5	0	1	0	0	0	0
Billeting	3	1	1	3229	17	1.5	5097.5	10	1.8	5900	6	2	2	5	0	1	0	0	0	0
Billeting	4	1	1	3229	17	1.5	5097.5	10	1.8	5900	6	2	2	5	0	1	0	0	0	0
Latrine	5	0	1	0	0	0	0	0	0	0	0	0	0	5	0	0	0	0	0	0
Billeting	6	1	1	3229	17	1.5	5097.5	10	1.8	5900	6	2	2	5	0	1	0	0	0	0
Billeting	7	1	1	3229	17	1.5	5097.5	10	1.8	5900	6	2	2	5	0	1	0	0	0	0
Billeting	8	1	1	3229	17	1.5	5097.5	10	1.8	5900	6	2	2	5	0	1	0	0	0	0
Billeting	9	1	1	3229	17	1.5	5097.5	10	1.8	5900	6	2	2	5	0	1	0	0	0	0
Latrine	10	0	1	0	0	0	0	0	0	0	0	0	0	5	0	0	0	0	0	0
Shower	11	1	1	3229	17	1.5	5097.5	10	1.8	5900	6	2	2	5	0	1	0	0	0	0
Shower	12	1	1	3229	17	1.5	5097.5	10	1.8	5900	6	2	2	5	0	1	0	0	0	0
Laundary	13	0	1	0	0	0	0	0	0	0	0	0	0	5	0	0	0	0	0	0
Kitchen	14	1	1	3229	17	1.5	5097.5	10	1.8	5900	6	2	2	5	0	1	0	0	0	0
COC	15	1	1	3229	17	1.5	5097.5	10	1.8	5900	6	2	2	5	1	0	0	0	0	0
COM	16	1	1	3229	17	1.5	5097.5	10	1.8	5900	6	2	2	5	0	1	0	0	0	0
Office	17	1	1	3229	17	1.5	5097.5	10	1.8	5900	6	2	2	5	0	1	0	0	0	0
Office	18	1	1	3229	17	1.5	5097.5	10	1.8	5900	6	2	2	5	0	1	0	0	0	0
	19	0	0	0	0	0	0	0	0	0	0	0	0	0	0	0	0	0	0	0
	20	0	0	0	0	0	0	0	0	0	0	0	0	0	0	0	0	0	0	0
	21	0	0	0	0	0	0	0	0	0	0	0	0	0	0	0	0	0	0	0
	22	0	0	0	0	0	0	0	0	0	0	0	0	0	0	0	0	0	0	0
	23	0	0	0	0	0	0	0	0	0	0	0	0	0	0	0	0	0	0	0
	24	0	0	0	0	0	0	0	0	0	0	0	0	0	0	0	0	0	0	0
	25	0	0	0	0	0	0	0	0	0	0	0	0	0	0	0	0	0	0	0
	26	0	0	0	0	0	0	0	0	0	0	0	0	0	0	0	0	0	0	0
	27	0	0	0	0	0	0	0	0	0	0	0	0	0	0	0	0	0	0	0
	28	0	0	0	0	0	0	0	0	0	0	0	0	0	0	0	0	0	0	0
	29	0	0	0	0	0	0	0	0	0	0	0	0	0	0	0	0	0	0	0
	30	0	0	0	0	0	0	0	0	0	0	0	0	0	0	0	0	0	0	0

Figure A.2: HVAC Parameters

Shelter		Wall Parameters		Room Parameters		Internal Load		Wall Parameters	
Name	Number	Thermal Capacitance [kJ/K]	Time Constant [Sec]	Volume [m^3]	Time Constant [Sec]	Heat Electrical Power Fraction	Heat Load Per Person [kW]	Thermal Capacitance [kJ/K]	Time Constant [Sec]
Billeting	1	28.00	28.00	650.00	28.00	0.8	0.1	25	25
Billeting	2	24.00	24.00	650.00	24.00	0.8	0.1	25	25
Billeting	3	26.00	26.00	650.00	26.00	0.8	0.1	25	25
Billeting	4	27.00	27.00	650.00	27.00	0.8	0.1	25	25
Latrine	5	28.00	8.00	650.00	53.00	0.8	0.1	25	5
Billeting	6	25.00	25.00	650.00	25.00	0.8	0.1	25	25
Billeting	7	21.00	21.00	650.00	21.00	0.8	0.1	25	25
Billeting	8	28.00	28.00	650.00	28.00	0.8	0.1	25	25
Billeting	9	26.00	26.00	650.00	26.00	0.8	0.1	25	25
Latrine	10	26.00	5.00	650.00	51.00	0.8	0.1	25	5
Shower	11	22.00	22.00	650.00	22.00	0.8	0.1	25	25
Shower	12	21.00	21.00	650.00	21.00	0.8	0.1	25	25
Laundary	13	29.00	5.00	650.00	29.00	0.8	0.1	25	5
Kitchen	14	18.00	153.00	650.00	153.00	0.8	0.1	15	150
COC	15	27.00	27.00	650.00	27.00	0.8	0.1	25	25
COM	16	21.00	21.00	650.00	21.00	0.8	0.1	25	25
Office	17	25.00	25.00	650.00	25.00	0.8	0.1	25	25
Office	18	26.00	26.00	650.00	26.00	0.8	0.1	25	25
	19	0	0	0	0	0	0	0	0
	20	0	0	0	0	0	0	0	0
	21	0	0	0	0	0	0	0	0
	22	0	0	0	0	0	0	0	0
	23	0	0	0	0	0	0	0	0
	24	0	0	0	0	0	0	0	0
	25	0	0	0	0	0	0	0	0
	26	0	0	0	0	0	0	0	0
	27	0	0	0	0	0	0	0	0
	28	0	0	0	0	0	0	0	0
	29	0	0	0	0	0	0	0	0
	30	0	0	0	0	0	0	0	0

Time Constant [Sec]
3.000
-1.000
1.000
2.000
3.000
0.000
-4.000
3.000
1.000
1.000
-3.000
-4.000
4.000
3.000
2.000
-4.000
0.000
1.000
0
0
0
0
0
0
0
0
0
0

Figure A.3: Shelter Parameters

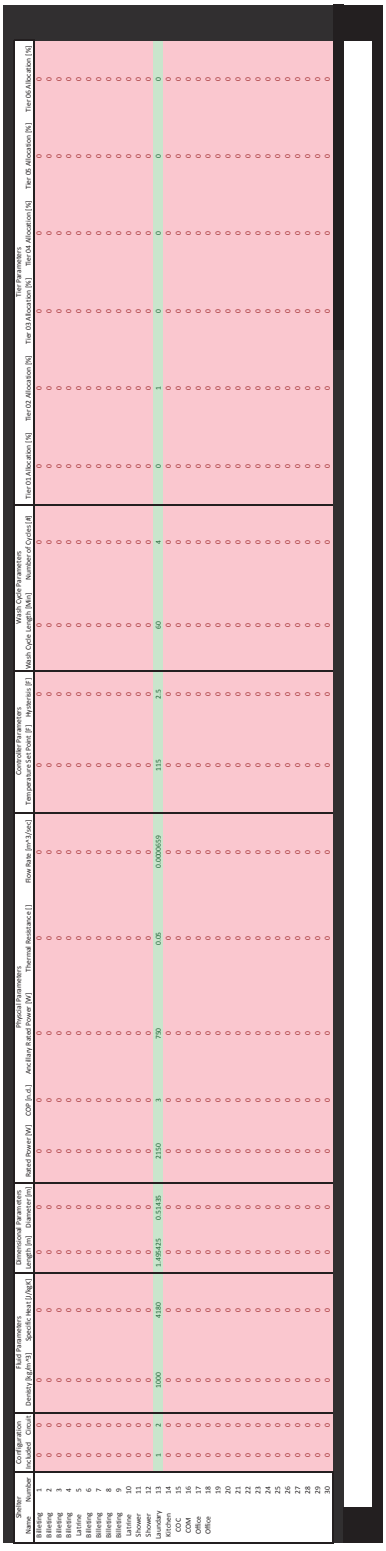

Figure A.4: Washing Machine Parameters

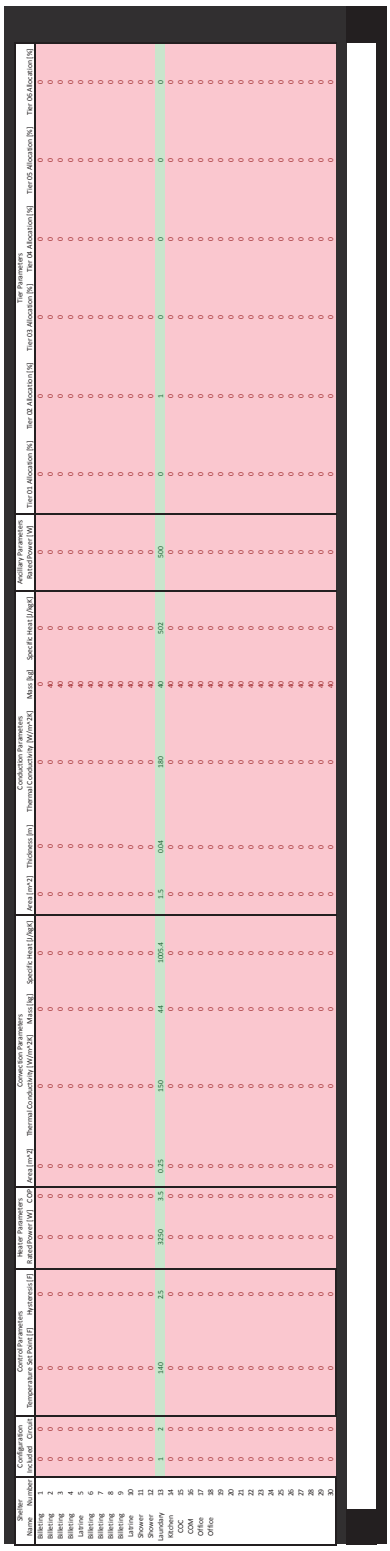

Figure A.5: Drying Machine Parameters

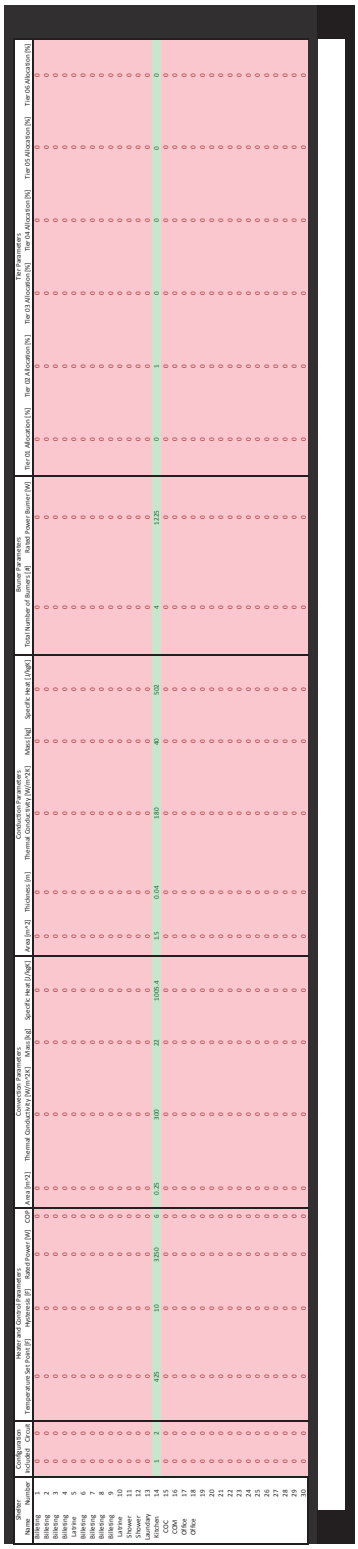

Figure A.6: Oven Parameters

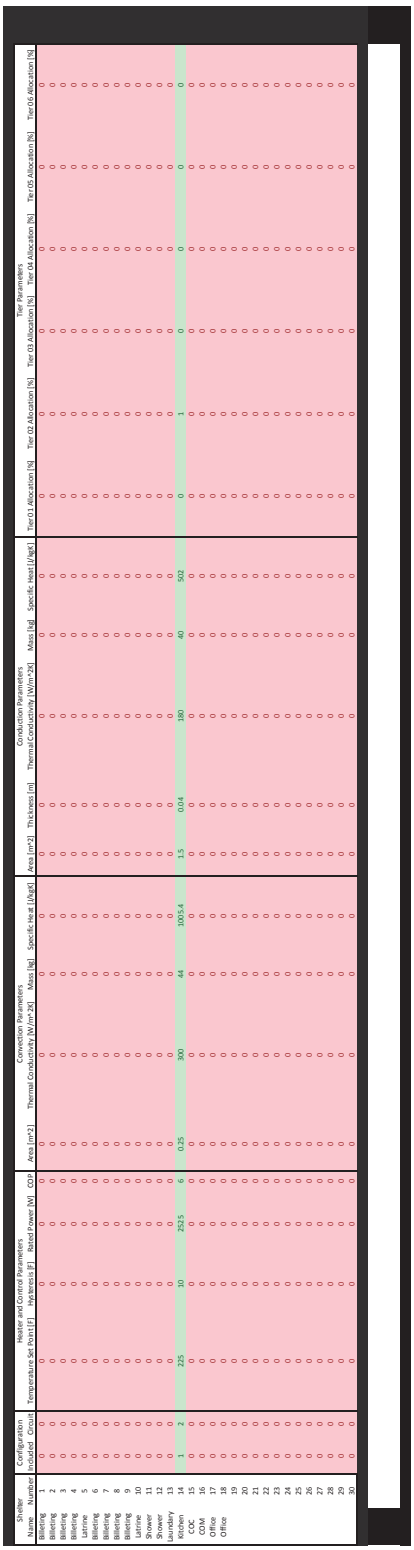

Figure A.7: Warmer Parameters

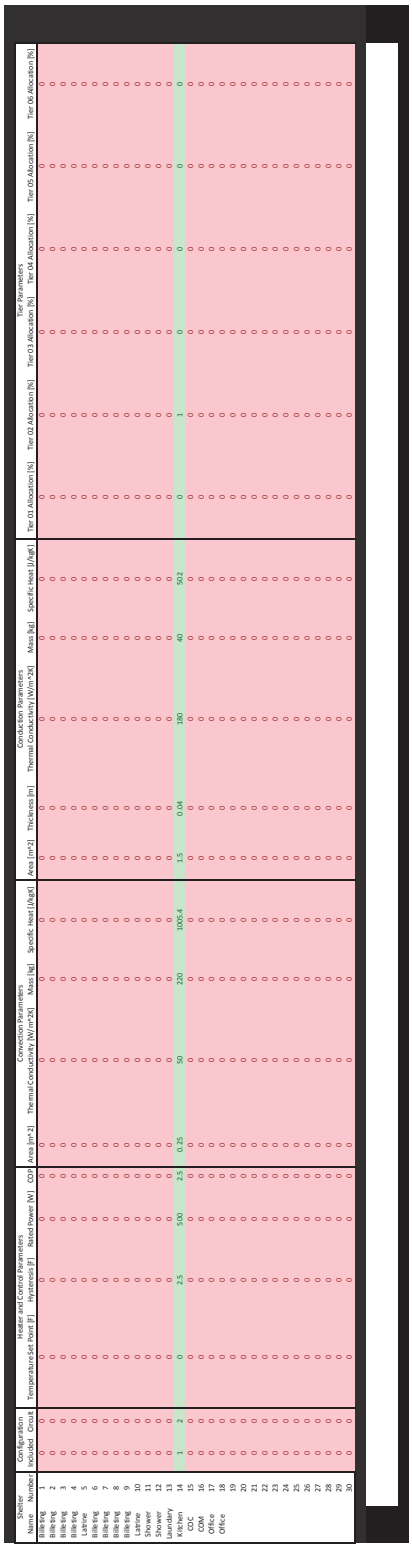

Figure A.8: Freezer Parameters

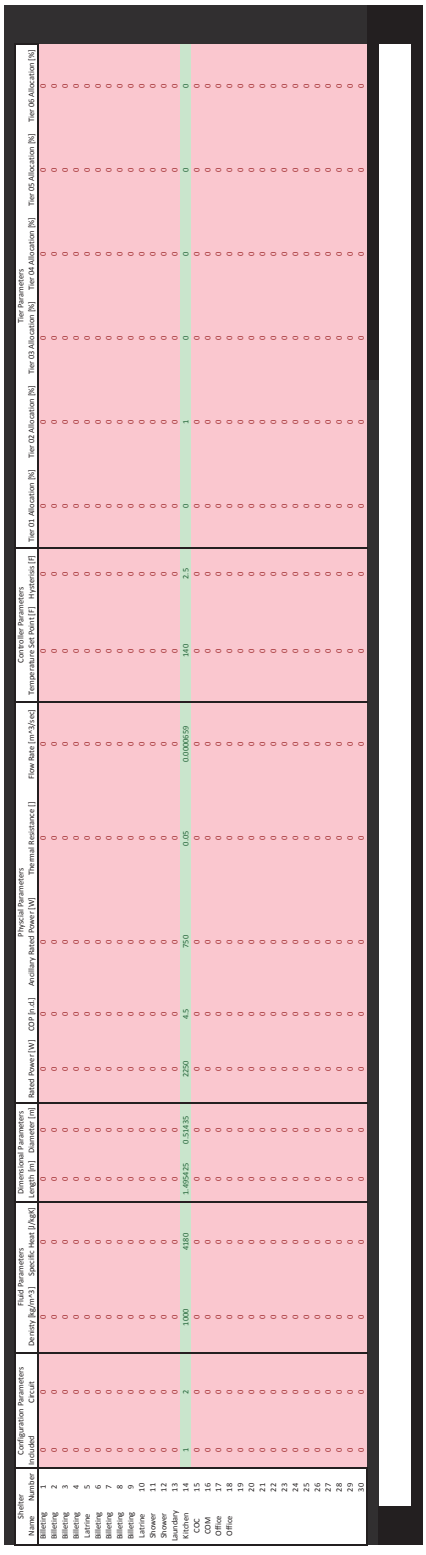

Figure A.9: Dishwasher Parameters

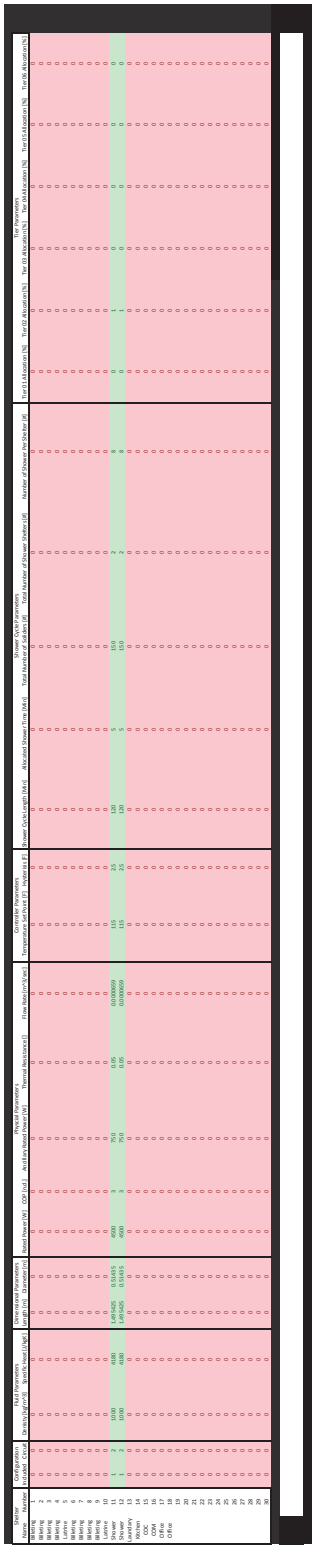

Figure A.10: Water Heater Parameters

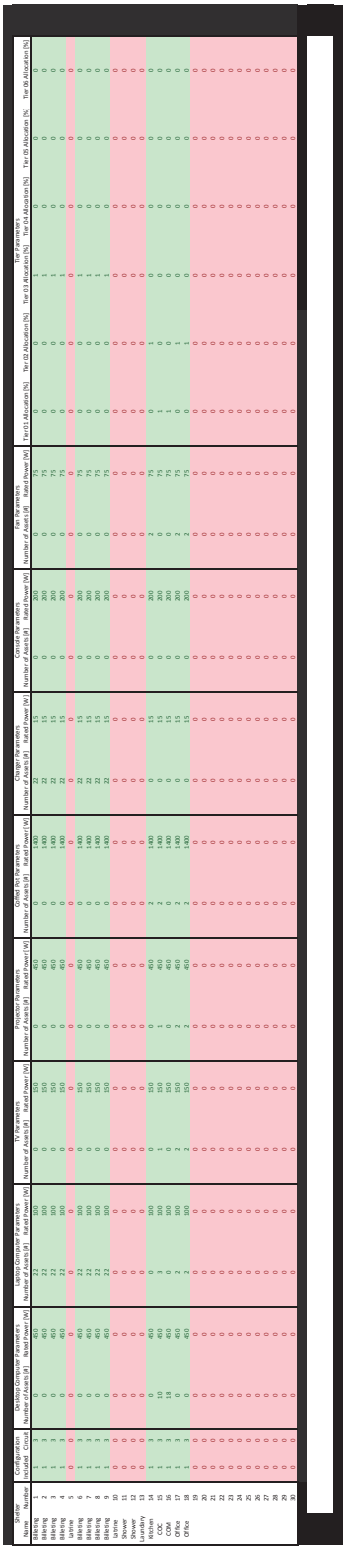

Figure A.11: Ancillary Parameters

Shelter		Configuration Parameters			Ancillary Parameters		Tier Parameters					
Name	Number	Included	Circuit	Circuit	Number of Lights	Rated Power [W]	Tier 01 Allocation [%]	Tier 02 Allocation [%]	Tier 03 Allocation [%]	Tier 04 Allocation [%]	Tier 05 Allocation [%]	Tier 06 Allocation [%]
Billeting	1	1	4	5	10	60	0	0	1	0	0	0
Billeting	2	1	4	5	10	60	0	0	1	0	0	0
Billeting	3	1	4	5	10	60	0	0	1	0	0	0
Billeting	4	1	4	5	10	60	0	0	1	0	0	0
Latrine	5	1	4	5	10	60	0	0	1	0	0	0
Billeting	6	1	4	5	10	60	0	0	1	0	0	0
Billeting	7	1	4	5	10	60	0	0	1	0	0	0
Billeting	8	1	4	5	10	60	0	0	1	0	0	0
Billeting	9	1	4	5	10	60	0	0	1	0	0	0
Latrine	10	1	4	5	10	60	0	0	1	0	0	0
Shower	11	1	4	5	10	60	0	0	1	0	0	0
Shower	12	1	4	5	10	60	0	0	1	0	0	0
Laundary	13	1	4	5	10	60	0	0	1	0	0	0
Kitchen	14	1	4	5	10	60	0	0	1	0	0	0
COC	15	1	4	5	10	60	0	0	1	0	0	0
COM	16	1	4	5	10	60	0	0	1	0	0	0
Office	17	1	4	5	10	60	0	0	1	0	0	0
Office	18	1	4	5	10	60	0	0	1	0	0	0
	19	0	0	0	0	0	0	0	0	0	0	0
	20	0	0	0	0	0	0	0	0	0	0	0
	21	0	0	0	0	0	0	0	0	0	0	0
	22	0	0	0	0	0	0	0	0	0	0	0
	23	0	0	0	0	0	0	0	0	0	0	0
	24	0	0	0	0	0	0	0	0	0	0	0
	25	0	0	0	0	0	0	0	0	0	0	0
	26	0	0	0	0	0	0	0	0	0	0	0
	27	0	0	0	0	0	0	0	0	0	0	0
	28	0	0	0	0	0	0	0	0	0	0	0
	29	0	0	0	0	0	0	0	0	0	0	0
	30	0	0	0	0	0	0	0	0	0	0	0

Figure A.12: Lighting Parameters

A.3 Meteorological Weather Profiles

The 2016 BCIL demo also contained meteorological weather data. The meteorological weather data which was integrated within the scenario generator included that of the ambient air temperature T_{amb} ^oF, the pressure P_{amb} inHg, the relative humidity RH %, the solar radiation G_{amb} W/m^2, the wind speed W_{speed} mph, and the wind direction $W_{direction}$ in degrees. The ambient air temperature and solar radiation profiles were required to incorporate renewable power generation. The ambient air temperature also affects the energy grid model's electrical load resulting from the use of an HVAC. Typical solar radiation and temperature profiles used within the dissertation was provided consistently throughout the earlier chapters, for this reason, no additional meteorological weather profiles were provided.

A.4 U.S. Army Relevant Event Schedules

Many of the energy management strategies provided within the previous chapters of this dissertation utilize model predictive control (MPC) in addition to a deterministic operational load profile which were directly tied to the U.S. Army relevant event schedule. During the initial development of the AAM, realistic data measured from the Dynamo II study and BCIL were obtained. Security restrictions made potential

use of the data directly within the AAM problematic. Additionally, insufficient record keeping regarding the relationship between known events and the operational load profiles contained within the Dynamo II or BCIL data sets made model predictive control extremely challenging.

In order for the MPC algorithms to operate, meteorological and deterministic event predictions were required, both required a quantifiable relationship to either (1) the power generated from a PV array or (2) the power consumed by the shelter's internal/external equipment. This kind of relationship would allow the MPC to predict future events, allowing the MPC to compute more energy efficient solutions. As this was not the case within the Dynamo II study, the U.S. Army relevant event schedule was generated via Mike Cook using his previous knowledge concerning military based operations. This event schedule was coupled with the preexisting data from the BCIL or Dynamo II studies, unfortunately, this deterministic relationship was unrealistic and produced operational load profiles which made further development of the energy management strategies and control architecture difficult.

It was at this point that the energy grid model was developed. Mathematical models for the various electrical equipment, as well as a heating, ventilation and air conditioning (HVAC) units were constructed. The event schedule was used as an input to drive the energy grid model, direct correlations between events and load increases or decreases were observed, yielding more reasonable behavior of the MPC, resulting in

improved energy management and control possibilities. The event schedule defines all active events, which took place within a scenario. The event schedule was directly tied to an operational load profile, which was generated using the energy grid model. An example event schedule are in Figure A.15. The event schedule was constructed directly from the Excel document presented in Section A.2, which defines the individual event trajectories as variably sized pulsed width signals with a fixed height and no set frequency, two example event trajectories which were ultimately used to make the event schedule shown in Figure A.15 are provided within Figure A.13 and Figure A.14.

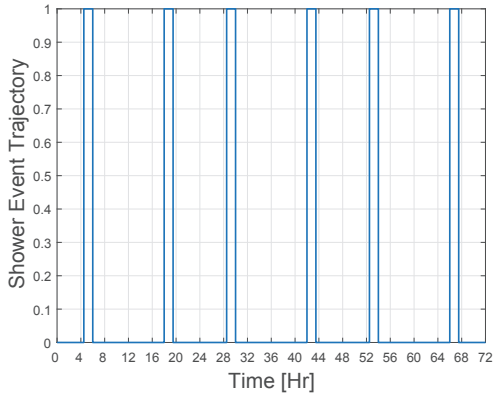

Figure A.13: Shower Event Trajectory

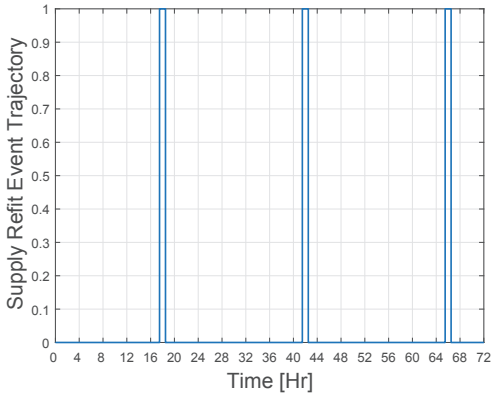

Figure A.14: Supply Refit Event Trajectory

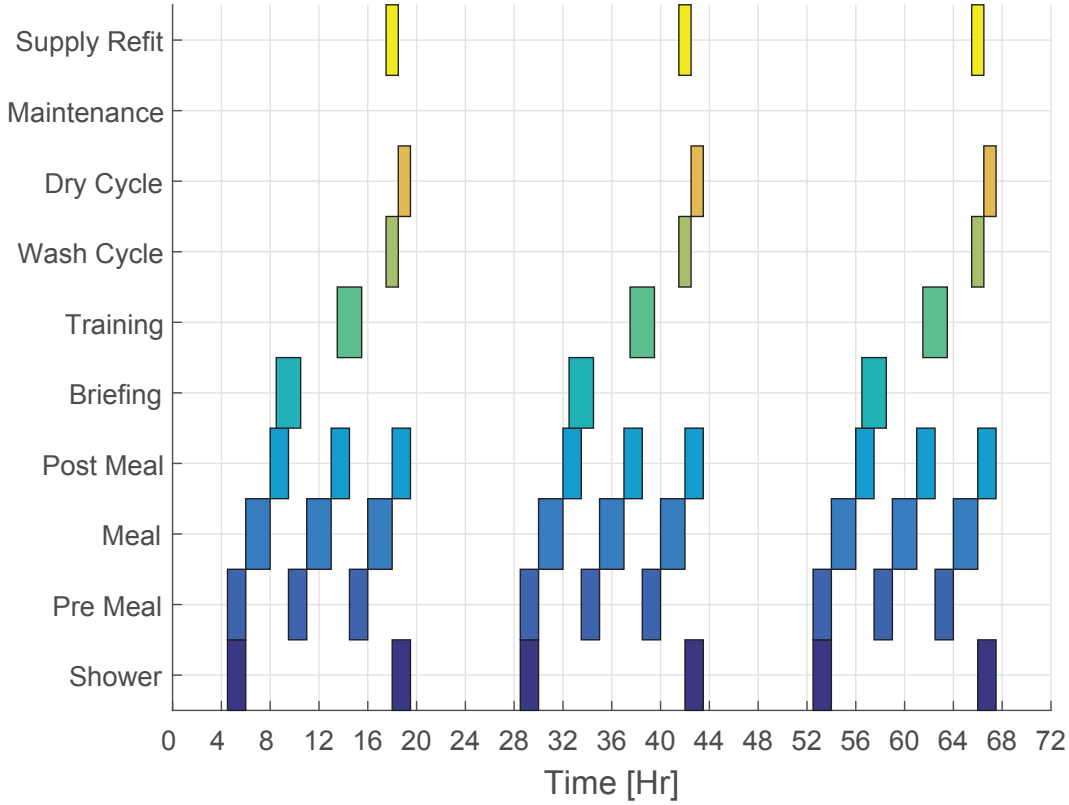

Figure A.15: Example event schedule. The individual colored rectangle indicates the event is active, while no colored rectangle indicates the event is inactive. An active event is defined within the event schedule trajectory using a one; conversely an inactive event is defined using a zero. The event schedule is closely tied to the shelter equipment list.

The event schedule should be constructed concurrently with the shelter equipment list as the event schedule was required to drive the energy grid model. The event schedule was also defined within a single Excel spreadsheet. The first sheet was used to define the event trajectories. Each additional sheet was used to visualize the various event trajectories.

The first sheet within the excel document defined the event trajectories, row one through row four defined the event times, which was separated into the military time, time in hours, time in minutes, and time in seconds respectively. It was assumed that the event schedule starts at 0 : 00 hours. Each time value was repeated within the event schedule, this allows the user to specify a variably sized pulse width signals which allowed an instantaneous step change to occur (active/inactive or the inverse). The minimum pulse width period was set to thirty minutes or a half hour. Every additional row within the first excel spreadsheet was used to define the various event trajectories. A one was used to indicate that an event was active, and a zero was used to indicate that an event was inactive. The sheet which defined the event trajectories are provided in Figure A.16. All other sheets were used to visualize the event trajectories.

Military Time	0:00:00		0:30:00		1:00:00		1:30:00	
Hours	0		0.5		1		1.5	
Mintues	0	0	30	30	60	60	90	90
Seconds	0	0	1800	1800	3600	3600	5400	5400
Shower	0	0	0	0	0	0	0	0
Pre-Meal	0	0	0	0	0	0	0	0
Meal	0	0	0	0	0	0	0	0
Post Meal	0	0	0	0	0	0	0	0
Briefing	0	0	0	0	0	0	0	0
Training	0	0	0	0	0	0	0	0
Wash Cycle	0	0	0	0	0	0	0	0
Dry Cycle	0	0	0	0	0	0	0	0
Maintenance	0	0	0	0	0	0	0	0
Supply Refit	0	0	0	0	0	0	0	0
Event 11	0	0	0	0	0	0	0	0
Event 12	0	0	0	0	0	0	0	0
Event 13	0	0	0	0	0	0	0	0
Event 14	0	0	0	0	0	0	0	0
Event 15	0	0	0	0	0	0	0	0
Event 16	0	0	0	0	0	0	0	0
Event 17	0	0	0	0	0	0	0	0
Event 18	0	0	0	0	0	0	0	0
Event 19	0	0	0	0	0	0	0	0
Event 20	0	0	0	0	0	0	0	0
Event 21	0	0	0	0	0	0	0	0
Event 22	0	0	0	0	0	0	0	0
Event 23	0	0	0	0	0	0	0	0
Event 24	0	0	0	0	0	0	0	0
Event 25	0	0	0	0	0	0	0	0
Event 26	0	0	0	0	0	0	0	0
Event 27	0	0	0	0	0	0	0	0
Event 28	0	0	0	0	0	0	0	0

Figure A.16: Event Schedule - Sheet 01 - The Excel sheet used to define the event schedule trajectories.

A.5 Energy Grid Model

The energy grid model was pragmatically generated, this allows the operational load profiles utilized to be extensible. In order to pragmatically construct the energy grid model, the amended configuration data structure was first generated. The custom files and functions of the scenario generator were then executed to construct the energy

grid model. The programmatic creation of the energy grid model currently supports creation of (1) a billeting shelter, (2) a latrine, (3) a shower shelter, (4) a laundry shelter, (5) a combat operations center (COC) shelter, a communication (COMM) shelter, (6) a kitchen shelter, and (7) an office shelter, provided in the subsequent subsections.

A.5.1 Billeting Shelter

The billeting shelter was programmed to include an HVAC unit coupled with a hysteresis controller, a thermal model of the shelter, ancillary electrical components, and lighting. The inner components of the billeting shelter subsystem are provided in Figure A.17.

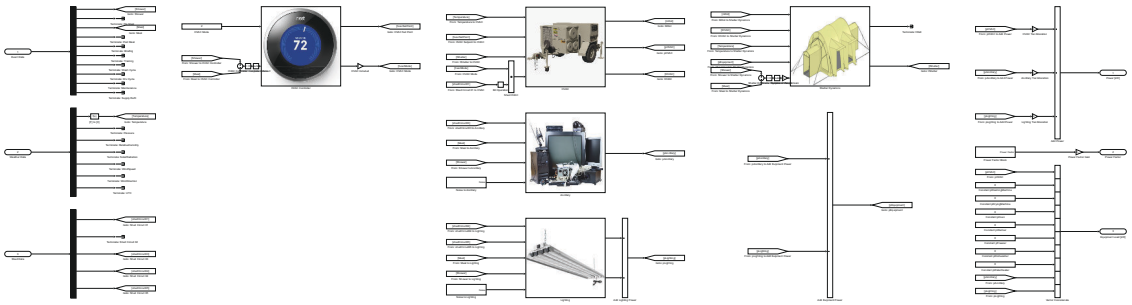

Figure A.17: Billeting Shelter Subsystem

A.5.2 Latrine Shelter

The latrine shelter was programmed to include an HVAC unit coupled with a hysteresis controller, a thermal model of the shelter, and lighting. The inner components of the latrine shelter subsystem are shown in Figure A.18.

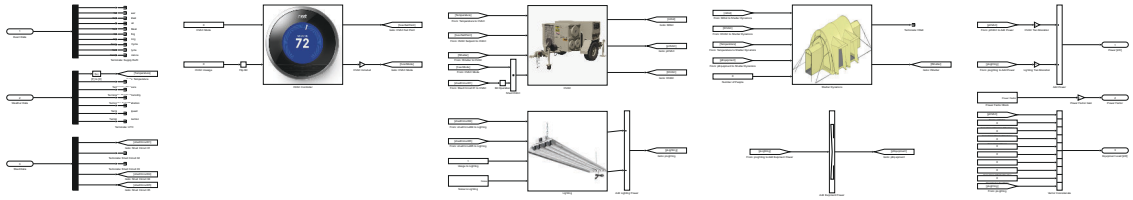

Figure A.18: Latrine Shelter Subsystem

A.5.3 Shower Shelter

The shower shelter was programmed to include an HVAC unit coupled with a hysteresis controller, a thermal model of the shelter, a hot water heater, and lighting. The inner components of the shower shelter subsystem are provided in Figure A.19.

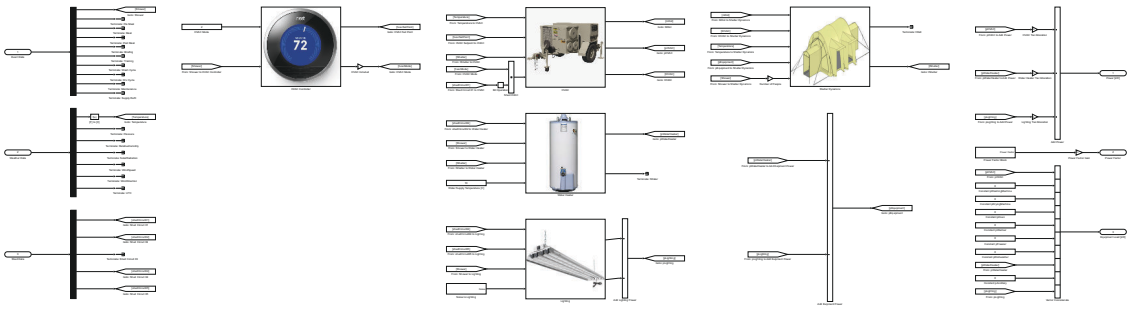

Figure A.19: Shower Shelter Subsystem

A.5.4 Laundry Shelter

The laundry shelter was programmed to include an HVAC unit coupled with a hysteresis controller, a thermal model of the shelter, a washing machine, a drying machine, and lighting. The inner components of the laundry shelter subsystem are presented in Figure A.20.

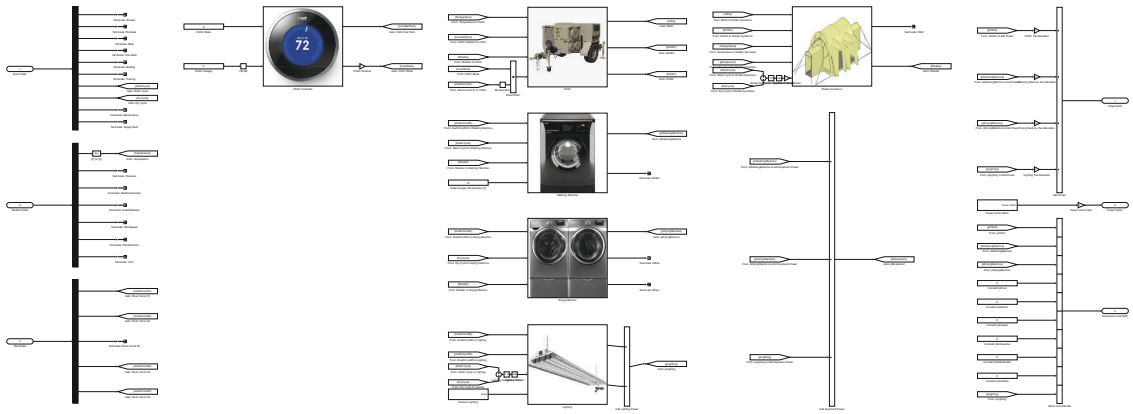

Figure A.20: Laundry Shelter Subsystem

A.5.5 Combat Operation Center (COC) Shelter

The COC shelter was programmed to include an HVAC unit coupled with a hysteresis controller, a thermal model of the shelter, ancillary electrical components, and lighting. The inner components of the COC shelter subsystem are provided in Figure A.21.

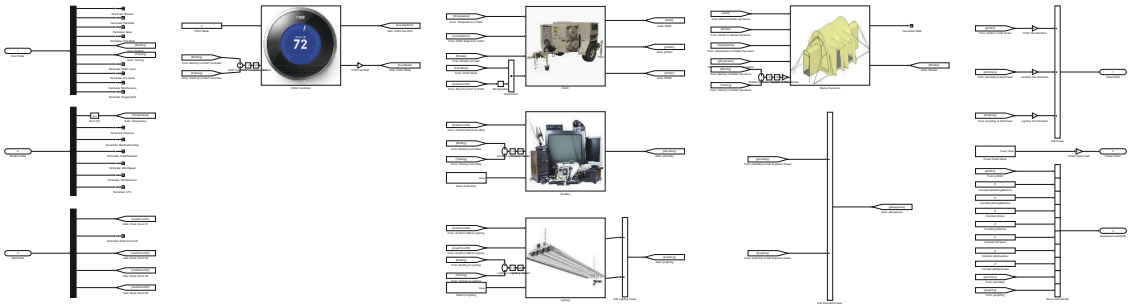

Figure A.21: COC Shelter Subsystem

A.5.6 Communication (COMM) Shelter

The COMM shelter was programmed to include an HVAC unit coupled with a hysteresis controller, a thermal model of the shelter, ancillary electrical components, and lighting. The inner components of the COMM shelter subsystem are shown in Figure A.22.

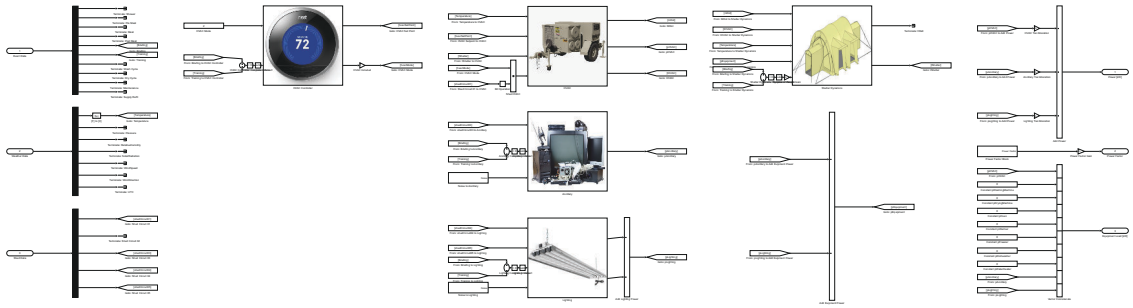

Figure A.22: Communication Shelter Subsystem

A.5.7 Kitchen Shelter

The kitchen shelter was programmed to include an HVAC unit coupled with a hysteresis controller, a thermal model of the shelter, an oven, a warmer, a freezer or refrigerator, a dishwasher, ancillary electrical components, and lighting. The inner components of the kitchen shelter subsystem are presented in Figure A.23.

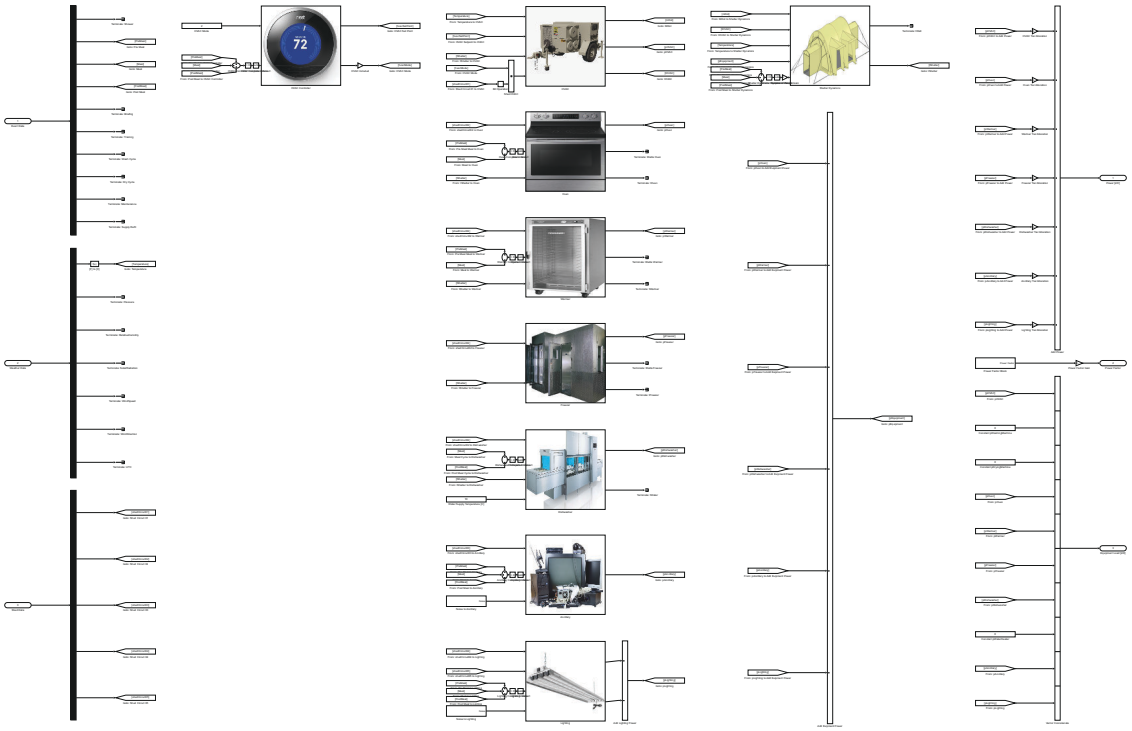

Figure A.23: Kitchen Shelter Subsystem

A.5.8 Office Shelter

The office shelter was programmed to include an HVAC unit coupled with a hysteresis controller, a thermal model of the shelter, ancillary electrical components, and lighting. The inner components of the office shelter subsystem are provided in Figure A.24.

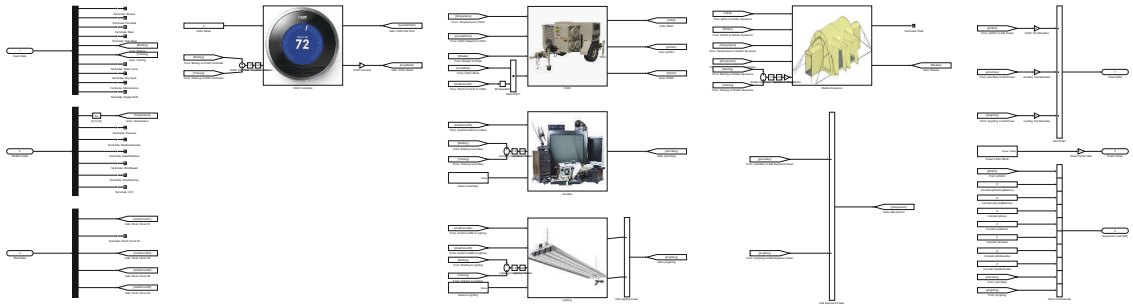

Figure A.24: Office Shelter Subsystem

A.5.9 Energy Grid Model Subsystem

Each of the previously mentioned shelters was contained within the energy grid model subsystem, the contents of which are shown within Figure A.25.

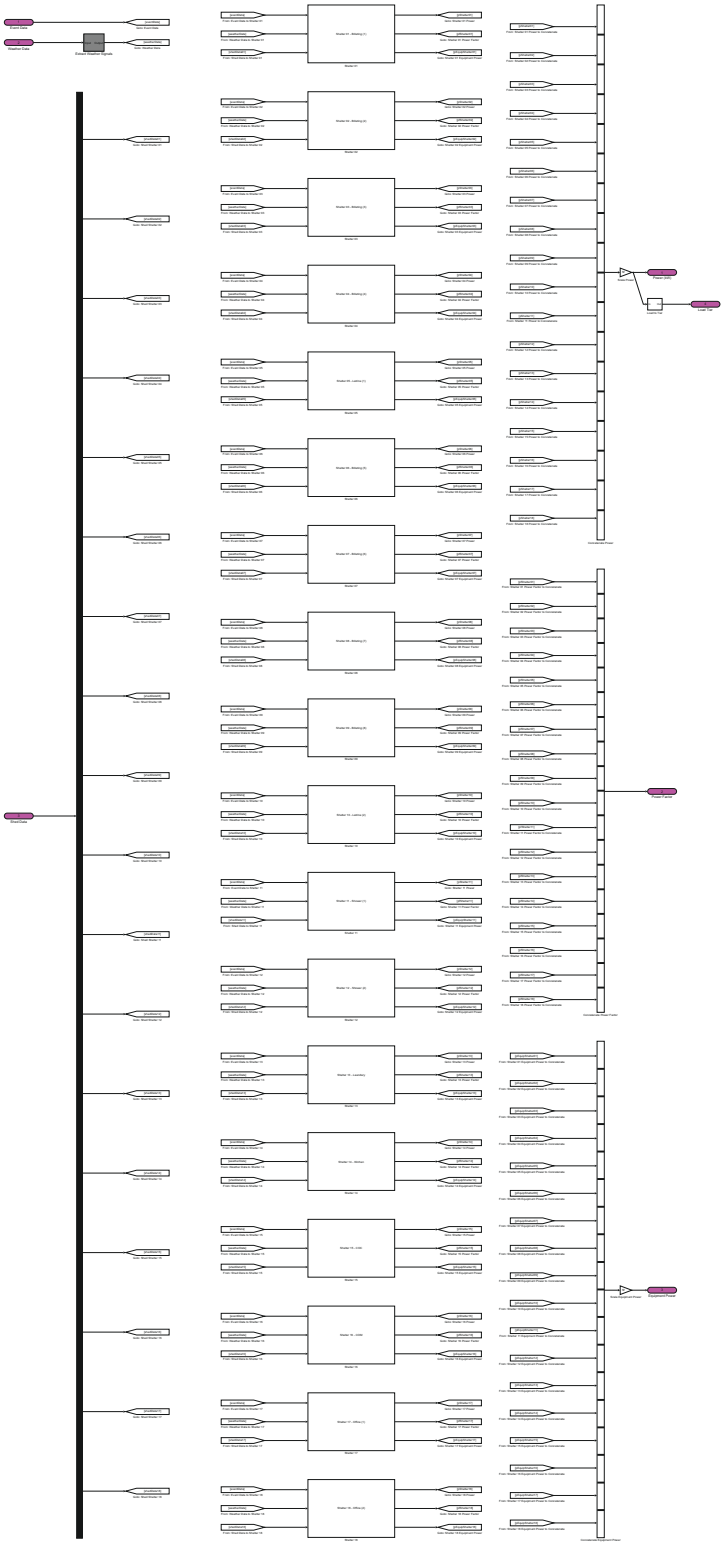

Figure A.25: The Shelter Load Subsystem Block Contents.

The energy grid model computes the electrical load for each shelter, which was decomposed into a prioritized load which includes three tiers, assuming tier one was the highest priority while tier three was the lowest priority load. Additionally, the energy grid model computes a power factor for each tiered load, as well as a complete set of electrical equipment power signals which allow the control algorithms to identify which electrical components within the shelter were operating. Some devices while not present within the model will be displayed as having zero power for a shelter. An example of the expected output from two of the many shelters defined using the energy grid model are shown in Figure A.26 - Figure A.35.

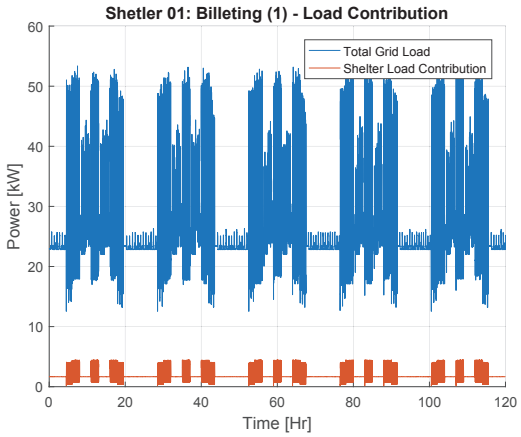

Figure A.26: Load Contribution for Shelter 01

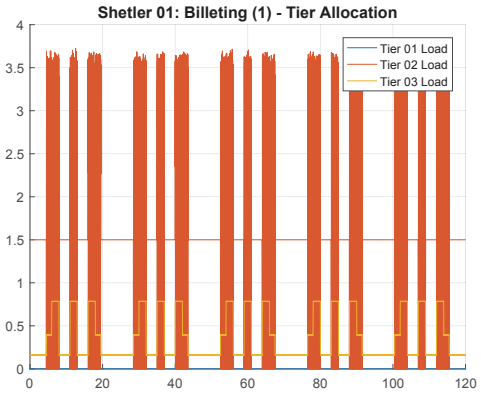

Figure A.27: Load Tier for Shelter 01

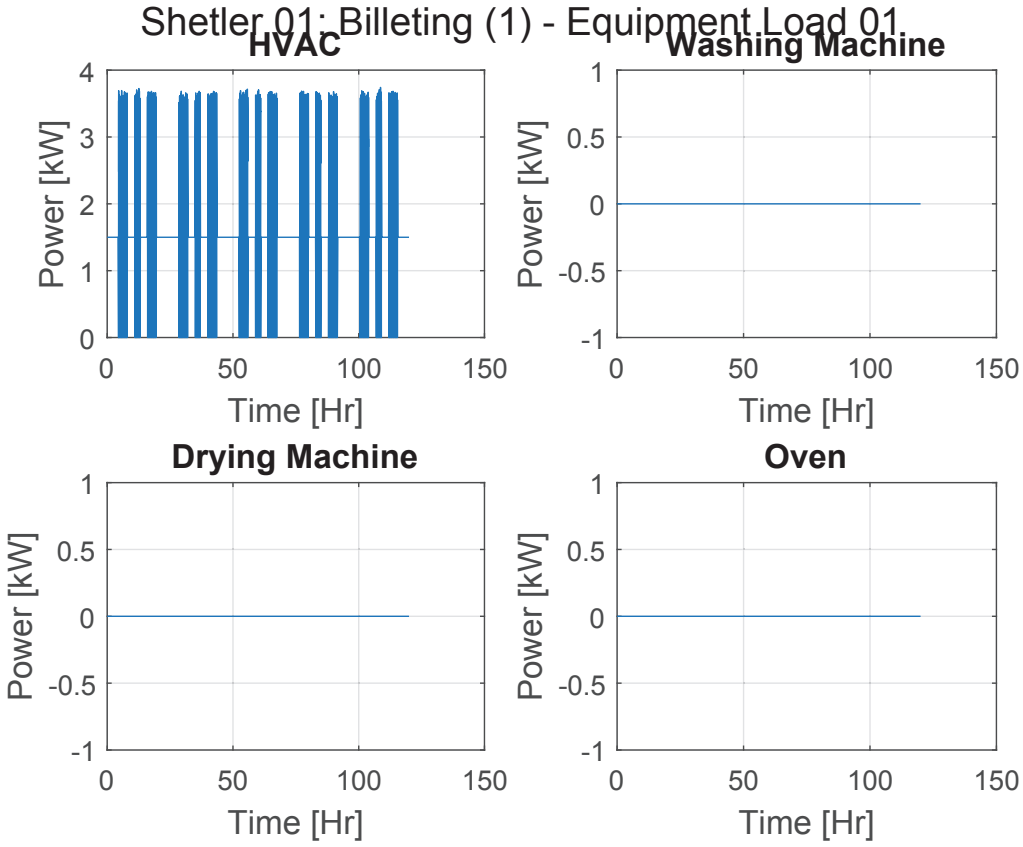

Figure A.28: Electrical Equipment Component 01 - 04 for Shelter 01

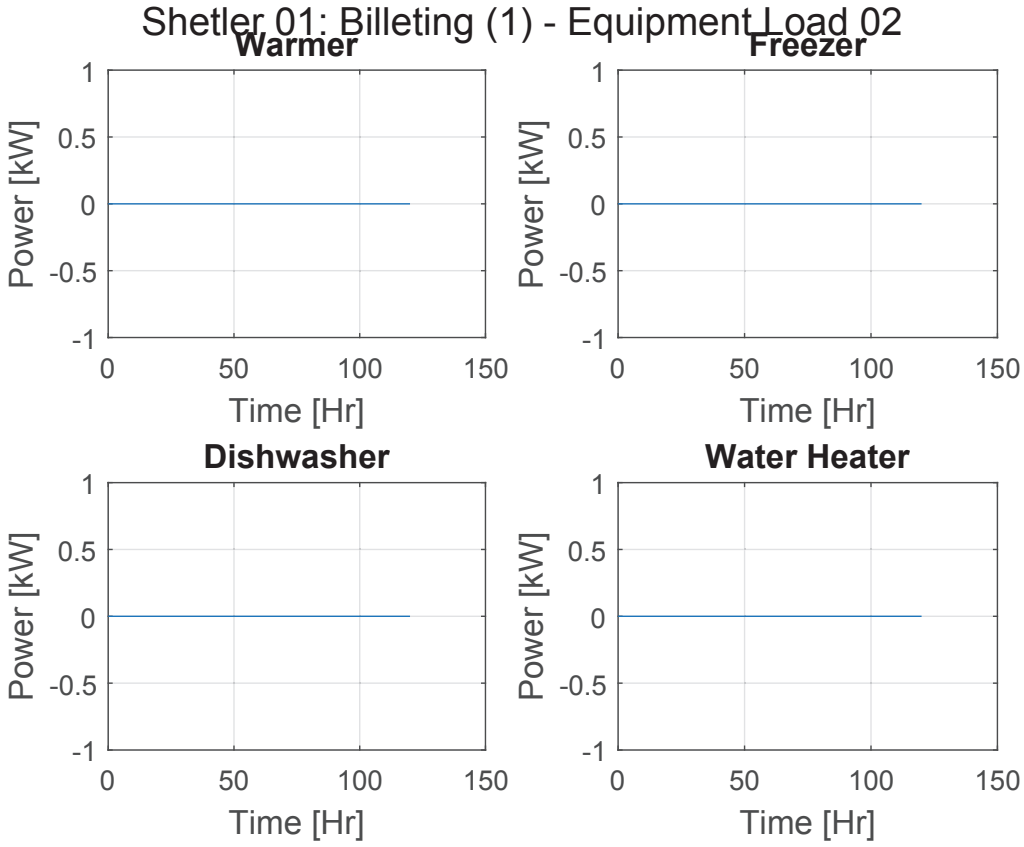

Figure A.29: Electrical Equipment Component 05 - 08 for Shelter 01

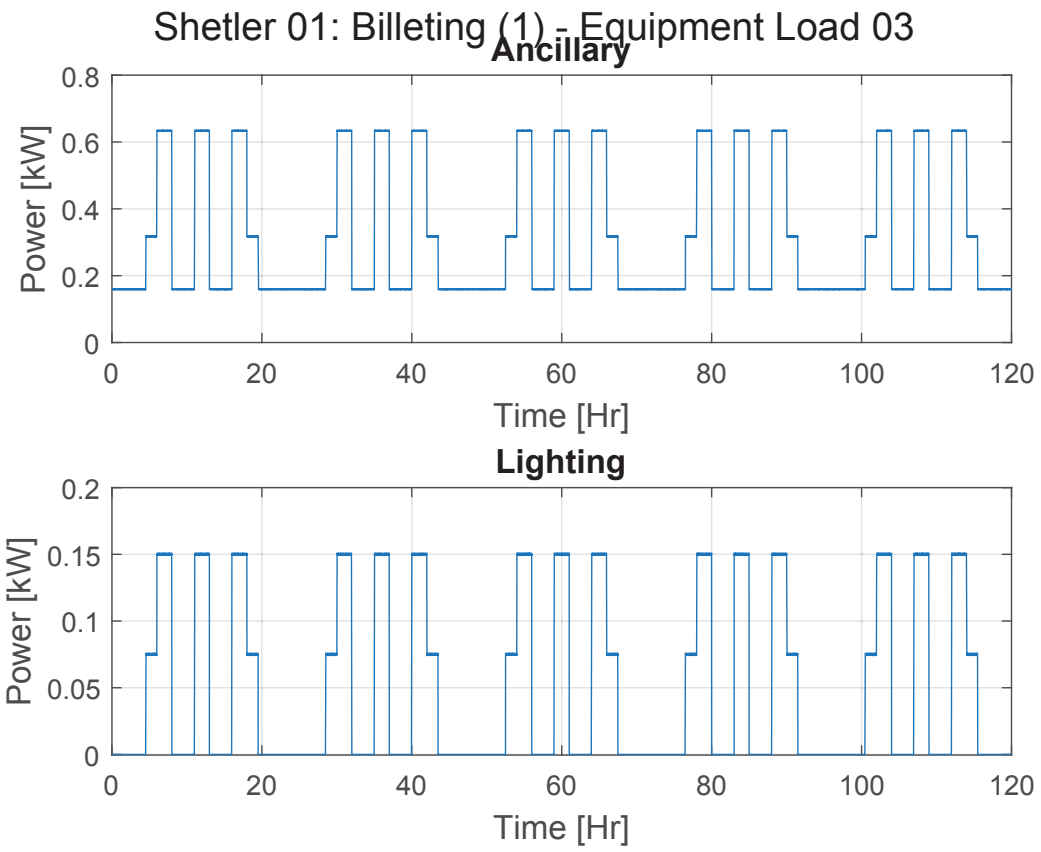

Figure A.30: Electrical Equipment Component 09 - 10 for Shelter 01

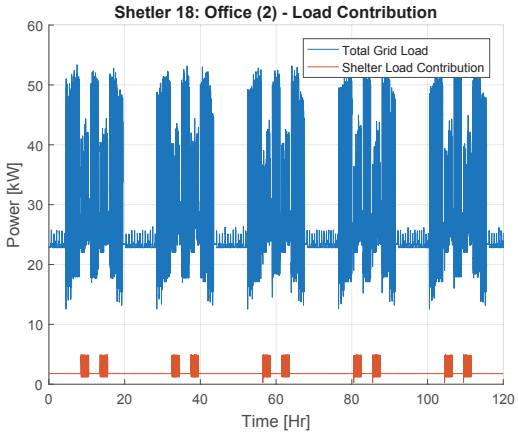

Figure A.31: Load Contribution for Shelter 02

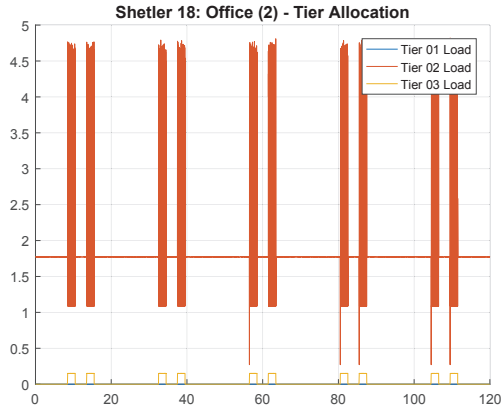

Figure A.32: Load Tier for Shelter 02

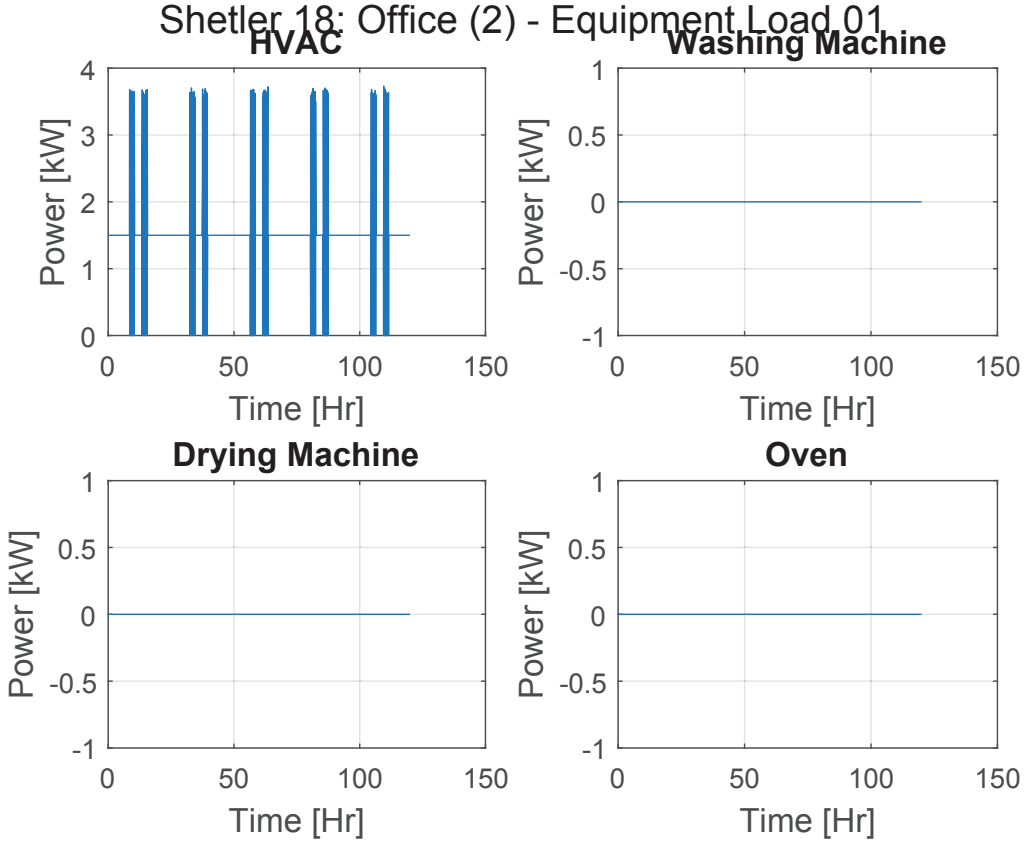

Figure A.33: Electrical Equipment Component 01 - 04 for Shelter 02

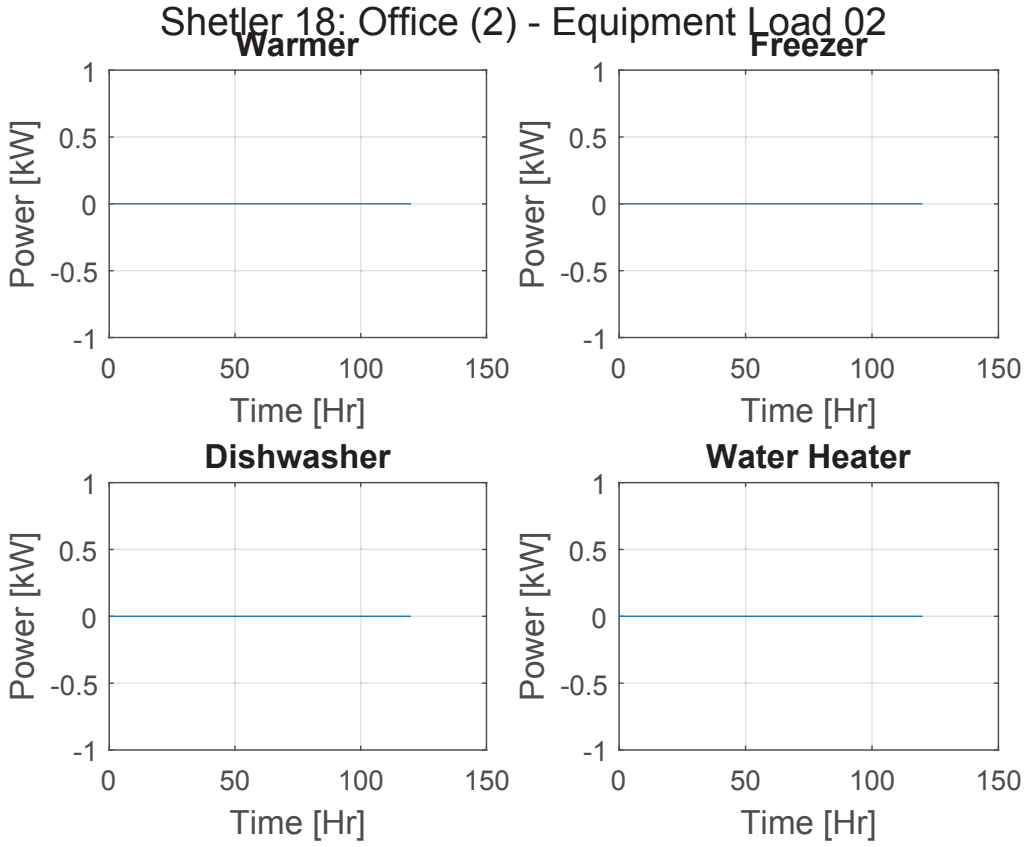

Figure A.34: Electrical Equipment Component 05 - 08 for Shelter 02

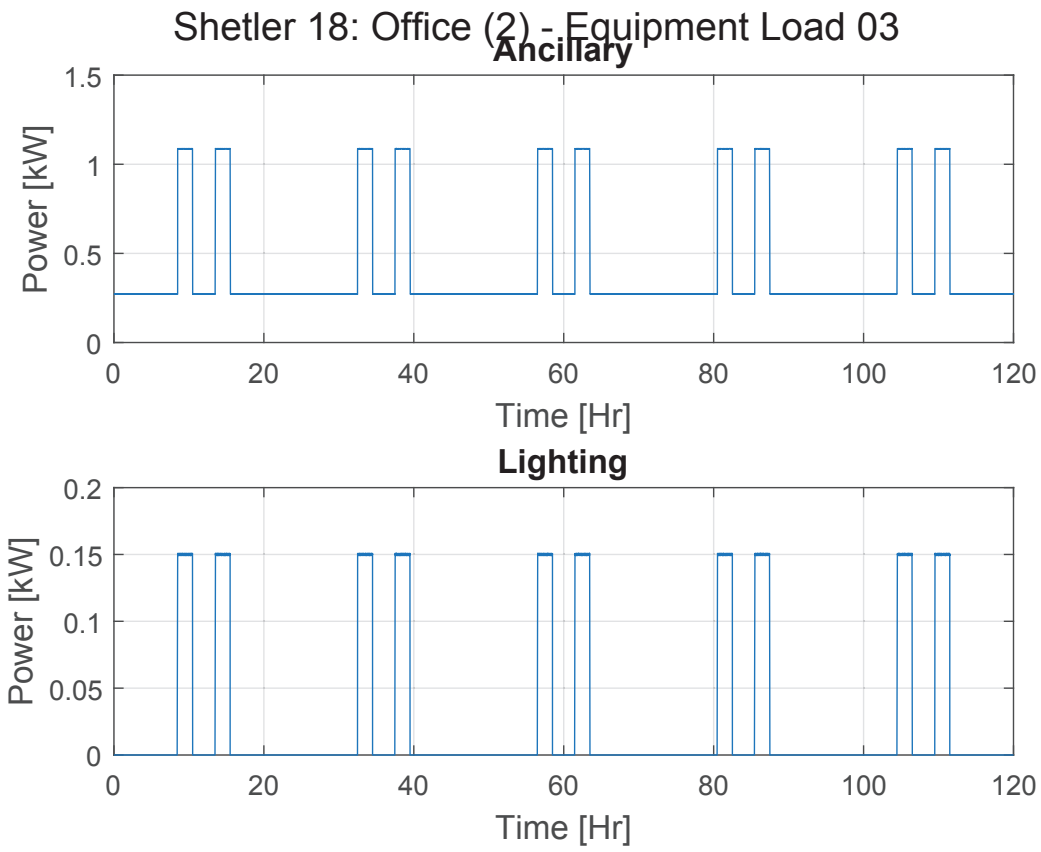

Figure A.35: Electrical Equipment Component 09 - 10 for Shelter 02

The energy grid model was ultimately constructed using multiple GUIs. The first GUI enabled the enabled the meteorological weather conditions from the BCIL data to be parsed, and coupled with the shelter equipment list, and event schedule to construct multiple data files. The data files were then loaded using the second GUI, which programmatically generated the *Simulink* model which contained the energy grid model of the time varying electrical load.

Appendix B

Weather Publication

Non-Normalized Sky Results

B.1 Electrical Load

There were eighteen shelters, of the eighteen shelters, there were eight distinctly different shelters, including (1) billeting, (2) latrine, (3) laundry, (4) shower, (5) kitchen, (6) the combat operations center (COC), (7) communication (COMM), and an office. The internal equipment electrical load of each shelter varied as a function of the event schedule and the shelter designation. The equipment electrical load was held constant throughout the case studies resulting from a constant event

schedule. The internal equipment electrical load for each of the eight distinctly different shelters were provided in Figure B.1 - Figure B.8.

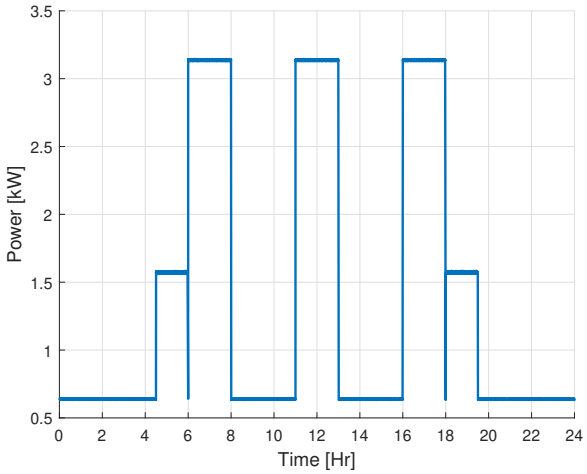

Figure B.1: Billeting Equipment Power

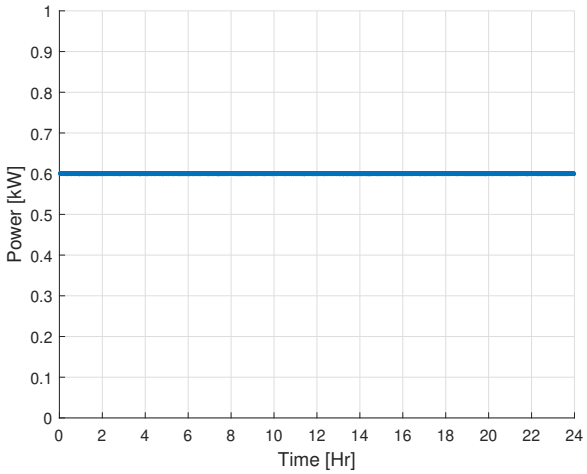

Figure B.2: Latrine Equipment Power

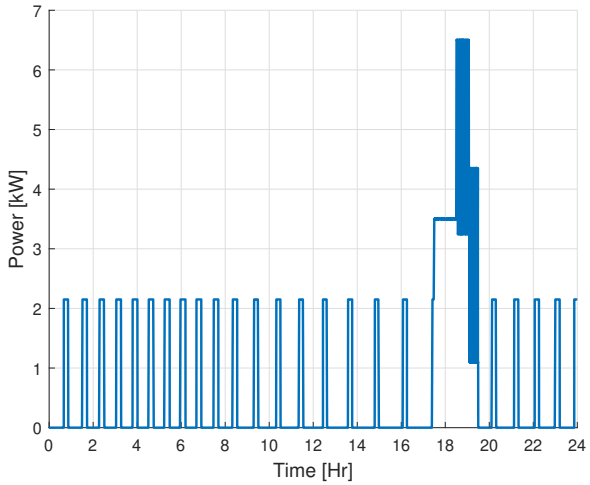

Figure B.3: Laundry Equipment Power

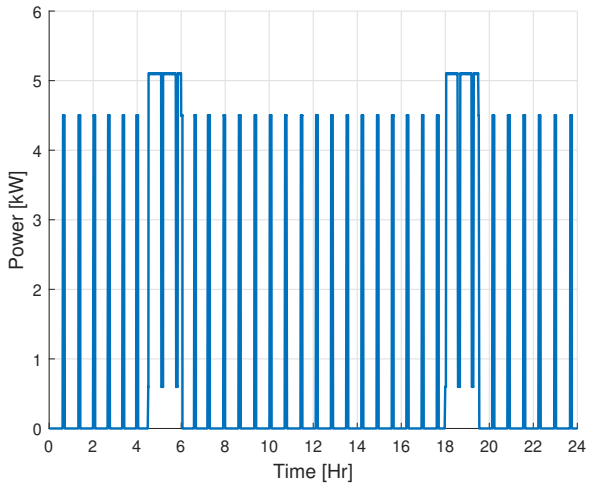

Figure B.4: Shower Equipment Power

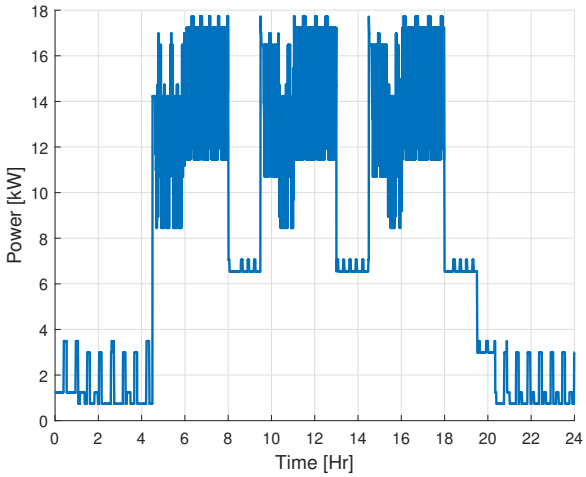

Figure B.5: Kitchen Equipment Power

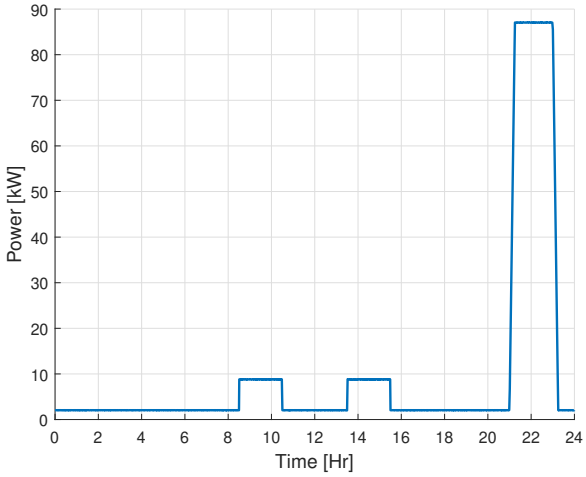

Figure B.6: COC Equipment Power

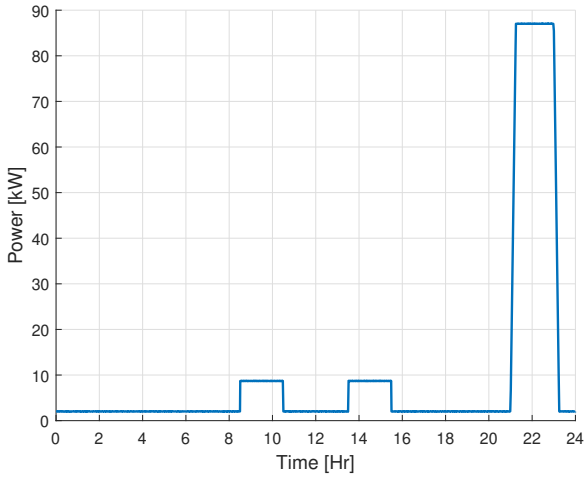

Figure B.7: COM Equipment Power

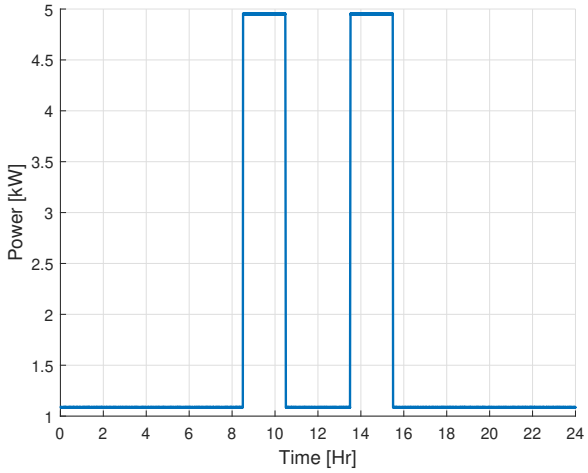

Figure B.8: Office Equipment Power

The energy management strategy was predicated on the idea that event schedule and meteorological conditions had a quantifiable relationship with the aggregate electrical load (equipment and HVAC). The operation of the HVAC units was then directly linked to the meteorological conditions and thermal parameters and constants which governed the heat transfer between a shelter and the ambient conditions, the thermal

parameters for the shelter are provided in Table B.1, and the thermal constants for each shelter are provided in Table B.2.

Symbol	Description	Unit	Value
$C_{p,air}$	Average Specific Heat of Air	kJ/kg/K	1.005
ρ_{air}	Density of Air	kg/m^3	1.19
V_{room}	Room Volume	m^3	650
C_{room}	Room Capacitance	kJ/kg	$C_{p,air}\rho_{air}V_{room}$
R_{room}	Room Thermal Resistance	kW/K	C_{room}/τ_{room}
R_{wall}	Wall Thermal Resistance	kW/K	C_{wall}/τ_{wall}

Table B.1
Shelter Thermal Parameters

Shelter	Shelter Type	Wall Capacitance C_{wall} kJ/kg	Wall Time Constant τ_{wall} sec	Room Time Constant τ_{room} sec
1	Billeting	23	23	23
2	Billeting	30	30	30
3	Billeting	29	29	29
4	Billeting	25	25	25
5	Latrine	26	26	26
6	Billeting	30	30	30
7	Billeting	23	23	23
8	Billeting	30	30	30
9	Billeting	28	28	28
10	Latrine	21	21	21
11	Shower	24	24	24
12	Shower	30	30	30
13	Laundry	29	29	29
14	Kitchen	12	147	147
15	COC	21	21	21
16	COM	26	26	26
17	Office	20	20	20
18	Office	27	27	27

Table B.2
Shelter Thermal Constants

Using the thermal parameters and constants in addition of the equipment electrical load profiles and the 1D heat transfer equations provided earlier, the aggregate electrical load profile was generated.

B.2 Sky Condition Results

For each of four atmospheric scenarios, two separate figures are provided. The first figure includes the fuel consumed by the generators. The consumed fuel considers (1) the fuel consumed to run the generators, (2) the amount of fuel consumed to charge the electrical storage to an initial value, and (3) the amount of fuel consumed or saved, which accounts for the differences between the final energy state and the initial energy state. The second figure contains the energy storage requirements as a whole, and is separated into the component requirements (bus storage and PV storage).

B.2.1 Clear Results

The fuel consumption and energy storage requirements for the clear sky conditions of Figure 5.4 and Figure 5.9 are provided in Figure B.9 - Figure B.10.

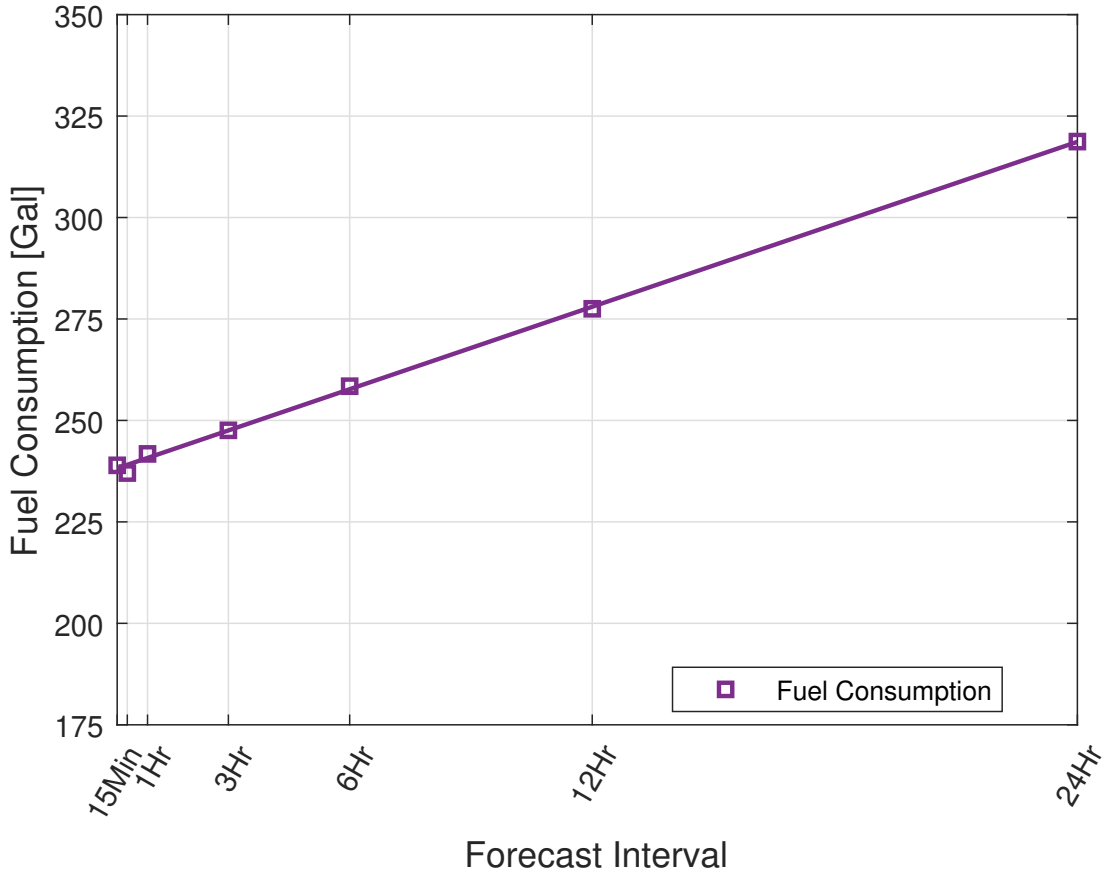

Figure B.9: The fuel consumed by the generators factoring in both the initial stored energy requirements, and the difference between the final energy state and the initial energy state for the bus and PV storage.

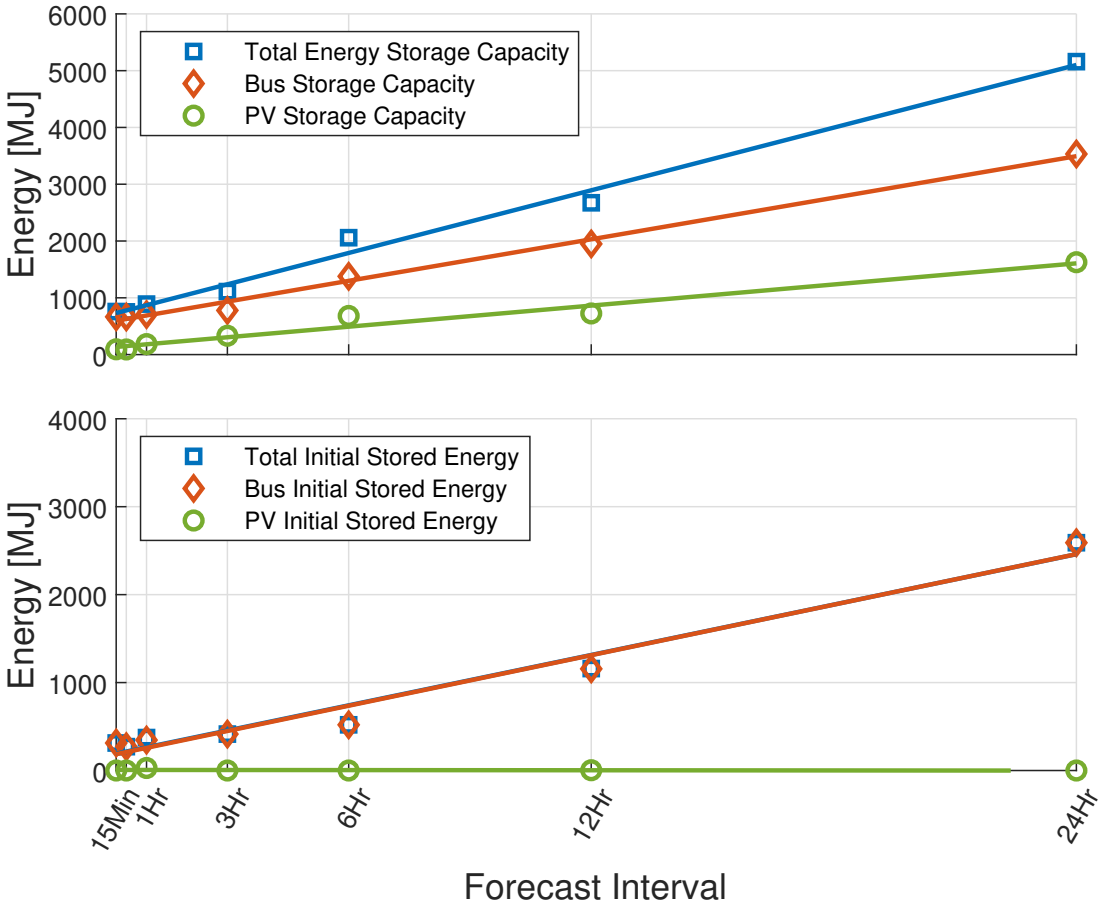

Figure B.10: Allocation of the total energy storage between the bus storage and the PV sites.

B.2.2 Cloudy Results

The fuel consumption and energy storage requirements for the cloudy sky conditions of Figure 5.5 and Figure 5.10 are provided in Figure B.11 - Figure B.12.

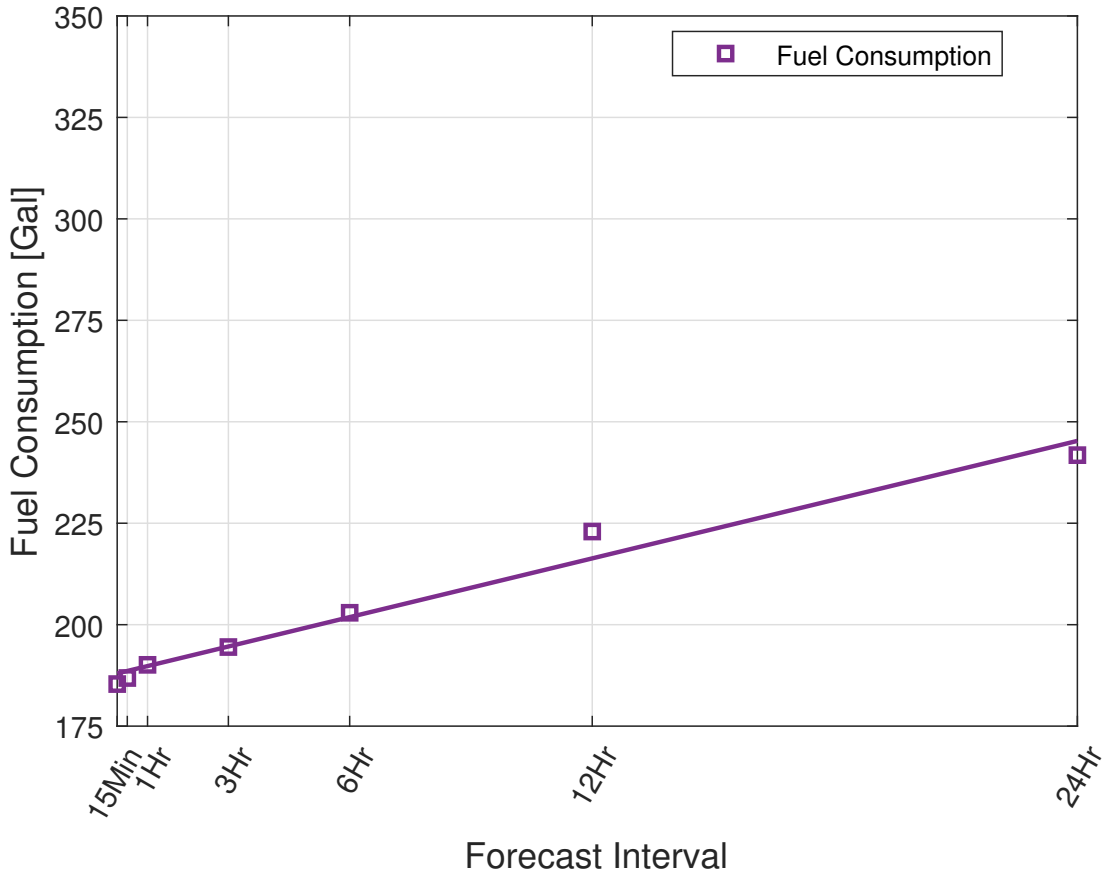

Figure B.11: The fuel consumed by the generators factoring in both the initial stored energy requirements, and the difference between the final energy state and the initial energy state for the bus and PV storage.

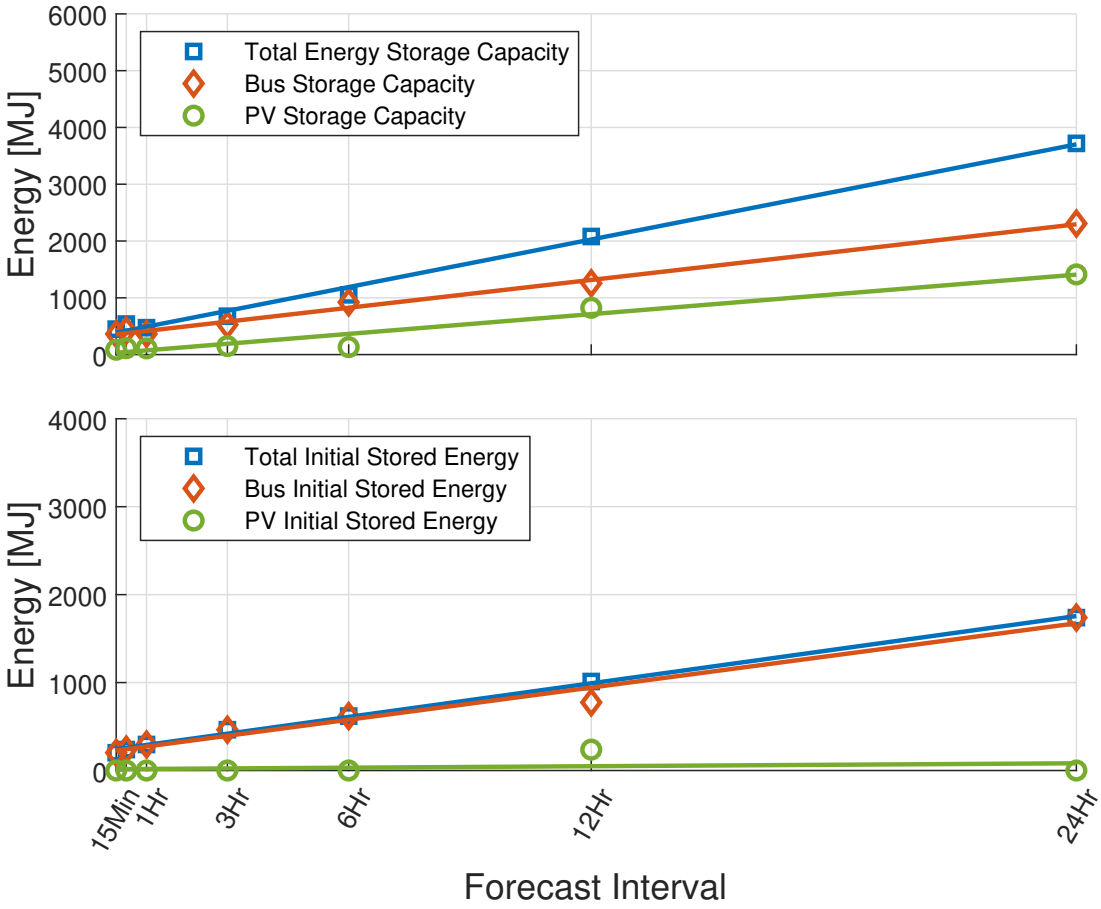

Figure B.12: Allocation of the total energy storage between the bus storage and the PV sites.

B.2.3 Overcast Results

The fuel consumption and energy storage requirements for the overcast sky conditions of Figure 5.6 and Figure 5.11 are provided in Figure B.13 - Figure B.14.

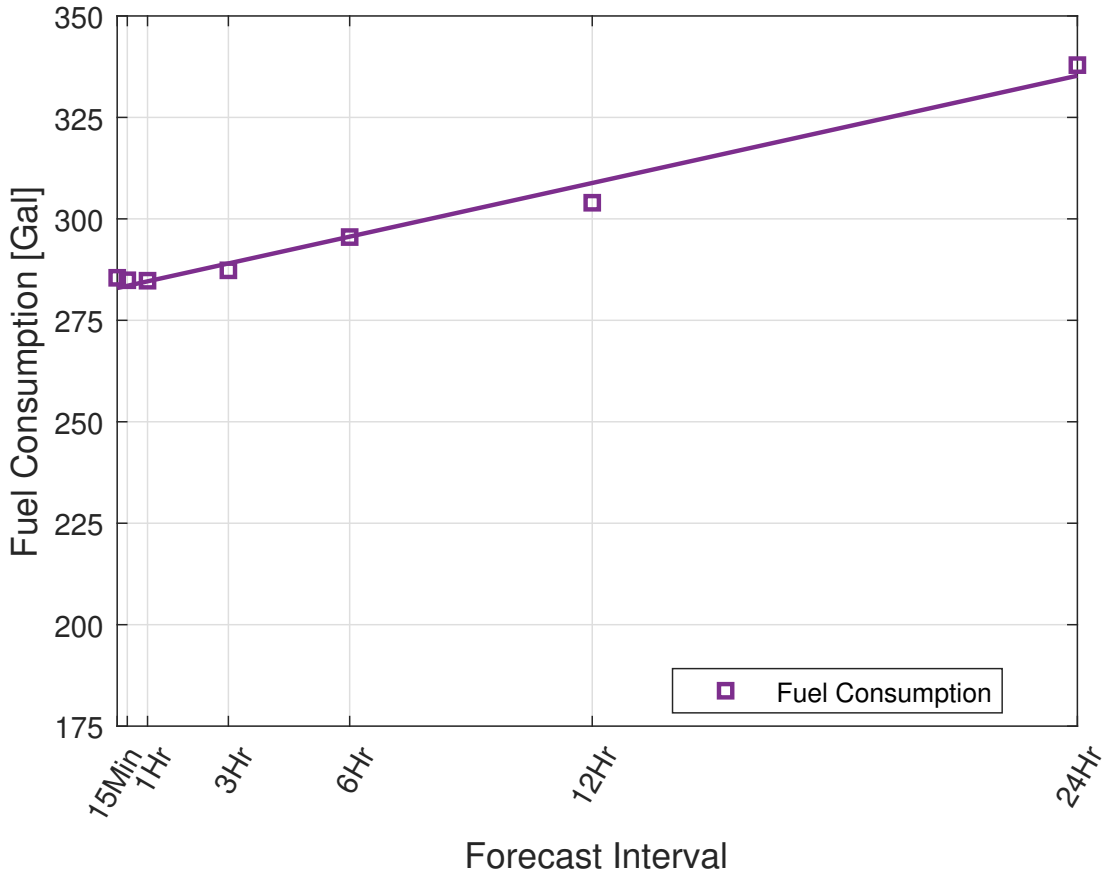

Figure B.13: The fuel consumed by the generators factoring in both the initial stored energy requirements, and the difference between the final energy state and the initial energy state for the bus and PV storage.

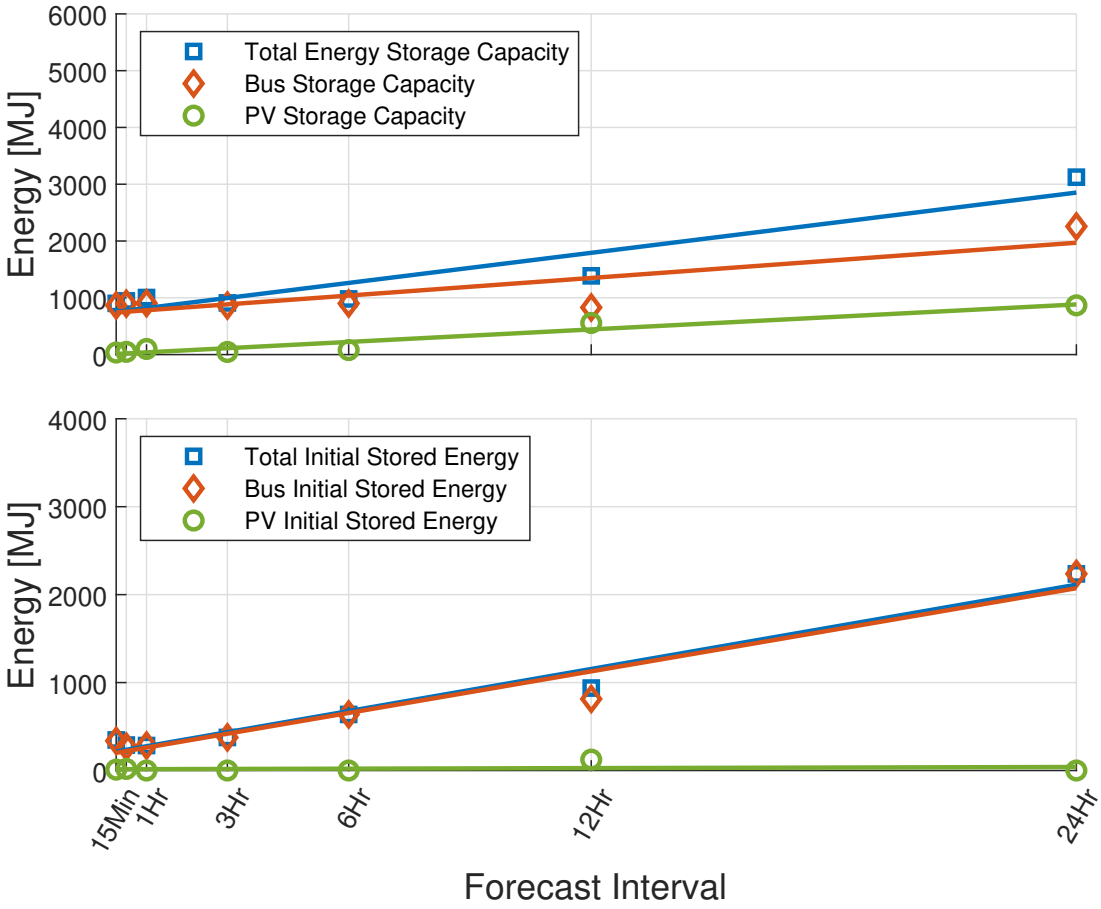

Figure B.14: Allocation of the total energy storage between the bus storage and the PV sites.

B.2.4 Monsoon Results

The fuel consumption and energy storage requirements for the monsoon sky conditions of Figure 5.7 and Figure 5.12 are provided in Figure B.15 - Figure B.16.

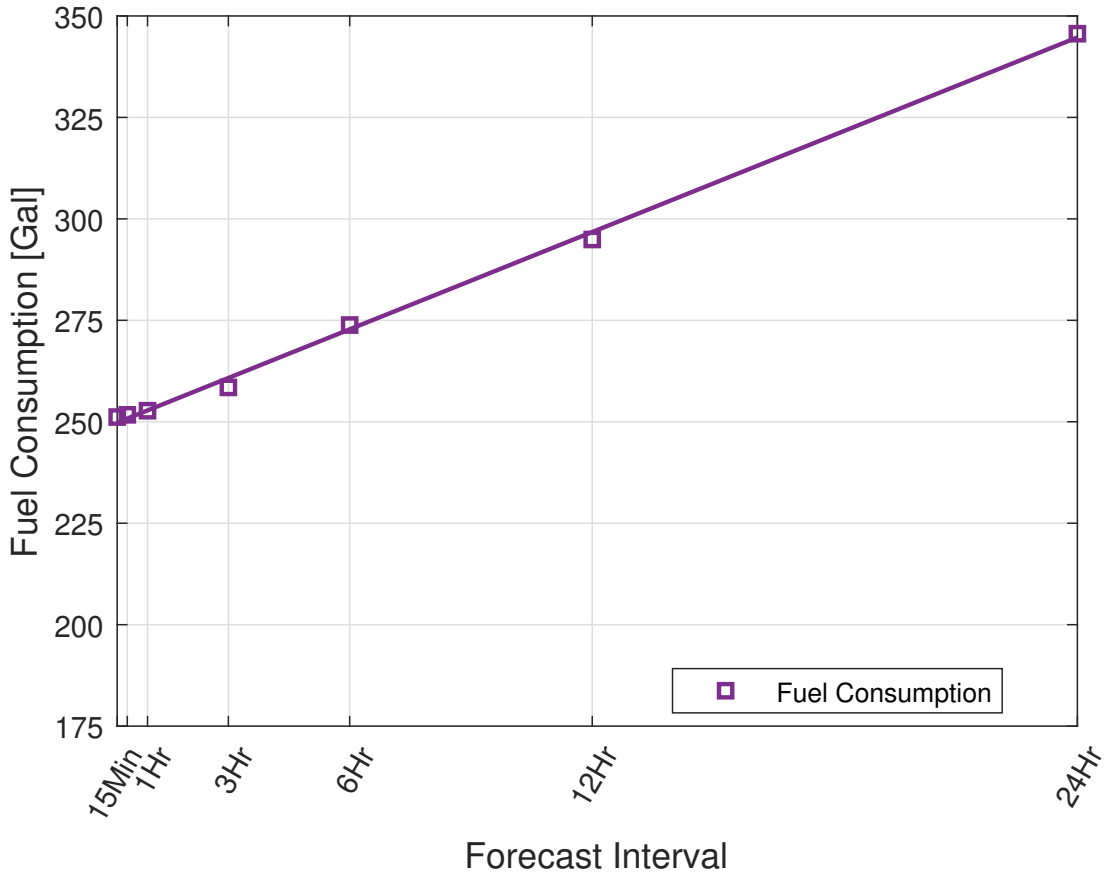

Figure B.15: The fuel consumed by the generators factoring in both the initial stored energy requirements, and the difference between the final energy state and the initial energy state for the bus and PV storage.

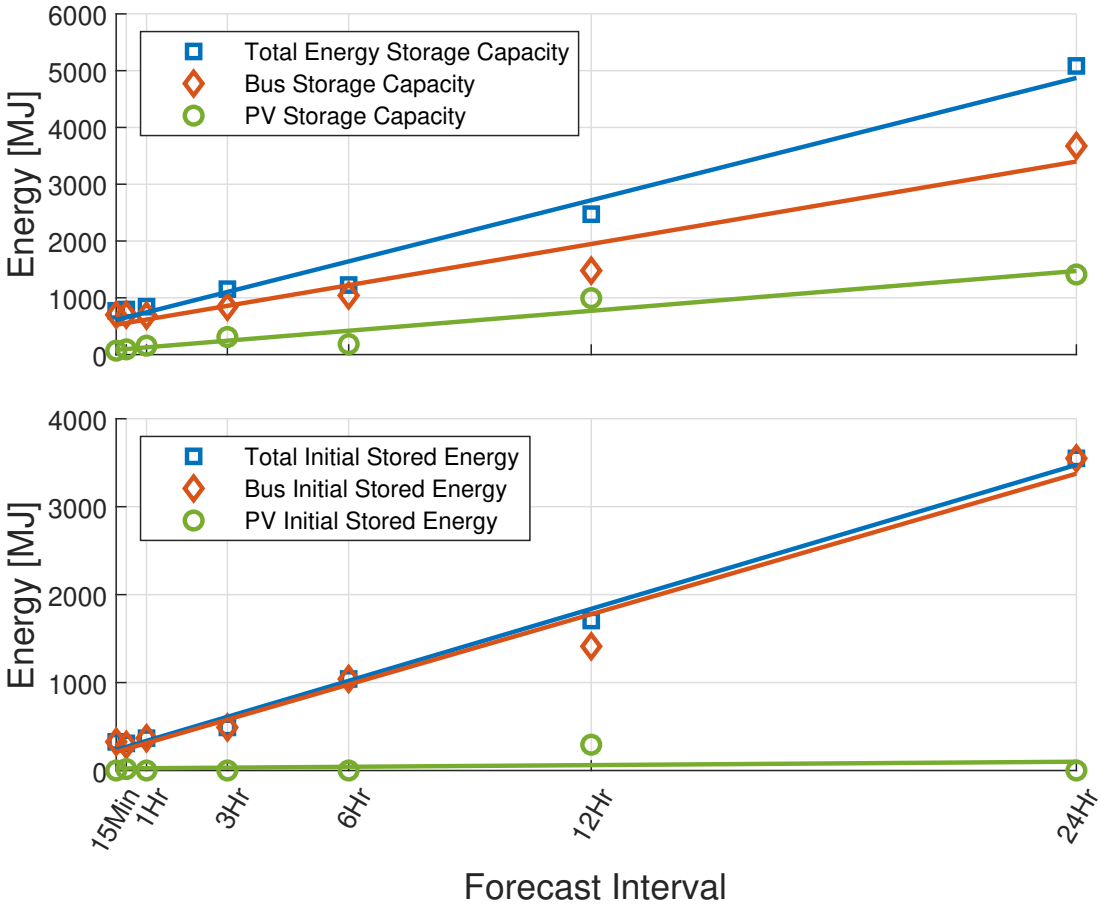

Figure B.16: Allocation of the total energy storage between the bus storage and the PV sites.

Appendix C

Blending of Heterogeneous Assets for Cooperative Control Additional Case Studies

This appendix contains additional case studies completed in response to the results collected from Chapter 6 concerning the development of a methodology to blend a diverse set of heterogeneous assets with competing objective functions, to achieve more optimal control.

Specifically, the additional case studies used the original scenario and energy management policies presented within Section 6.4. Minor modifications to the energy

management strategy or policy to try and achieve more optimal energy usage of the generation assets when compared to the results collected in Section 6.3.

C.1 Reduction of the Forecast Interval

The results collected and tabulated within Chapter 5 showed that as the forecast interval increased from 15 Min, 30 Min, 1 Hr, 3 Hr, 6 Hr, 12 Hr, to $24Hrs$, the equivalent fuel consumption increased non-linearly following a trend similar to exponential growth. For smaller forecast intervals, of 15 Min, 30 Min, and 1 Hr there was not much difference regarding the optimality of the solutions, for progressively larger forecast intervals, more substantial differences regarding the optimality of the solutions was observed. The results presented in Section 6.4 were generated assuming the LTO was executed periodically every 900 seconds, and the forecast interval was that of 15 Min. For the subsequently provided results, the forecast interval was reduced to 1 Min. The results collected are provided in Figure C.1 - Figure C.11.

Similarly, to the results collected in Section 6.4, the results provided within this section contain all active power contribution figures for each of the three separate power apportionment strategies, in addition to the combined bus storage and dedicated 60 kW RESCU electrical storage energy trajectories, the renewable asset's energy storage trajectories, the vehicle assets energy storage trajectories, the tracked fuel

consumption, and the equivalent fuel consumption.

The results collected, provided that the forecast interval was decreased from a 15 Min persistent forecast to a 1 Min persistent forecast are shown in Figure C.1 - Figure C.11. The results from Section 6.3 showed that the diesel fuel based assets consumed approximately 290, 388, and 270 gallons for Case A, B, and C respectively. Keep in mind that the results provided in Section 6.3 did not consider the 60 kW electrical storage, however the results in Section 6.4 did, which showed that the diesel fuel based assets consumed approximately 312, 390, and 300 gallons for Case A, B, and C respectively. With the decreased forecast interval, the diesel fuel based assets consumed approximately 312, 368.4, and 300 gallons for Case A, B, and C respectively. Negligible fuel differences arose from for Case A and C, however, there was a decrease in total fuel consumption for Case B. Unfortunately, the reduction of the forecast interval has not achieved more optimal energy usage when compared to Section 6.3. However, the results collected within this section support the results and conclusions presented in Chapter 5, which showed that there was not much difference regarding the optimality of the solutions for small forecast intervals.

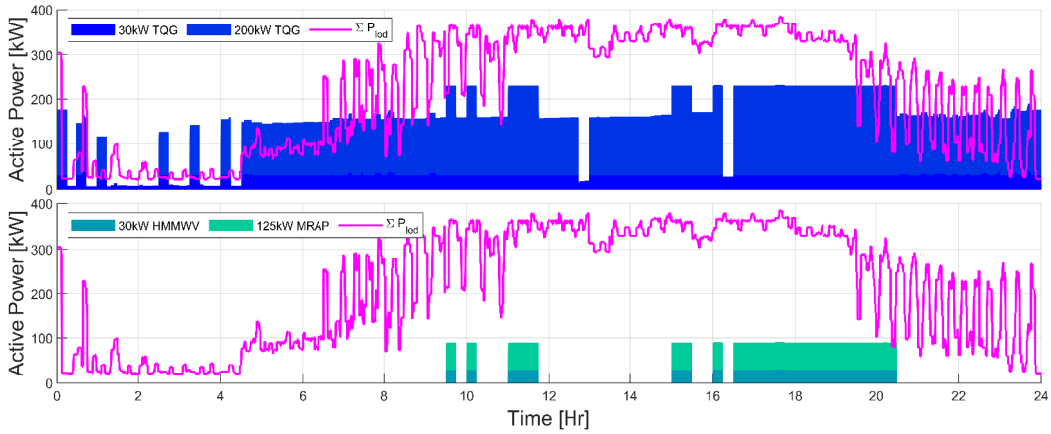

Figure C.1: Case A - Diesel Fuel Based Asset Electrical Power Contribution compared to the Aggregate Electrical Load

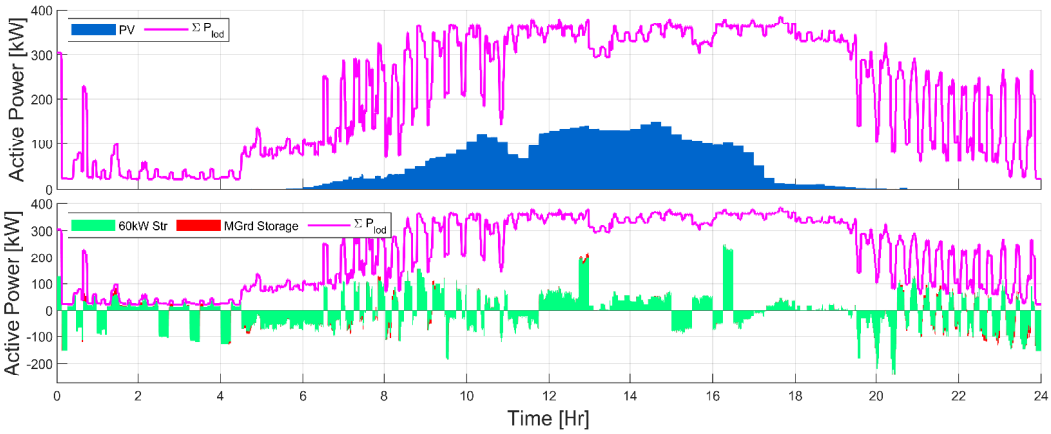

Figure C.2: Case A - Electrical Storage Based Asset Electrical Power Contribution compared to the Aggregate Electrical Load

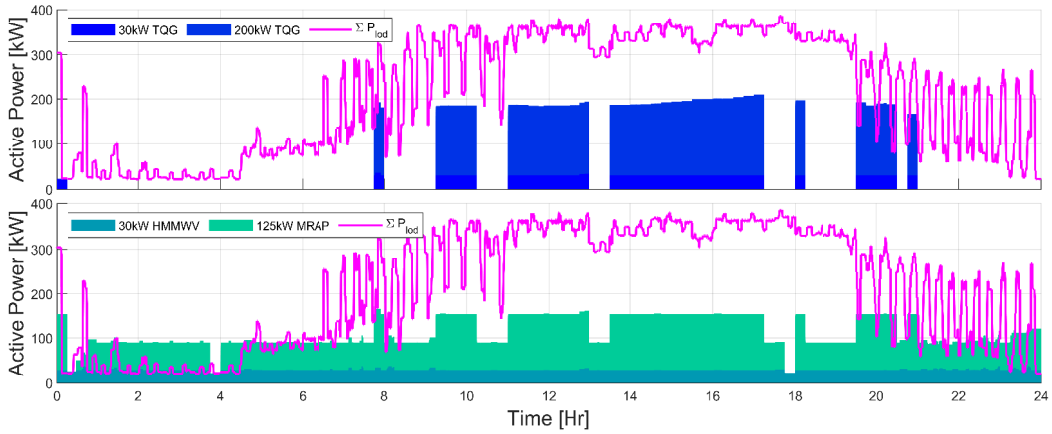

Figure C.3: Case B - Diesel Fuel Based Asset Electrical Power Contribution compared to the Aggregate Electrical Load

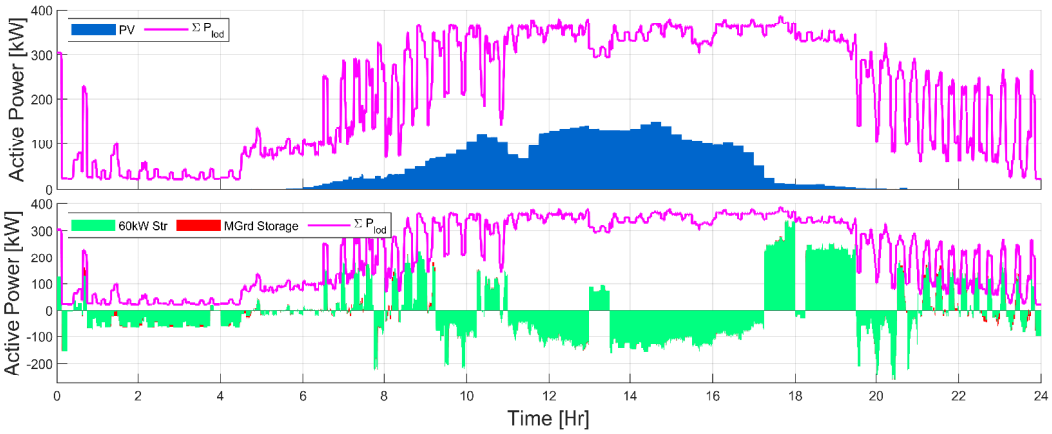

Figure C.4: Case B - Electrical Storage Based Asset Electrical Power Contribution compared to the Aggregate Electrical Load

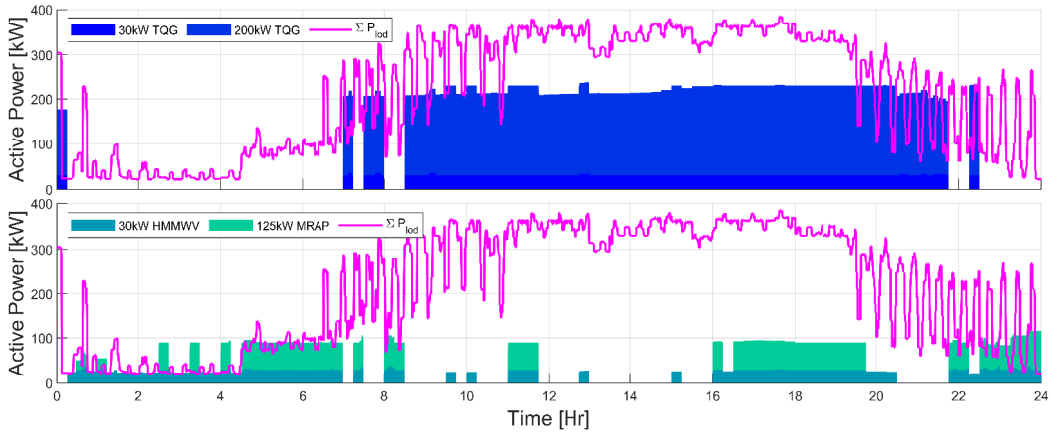

Figure C.5: Case C - Diesel Fuel Based Asset Electrical Power Contribution compared to the Aggregate Electrical Load

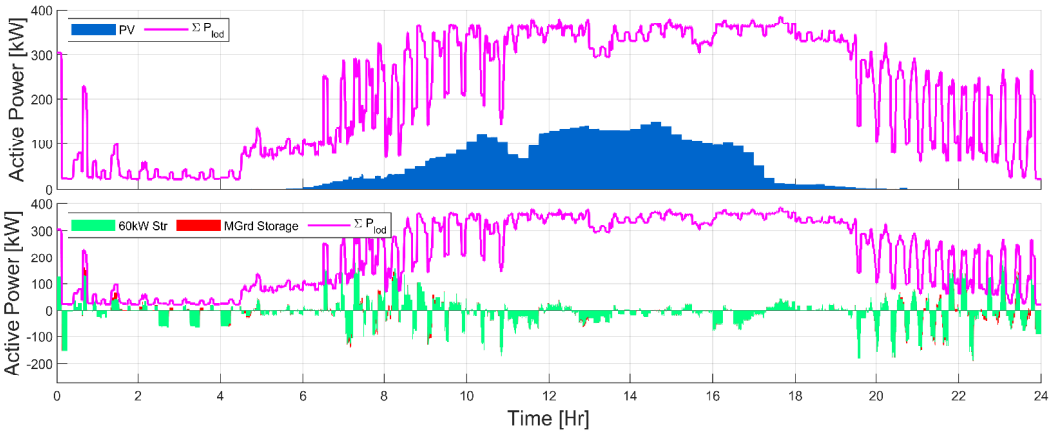

Figure C.6: Case C - Electrical Storage Based Asset Electrical Power Contribution compared to the Aggregate Electrical Load

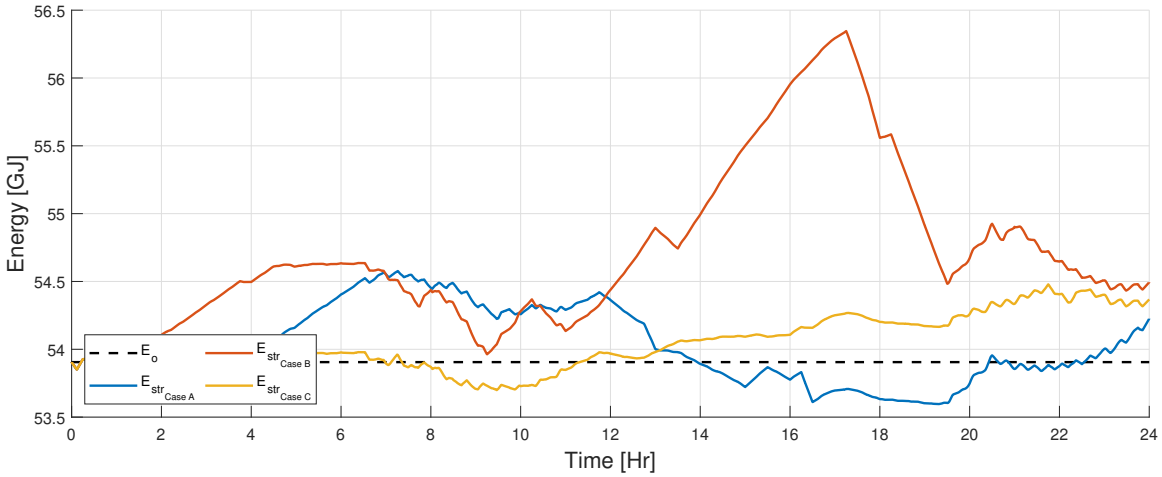

Figure C.7: The electrical storage asset's energy usage throughout across the three case studies throughout simulation epoch.

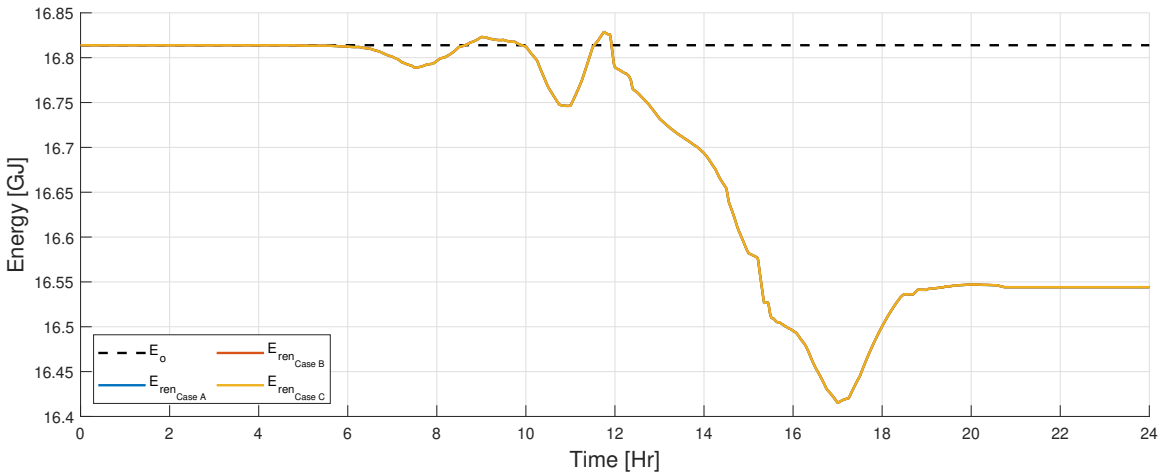

Figure C.8: The electrical storage energy for the renewable's collocated electrical storage asset for each of the three case studies.

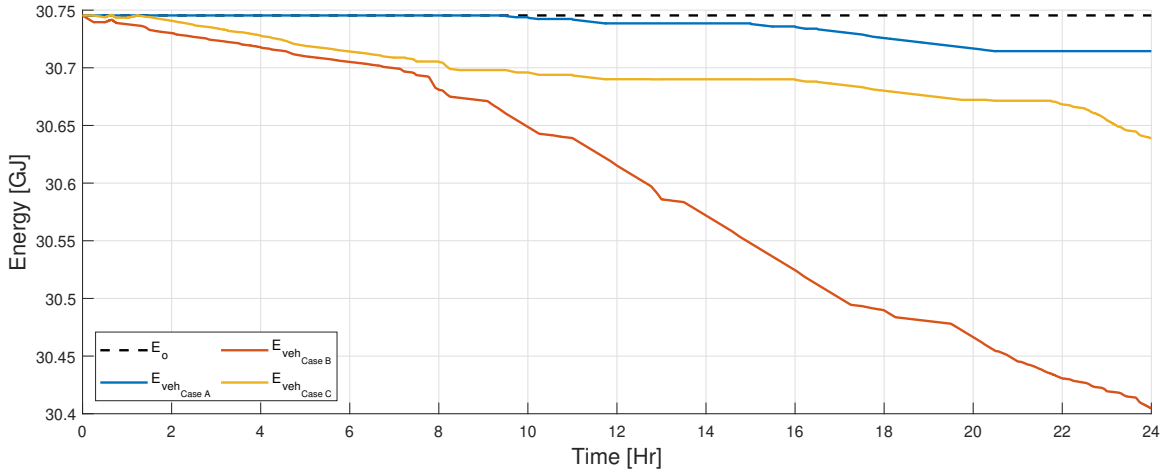

Figure C.9: The electrical storage energy for the vehicle's collocated electrical storage asset for each of the three case studies.

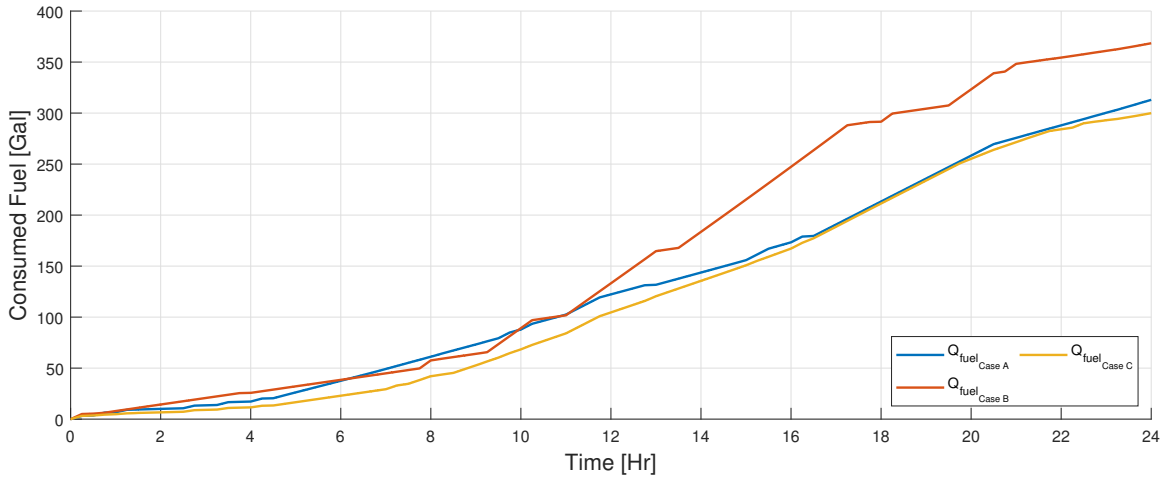

Figure C.10: The combined fuel consumed by the contingent of the diesel generators and military type vehicles.

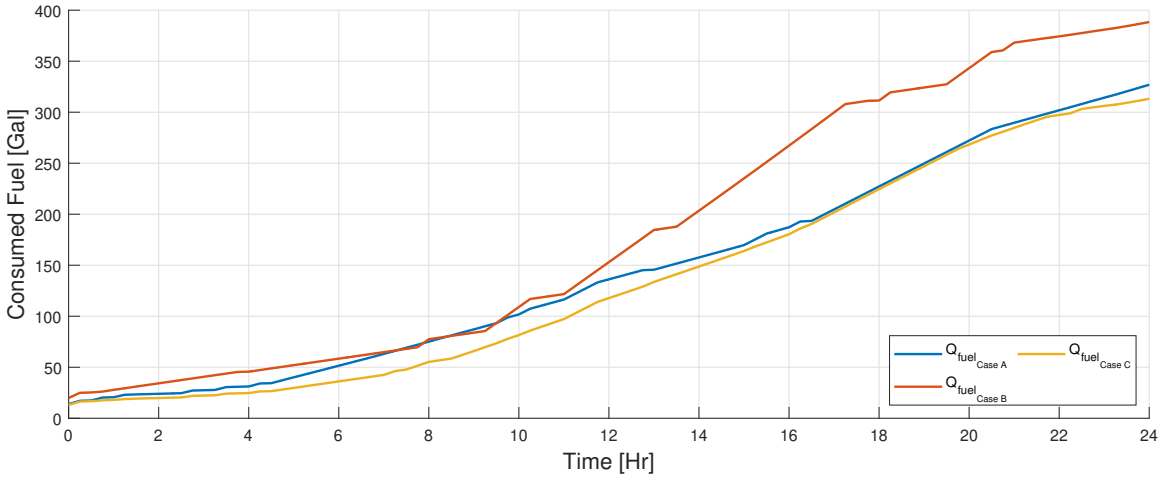

Figure C.11: The equivalent fuel consumption for each of the three case studies.

C.2 Increase the LTO Execution Rate with a Reduction of Forecast Interval

The results collected and tabulated within Chapter 5 showed that as the forecast interval increased from 15 Min, 30 Min, 1 Hr, 3 Hr, 6 Hr, 12 Hr, to $24Hrs$, the equivalent fuel consumption increased non-linearly following a trend similar to exponential growth. For smaller forecast intervals, of 15 Min, 30 Min, and 1 Hr there was not much difference regarding the optimality of the solutions, for progressively larger forecast intervals, more substantial differences regarding the optimality of the solutions was observed. The results presented in Section 6.4 were generated assuming the LTO was executed periodically every 900 seconds, and the forecast interval was that of 15 Min. For the subsequently provided results, the LTO execution rate was decreased to 1 Min, similarly, the forecast interval was also reduced to 1 Min. The results collected are provided Figure C.12 - Figure C.22.

Similarly to the results collected in Section 6.4, the results provided within this section contain all active power contribution figures for each of the three separate power apportionment strategies, in addition to the combined bus storage and dedicated 60 kW RESCU electrical storage energy trajectories, the renewable asset's energy storage trajectories, the vehicle assets energy storage trajectories, the tracked fuel

consumption, and the equivalent fuel consumption.

The results collected, provided that the forecast interval was decreased from a 15 Min persistent forecast to a 1 Min persistent forecast are shown in Figure C.1 - Figure C.11. The results from Section 6.3 showed that the diesel fuel based assets consumed approximately 290, 388, and 270 gallons for Case A, B, and C respectively. Keep in mind that the results provided in Section 6.3 did not consider the 60 kW electrical storage, however the results in Section 6.4 did, which showed that the diesel fuel based assets consumed approximately 312, 390, and 300 gallons for Case A, B, and C respectively. With the decreased forecast interval, the diesel fuel based assets consumed approximately 31.34, 389, and 299.30 gallons for Case A, B, and C respectively. Negligible fuel differences arose from for all cases, most notably, the increased execution frequency of the LTO increases the fuel consumption of Case B, however the end value was still slightly better than the fuel consumption of Section 6.4, Case B. Unfortunately, the reduction of the forecast interval and an increased execution rate of the LTO did not achieved more optimal energy usage when compared to Section 6.3. However, the results collected within this section support the results and conclusions presented in Chapter 5, which showed that there was not much difference regarding the optimality of the solutions for small forecast intervals.

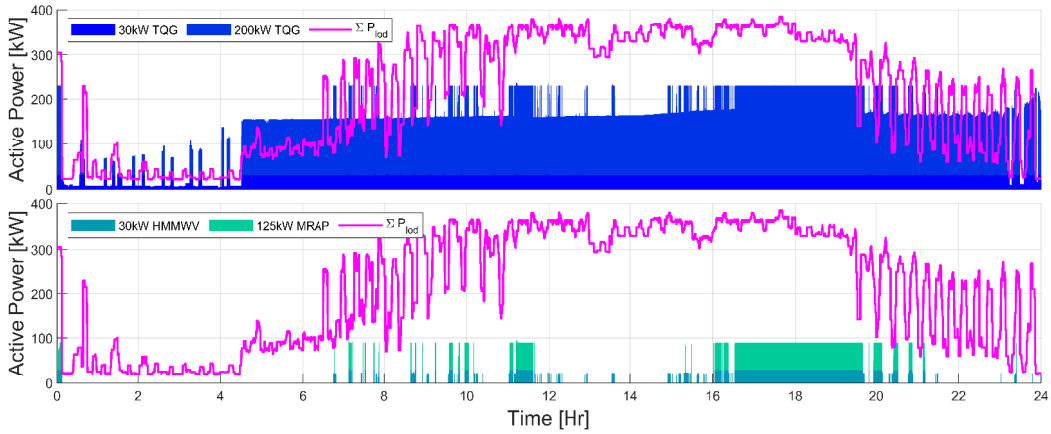

Figure C.12: Case A - Diesel Fuel Based Asset Electrical Power Contribution compared to the Aggregate Electrical Load

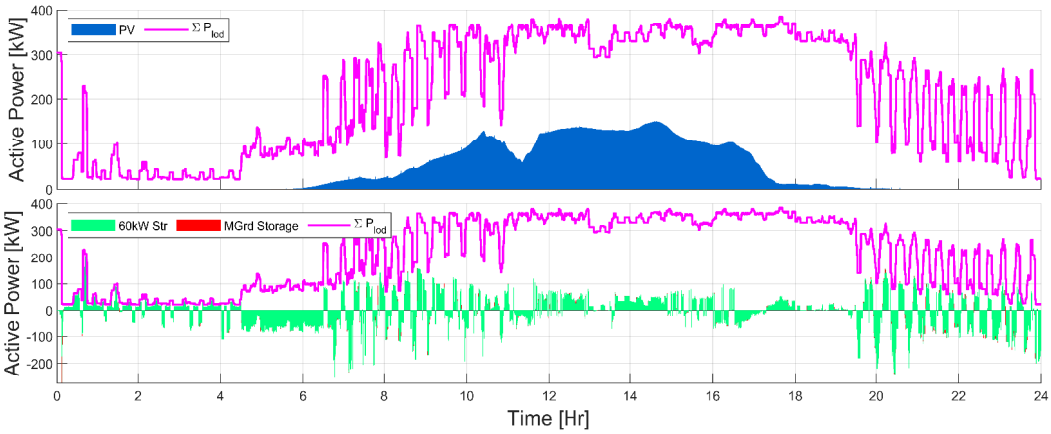

Figure C.13: Case A - Electrical Storage Based Asset Electrical Power Contribution compared to the Aggregate Electrical Load

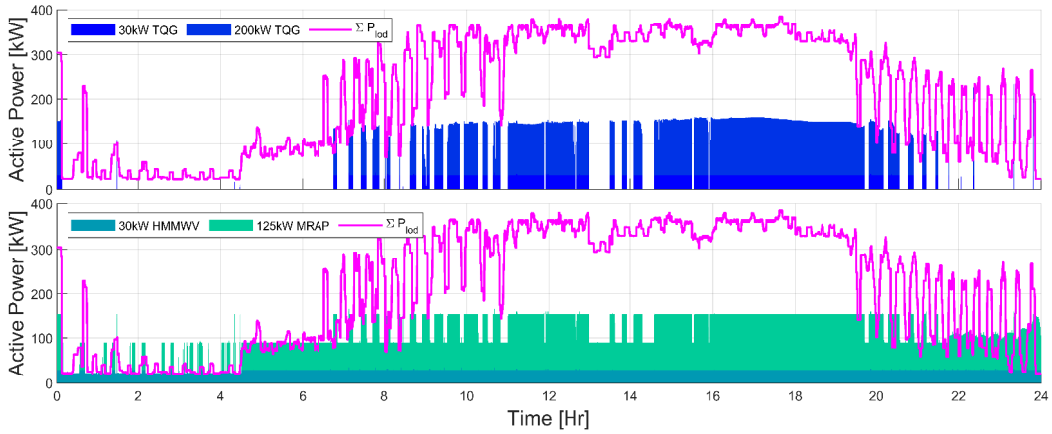

Figure C.14: Case B - Diesel Fuel Based Asset Electrical Power Contribution compared to the Aggregate Electrical Load

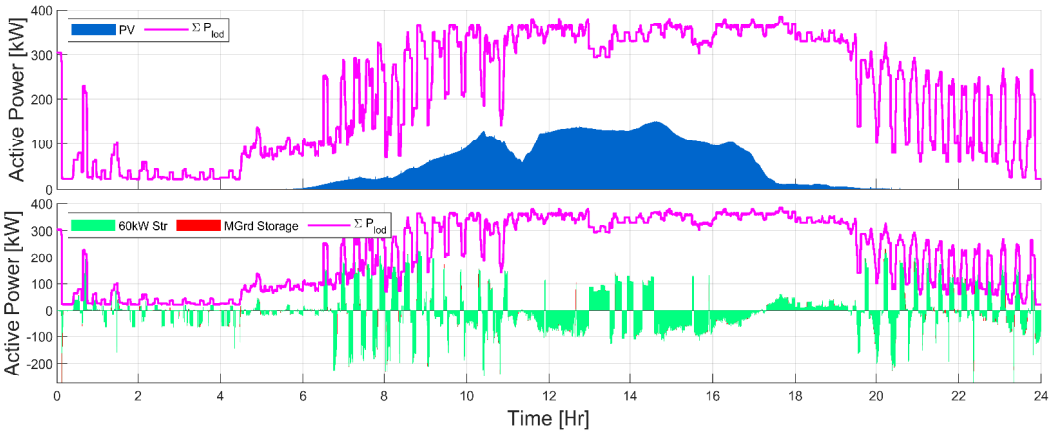

Figure C.15: Case B - Electrical Storage Based Asset Electrical Power Contribution compared to the Aggregate Electrical Load

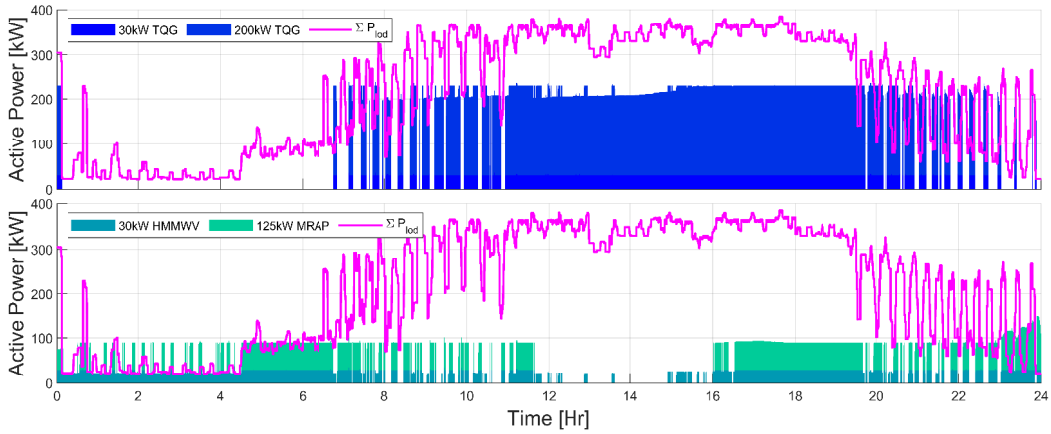

Figure C.16: Case C - Diesel Fuel Based Asset Electrical Power Contribution compared to the Aggregate Electrical Load

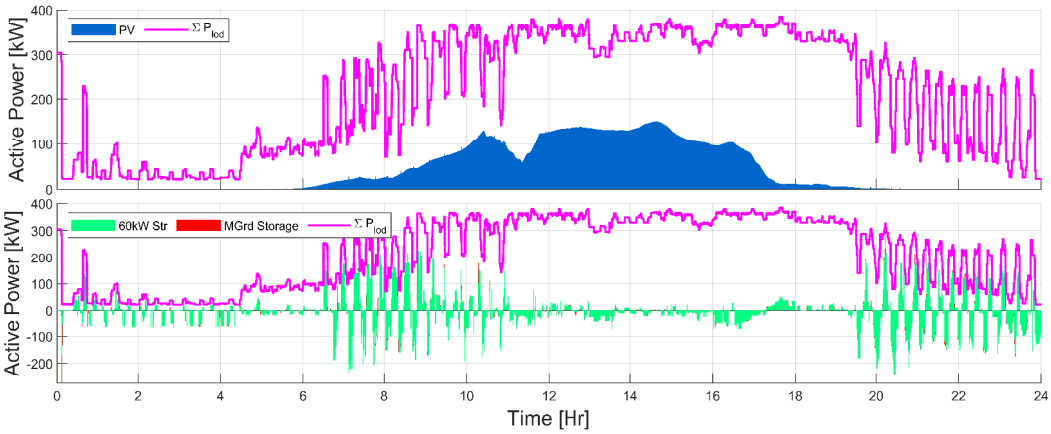

Figure C.17: Case C - Electrical Storage Based Asset Electrical Power Contribution compared to the Aggregate Electrical Load

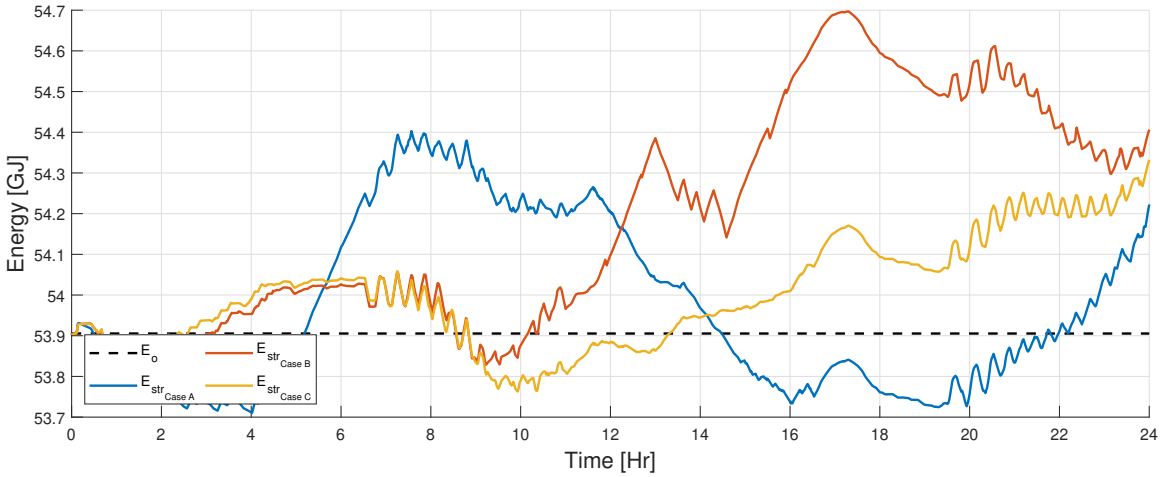

Figure C.18: The electrical storage asset's energy usage throughout across the three case studies throughout simulation epoch.

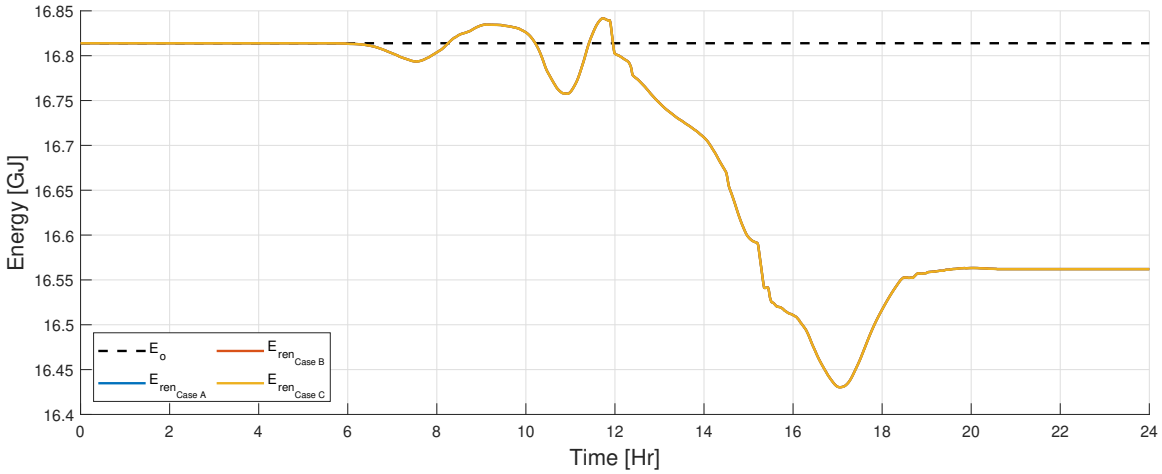

Figure C.19: The electrical storage energy for the renewable's collocated electrical storage asset for each of the three case studies.

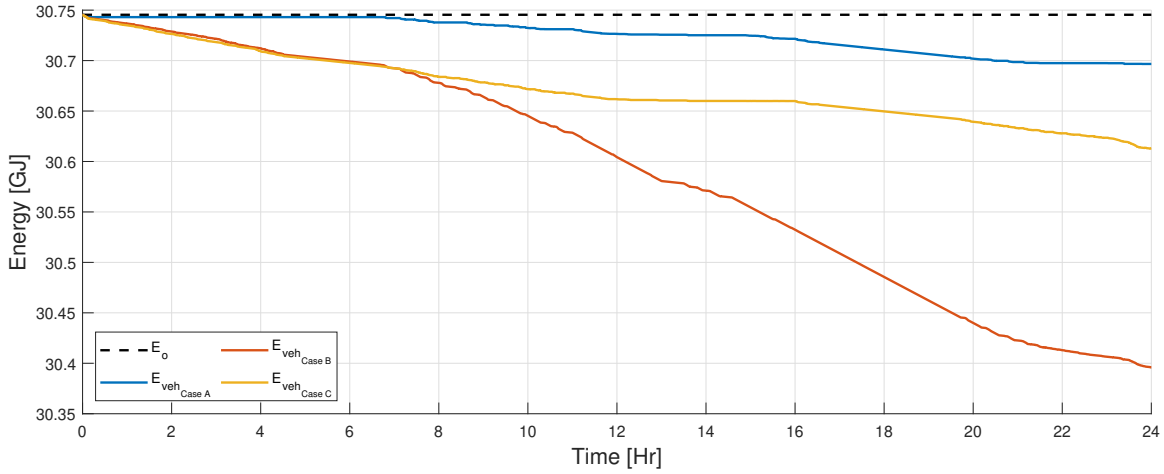

Figure C.20: The electrical storage energy for the vehicle's collocated electrical storage asset for each of the three case studies.

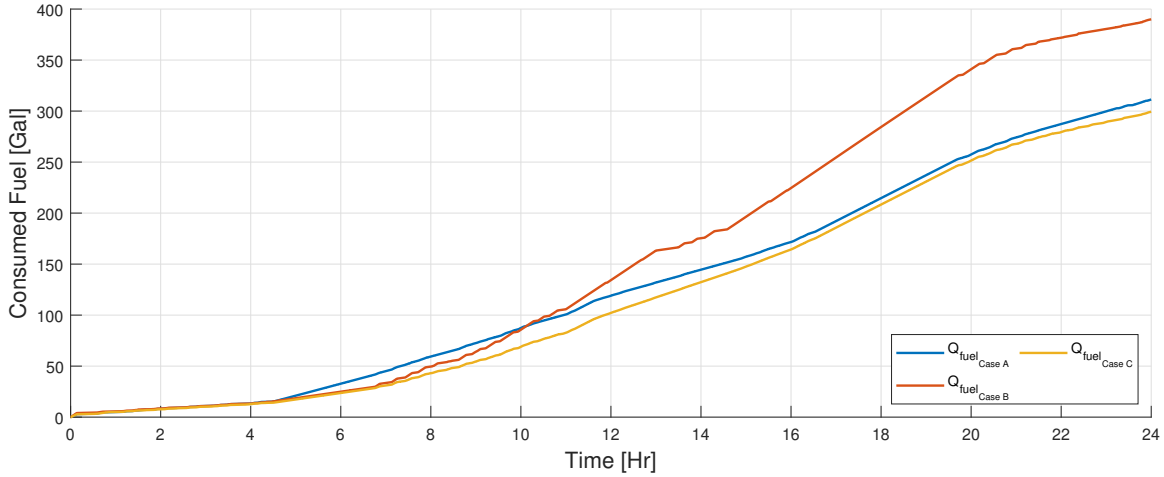

Figure C.21: The combined fuel consumed by the contingent of the diesel generators and military type vehicles.

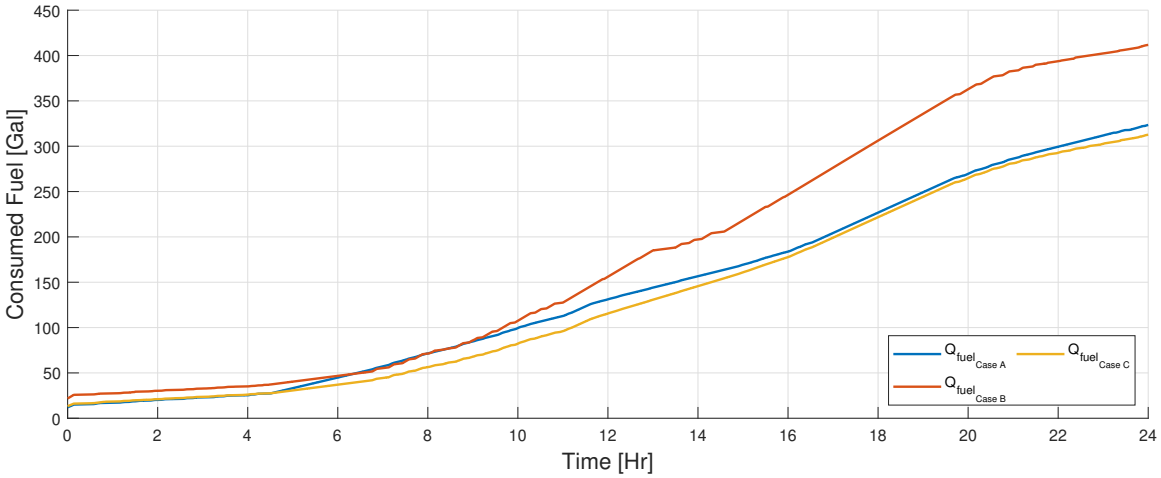

Figure C.22: The equivalent fuel consumption for each of the three case studies.

C.3 Continuous Vs. Discontinuous Optimization

In this section, discontinuous execution of the LTO's energy management policy was compared to continuous execution of the LTO's energy management policy. Discontinuous optimization refers to the frequency of the LTO's execution. For discontinuous execution of the LTO, the LTO will execute at the beginning of the simulation, the solution was parsed appropriately and passed throughout the simulation. For continuous optimization, the LTO will execute at fixed intervals, and generate new optimal commands based on updated measurement data. Two different LTO execution rates of 15 Min and 60 Sec will be simulated with two different forecast intervals of 15 Min and 60 Sec.

C.3.1 LTO Execution Every Fifteen Minutes with a Forecast Interval of Fifteen Minutes

Five different figures are shown in this section to illustrate the difference between the discontinuous and continuous optimization, including (1) the electrical energy of the electrical storage asset, (2) the electrical energy of the PV's electrical storage assets, (3) the electrical energy of the vehicles electrical storage assets, (4) the fuel consumption of the diesel fuel based assets, and (5) the equivalent fuel consumption which accounts for the final and initial energy storage requirements of all electrical storage assets. The results are shown in Figure C.23 - Figure C.27.

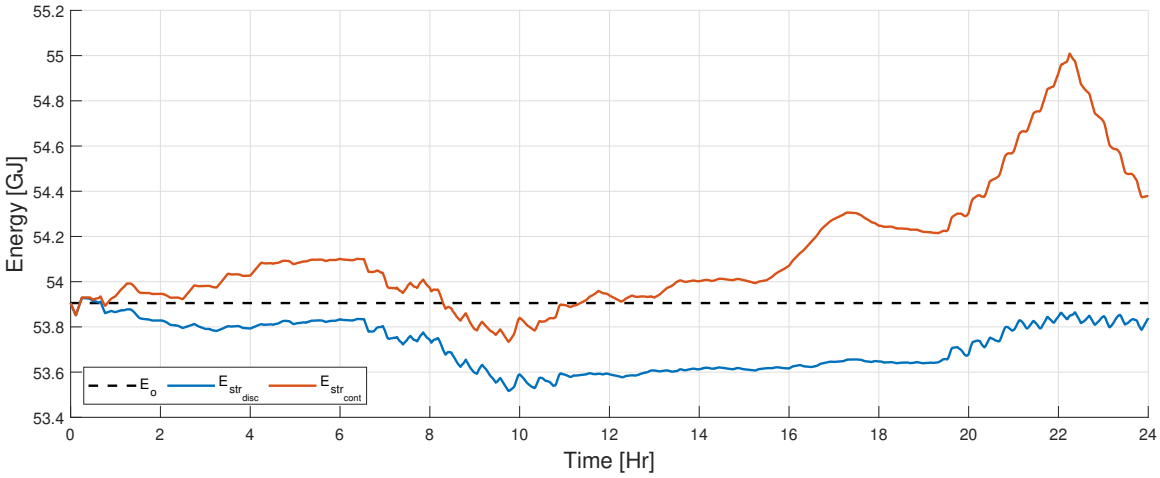

Figure C.23: The electrical storage energy for the discontinuous and continuous optimization of the LTO.

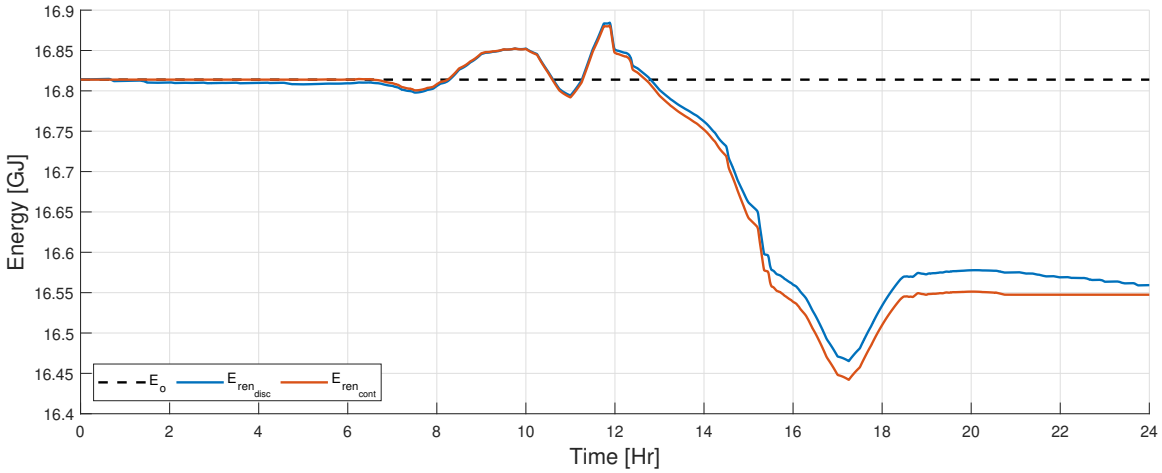

Figure C.24: The electrical storage energy for the renewable's collocated electrical storage asset for both the discontinuous and continuous optimization of the LTO.

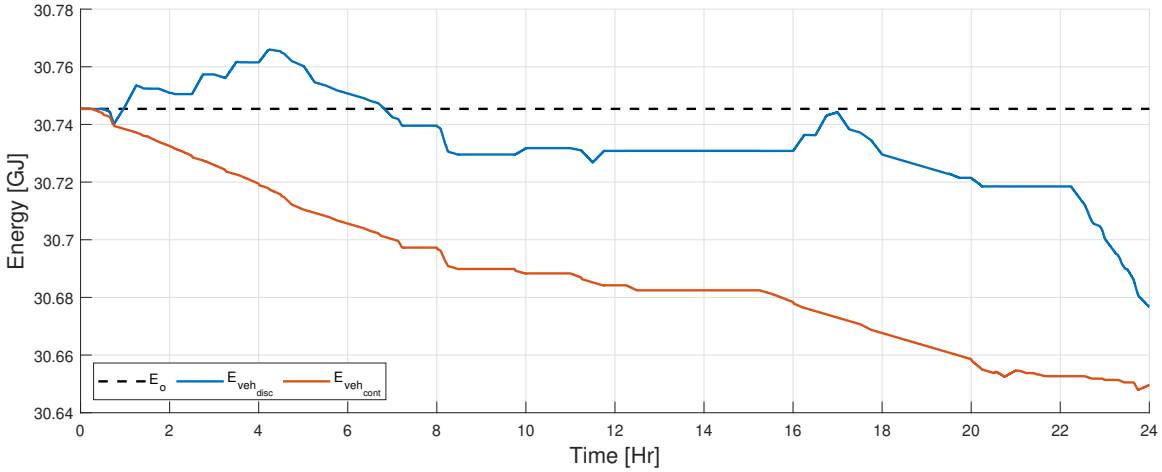

Figure C.25: The electrical storage energy for the vehicle's collocated electrical storage asset for both the discontinuous and continuous optimization of the LTO.

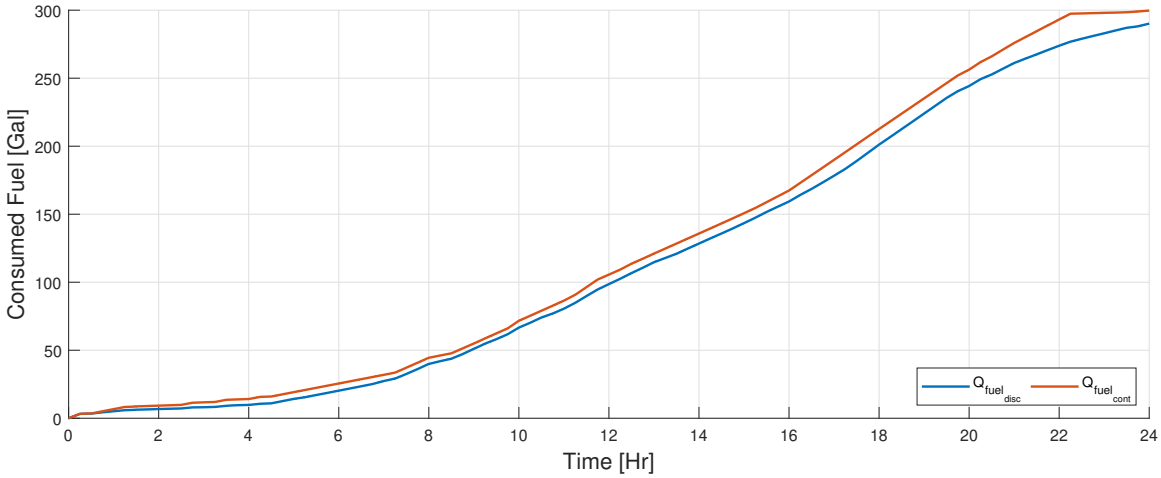

Figure C.26: The combined fuel consumed by the contingent of the diesel generators and military type vehicles for both the discontinuous and continuous optimization of the LTO.

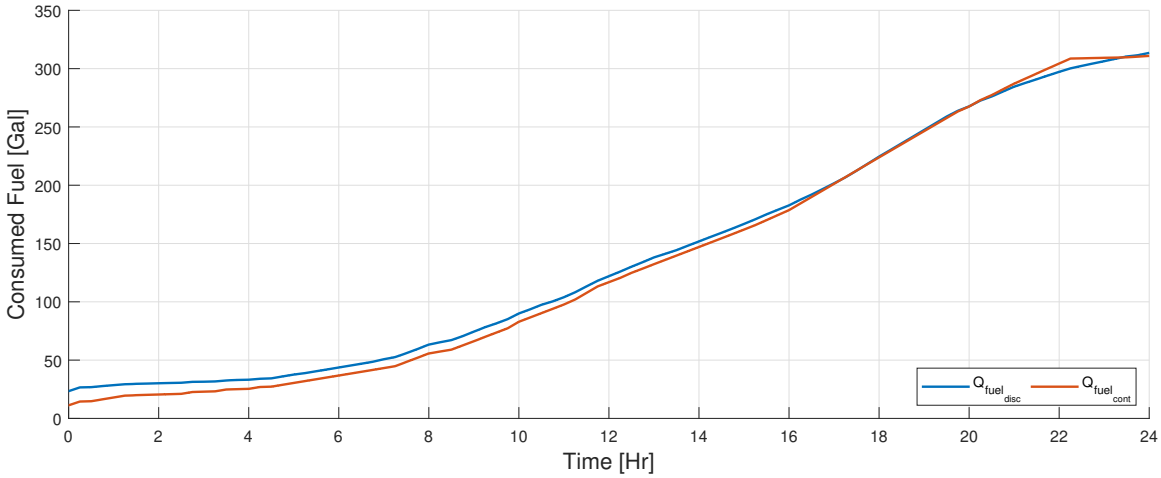

Figure C.27: The combined equivalent fuel consumed by the contingent of the diesel generators and military type vehicles for both the discontinuous and continuous optimization of the LTO.

The results provided in Figure C.23 - Figure C.27 indicate that straight fuel consumption of the diesel fuel based assets was lower for discontinuous optimization as opposed to continuous optimization. The results indicate that the use of continuous

optimization over discontinuous optimization will yield a 3% increase in total fuel consumption, interestingly enough, a 97% increase in the total electrical storage capacity. The most notable difference observed within the results was that the resulting final energy state of the total electrical storage asset exceeds that of the initial energy storage state, where the discontinuous energy storage state ends at a lower energy state. When the equivalent fuel consumption metric was computed, continuous optimization yields more optimal energy usage as opposed to discontinuous optimization consuming 1% less fuel which equates to about three gallons difference.

C.3.2 LTO Execution Every Sixty Seconds

Five different figures are provided within this section to illustrate the difference between the discontinuous and continuous optimization, including (1) the electrical energy of the electrical storage asset, (2) the electrical energy of the PV's electrical storage assets, (3) the electrical energy of the vehicles electrical storage assets, (4) the fuel consumption of the diesel fuel based assets, and (5) the equivalent fuel consumption which accounts for the final and initial energy storage requirements of all electrical storage assets. The results are shown in Figure C.28 - Figure C.32.

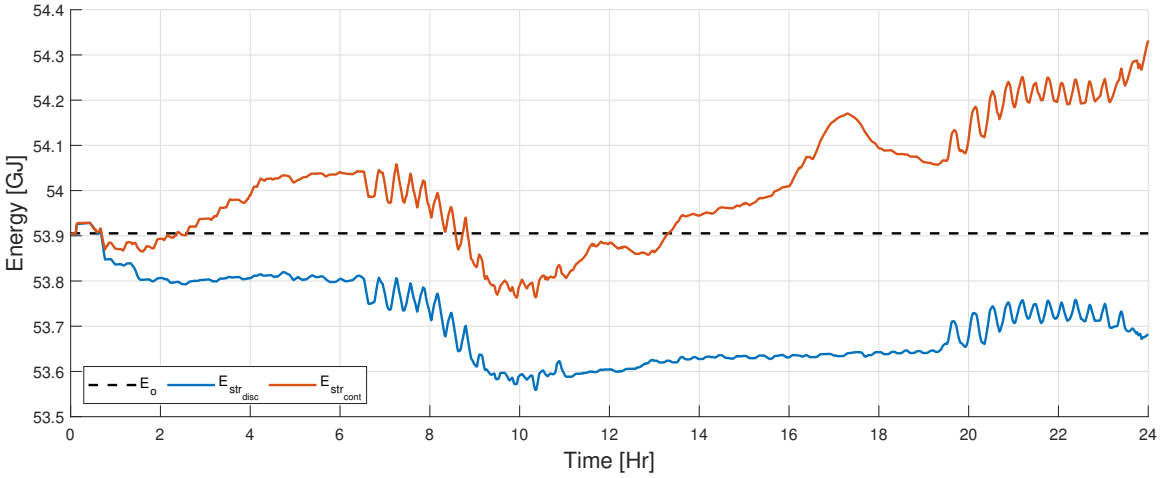

Figure C.28: The electrical storage energy for the discontinuous and continuous optimization of the LTO.

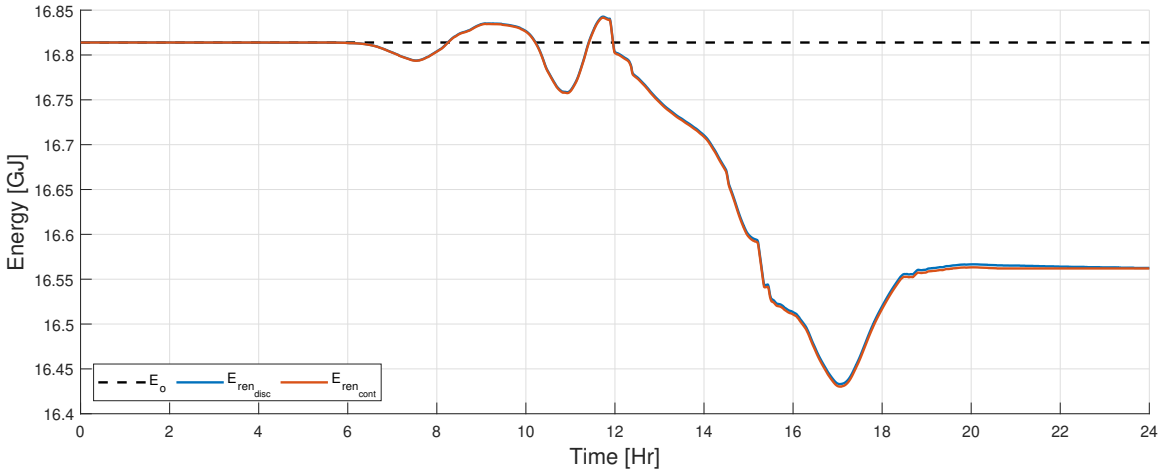

Figure C.29: The electrical storage energy for the renewable's collocated electrical storage asset for both the discontinuous and continuous optimization of the LTO.

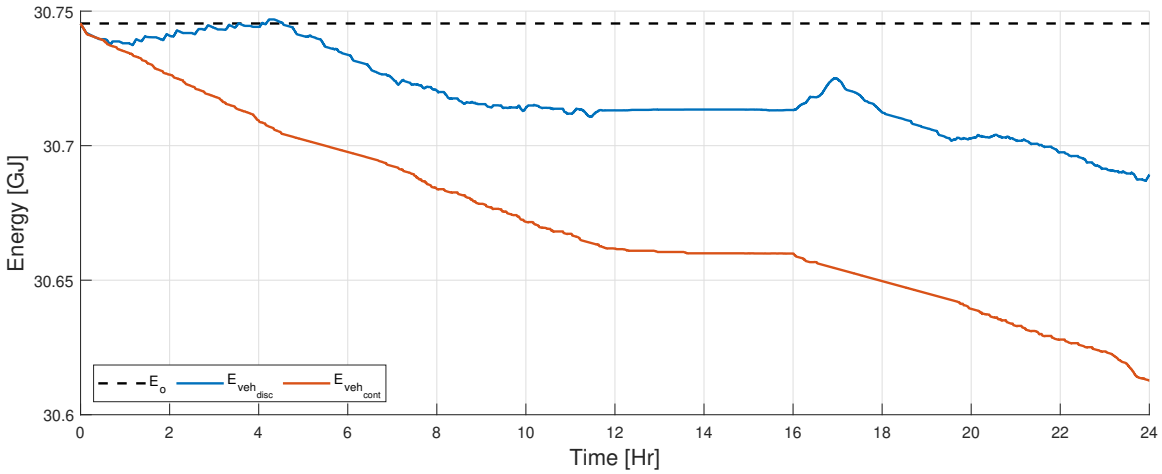

Figure C.30: The electrical storage energy for the vehicle's collocated electrical storage asset for both the discontinuous and continuous optimization of the LTO.

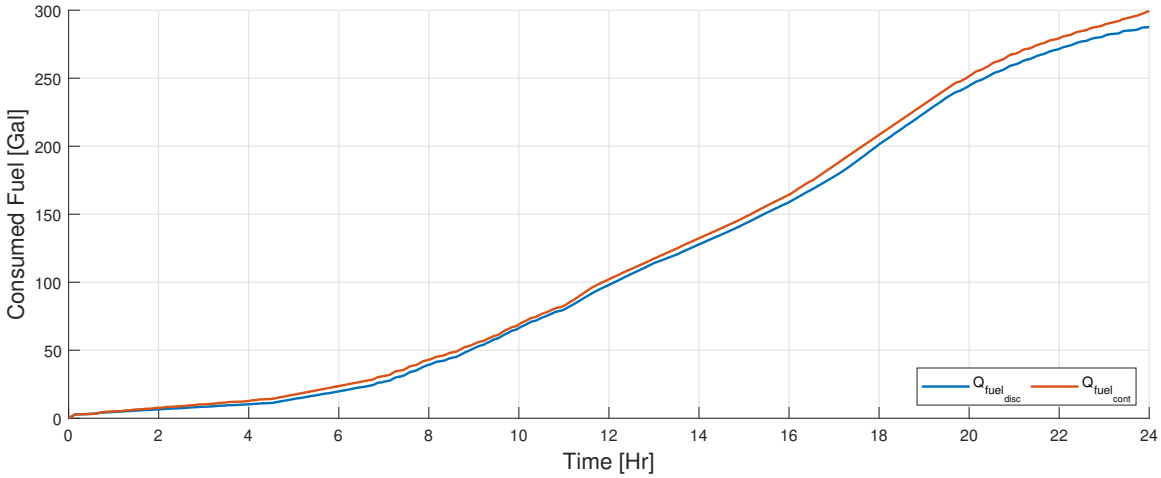

Figure C.31: The combined fuel consumed by the contingent of the diesel generators and military type vehicles for both the discontinuous and continuous optimization of the LTO.

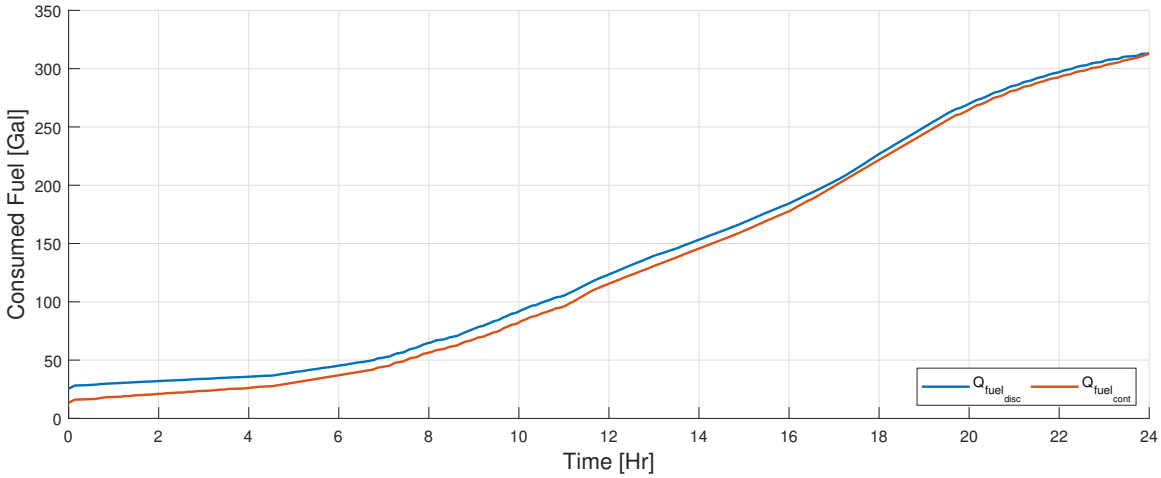

Figure C.32: The combined equivalent fuel consumed by the contingent of the diesel generators and military type vehicles for both the discontinuous and continuous optimization of the LTO.

The results provided in Figure C.28 - Figure C.32 indicate that straight fuel consumption of the diesel fuel based assets was lower for discontinuous optimization as opposed to continuous optimization. The results indicate that the use of continuous

optimization over discontinuous optimization will yield a 4% increase in total fuel consumption, interestingly enough, a 33% increase in the total electrical storage capacity. The most notable difference observed within the results was that the resulting final energy state of the total electrical storage asset exceeds that of the initial energy storage state, where the discontinuous energy storage state ends at a lower energy state. When the equivalent fuel consumption metric was computed, it was determined that continuous optimization yields more optimal energy usage as opposed to discontinuous optimization consuming 0.13% less fuel which equates to about half of a gallon difference.

C.4 Summary

The results provided within this appendix support the results collected and tabulated within Chapter 6. This appendix was added to further investigate if more optimal energy management could be achieved when compared to the results collected in Section 6.3 by (1) reducing the forecast interval and (2) increasing the LTO's execution rate. Further, the difference between discontinuous and continuous optimization of the LTO was investigated using variable LTO execution rates and variable forecast intervals.

Unfortunately, the reduction of the forecast interval and the increased LTO execution

rate did not enable more optimal energy behavior to be obtained when compared to the results collected within Section 6.3. This was primarily because the energy management strategy did not require the additional electrical storage asset, meaning on average, less electrical losses would be incurred when compared to the energy management strategy of Section 6.4. Less electrical losses for a prolonged period of time would inhibit the ability of the energy management policy to reduce energy usage while using an additional generation asset. Conversely, the results collected within Section C.1 and Section C.2 yielded similar or slightly more optimal energy usage when compared to the results of Section 6.4. This supports the results collected within Chapter 5 which indicated that for certain scenarios, a reduction of forecast interval may minimally affect the LTO's ability to provide more optimal fuel or energy usage with small forecast intervals of 15 Min, 30 Min, and 1 Hr.

Finally, regarding the difference between discontinuous and continuous execution of the LTO's energy management policy subject to variable forecast intervals and variable execution rates, the results collected showed that less fuel optimal behavior was observed for continuous optimization as opposed to discontinuous optimization. Additionally, larger electrical storage metrics were also observed, however, due to continuous updates, the continuous optimization leads to more energy optimal behavior when all electrical storage and fuel consumption metrics when tabulated. It is expected that if larger forecast intervals are used in conjunction with a fixed LTO execution rate of 900 seconds, that substantial differences within the weather forecast

would lead to less optimal fuel usage for discontinuous optimization as opposed to continuous optimization.

Appendix D

Letter of Permission

D.1 Copy Right Permission Request 01

Dear Editor:

I would like to use a paper published in SAE for my PhD dissertation:

Jane, R., Parker, G., Weaver, W., Matthews, R. et al., "Optimal Power Management of Vehicle Sourced Military Outposts," SAE Int. J. Commer. Veh. 10(1):132-143, 2017, https://doi.org/10.4271/2017-01-0271.

Is this permitted, if so is there any additional paper work which is required to complete

to include the paper within my dissertation.

Thank you for your time.

Robert. S. Jane

D.2 Copy Right Permission Request 02

I emailed previously concerning including a different SAE paper within my PhD dissertation, and would also like to include components of a another paper:

Fuel-Optimal Strategies for Vehicle Supported Military Microgrids Technical Paper2016-01-0312 ISSN 0148-7191 DOI: https://doi.org/10.4271/2016-01-0312 Published April 5, 2016 by SAE International in United States

Is this permitted, if so is there any additional paper work which is required to complete to include the paper within my dissertation.

Thank you for your time.

Robert. S. Jane

D.3 Copyright Permission Request Response

Hello Robert,

SAE International has partnered with Copyright Clearance Center to make it easier to request permissions to reuse SAE International content. A separate permission request must be submitted for additional usage of SAE copyright material. Please follow the steps below:

To request republication of content, please click on the following link www.copyright.com and follow the prompts.

Enter the title, ISBN or ISSN number of the publication you'd like to reuse and hit "Go" After finding the title you'd like, choose "Pay-Per-Use Options" Enter the publication year of the content you'd like to reuse Scroll down the list to find the type of reuse you want to request Select the corresponding bubble and click "Price & Order" Fill out any required information and follow the prompts to acquire the proper permissions to reuse the selected content

For questions regarding process or assistance from the Copyright Clearance Center in obtaining republication grants, please contact info@copyright.com or:

Copyright Clearance Center 222 Rosewood Drive Danvers, MA 01923 Phone: +1-(978) 750-8400 Fax: +1-(978) 750-4470

For questions regarding process or assistance from SAE International, please contact copyright@sae.org.

Heather Kindsvatter Intellectual Property Specialist Content Management

SAE International 400 Commonwealth Drive Warrendale, PA 15096

o: 1.724.772.8515 e: heather.kindsvatter@sae.org www.sae.org

D.4 Citation Information

Fuel-Optimal Strategies for Vehicle Supported Military Microgrids by Jane, Robert Reproduced with permission of SAE International in the format Thesis/Dissertation via Copyright Clearance Center.

Optimal Power Management of Vehicle Sourced Military Outposts by Jane, Robert Reproduced with permission of SAE International in the format Thesis/Dissertation via Copyright Clearance Center.

D.5 Copyright Permission Status 01

Copyright Clearance Center

Note: Copyright.com supplies permissions but not the copyrighted content itself.

1 PAYMENT 2 REVIEW 3 CONFIRMATION

Step 3: Order Confirmation

Thank you for your order! A confirmation for your order will be sent to your account email address. If you have questions about your order, you can call us 24 hrs/day, M-F at +1.855.239.3415 Toll Free, or write to us at info@copyright.com. This is not an invoice.

Confirmation Number: 11805137
Order Date: 04/05/2019

If you paid by credit card, your order will be finalized and your card will be charged within 24 hours. If you choose to be invoiced, you can change or cancel your order until the invoice is generated.

Payment Information

Robert Jane
rsjane@mtu.edu
+1 (248) 933-1357
Payment Method: n/a

Order Details

Optimal Power Management of Vehicle Sourced Military Outposts

Order detail ID:	71870459
Order License Id:	4562530778144
Report ID:	2017-01-0271
Publication Type:	Report
Volume:	
Issue:	
Start page:	
Publisher:	SAE International
Author/Editor:	Jane, Robert

Permission Status: Granted
Permission type: Republish or display content
Type of use: Thesis/Dissertation

Requestor type	Author of requested content
Format	Print, Electronic
Portion	chapter/article
The requesting person/organization	Robert S. Jane
Title or numeric reference of the portion(s)	Chapter 3 of my PhD Dissertation.
Title of the article or chapter the portion is from	N/A
Editor of portion(s)	N/A
Author of portion(s)	N/A

D.6 Copyright Permission Status 02

Copyright Clearance Center

Note: Copyright.com supplies permissions but not the copyrighted content itself.

1 PAYMENT 2 REVIEW 3 CONFIRMATION

Step 3: Order Confirmation

Thank you for your order! A confirmation for your order will be sent to your account email address. If you have questions about your order, you can call us 24 hrs/day, M-F at +1.855.239.3415 Toll Free, or write to us at info@copyright.com. This is not an invoice.

Confirmation Number: 11805136
Order Date: 04/05/2019

If you paid by credit card, your order will be finalized and your card will be charged within 24 hours. If you choose to be invoiced, you can change or cancel your order until the invoice is generated.

Payment Information

Robert Jane
rsjane@mtu.edu
+1 (248) 933-1357
Payment Method: n/a

Order Details

Fuel-Optimal Strategies for Vehicle Supported Military Microgrids

Order detail ID:	71870454
Order License Id:	4562530489316
Report ID:	2016-01-0312
Publication Type:	Report
Volume:	
Issue:	
Start page:	
Publisher:	SAE International
Author/Editor:	Jane, Robert

Permission Status: Granted
Permission type: Republish or display content
Type of use: Thesis/Dissertation

Requestor type	Author of requested content
Format	Print, Electronic
Portion	chapter/article
The requesting person/organization	Robert S. Jane
Title or numeric reference of the portion(s)	Portions of the Publication may be used in Chapter 2 of my PhD dissertation.
Title of the article or chapter the portion is from	N/A
Editor of portion(s)	N/A
Author of portion(s)	N/A